Vandetanib-eluting radiopaque beads and stereotactic body radiotherapy in the treatment of liver cancers

Dr Laura Elizabeth Beaton
MBBS BSc MRCP FRCR

Submitted for MD (Res) to
University College London

DECLARATION

I, Laura Beaton, confirm that the work presented in this thesis is my own. Where information has been derived from other sources, I confirm that this has been indicated in the thesis.

This research was undertaken at University College London. The MD (Res) is registered with the Cancer Institute, UCL. I would like to thank Professor Ricky Sharma (UCL) and Dr Scott Tyldesley (BC Cancer, Vancouver) for their invaluable help and support as supervisors.

The VEROnA study was undertaken in close collaboration with the Clinical Trials Centre at UCL, and the clinical teams at University College London Hospitals and Royal Free Hospitals NHS trust. This thesis also includes research from work initially undertaken at BC Cancer, Vancouver.

I acknowledge the contributions of:

Nicholas Counsell: Statistical analysis (Chapters 2, 3 and 5)

Samantha Ryan: Pharmacokinetic analysis (Chapter 3)

Helen Lowe and the UCL GCLP laboratory: Cytokine data (Chapter 3)

York Bioanalytical Solutions Ltd: Vandetanib tissue and plasma concentrations (Chapter 3)

Dr Marnix Jansen: Histopathological sampling and analysis (Chapter 4)

Dr Julian Hague, Dr Graham Munneke, Dr Steven Bandula, Dr Manil Chouhan: DCE-MRI and perfusion CT post-processing and tumour contouring (Chapter 5)

Henry Tregidgo: DCE-MRI post-processing (Chapter 5) and Go-ICP algorithm (Chapter 7)

Dr Roy Ma, Dr Devin Schellenberg, Dr Mitchell Liu, Dr Rosanna Yeung, Dr Emma Dunne: Patient data and treatment plans (Chapter 6)

Dr Colin Mar and Dr Charlotte Yong-Hing: Radiology reporting (Chapter 6)

Kimberly DeVries: Statistical analysis (Chapter 6)

Mairead Daly, Syed Moinuddin, Helen Grimes and Chris Stacey: Acquisition of radiotherapy images (Chapter 7)

This work is dedicated to my husband David, my sister, and my parents for their never-ending support throughout my career.

ABSTRACT

Background

Current treatment options for unresectable hepatocellular carcinoma (HCC) and colorectal liver metastases (mCRC) include transarterial chemoembolisation (TACE) and stereotactic body radiotherapy (SBRT). The objectives of this project were:

1. To assess a novel drug-eluting bead for TACE
2. To report on the safety and efficacy of SBRT in HCC
3. To assess the feasibility of using radiopaque beads as fiducial markers for SBRT

Methods

In Part 1, a first-in-human trial was performed in patients with HCC and mCRC using a novel vandetanib-eluting radiopaque bead, BTG-002814. Primary trial endpoints were safety/tolerability and the concentrations of vandetanib and its major metabolite in plasma and resected tissue. Biomarker studies included blood cytokines and perfusion imaging parameters. In Part 2, the efficacy of SBRT was explored in a retrospective study of 31 patients with HCC tumours ≤5 cm and in a phase II study of 13 patients with larger tumours. In Part 3 the feasibility of using radiopaque beads as fiducial markers for SBRT was investigated.

Results

BTG-002814 was shown to have a satisfactory safety profile in 8 patients. Vandetanib was present in the plasma of all patients 12 days post-TACE, and present in resected liver tissue up to 32 days post-treatment. There were no significant changes in perfusion parameters. Blood biomarker studies showed increases in leptin, osteopontin and sTie2. SBRT offered 1-year local control rates of 94% in small HCCs and 92% in larger tumours. Radiopaque beads were visible on 4D-CT and CBCT images in all 8 cases and matching successfully performed.

Conclusions

The safety profile and pharmacokinetic characteristics for this novel technology are adequate to proceed to a Phase I/II trial. SBRT is an effective local treatment for HCC. The role of radiopaque beads as fiducial markers is feasible and warrants further exploration as a clinical trial of TACE with SBRT.

IMPACT STATEMENT

In order to improve clinical outcomes for patients with unresectable liver cancers, local directed therapies need to be optimised. Transarterial chemoembolisation (TACE) is the commonest procedure performed worldwide to treat primary liver cancer. Despite recent advances, including the development of drug-eluting bead (DEB) -TACE, tumour progression occurs in the majority. Given these high recurrence rates, new anti-cancer drugs that can be delivered directly to the tumour on pre-loaded beads are required. As TACE enhances the production of anti-angiogenic factors such as VEGF, combining TACE with anti-angiogenic agents may provide a mechanism for improving outcomes. Furthermore, the combination of TACE with stereotactic body radiotherapy (SBRT) may further improve clinical outcomes for patients with unresectable liver cancers.

This project comprises the first clinical trial to load a targeted anti-angiogenic agent onto radiopaque DEBs and study bead distribution on imaging and in tissue, the toxicity profile and the pharmacokinetic characteristics in patients with primary and secondary liver tumours. This study also demonstrates that the novel vandetanib-eluting radiopaque bead (BTG-002814) has an acceptable safety profile and is feasible to deliver to patients with hepatocellular carcinoma (HCC) and liver-limited metastases from colorectal cancer (mCRC). It shows that minimal vandetanib enters the systemic circulation and demonstrates sustained release from the loaded beads with levels of vandetanib being present in resected liver tissue up to 32 days post-TACE. The radiopaque beads are also used to quantify anatomical distribution following treatment. As such, the location of radiopaque beads is correlated with surgical resection specimens, allowing highly accurate quantification of on-target and off-target bead delivery.

This is the first study to report such a correlation in patients with liver cancer. Despite the relatively low proportion of beads within the tumour, this study reports evidence of anti-tumour efficacy demonstrating the need to load effective anticancer drugs onto TACE beads. This represents the first of a new targeted class of liver-directed agents being available to treat patients with HCC and mCRC. The ability to safely deliver vandetanib locally *via* TACE is an exciting

new development in the field and this data suggest that it warrants further exploration in future phase I-II trials.

This project also explores the role of SBRT in the treatment of small (≤5 cm) and large (>5 cm) HCC tumours. These two clinical studies are important contributions to the current evidence base, by demonstrating that SBRT is well-tolerated and offers excellent local control for patients not suitable, or refractory, to other liver-directed therapies, including TACE.

The final part of this project is the first systematic study in phantoms and in cancer patients to demonstrate the feasibility of using radiopaque TACE beads as fiducial markers for liver SBRT. This is an important contribution to the literature. As SBRT has been shown to be an effective local treatment for HCC, and as the role of radiopaque beads as fiducial markers is feasible, further exploration in combination studies of TACE followed by SBRT for liver tumours is warranted and holds the promise of improved clinical outcomes for these patients.

TABLE OF CONTENTS **Page**

Appendices

LIST OF TABLES **Page**

2. VEROnA clinical trial: Study design and safety of BTG-002814

3. Pharmacokinetics of BTG-002814 in the VEROnA trial

4. Histopathological and cytokine response following treatment with BTG-002814

5. Perfusion Imaging of Primary and Secondary Liver Tumours

6. Stereotactic body radiotherapy for hepatocellular carcinoma

7. Radiopaque beads as fiducial markers for liver stereotactic radiotherapy

LIST OF FIGURES **Page**

5. Perfusion Imaging of Primary and Secondary Liver Tumours

6. Stereotactic body radiotherapy for hepatocellular carcinoma

7. Radiopaque beads as fiducial markers for liver stereotactic radiotherapy

1 INTRODUCTION AND OVERVIEW OF THESIS

1.1 DISEASE BACKGROUND

1.1.1 Hepatocellular carcinoma

Primary liver cancer, of which hepatocellular carcinoma (HCC) comprises 75-85% of cases, is the sixth most common cancer and the fourth leading cause of cancer related death worldwide. Of the 841,080 new cases diagnosed globally in 2018, 66% were from Eastern and South Eastern Asia, a rate attributed to the high endemicity of chronic hepatitis B (HBV) and increasing rates of hepatitis C (HCV) infection in this region [1]. Comparatively, the incidence of liver cancer in Europe and North America is lower. However, over the last decade there has been a significant increase in the number of cases recorded likely due to the increasing prevalence of lifestyle risk factors such as obesity, smoking and alcoholic liver disease [2, 3].

Overall, HCC has a poor prognosis. The development of surveillance programs in high-risk patient groups enables the detection of early-stage tumours that may be amenable to curative therapies [4, 5]. These include surgical resection and orthotopic liver transplant, with the latter providing a long-term survival of up to 70-85% at four years [6]. For small tumours, typically <3 cm, radiofrequency ablation (RFA) and percutaneous ethanol injection (PEI) have also been used as curative options [4, 5]. However, at diagnosis, fewer than 30% of patients are suitable for curative treatment. This is due to poor baseline liver function, underlying co-morbidities, vascular invasion, or large tumour burden, with over a third of patients presenting with tumours >5 cm [7-9].

The classification of HCC is based on the Barcelona Clinic Liver Cancer (BCLC) staging classification. This staging system defines five subclasses, based on prognostic variables related to tumour size, liver function and underlying performance status (Figure 1) [4]. The BCLC algorithm provides a treatment algorithm for each subclass.

Current international guidelines from the American Association for the Study of Liver Disease (AASLD) and the European Association for the Study of the Liver (EASL) recommend transarterial chemoembolisation (TACE) as the standard of care for patients with limited unresectable disease in the absence of vascular invasion and extrahepatic spread (Barcelona Clinic Liver Cancer (BCLC), intermediate-stage disease) [4, 9]. It has been shown to provide a survival advantage when compared to best supportive care in both randomised controlled trials and meta-analyses [10-13]. However, TACE is not considered curative and, although the procedure can be repeated several times, tumours ultimately become resistant to treatment. In patients who progress, or for those unsuitable for TACE, systemic therapy is often the only remining therapeutic option [11, 14, 15].

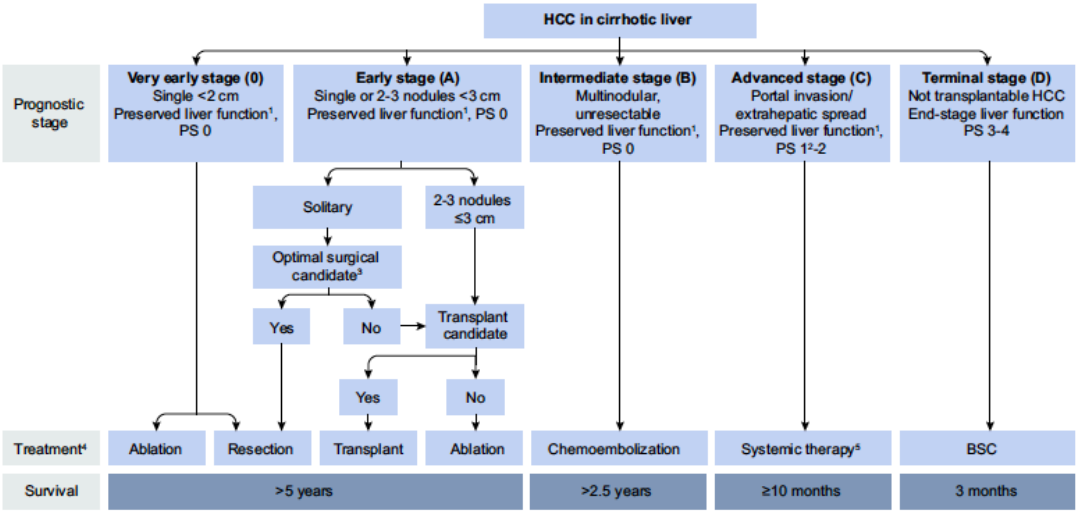

Figure 1: Modified BCLC staging system and treatment strategy [4].
Abbreviations: HCC, hepatocellular carcinoma; PS, performance status; BSC, best supportive care

In the setting of advanced disease, HCC is generally refractory to conventional chemotherapy with objective response rates less than 10% [16]. As such, we have had to advance our knowledge of the genetic alterations and signalling pathways involved in hepatocarcinogenesis, in order to identify novel key targets. In HCC, a number of key pathways have already been identified, including various growth factors such as epidermal growth factor (EGF), vascular endothelial growth receptor (VEGF), hepatocyte growth factor (HGF), insulin-like growth factor and regulating specific intracellular pathways such as

RAF/MEK/ERK and PI3K/PTEN/Akt/mTOR and Wnt/B-catenin pathways [17, 18].

Sorafenib, a multi-kinase inhibitor, has been shown to prolong median overall survival (OS) in patients with advanced HCC from 7.9 to 10.7 months (the SHARP trial), provided there is preserved liver function [Child-Pugh (CP) A] [19-21]. As a result, sorafenib is the standard of care in many countries. However, in the REFLECT trial, an open label, phase 3, multicentre, non-inferiority trial of 1492 patients with unresectable HCC (BCLC stage B or C, CP A and PS 0 – 1), lenvatinib was shown to be non-inferior to sorafenib with a median OS of 13.6 months (95% CI, 12.1–14.9). As such, some countries have now approved the use of lenvatinib in the first-line setting [22]. Furthermore, the IMbrave150 trial has recently shown a promising role for the combination of bevacizumab (a monoclonal antibody that targets VEGF) with atezolizumab, a PD-L1 inhibitor. In this phase 3 randomised controlled trial atezolizumab combined with bevacizumab resulted in better overall and progression-free survival (PFS) outcomes than sorafenib. Overall survival at 12 months was 67.2% (95% CI, 61.3 to 73.1) with atezolizumab–bevacizumab and 54.6% (95% CI, 45.2 to 64.0) with sorafenib, whilst median PFS was 6.8 months (95% CI, 5.7 to 8.3) vs 4.3 months (95% CI, 4.0 to 5.6) in the respective groups [23]. As such, this combination is now licensed for use in the UK. Other systemic therapies that have been explored in the first-line setting include brivanib (a fibroblast growth factor receptor and VEGFR inhibitor), sunitinib (a KIT, VEGR and PDGFR inhibitor), linifanib (a VEGFR and PDGFR inhibitor), and erlotinib (an EGFR inhibitor) [24].

There is therefore a clinical need to improve current treatment options for patients with HCC. Stereotactic body radiotherapy (SBRT) has recently emerged as a feasible and safe treatment option for patients with HCC ineligible for other local treatments, with local control (LC) rates of 70-100% [25-35]. Furthermore, selective internal radiotherapy (SIRT) with yttrium-90 (Y^{90}) has been recently proposed as an alternative treatment option for patients with locally-advanced HCC, with cohort studies reporting objective response rates ranging from 35-50% [35, 36]. However, recent studies have failed to demonstrate a significant OS benefit from SIRT [38, 39].

In order to improve treatment outcomes for patients with HCC, focus needs to be placed on the discovery of new targeted therapies, and their use in combination with locally targeted therapies.

1.1.2 Liver metastases from colorectal cancer

Secondary liver tumours (metastatic to the liver from a primary site outside the liver) are the most common form of hepatic malignancies and are even more common than HCC [40]. The most common sites of primary tumours which spread to the liver are colorectal cancer (CRC), breast cancer and lung cancer.

Worldwide, CRC is the third most commonly occurring cancer in men and the second most commonly occurring cancer in women [41]. Around 25% of patients present with metastatic CRC (mCRC), and approximately 35-55% of CRC patients will develop liver metastases at some point during the course of their disease. Surgical resection is the treatment of choice, offering a potentially curative therapy; retrospective studies show favourable 5-year survival rates of 25% to 47% in patients treated with surgical resection for mCRC [42]. However, only 15%-20% of patients that develop mCRC will be resectable at presentation due to presence of multifocal tumours, limited hepatic reserve or underlying co-morbidities [43, 44].

In patients unsuitable for surgical resection, alternative liver-directed therapies offer the potential of disease control. For patients with oligometastatic disease, characterised by the existence of metastases at up to two, or three sites (generally less than five lesions) the European Society for Medical Oncology (ESMO) suggest there is now a ‘toolbox’ of loco-regional therapies that can be considered [45]. These include TACE, SIRT, RFA and SBRT, either alone or in combination with systemic chemotherapy [45, 46].

With regards to systemic therapy for mCRC, there have already been a number of advancements in the development of novel targeted therapies. Biological agents including bevacizumab, a humanised monoclonal antibody that targets vascular endothelial growth factor (VEGF), a central regulator of angiogenesis, and cetuximab/panitumumab, monoclonal antibodies directed against endothelial growth factor receptors (EGFR), have been shown to improve the clinical

outcome of patients with mCRC [47-49].

1.2 TRANSARTERIAL CHEMOEMBOLISATION (TACE)

1.2.1 TAE and cTACE

In 1977, Yamada *et al* developed a technique called transarterial embolisation (TAE), a minimally invasive procedure that aimed to restrict the vascular supply to liver tumours. By working on the understanding that liver has a dual vascular supply, from the hepatic artery and portal vein, and that liver tumours are vascularised by the hepatic artery, by blocking this supply it blocks the tumour's main nutrient source resulting in ischaemic necrosis. As the liver parenchyma is supplied by the portal vein, liver function is maintained [50, 51]. Over time, conventional TACE (cTACE) was developed, whereby a chemotherapeutic drug is introduced into arteries feeding the tumour, followed by an embolic agent. The most common anticancer cytotoxic drugs for local delivery via TACE are doxorubicin, cisplatin, epirubicin, mitoxantrone and mitomycin C.

In 2002, two groups reported a survival benefit of TACE compared to best supportive care (BSC) in patients with locally advanced HCC [11, 12]. Llovet *et al* used doxorubicin-based TACE, whilst Lo *et a*l compared cisplatin-based TACE to BSC. These trials were included in a subsequent meta-analysis of seven trials including 545 patients, which concluded that TACE was associated with a significant 2-year survival benefit over BSC [10]. As a result, TACE is the standard of care for patients with intermediate-stage HCC.

1.2.2. Drug-eluting bead TACE

Although cTACE enables the delivery of anti-cancer drugs directly into the tumour, the systemic release of the cytotoxic was found to cause systemic side effects. As such, an alternative method of local drug delivery was sought. This led to the innovative idea of combining a cytotoxic drug with microspheres, to create drug-eluting bead TACE (DEB-TACE). The DEBs, DC Beads™ (BTG, United Kingdom) are non-biodegradable poly-vinyl alcohol microspheres, that can be loaded with calibrated cytotoxic drugs. Embolic microspheres have the ability to sequester chemotherapeutic agents and release them in a controlled mode over a one-week period [4].

TACE using DEBs loaded with doxorubicin (DEBDOX) has been extensively used in patients with HCC [52, 53]. Studies have shown that the drug-eluting microspheres (DC Bead™) achieve higher intra-tumoural concentrations and lower systemic concentrations of cytotoxic drugs than cTACE, thereby reducing the potential liver toxicity of treatment and systemic side effects [54,55]. A randomised phase II study comparing the short-term outcomes of DEB-TACE and cTACE indicated some advantages of DEB-TACE in terms of toxicity and radiological tumour response, particularly in advanced disease [53].

There is also increasing evidence to support the used of DEB-TACE in patients with mCRC. In this case, DEBs loaded with irinotecan are typically used (DEBIRI) [56]. TACE has been shown to be an effective treatment option for these patients, potentially offering an improvement in quality of life and OS. A systemic review of 13 studies, comprising 850 patients with mCRC treated using DEBIRI, demonstrated an average response rate of 56.2% by RECIST (Response Evaluation Criteria in Solid Tumours) and 51.2% by modified RECIST/EASL response criteria. The average OS was 16 months [57]. The improvement in quality in life is mainly related to the reduced systemic side effects of the chemotherapy drug [58, 59]. DEB-TACE is therefore a palliative locoregional treatment option that can be considered for mCRC patients with unresectable liver metastases [45].

1.2.3 TACE vs bland embolisation

To date, there has been no prospective trial that has demonstrated the superiority of TACE compared with bland embolisation (TAE). Furthermore, meta-analyses from 2002, 2007 and 2014 all concluded that the OS was statistically similar between the two groups [13, 60, 61]. A randomised phase II trial used cisplatin-based TACE compared with TAE using polyvinyl alcohol (PVA) particles alone and again found no difference in survival. However, this study did find a higher response rate with cisplatin-based TACE compared to TAE [62]. More recently, a randomised trial of 101 patients did not find differences between TACE and TAE in terms of tumour response, progression-free survival (PFS) and OS [63]. However, as TACE is the only approach that has demonstrated a survival

advantage when compared to BSC, it remains the standard of care, with few institutions performing TAE only [4].

Although TACE can be repeated several times, it is not a curative treatment option and recurrence occurs in the majority of patients [14]. The 5-year survival rate post-TACE is poor at <20% [10]. As such, there is a clinical need to improve outcomes following TACE in patients with both primary and secondary liver tumours. This involves improving the technical delivery of DEBs to the tumour, in addition to exploring new, more effective, targeted anticancer drugs that can be delivered directly to the tumour. As tumour hypoxia induced by embolisation therapy leads to upregulation of pro-angiogenic pathways, interest has grown into the possibility of loading newer small-molecule targeted therapeutic agents on to DEBs, that are designed to block cell proliferation and angiogenesis [64, 65].

1.3 VANDETANIB-ELUTING RADIOPAQUE BEADS

1.3.1 Radiopaque beads

One of the proposed reasons for the failure of TACE is not being able to assess the final location of tumour embolisation. As such, there is a need to improve the accuracy of delivery of the embolic agent, and furthermore a method of establishing whether or not the embolisation procedure has been successful. The recent development of a radiopaque (RO) bead, which can be visualised with computed tomography (CT) and fluoroscopic imaging [66], has the advantage of providing intra- and post-procedural confirmation of bead location, enabling real-time adjustments to optimise patient treatment and evaluation of the completeness of tumour treatment [67].

The RO bead is a permanent implant. The beads are formed from a sulphonate modified PVA polymer containing a radiopaque moiety derived from triiodobenzyl aldehyde (2,3,5-trioodobenzaldehyde) that is covalently bonded with the hydrogel structure. The incorporation of this radiopaque moiety into the co-polymer imparts X-ray imageability by rendering the microspheres radiopaque. The beads are formed into microspheres of 60-160 μm diameter.

1.3.2 Vandetanib

It is well established that embolisation of hepatic tumours leads to ischaemia by cutting off the arterial supply, resulting in tumour necrosis. The issue with the creation of an ischaemic and ultimately hypoxic tumour environment is that this can lead to the release of vascular endothelial growth factor (VEGF), a potent stimulator of new blood vessel growth (angiogenesis), which can lead to eventual tumour recurrence [68-70]. One approach is to inhibit the VEGF pathway by combining TACE with an anti-angiogenic agent.

Vandetanib is a potent inhibitor of the tyrosine kinase activity of VEGFR-2, an endothelial cell receptor for VEGF. It also possesses activity against EGFR and REarranged during Transfection (RET) tyrosine kinases. By targeting both angiogenesis and EGFR- and RET-dependent tumour cell growth, it is hypothesised that the growth of tumours will be controlled, with relative sparing of normal tissues [71]. Vandetanib, in its oral form, has been shown to significantly prolong PFS of patients with advanced medullary thyroid cancer [72]. It has also been assessed as a second line treatment option for patients with advanced non-small-cell lung cancer (NSCLC) and was found not to be inferior to erlotinib, an EGFR inhibitor [73]. Vandetanib combined with docetaxel has also been reported to significantly prolong PFS, compared with docetaxel alone, in patients with advanced NSCLC who have progressed after first-line chemotherapy [74].

To date, there has been only one trial that has assessed the efficacy of oral vandetanib in HCC patients. This study, by Hsu *et* al, involved randomising 67 HCC patients to oral vandetanib 300 mg (n=19), oral vandetanib 100 mg (n=25) or placebo (n=23). Twenty-nine patients subsequently entered open-label treatment. In both vandetanib treatment arms, tumour stabilisation rate was not significantly different from placebo. Although trends towards improved PFS and OS after vandetanib treatment were found, they were not statistically significant. The most common adverse events were diarrhoea and rash in both treatment groups [75].

In patients with mCRC, several phase I dose escalation studies have been conducted to determine the maximum tolerated dose (MTD) of oral vandetanib in

combination with different therapeutic agents and regimens. Combinations that have so far been investigated include combining vandetanib with FOLFIRI [76], cetuximab and irinotecan [77], FOLFOX [78] and capecitabine plus oxaliplatin [79]. Bevacizumab, however, was not well tolerated with vandetanib and XELOX in combination [79].

Although these studies have reported expected and manageable toxicity profiles, the observed efficacy rates have raised concern for moving forward with these combinations of systemic agents. The rationale in this project is to therefore consider delivery of vandetanib directly into the liver via TACE.

1.3.3 Vandetanib-eluting radiopaque beads

BTG-002814 (vandetanib-eluting radiopaque bead) is an investigational medicinal product intended for the treatment of hypervascular tumours such as HCC and liver metastases from CRC. The drug vandetanib is bound reversibly to the beads and is able to elute in situ into the liver tumour following targeted delivery [64]. Elution in situ is aimed to reduce the systemic concentration of the drug in plasma and increase the local concentration of vandetanib at the site of the delivery. BTG-002814 is precisely calibrated in size (60-160 μm) and spherical in design, which increases the surface area of the bead exposed to the surrounding liver tissue when compared to larger drug-eluting products.

1.3.4 Pre-clinical trials of vandetanib-eluting radiopaque beads

The safety of the vandetanib-eluting bead has already been evaluated in a GLP swine liver embolisation model. In this model, vandetanib-loaded radiopaque beads (100 mg vandetanib per 1 ml bead) were delivered to healthy liver by hepatic intra-arterial administration. Up to 1 ml of vandetanib-loaded bead was administered, equating to the delivery of 100 mg vandetanib to the targeted liver lobe. The animals were maintained for either 30 or 90 days, and there were no treatment-related effects evident. Transient changes in coagulation and clinical chemistry parameters were observed, likely to be related to the hepatic embolisation procedure. There were expected microscopic findings associated with hepatic embolisation following intrahepatic administration of vandetanib-loaded bead. The study indicated that intrahepatic administration of up to 1 ml vandetanib-loaded radiopaque bead containing 100 mg of vandetanib was well

tolerated and did not produce any systemic toxicity [65]. The next step is to therefore assess the feasibility of delivering vandetanib-eluting radiopaque beads in humans.

1.4 PERFUSION IMAGING IN ASSESSING TUMOUR RESPONSE

Tumour response to treatment has historically been classified on imaging according to Response Evaluation Criteria in Solid Tumour (RECIST). This is based on the anatomic unidimensional assessment of tumour burden as assessed by CT imaging, although criteria have now been updated to include the use of FDG-PET as an adjunct to determination of progression [80, 81]. Objective response by size criteria is therefore a common method of response that is assessed in clinical trials. However, RECIST guidelines were initially designed to evaluate the response to cytotoxic drugs and do not take into account measures of anti-tumour activity other than size [81]. This limitation in the assessment of response by RECIST has already been recognised in the case of HCC, with recent studies showing a poor correlation between the clinical benefit of novel agents and liver directed therapies with conventional methods of response [19, 82, 83]. This has led to the development of the modified RECIST (mRECIST) criteria for the assessment of HCC, which takes into account tumour necrosis induced by treatment and measures only the viable portion of the target lesion [83].

Despite improvements in CT and MR imaging, treatment with novel molecularly targeted therapies may induce changes in the tumour and surrounding vasculature that are not fully appreciated or quantified by such methods of imaging. Studies have therefore started to explore novel imaging techniques in order to identify imaging biomarkers that can predict response to treatment. This is particularly important in the assessment of response to anti-angiogenic drugs which are known to induce vascular changes.

Functional imaging techniques, such as dynamic contrast-enhanced MRI (DCE-MRI) and multi-detector row perfusion CT (pCT), allow a non-invasive approach of imaging changes in vasculature and offer a novel method of assessing response to treatments that impact on tumour vasculature. DCE-MRI and pCT

imaging techniques have already been utilised in a number of clinical trials to assess tumour vascularity and changes in blood flow, following both TACE and anti-angiogenic therapy [75, 84-91].

1.5 STEREOTACTIC BODY RADIOTHERAPY (SBRT)

1.5.1 Overview of SBRT

Traditionally external beam radiation treatments are fractionated into daily doses of 1.8–2.0 Gy to maximise the therapeutic ratio between the dose to the tumour and dose to normal tissue. Stereotactic body radiotherapy (SBRT) is an emerging novel radiation technique that enables the delivery of high dose, highly focussed external beam radiotherapy in a small number of fractions (usually 1-5) [92, 93]. The doses delivered in SBRT are therefore 'ablative' and, accordingly, the safe delivery of such large doses per fraction necessitates effective patient immobilisation, precise target localisation, accurate treatment delivery and daily image guidance to allow very steep isodose gradients between target volumes and surrounding normal tissues [92, 94].

The excellent results achieved with ablative doses suggest that the anti-tumour effects of SBRT are different to those induced by conventional fractionation. Endothelial cell damage, enhanced anti-tumour immunity and a lack of time for reoxygenation and repopulation are possible underlying mechanisms for the increased efficacy of SBRT [95].

Although initially utilised for the radical treatment of lung tumours, SBRT has recently been shown to have benefit in the treatment of oligometastases. The oligometastatic paradigm implies that patients who develop a small number of metastatic lesions might achieve long-term survival if all these lesions are ablated with surgery or SBRT [96]. Until recently, most of the evidence supporting this paradigm was from observational studies. However, the results from the COMET-SABR trial, a randomised phase II trial of 99 patients with oligometastatic disease randomised to palliative standard of care alone (control group), or standard of care plus SBRT to all metastatic lesions (SBRT group), has shown that SBRT is associated with an improvement in survival. In this trial, median OS was longer with SBRT than with no ablative treatment, 41 months versus 28 months

(HR 0.57, 95% CI 0.30–1.10; $p = 0.09$), as was median PFS, 12.0 months versus 6.0 months (HR 0.47, 95% CI 0.30–0.76; $p = 0.0012$) [97]. As such, the number of patients with oligometastatic disease receiving treatment with SBRT is increasing rapidly.

1.5.2 Liver SBRT

Historically, radiotherapy to the liver was not regarded as a safe or effective treatment option due to high rates of radiation-induced liver disease (RILD) [98]. Recent advances in both technology, and in the biological understanding of liver radiation tolerances, has led to the development of more conformal radiotherapy techniques allowing for partial liver irradiation, significantly reducing the risk of RILD. SBRT offers the additional advantage of potentially delivering higher effective tumour doses due to sharper dose gradients around the tumour. SBRT to the liver is therefore becoming increasingly used as a local ablative therapy in the treatment of primary liver cancers, in addition to the treatment of liver metastases from CRC.

A number of studies have now shown that SBRT is a feasible and safe treatment option for patients with HCC ineligible for other local treatments [25-35], with reported outcomes similar to those of RFA in small HCC tumours. In a study of 224 patients with inoperable HCC, one- and two-year freedom from local progression (FFLP) for tumours treated with RFA were 83.6% and 80.2% versus 97.4% and 83.8% for SBRT. For tumours ≥ 2 cm there was decreased FFLP for RFA compared with SBRT suggesting that for HCC ≥ 2 cm, SBRT may even offer superior LC when compared with RFA [35]. Furthermore, SBRT can also be used as a bridge to transplant [99-102], as well as having a role in combination with, or as an alternative to, other treatment modalities [30, 103-107]. As a result, the 2018 National Comprehensive Cancer Network (NCCN) guidelines now recommend that SBRT can be used as an alternative to RFA/TACE in inoperable HCC [108].

Although surgery remains the preferred option for isolated, operable liver metastases, for those not suitable for resection, RFA and SBRT are both widely used focal liver therapies, as both have prospectively been shown to provide good LC, with reported local recurrence rates < 20% [109-111]. A recent systemic

review of 656 patients showed that local therapy with SBRT resulted in long term LC in relapsing or progressing patients with oligometastatic CRC liver metastases (1- and 2-year LC rates of 67% and 59%) with similar one- and two-year OS (67 and 56%). Median OS and PFS were 31 and 11 months [112].

A recent study of 161 patients with 282 pathologically diagnosed unresectable liver metastases showed that treatment with SBRT or RFA was well tolerated and provided excellent and similar LC for intrahepatic metastases <2 cm in size. The 2-year FFLP was 88.2% compared with 73.9%, favouring SBRT (p=0.06). The 2-year OS rate was 51.1%, with no difference between groups. For tumours ≥2 cm in size treatment with SBRT was associated with improved FFLP [113].

Although the role of SBRT in the treatment of both primary and metastatic liver cancers is starting to change, historically SBRT has only been used when other local treatments are no longer an option. As a result, patients frequently considered for SBRT have often been heavily pre-treated with other local therapies, including TACE. Recent studies have shown that SBRT can be used safely in both the adjuvant setting, and as a salvage treatment post-TACE [30, 105, 114]. Given that TACE remains a palliative procedure, and with increasingly good outcomes with SBRT, there is now a rationale to investigate the feasibility of combining TACE with SBRT.

1.6 SUMMARY

In summary, there is a clear need to improve treatment outcomes for patients with inoperable primary and secondary liver cancers. Although TACE is the current standard of care for inoperable HCC, it is not curative and treatment needs to be improved. SBRT offers excellent LC rates for HCC tumours, and can also be used safely in both the adjuvant setting, and as a salvage treatment post TACE failure. Combination approaches of TACE with SBRT therefore need to be considered.

1.7 THESIS OBJECTIVES

The objectives of this project were to assess a novel drug-eluting bead for TACE, to report on the safety and efficacy and SBRT in HCC and to assess the feasibility of using radiopaque beads as fiducial markers for SBRT.

The first part of this thesis focuses on a novel DEB-TACE treatment developed for HCC and mCRC. The VEROnA study explores the feasibility of administering a vandetanib-eluting radiopaque embolisation bead (BTG-022814). It is the first time that BTG-002814 has been administered to humans. The primary objectives of the VEROnA study were to evaluate the safety and tolerability of vandetanib-eluting radiopaque embolic beads (BTG-002814) in patients with resectable liver malignancies, and to determine concentrations of vandetanib and the N-desmethyl metabolite in plasma and resected liver following treatment with BTG-002814. The novel design of this phase 0 study provides a unique 'window-of-opportunity' in which a number of exploratory circulating biomarkers can be measured prior to and following treatment, with the aim of identify biomarkers that may indicate response to treatment or provide a potential explanation for resistance. Furthermore, the trial design incorporates a number of novel imaging techniques that can be used to identify imaging biomarkers.

The second part of this project focuses on the role of SBRT for primary HCC. The efficacy of SBRT for HCC is first explored in a retrospective study of 31 patients with tumours ≤5 cm diameter. The safety and efficacy of SBRT in patients with large unresectable HCCs (>5 cm) who were not eligible for, or who had failed, previous liver-directed therapies (LDTs) is then explored in a phase II clinical study of 13 patients.

The final part of this thesis explores the potential for future clinical trials of combining TACE with liver SBRT. As vandetanib-eluting radiopaque embolic beads are visible on CT imaging, I explore the possibility of using the radiopaque beads as fiducial markers for liver stereotactic body radiotherapy (SBRT).

1.6.1 Specific aims of this research project:

1. To assess the safety and tolerability of radiopaque vandetanib-eluting chemo-embolisation beads, BTG-002814 (Chapter 2)

2. To measure concentrations of vandetanib and N-desmethyl metabolite in plasma and resected tissue following treatment with BTG-002814 (Chapter 3)

3. To study exploratory blood biomarkers with the potential to identify patients likely to respond to BTG-002814 (Chapter 4)

4. To assess changes in blood flow on perfusion CT and dynamic contrast-enhanced MRI imaging following treatment with BTG-002814 (Chapter 5)

5. To report on the clinical outcomes and toxicities of patients with small (≤5 cm) and large (>5 cm) HCC treated with SBRT (Chapter 6)

6. To assess whether radiopaque beads can function as fiducial markers for liver SBRT (Chapter 7)

1.8 REFERENCES

[1] Bray F, Ferlay J, Soerjomataram I, Siegel RL, Torre LA, Jemal A. Global cancer statistics 2018: GLOBOCAN estimates of incidence and mortality worldwide for 36 cancers in 185 countries. CA Cancer J Clin. 2018;68:394-424.

[2] Sanyal AJ, Yoon SK, Lencioni R. The etiology of hepatocellular carcinoma and consequences for treatment. Oncologist. 2010;15 Suppl 4:14-22.

[3] Knudsen ES, Gopal P, Singal AG. The changing landscape of hepatocellular carcinoma: etiology, genetics, and therapy. Am J Pathol. 2014;184:574-83.

[4] EASL Clinical Practice Guidelines: Management of hepatocellular carcinoma. Journal of hepatology. 2018;69:182-236.

[5] Forner A, Llovet JM, Bruix J. Hepatocellular carcinoma. The Lancet. 2012;379:1245-55.

[6] Mazzaferro V, Regalia E, Doci R, Andreola S, Pulvirenti A, Bozzetti F, et al. Liver transplantation for the treatment of small hepatocellular carcinomas in patients with cirrhosis. The New England journal of medicine. 1996;334:693-9.

[7] Tsoulfas G, Mekras A, Agorastou P, Kiskinis D. Surgical treatment for large hepatocellular carcinoma: does size matter? ANZ journal of surgery. 2012;82:510-7.

[8] Pawlik TM, Poon RT, Abdalla EK, Zorzi D, Ikai I, Curley SA, et al. Critical appraisal of the clinical and pathologic predictors of survival after resection of large hepatocellular carcinoma. Archives of surgery (Chicago, Ill : 1960). 2005;140:450-7; discussion 7-8.

[9] Bruix J, Sherman M. Management of hepatocellular carcinoma: an update. Hepatology (Baltimore, Md). 2011;53:1020-2.

[10] Llovet JM, Bruix J. Systematic review of randomized trials for unresectable hepatocellular carcinoma: Chemoembolization improves survival. Hepatology (Baltimore, Md). 2003;37:429-42.

[11] Llovet JM, Real MI, Montana X, Planas R, Coll S, Aponte J, et al. Arterial embolisation or chemoembolisation versus symptomatic treatment in patients with unresectable hepatocellular carcinoma: a randomised controlled trial. Lancet (London, England). 2002;359:1734-9.

[12] Lo CM, Ngan H, Tso WK, Liu CL, Lam CM, Poon RT, et al. Randomized controlled trial of transarterial lipiodol chemoembolization for unresectable hepatocellular carcinoma. Hepatology (Baltimore, Md). 2002;35:1164-71.

[13] Camma C, Schepis F, Orlando A, Albanese M, Shahied L, Trevisani F, et al. Transarterial chemoembolization for unresectable hepatocellular carcinoma: meta-analysis of randomized controlled trials. Radiology. 2002;224:47-54.
[14] Park W, Chung YH, Kim JA, Jin YJ, Lee D, Shim JH, et al. Recurrences of hepatocellular carcinoma following complete remission by transarterial chemoembolization or radiofrequency therapy: Focused on the recurrence patterns. Hepatology research : the official journal of the Japan Society of Hepatology. 2013;43:1304-12.
[15] Golfieri R, Renzulli M, Mosconi C, Forlani L, Giampalma E, Piscaglia F, et al. Hepatocellular carcinoma responding to superselective transarterial chemoembolization: an issue of nodule dimension? Journal of vascular and interventional radiology : JVIR. 2013;24:509-17.
[16] Lopez PM, Villanueva A, Llovet JM. Systematic review: evidence-based management of hepatocellular carcinoma--an updated analysis of randomized controlled trials. Alimentary pharmacology & therapeutics. 2006;23:1535-47.
[17] Kudo M. Signaling pathway/molecular targets and new targeted agents under development in hepatocellular carcinoma. World J Gastroenterol. 2012;18:6005-17.
[18] Raza A, Sood GK. Hepatocellular carcinoma review: current treatment, and evidence-based medicine. World J Gastroenterol. 2014;20:4115-27.
[19] Llovet JM, Ricci S, Mazzaferro V, Hilgard P, Gane E, Blanc JF, et al. Sorafenib in advanced hepatocellular carcinoma. The New England journal of medicine. 2008;359:378-90.
[20] Abou-Alfa GK, Schwartz L, Ricci S, Amadori D, Santoro A, Figer A, et al. Phase II study of sorafenib in patients with advanced hepatocellular carcinoma. J Clin Oncol. 2006;24:4293-300.
[21] Cheng A-L, Kang Y-K, Chen Z, Tsao C-J, Qin S, Kim JS, et al. Efficacy and safety of sorafenib in patients in the Asia-Pacific region with advanced hepatocellular carcinoma: a phase III randomised, double-blind, placebo-controlled trial. The Lancet Oncology. 2009;10:25-34.
[22] Kudo M, Finn RS, Qin S, Han KH, Ikeda K, Piscaglia F, et al. Lenvatinib versus sorafenib in first-line treatment of patients with unresectable hepatocellular carcinoma: a randomised phase 3 non-inferiority trial. Lancet (London, England). 2018;391:1163-73.

[23] Finn RS, Qin S, Ikeda M, Galle PR, Ducreux M, Kim TY, et al. Atezolizumab plus Bevacizumab in Unresectable Hepatocellular Carcinoma. The New England journal of medicine. 2020;382:1894-905.
[24] Llovet JM, Zucman-Rossi J, Pikarsky E, Sangro B, Schwartz M, Sherman M, et al. Hepatocellular carcinoma. Nat Rev Dis Primers. 2016;2:16018.
[25] Cardenes HR, Price TR, Perkins SM, Maluccio M, Kwo P, Breen TE, et al. Phase I feasibility trial of stereotactic body radiation therapy for primary hepatocellular carcinoma. Clinical & translational oncology : official publication of the Federation of Spanish Oncology Societies and of the National Cancer Institute of Mexico. 2010;12:218-25.
[26] Yamashita H, Onishi H, Murakami N, Matsumoto Y, Matsuo Y, Nomiya T, et al. Survival outcomes after stereotactic body radiotherapy for 79 Japanese patients with hepatocellular carcinoma. J Radiat Res. 2015;56:561-7.
[27] Huertas A, Baumann AS, Saunier-Kubs F, Salleron J, Oldrini G, Croise-Laurent V, et al. Stereotactic body radiation therapy as an ablative treatment for inoperable hepatocellular carcinoma. Radiother Oncol. 2015;115:211-6.
[28] Tse RV, Hawkins M, Lockwood G, Kim JJ, Cummings B, Knox J, et al. Phase I study of individualized stereotactic body radiotherapy for hepatocellular carcinoma and intrahepatic cholangiocarcinoma. J Clin Oncol. 2008;26:657-64.
[29] Andolino DL, Johnson CS, Maluccio M, Kwo P, Tector AJ, Zook J, et al. Stereotactic Body Radiotherapy for Primary Hepatocellular Carcinoma. International Journal of Radiation Oncology*Biology*Physics. 2011;81:e447-e53.
[30] Kang JK, Kim MS, Cho CK, Yang KM, Yoo HJ, Kim JH, et al. Stereotactic body radiation therapy for inoperable hepatocellular carcinoma as a local salvage treatment after incomplete transarterial chemoembolization. Cancer. 2012;118:5424-31.
[31] Bujold A, Massey CA, Kim JJ, Brierley J, Cho C, Wong RK, et al. Sequential phase I and II trials of stereotactic body radiotherapy for locally advanced hepatocellular carcinoma. J Clin Oncol. 2013;31:1631-9.
[32] Sanuki N, Takeda A, Oku Y, Mizuno T, Aoki Y, Eriguchi T, et al. Stereotactic body radiotherapy for small hepatocellular carcinoma: a retrospective outcome analysis in 185 patients. Acta Oncol. 2014;53:399-404.
[33] Scorsetti M, Comito T, Cozzi L, Clerici E, Tozzi A, Franzese C, et al. The challenge of inoperable hepatocellular carcinoma (HCC): results of a single-

institutional experience on stereotactic body radiation therapy (SBRT). Journal of cancer research and clinical oncology. 2015;141:1301-9.
[34] Lasley FD, Mannina EM, Johnson CS, Perkins SM, Althouse S, Maluccio M, et al. Treatment variables related to liver toxicity in patients with hepatocellular carcinoma, Child-Pugh class A and B enrolled in a phase 1-2 trial of stereotactic body radiation therapy. Pract Radiat Oncol. 2015;5:e443-e9.
[35] Wahl DR, Stenmark MH, Tao Y, Pollom EL, Caoili EM, Lawrence TS, et al. Outcomes After Stereotactic Body Radiotherapy or Radiofrequency Ablation for Hepatocellular Carcinoma. Journal of clinical oncology : official journal of the American Society of Clinical Oncology. 2016;34:452-9.
[36] Hilgard P, Hamami M, Fouly AE, Scherag A, Muller S, Ertle J, et al. Radioembolization with yttrium-90 glass microspheres in hepatocellular carcinoma: European experience on safety and long-term survival. Hepatology (Baltimore, Md). 2010;52:1741-9.
[37] Salem R, Lewandowski RJ, Mulcahy MF, Riaz A, Ryu RK, Ibrahim S, et al. Radioembolization for hepatocellular carcinoma using Yttrium-90 microspheres: a comprehensive report of long-term outcomes. Gastroenterology. 2010;138:52-64.
[38] Chow PKH, Gandhi M, Tan SB, Khin MW, Khasbazar A, Ong J, et al. SIRveNIB: Selective Internal Radiation Therapy Versus Sorafenib in Asia-Pacific Patients With Hepatocellular Carcinoma. J Clin Oncol. 2018;36:1913-21.
[39] Vilgrain V, Pereira H, Assenat E, Guiu B, Ilonca AD, Pageaux G-P, et al. Efficacy and safety of selective internal radiotherapy with yttrium-90 resin microspheres compared with sorafenib in locally advanced and inoperable hepatocellular carcinoma (SARAH): an open-label randomised controlled phase 3 trial. The Lancet Oncology. 2017;18:1624-36.
[40] Lewandowski RJ, Thurston KG, Goin JE, Wong CY, Gates VL, Van Buskirk M, et al. 90Y microsphere (TheraSphere) treatment for unresectable colorectal cancer metastases of the liver: response to treatment at targeted doses of 135-150 Gy as measured by [18F]fluorodeoxyglucose positron emission tomography and computed tomographic imaging. Journal of vascular and interventional radiology : JVIR. 2005;16:1641-51.
[41] Ferlay J, Soerjomataram I, Ervik M, Dikshit R, Eser S, Mathers C, et al. Cancer Incidence and Mortality Worldwide: IARC CancerBase No. 11 GLOBOCAN 2012 v10, Cancer Incidence and Mortality Worldwide: IARC

CancerBase No 11 [Internet] Available at: http://globocaniarcfr Last accessed September 20152013.
[42] Hoyer M, Swaminath A, Bydder S, Lock M, Mendez Romero A, Kavanagh B, et al. Radiotherapy for liver metastases: a review of evidence. International journal of radiation oncology, biology, physics. 2012;82:1047-57.
[43] Adam R, De Gramont A, Figueras J, Guthrie A, Kokudo N, Kunstlinger F, et al. The oncosurgery approach to managing liver metastases from colorectal cancer: a multidisciplinary international consensus. Oncologist. 2012;17:1225-39.
[44] Akgul O, Cetinkaya E, Ersoz S, Tez M. Role of surgery in colorectal cancer liver metastases. World J Gastroenterol. 2014;20:6113-22.
[45] Van Cutsem E, Cervantes A, Adam R, Sobrero A, Van Krieken JH, Aderka D, et al. ESMO consensus guidelines for the management of patients with metastatic colorectal cancer. Ann Oncol. 2016;27:1386-422.
[46] De Groote K, Prenen H. Intrahepatic therapy for liver-dominant metastatic colorectal cancer. World J Gastrointest Oncol. 2015;7:148-52.
[47] Douillard JY, Oliner KS, Siena S, Tabernero J, Burkes R, Barugel M, et al. Panitumumab-FOLFOX4 treatment and RAS mutations in colorectal cancer. The New England journal of medicine. 2013;369:1023-34.
[48] Van Cutsem E, Lenz HJ, Kohne CH, Heinemann V, Tejpar S, Melezinek I, et al. Fluorouracil, leucovorin, and irinotecan plus cetuximab treatment and RAS mutations in colorectal cancer. J Clin Oncol. 2015;33:692-700.
[49] Saltz LB, Clarke S, Diaz-Rubio E, Scheithauer W, Figer A, Wong R, et al. Bevacizumab in combination with oxaliplatin-based chemotherapy as first-line therapy in metastatic colorectal cancer: a randomized phase III study. J Clin Oncol. 2008;26:2013-9.
[50] Duran R, Chapiro J, Schernthaner RE, Geschwind JF. Systematic review of catheter-based intra-arterial therapies in hepatocellular carcinoma: state of the art and future directions. Br J Radiol. 2015;88:20140564.
[51] Tsurusaki M, Murakami T. Surgical and Locoregional Therapy of HCC: TACE. Liver Cancer. 2015;4:165-75.
[52] Lencioni R, Petruzzi P, Crocetti L. Chemoembolization of hepatocellular carcinoma. Semin Intervent Radiol. 2013;30:3-11.
[53] Lammer J, Malagari K, Vogl T, Pilleul F, Denys A, Watkinson A, et al. Prospective randomized study of doxorubicin-eluting-bead embolization in the

treatment of hepatocellular carcinoma: results of the PRECISION V study. Cardiovasc Intervent Radiol. 2010;33:41-52.
[54] Poon RT, Tso WK, Pang RW, Ng KK, Woo R, Tai KS, et al. A phase I/II trial of chemoembolization for hepatocellular carcinoma using a novel intra-arterial drug-eluting bead. Clinical gastroenterology and hepatology : the official clinical practice journal of the American Gastroenterological Association. 2007;5:1100-8.
[55] Varela M, Real MI, Burrel M, Forner A, Sala M, Brunet M, et al. Chemoembolization of hepatocellular carcinoma with drug eluting beads: efficacy and doxorubicin pharmacokinetics. Journal of hepatology. 2007;46:474-81.
[56] Martin RC, Joshi J, Robbins K, Tomalty D, Bosnjakovik P, Derner M, et al. Hepatic intra-arterial injection of drug-eluting bead, irinotecan (DEBIRI) in unresectable colorectal liver metastases refractory to systemic chemotherapy: results of multi-institutional study. Ann Surg Oncol. 2011;18:192-8.
[57] Akinwande O, Dendy M, Ludwig JM, Kim HS. Hepatic intra-arterial injection of irinotecan drug eluting beads (DEBIRI) for patients with unresectable colorectal liver metastases: A systematic review. Surg Oncol. 2017;26:268-75.
[58] Narayanan G, Barbery K, Suthar R, Guerrero G, Arora G. Transarterial chemoembolization using DEBIRI for treatment of hepatic metastases from colorectal cancer. Anticancer research. 2013;33:2077-83.
[59] Fiorentini G, Aliberti C, Turrisi G, Del Conte A, Rossi S, Benea G, et al. Intraarterial hepatic chemoembolization of liver metastases from colorectal cancer adopting irinotecan-eluting beads: results of a phase II clinical study. In vivo (Athens, Greece). 2007;21:1085-91.
[60] Marelli L, Stigliano R, Triantos C, Senzolo M, Cholongitas E, Davies N, et al. Transarterial therapy for hepatocellular carcinoma: which technique is more effective? A systematic review of cohort and randomized studies. Cardiovasc Intervent Radiol. 2007;30:6-25.
[61] Xie ZB, Ma L, Wang XB, Bai T, Ye JZ, Zhong JH, et al. Transarterial embolization with or without chemotherapy for advanced hepatocellular carcinoma: a systematic review. Tumour Biol. 2014;35:8451-9.
[62] Meyer T, Kirkwood A, Roughton M, Beare S, Tsochatzis E, Yu D, et al. A randomised phase II/III trial of 3-weekly cisplatin-based sequential transarterial chemoembolisation vs embolisation alone for hepatocellular carcinoma. Br J Cancer. 2013;108:1252-9.

[63] Brown KT, Do RK, Gonen M, Covey AM, Getrajdman GI, Sofocleous CT, et al. Randomized Trial of Hepatic Artery Embolization for Hepatocellular Carcinoma Using Doxorubicin-Eluting Microspheres Compared With Embolization With Microspheres Alone. J Clin Oncol. 2016;34:2046-53.
[64] Hagan A, Phillips GJ, Macfarlane WM, Lloyd AW, Czuczman P, Lewis AL. Preparation and characterisation of vandetanib-eluting radiopaque beads for locoregional treatment of hepatic malignancies. Eur J Pharm Sci. 2017;101:22-30.
[65] Denys A, Czuczman P, Grey D, Bascal Z, Whomsley R, Kilpatrick H, et al. Vandetanib-eluting Radiopaque Beads: In vivo Pharmacokinetics, Safety and Toxicity Evaluation following Swine Liver Embolization. Theranostics. 2017;7:2164-76.
[66] Lewis AL, Willis SL, Dreher MR, Tang Y, Ashrafi K, Wood BJ, et al. Bench-to-clinic development of imageable drug-eluting embolization beads: finding the balance. Future Oncol. 2018;14:2741-60.
[67] Levy EB, Krishnasamy VP, Lewis AL, Willis S, Macfarlane C, Anderson V, et al. First Human Experience with Directly Image-able Iodinated Embolization Microbeads. Cardiovasc Intervent Radiol. 2016;39:1177-86.
[68] Li X, Feng GS, Zheng CS, Zhuo CK, Liu X. Expression of plasma vascular endothelial growth factor in patients with hepatocellular carcinoma and effect of transcatheter arterial chemoembolization therapy on plasma vascular endothelial growth factor level. World J Gastroenterol. 2004;10:2878-82.
[69] Chao Y, Wu CY, Kuo CY, Wang JP, Luo JC, Kao CH, et al. Cytokines are associated with postembolization fever and survival in hepatocellular carcinoma patients receiving transcatheter arterial chemoembolization. Hepatol Int. 2013;7:883-92.
[70] Ranieri G, Ammendola M, Marech I, Laterza A, Abbate I, Oakley C, et al. Vascular endothelial growth factor and tryptase changes after chemoembolization in hepatocarcinoma patients. World J Gastroenterol. 2015;21:6018-25.
[71] Morabito A, Piccirillo MC, Falasconi F, De Feo G, Del Giudice A, Bryce J, et al. Vandetanib (ZD6474), a dual inhibitor of vascular endothelial growth factor receptor (VEGFR) and epidermal growth factor receptor (EGFR) tyrosine kinases: current status and future directions. Oncologist. 2009;14:378-90.

[72] Wells SA, Jr., Gosnell JE, Gagel RF, Moley J, Pfister D, Sosa JA, et al. Vandetanib for the treatment of patients with locally advanced or metastatic hereditary medullary thyroid cancer. J Clin Oncol. 2010;28:767-72.
[73] Natale RB, Thongprasert S, Greco FA, Thomas M, Tsai CM, Sunpaweravong P, et al. Phase III trial of vandetanib compared with erlotinib in patients with previously treated advanced non-small-cell lung cancer. J Clin Oncol. 2011;29:1059-66.
[74] Herbst RS, Sun Y, Eberhardt WE, Germonpre P, Saijo N, Zhou C, et al. Vandetanib plus docetaxel versus docetaxel as second-line treatment for patients with advanced non-small-cell lung cancer (ZODIAC): a double-blind, randomised, phase 3 trial. The Lancet Oncology. 2010;11:619-26.
[75] Hsu C, Yang TS, Huo TI, Hsieh RK, Yu CW, Hwang WS, et al. Vandetanib in patients with inoperable hepatocellular carcinoma: a phase II, randomized, double-blind, placebo-controlled study. Journal of hepatology. 2012;56:1097-103.
[76] Saunders MP, Wilson R, Peeters M, Smith R, Godwood A, Oliver S, et al. Vandetanib with FOLFIRI in patients with advanced colorectal adenocarcinoma: results from an open-label, multicentre Phase I study. Cancer Chemother Pharmacol. 2009;64:665-72.
[77] Meyerhardt JA, Ancukiewicz M, Abrams TA, Schrag D, Enzinger PC, Chan JA, et al. Phase I study of cetuximab, irinotecan, and vandetanib (ZD6474) as therapy for patients with previously treated metastastic colorectal cancer. PloS one. 2012;7:e38231.
[78] Michael M, Gibbs P, Smith R, Godwood A, Oliver S, Tebbutt N. Open-label phase I trial of vandetanib in combination with mFOLFOX6 in patients with advanced colorectal cancer. Investigational new drugs. 2009;27:253-61.
[79] Cabebe EC, Fisher GA, Sikic BI. A phase I trial of vandetanib combined with capecitabine, oxaliplatin and bevacizumab for the first-line treatment of metastatic colorectal cancer. Investigational new drugs. 2012;30:1082-7.
[80] Therasse P, Arbuck SG, Eisenhauer EA, Wanders J, Kaplan RS, Rubinstein L, et al. New guidelines to evaluate the response to treatment in solid tumors. European Organization for Research and Treatment of Cancer, National Cancer Institute of the United States, National Cancer Institute of Canada. J Natl Cancer Inst. 2000;92:205-16.

[81] Eisenhauer EA, Therasse P, Bogaerts J, Schwartz LH, Sargent D, Ford R, et al. New response evaluation criteria in solid tumours: revised RECIST guideline (version 1.1). European journal of cancer (Oxford, England : 1990). 2009;45:228-47.

[82] Forner A, Ayuso C, Varela M, Rimola J, Hessheimer AJ, de Lope CR, et al. Evaluation of tumor response after locoregional therapies in hepatocellular carcinoma: are response evaluation criteria in solid tumors reliable? Cancer. 2009;115:616-23.

[83] Lencioni R, Llovet JM. Modified RECIST (mRECIST) assessment for hepatocellular carcinoma. Seminars in liver disease. 2010;30:52-60.

[84] Ippolito D, Querques G, Okolicsanyi S, Franzesi CT, Strazzabosco M, Sironi S. Diagnostic value of dynamic contrast-enhanced CT with perfusion imaging in the quantitative assessment of tumor response to sorafenib in patients with advanced hepatocellular carcinoma: A feasibility study. Eur J Radiol. 2017;90:34-41.

[85] Tamandl D, Waneck F, Sieghart W, Unterhumer S, Kolblinger C, Baltzer P, et al. Early response evaluation using CT-perfusion one day after transarterial chemoembolization for HCC predicts treatment response and long-term disease control. Eur J Radiol. 2017;90:73-80.

[86] Ippolito D, Fior D, Bonaffini PA, Capraro C, Leni D, Corso R, et al. Quantitative evaluation of CT-perfusion map as indicator of tumor response to transarterial chemoembolization and radiofrequency ablation in HCC patients. Eur J Radiol. 2014;83:1665-71.

[87] Mross K, Fasol U, Frost A, Benkelmann R, Kuhlmann J, Buchert M, et al. DCE-MRI assessment of the effect of vandetanib on tumor vasculature in patients with advanced colorectal cancer and liver metastases: a randomized phase I study. Journal of angiogenesis research. 2009;1:5.

[88] Wimmer T, Steiner J, Talakic E, Stauber R, Quehenberger F, Portugaller RH, et al. Computed Tomography Perfusion Following Transarterial Chemoembolization of Hepatocellular Carcinoma: A Feasibility Study in the Early Period. J Comput Assist Tomogr. 2017;41:708-12.

[89] Kim DH, Kim SH, Im SA, Han SW, Goo JM, Willmann JK, et al. Intermodality comparison between 3D perfusion CT and 18F-FDG PET/CT imaging for predicting early tumor response in patients with liver metastasis after

chemotherapy: preliminary results of a prospective study. Eur J Radiol. 2012;81:3542-50.
[90] Saito K, Ledsam J, Sugimoto K, Sourbron S, Araki Y, Tokuuye K. DCE-MRI for Early Prediction of Response in Hepatocellular Carcinoma after TACE and Sorafenib Therapy: A Pilot Study. J Belg Soc Radiol. 2018;102:40.
[91] Nakamura Y, Kawaoka T, Higaki T, Fukumoto W, Honda Y, Iida M, et al. Hepatocellular carcinoma treated with sorafenib: Arterial tumor perfusion in dynamic contrast-enhanced CT as early imaging biomarkers for survival. Eur J Radiol. 2018;98:41-9.
[92] Martin A, Gaya A. Stereotactic body radiotherapy: a review. Clin Oncol (R Coll Radiol). 2010;22:157-72.
[93] Guckenberger M, Andratschke N, Alheit H, Holy R, Moustakis C, Nestle U, et al. Definition of stereotactic body radiotherapy: principles and practice for the treatment of stage I non-small cell lung cancer. Strahlenther Onkol. 2014;190:26-33.
[94] Lo SS, Fakiris AJ, Chang EL, Mayr NA, Wang JZ, Papiez L, et al. Stereotactic body radiation therapy: a novel treatment modality. Nat Rev Clin Oncol. 2010;7:44-54.
[95] Brown JM, Carlson DJ, Brenner DJ. The tumor radiobiology of SRS and SBRT: are more than the 5 Rs involved? Int J Radiat Oncol Biol Phys. 2014;88:254-62.
[96] Palma DA, Salama JK, Lo SS, Senan S, Treasure T, Govindan R, et al. The oligometastatic state - separating truth from wishful thinking. Nat Rev Clin Oncol. 2014;11:549-57.
[97] Palma DA, Olson R, Harrow S, Gaede S, Louie AV, Haasbeek C, et al. Stereotactic ablative radiotherapy versus standard of care palliative treatment in patients with oligometastatic cancers (SABR-COMET): a randomised, phase 2, open-label trial. Lancet (London, England). 2019;393:2051-8.
[98] https://clinicaltrials.gov/ct2/show/NCT01730937. Sorafenib Tosylate With or Without Stereotactic Body Radiation Therapy in Treating Patients With Liver Cancer
[99] O'Connor JK, Trotter J, Davis GL, Dempster J, Klintmalm GB, Goldstein RM. Long-term outcomes of stereotactic body radiation therapy in the treatment of hepatocellular cancer as a bridge to transplantation. Liver transplantation : official

publication of the American Association for the Study of Liver Diseases and the International Liver Transplantation Society. 2012;18:949-54.
[100] Moore A, Cohen-Naftaly M, Tobar A, Kundel Y, Benjaminov O, Braun M, et al. Stereotactic body radiation therapy (SBRT) for definitive treatment and as a bridge to liver transplantation in early stage inoperable Hepatocellular carcinoma. Radiation Oncology (London, England). 2017;12:163.
[101] Facciuto ME, Singh MK, Rochon C, Sharma J, Gimenez C, Katta U, et al. Stereotactic body radiation therapy in hepatocellular carcinoma and cirrhosis: evaluation of radiological and pathological response. J Surg Oncol. 2012;105:692-8.
[102] Sapisochin G, Barry A, Doherty M, Fischer S, Goldaracena N, Rosales R, et al. Stereotactic body radiotherapy vs. TACE or RFA as a bridge to transplant in patients with hepatocellular carcinoma. An intention-to-treat analysis. Journal of hepatology. 2017;67:92-9.
[103] Choi BO, Choi IB, Jang HS, Kang YN, Jang JS, Bae SH, et al. Stereotactic body radiation therapy with or without transarterial chemoembolization for patients with primary hepatocellular carcinoma: preliminary analysis. BMC cancer. 2008;8:351.
[104] Meng MB, Cui YL, Lu Y, She B, Chen Y, Guan YS, et al. Transcatheter arterial chemoembolization in combination with radiotherapy for unresectable hepatocellular carcinoma: a systematic review and meta-analysis. Radiother Oncol. 2009;92:184-94.
[105] Paik EK, Kim MS, Jang WI, Seo YS, Cho CK, Yoo HJ, et al. Benefits of stereotactic ablative radiotherapy combined with incomplete transcatheter arterial chemoembolization in hepatocellular carcinoma. Radiation oncology (London, England). 2016;11:22.
[106] Shim SJ, Seong J, Han KH, Chon CY, Suh CO, Lee JT. Local radiotherapy as a complement to incomplete transcatheter arterial chemoembolization in locally advanced hepatocellular carcinoma. Liver Int. 2005;25:1189-96.
[107] Huo YR, Eslick GD. Transcatheter Arterial Chemoembolization Plus Radiotherapy Compared With Chemoembolization Alone for Hepatocellular Carcinoma: A Systematic Review and Meta-analysis. JAMA Oncol. 2015;1:756-65.
[108] Network NCC. Hepatobiliary cancers (version 2.2018). 2018.

[109] Lee MT, Kim JJ, Dinniwell R, Brierley J, Lockwood G, Wong R, et al. Phase I study of individualized stereotactic body radiotherapy of liver metastases. J Clin Oncol. 2009;27:1585-91.
[110] Rusthoven KE, Kavanagh BD, Cardenes H, Stieber VW, Burri SH, Feigenberg SJ, et al. Multi-institutional phase I/II trial of stereotactic body radiation therapy for liver metastases. J Clin Oncol. 2009;27:1572-8.
[111] Scorsetti M, Comito T, Tozzi A, Navarria P, Fogliata A, Clerici E, et al. Final results of a phase II trial for stereotactic body radiation therapy for patients with inoperable liver metastases from colorectal cancer. Journal of cancer research and clinical oncology. 2015;141:543-53.
[112] Petrelli F, Comito T, Barni S, Pancera G, Scorsetti M, Ghidini A, et al. Stereotactic body radiotherapy for colorectal cancer liver metastases: A systematic review. Radiother Oncol. 2018;129:427-34.
[113] Jackson WC, Tao Y, Mendiratta-Lala M, Bazzi L, Wahl DR, Schipper MJ, et al. Comparison of Stereotactic Body Radiation Therapy and Radiofrequency Ablation in the Treatment of Intrahepatic Metastases. Int J Radiat Oncol Biol Phys. 2018;100:950-8.
[114] Jacob R, Turley F, Redden DT, Saddekni S, Aal AK, Keene K, et al. Adjuvant stereotactic body radiotherapy following transarterial chemoembolization in patients with non-resectable hepatocellular carcinoma tumours of >/= 3 cm. HPB (Oxford). 2015;17:140-9.

2 VERONA CLINICAL TRIAL – STUDY DESIGN AND SAFETY OF BTG-002814

2.1 INTRODUCTION

Transarterial chemoembolisation (TACE) is the current standard of care for patients with intermediate-stage hepatocellular carcinoma (HCC) [1, 2] and a treatment option for patients with liver-limited metastatic colorectal cancer (mCRC) [3]. Despite recent advances, including the development of drug eluting bead (DEB)-TACE, tumour progression occurs in the majority [4, 5]. Improving administration techniques and investigating the local delivery of new anti-cancer drugs via TACE are important research approaches to potentially improving clinical outcomes for patients with primary and secondary liver cancers [6, 7].

A current limitation in improving the accuracy of embolic administration during DEB-TACE and in understanding how well the treatment reaches its target is the inability to visualise the beads on imaging following local delivery within the liver. The recent development of a radiopaque (RO) bead, which can be visualised with computed tomography (CT) and fluoroscopic imaging [8], has the advantage of providing intra- and post-procedural confirmation of bead location, enabling real-time adjustments to optimise patient treatment [9]. As TACE enhances the production of anti-angiogenic factors such as VEGF, combining TACE with anti-angiogenic agents may provide a mechanism for improving outcomes. Vandetanib is an inhibitor of the tyrosine kinase activity of vascular endothelial growth factor receptor-2 (VEGFR-2), an endothelial cell receptor for VEGF. It also possesses activity against EGFR and REarranged during Transfection (RET) tyrosine kinases [10].

BTG-002814 is an innovative bead that combines two novel approaches into one new therapy: radiopacity for bead imaging and vandetanib-elution for treatment efficacy. The safety of BTG-002814 has been investigated in a pre-clinical swine study, where the administration of up to 1 ml was well tolerated, did not produce any obvious systemic toxicity and resulted in the expected microscopic findings associated with hepatic embolisation and subsequent healing [7]. Furthermore, an efficacy study conducted in a VX2-rabbit model showed that vandetanib-

loaded beads had superior anti-tumoural activity compared to unloaded beads [11].

We conducted a first-in-human study of BTG-002814 in patients with resectable liver tumours, thereby utilising a window-of-opportunity in clinical practice to measure levels of vandetanib in the resected liver sample as well as assessing the safety and tolerability of BTG-002814.

2.2 METHODS AND MATERIALS

2.2.1 Patient selection

The VEROnA clinical study was a first-in-human, open-label, phase 0, single-arm, window-of-opportunity study to establish the safety of BTG 002814 (Figure 1). Patients were recruited and treated at two centres in London, United Kingdom. Patients were initially identified from regional multi-disciplinary meetings and deemed 'potentially suitable' for the trial if they had resectable HCC or mCRC with low-risk of morbidity, without prior radiofrequency ablation (RFA), TACE or radioembolisation with yttrium Y^{90}. Patients were provisionally screened at the time of first review in the surgical clinic, in order to identify key exclusion criteria. If suitable, patients were provided with a patient information sheet (PIS) and contacted 24-hours later. If the patient was interested in participating in the trial, a specific trial screening visit was arranged. Following written consent, additional screening procedures included full medical, surgical and medication history; complete physical examination; vital signs; WHO performance status (PS); 12 lead electrocardiogram (ECG); clinical laboratory assessments (haematology, chemistry, coagulation, urine pregnancy test). Inclusion and exclusion criteria are outlined in Table 1.

.

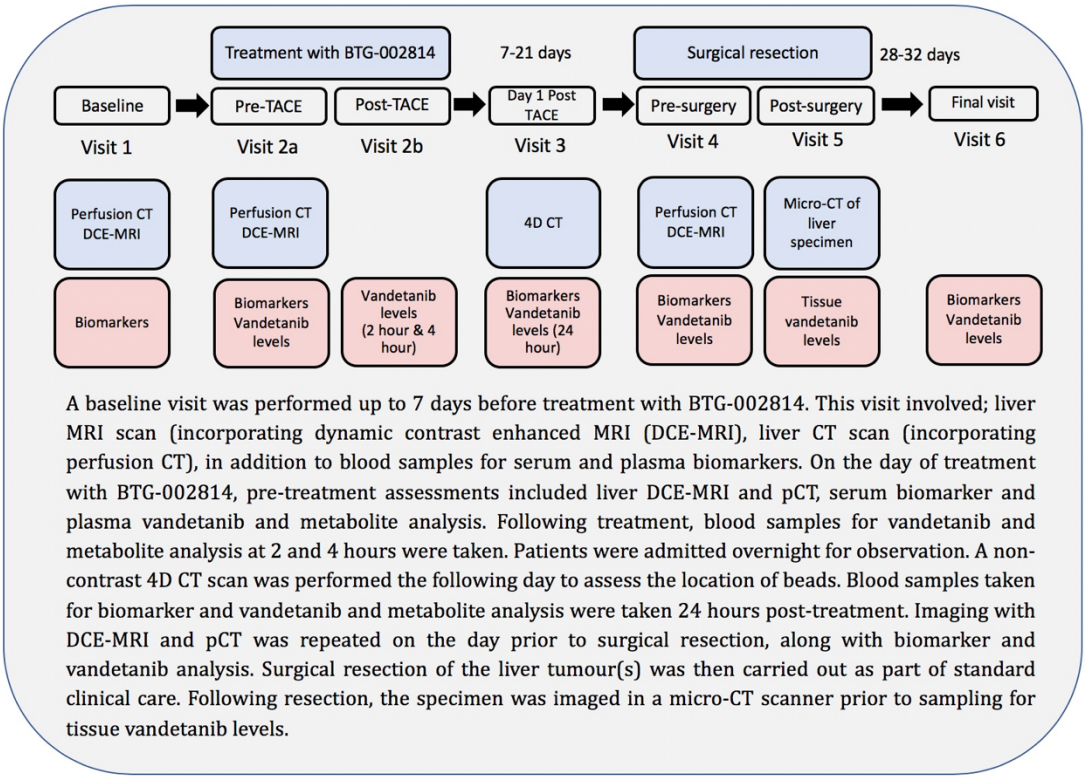

Figure 1: Trial schema for the VEROnA trial

2.2.2 Ethical Considerations

The VEROnA study (NCT03291379) was conducted and documented in accordance with the Declaration of Helsinki and was approved by the Health Research Authority London-Chelsea Research Ethics Service Committee (17/LO/00/11) and the Medicines and Healthcare Products Regulatory Agency (Clinical Trials Authorisation number 2016-004164-19).

Table 1: VEROnA Study: Inclusion/Exclusion criteria

Inclusion criteria	Exclusion criteria
1. Male or female adults (≥ 18 years old)	1. Any systemic chemotherapy within 3 months of the screening visit or any plan to administer systemic chemotherapy prior to surgery
2. Resectable HCC (Child Pugh A, INR ≤1.5) or resectable liver metastases from CRC and a candidate for liver surgery	2. Previous treatment with transarterial embolisation (with or without chemotherapy) of the liver, prior radiotherapy or ablation therapy to the liver or prior yttrium-90 microsphere therapy
3. Low risk for morbidity and mortality from liver surgery	3. Any contraindication to vandetanib according to its local label including: • Hypersensitivity to the active substance • Congenital long QTc syndrome • Patients known to have a QTc interval over 480 milliseconds • Concomitant use of medicinal products known to also prolong the QTc interval and/or induce Torsades de pointes
4. WHO performance status 0- 2	4. Any contraindication to hepatic artery catheterisation or hepatic embolisation procedures
5. Adequate haematological function with Hb >90 g/L, absolute neutrophil count >1.5 x 10^9/L, Plt >75 x 10^9/L	5. Women of child-bearing potential not using effective contraception or women who are breast feeding
6. Adequate liver function with serum bilirubin <1.5 x ULN, ALT (or AST if ALT not available) ≤5 x ULN, ALP <5 x ULN	6. Confirmed allergy to iodine-based intravenous contrast media
7. Adequate renal function with serum creatinine ≤1.5 x ULN and calculated creatinine clearance (GFR) ≥50 mL/min estimated	7. Patients who cannot have CT, MRI or DCE-MRI Imaging (according to site policy)

Inclusion criteria	Exclusion criteria
using a validated creatinine clearance calculation (e.g. Cockcroft-Gault or Wright formula).	
8. Willing to provide blood samples, and tissue samples at surgical resection, for research purposes	8. Active uncontrolled cardiovascular disease
9. Willing & able to provide written informed consent	9. Any co-morbid disease or condition or event that, in the investigator's judgment, would place the patient at undue risk and would preclude the safe use of BTG-002814
	10. Levels of potassium, calcium, magnesium or thyroid stimulating hormone (TSH) outside the normal ranges, and that in the investigator's judgement are clinically significant, or other laboratory findings that in the view of the investigator makes it undesirable for the patient to participate in the study
	11. Participation in another clinical trial with an investigational product within 4 weeks prior to the screening visit

2.2.3 Study Design

Three patients, with either HCC or mCRC, who were candidates for liver surgery were initially enrolled and underwent treatment with BTG-002814. Once these three patients had completed the final follow-up visit scheduled at 4 weeks after surgery (Figure 1), a planned interim analysis was conducted by a safety committee. The recommendation of the committee was to continue the study without any changes to the dose or trial design, as there were no significant unexpected toxicities related to BTG-002814. The target recruitment was 12 patents, six with HCC and six with mCRC. Replacement of up to two patients was permitted if patients did not complete the study investigations and follow-up, taking the maximum total sample size to 14 [12].

This study was funded by Biocompatibles UK Ltd, a BTG International group company and was registered with ClincialTrials.gov, trial number NCT03291379.

2.2.4 Adverse Event Reporting

Safety assessments were performed at each clinical trial visit and included physical examination, vital signs, PS assessment, ECG and clinical laboratory assessments. Toxicities were graded and documented according to the National Cancer Institute (NCI) Common Terminology Criteria for Adverse Events (CTCAE) v 4.0. Any adverse event (AE) since screening was documented and causality to TACE or vandetanib recorded. At the safety review committee, all AEs and serious adverse events (SAEs) were reviewed. ECG QT prolongation is an identified risk associated with vandetanib and was considered an AE of particular interest. As such, it was closely monitored following treatment with BTG-002814.

2.2.5 Study Procedures

Following screening and written consent, all eligible patients were treated with 1 ml of BTG-002814, delivered transarterially, 7 to 21 days before surgical resection of the liver. All TACE procedures were performed by interventional radiologists: Dr Julian Hague, Dr Graham Munneke and Dr Jowad Raja.

One vial of BTG-002814, containing 100 mg vandetanib, was used for each patient. To hydrate BTG 002814, 1 ml of Water for Injection, followed by 9 ml of Omnipaque 350 contrast agent was added to the vial. Prior to BTG-002814 delivery, diagnostic visceral arteriography was performed to delineate the arterial supply to the tumour, determine the presence of variant arterial anatomy and to confirm patency of the portal vein. Once the arterial anatomy was delineated, a catheter was advanced into the right or left hepatic artery distal to the cystic artery (if visualised). The treatment plan was based on the fluoroscopic appearances during arteriography.

Following trans-femoral catheterisation of the hepatic arterial vasculature, once the catheter was placed within the artery feeding the tumour, the reconstituted BTG-002814 suspension was slowly infused into the artery (approximately 1 ml

per minute). The end point of the procedure was either full delivery of the reconstituted bead volume (i.e. 1 ml vandetanib-loaded beads in contrast) or near-stasis in the tumoural vessel over 6 cardiac cycles. If the embolisation endpoint was achieved before the delivery of 1ml of bead, the injection was stopped and the volume of beads administered was recorded. For all patients a super selective (segmental/subsegmental) approach was taken with the catheter being placed as selectively as possible while maintaining sufficient flow to the tumour. In the case of multiple tumours being present, since all eligible patients had resectable disease, it was not a requirement of the protocol that all lesions visible on computed tomography (CT) were treated with BTG-002814; this decision was at the discretion of the treating investigator. Patients all underwent planned surgical resection 7-21 days following treatment with BTG-002814.

Blood samples for vandetanib and N-desmethyl vandetanib concentrations were taken at set time points throughout the study to assess the pharmacokinetic properties of vandetanib (Figure 1). Tissue samples for vandetanib and N-desmethyl vandetanib concentrations were taken from the resected liver tumours immediately following surgery. Vandetanib and N-desmethyl vandetanib metabolite concentrations in plasma and tissue samples were determined using solid phase extraction followed by liquid chromatography coupled to mass spectrometry (York Bioanalytical Solutions Ltd, York, United Kingdom) (Chapter 3).

Following tissue sampling for vandetanib, standard haematoxylin and eosin stain sections were cut, and the extent of tumour necrosis, viable tumour and presence of vascular changes reported (Chapter 4).

All patients underwent perfusion imaging with dynamic contrast-enhanced magnetic resonance imaging (DCE-MRI) and perfusion CT (pCT) at baseline, and following treatment with BTG-002814, on the day prior to resection.. Two baseline scans were performed for each patient, within 7 days of each other, in order to assess perfusion parameter variation (Chapter 5).

Following tumour resection, prior to tissue sampling, the resected specimen was imaged on a Mediso nanoScan Positron Emission Tomography/CT. Embolised

vasculature were aligned between the two images using a novel surface-based segment-matching algorithm and alignment verified using manually selected fiducial points. Using this alignment and calibrated scans of the RO beads, volumes of beads were calculated within the tumour, resection specimen, and liver (Chapter 4).

Thirty-seven exploratory blood biomarkers were measured throughout the study at set time-points to indicate the potential activity of BTG-002814. Specifically, pro- and anti-angiogenic factors, hypoxia markers, haemopoietic growth factors, inflammatory factors, and markers of endothelial function were measured (Chapter 4).

2.2.6 Study Objectives

The primary aim of the VEROnA clinical study was to assess the safety and tolerability of vandetanib-eluting radiopaque embolic beads (BTG-002814).

Co-Primary endpoints

- Adverse events related to treatment with BTG-002814 using the standardised grading criteria NCI CTCAE v 4.0.
- Concentration of vandetanib and N-desmethyl vandetanib in plasma and in resected liver tissue following treatment with BTG-002814 (Chapter 3).

Secondary endpoints

- Distribution of BTG-002814 on non-contrast enhanced imaging of tumour vasculature (Chapter 4).
- Evaluation of histopathological features in the surgical specimen (malignant and non-malignant liver tissue): tumour necrosis, viable tumour, vascular changes (Chapter 4).
- Assessment of changes in blood flow on dynamic contrast enhanced magnetic resonance imaging (DCE-MRI) following treatment with BTG-002814 (Chapter 5).

Exploratory endpoints

- Blood biomarkers with the potential to identify patients likely to respond to treatment with BTG-002814 (Chapter 4).

2.2.7 Study schedule

Figure 1 shows an overview of the study schema. Table 2 outlines the assessments undertaken at each study visit.

Table 2: Outline of study schedule and assessments

Study Visit	**Visit 0**	**Visit 1**	**Visit 2**		**Visit 3**	**Visit 4**	**Visit 5**	**Visit 6**
Assessment	**Screening**	**Baseline**	**Treatment Day**		**Day one post-treatment**	**Day pre resection**	**Surgical resection**	**End of Study**
			Pre	**Post**				
Informed Consent	X							
Patient Demographics	X							
Medical and Prior Treatment History	X							
Eligibility Assessment (Inclusion/Exclusion Criteria)	X							
Child Pugh Assessment (HCC patients only)	X							
Physical Examination	X	X				X		X
Vital Signs	X	X	X	X	X	X	X	X
WHO Performance Status	X	X				X		X
Concomitant Medications	X	X	X	X	X	X	X	X
Assessment of Adverse Events	X	X	X	X	X	X	X	X
Biochemistry	X	X			X	X		X
Haematology	X	X			X	X		X
Coagulation Tests	X	X				X		X
12-Lead ECG	X	X	X	X		X		X
Serum Pregnancy Test	X	X[2]						

Study Visit	**Visit 0**	**Visit 1**	**Visit 2**		**Visit 3**	**Visit 4**	**Visit 5**	**Visit 6**
Assessment	**Screening**	**Baseline**	**Treatment Day**		**Day one post-treatment**	**Day pre resection**	**Surgical resection**	**End of Study**
			Pre	**Post**				
Liver DCE- MRI		X	X			X		
Perfusion CT of Liver		X	X			X		
4D-CT Scan Liver					X			
Blood Biomarker Analysis		X	X		X	X		X
Serum Tumor Markers		X	X			X		
Vandetanib and N-desmethyl Metabolite Plasma Sampling			X	X	X	X		X
Vandetanib and N-desmethyl metabolite Tissue Sampling, Histopathological and Biomarker Analysis							X	

For women of child-bearing potential, a negative pregnancy test must have been obtained prior to treatment. For baseline blood tests, vital signs and ECG (visit 1) did not need repeating if screening assessments were performed within 7 days prior to treatment. Visit 3 CT and MRI scans could be performed the day before treatment. If surgery was delayed > 7 days, then all visit 4 assessments needed to be repeated the day before the rescheduled surgery.

2.3 STATISTICAL ANALYSIS

The statistical analysis in this study was primarily descriptive, to assess the safety and tolerability of the study treatment, as well as the distribution of the product following delivery. As such, the study was not powered for any statistical hypotheses. Based on pre-clinical trials, a target size of six patients with each primary diagnosis was deemed sufficient to assess safety and drug concentrations in plasma and resected specimens following treatment [7]. All patients who received treatment with BTG-002814 in the study were included in the analysis population.

2.4 RESULTS

2.4.1 Patient characteristics

Between August 2017 and February 2019, eight patients were enrolled into this study; two with HCC and six with mCRC (Figure 2). Median age of all eight patients was 62.5 years (range 50-69 years). All patients had solitary lesions except one patient with two lesions and one with five lesions (both mCRC). Patient and tumour baseline characteristics are summarised in Table 3. Enrolment was stopped prior to full accrual due to expiration of the investigational medicine product (BTG-002814) in February 2019.

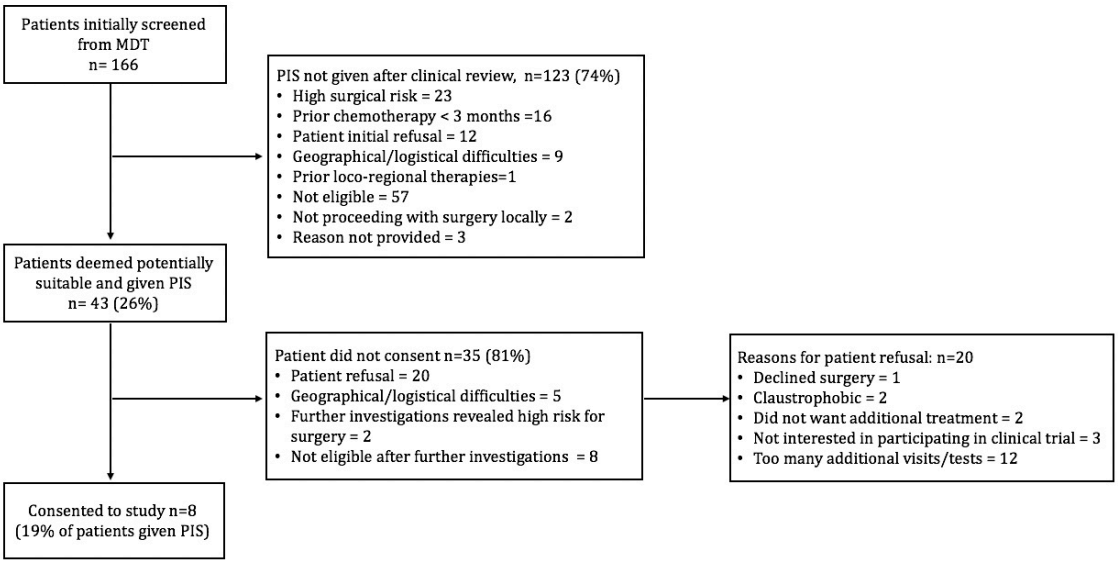

Figure 2: CONSORT diagram

Abbreviations: PIS, patient information sheet; MDT, multi-disciplinary meeting

Table 3: Baseline patient characteristics

Baseline characteristic	mCRC n=6	HCC n=2 (absolute values)	Total n=8
Sex			
Male	5 (83.3%)	2 (100%)	7 (87.5%)
Female	1 (16.7%)	0 (0%)	1 (12.5%)
Age (years), median (range)	61 (50-69)	57 & 69	62.5 (50-69)
WHO performance status			
0	6 (100%)	2 (100%)	8 (100%)
1	0 (0%)	0 (0%)	0 (0%)
2	0 (0%)	0 (0%)	0 (0%)
ALT(IU/L), median (range)	20.0 (15.0-31.0)	37.0 & 74.0	26.0 (15.0-74.0)
ALP (IU/L), median (range)	64.5 (45.0-105.0)	58.0 & 77.0	64.5 (45.0-105.0)
Albumin (g/L)	45.5 (42.0-50.0)	41.0 & 45.0	45.0 (41.0-50.0)
Total Bilirubin (µmol/L)	12.0 (5.0-26.0)	12.0 & 13.0	12.5 (5.0-26.0)
Haemoglobin (g/L)	142.0 (120.0-167.0)	123.0 & 130.0	137.0 (120.0-167.0)
INR	0.9 (0.9-1.0)	1.0 & 1.1	1.0 (0.9-1.1)
Serum creatinine (µmol/L)	90.5 (56.0-101.0)	81.0 & 87.0	88.5 (56.0-101.0)
Child-Pugh Score			
A5	NA	2 (100%)	NA
A6	NA	0 (0%)	NA
Baseline tumour marker			
AFP (kU/L)	NA	3.9 & 4.1	NA
CEA (µg/L)	9.1 (2.0-201.0)	NA	NA
CA19-9 (kU/L)	17.5 (9.0-195.0)	NA	NA
CA125 (kU/L)	9.0 (4.0-12.0)	NA	NA
Baseline ECG QTc (ms)	410.5 (384-427)	384 & 410	407 (384-427)
Number of liver tumours			
Median (range)	1 (1-5)	1 & 1	1 (1-5)
Tumour size (sum of longest diameters)			
Baseline CT (mm)	25 (8-133)	33 & 82	29.5 (8-133)
Baseline MRI (mm)	26 (8-120)	30 & 82	28 (8-120)

Abbreviations: ALT, alanine transferase; ALP, alkaline phosphatase; INR, international normalised ratio; AFP, alpha fetoprotein; CEA, carcinoembryonic antigen; CA 19-9, cancer antigen 19-9; CA 125, cancer antigen 125; CT, computed tomography; MRI, magnetic resonance imaging.

2.4.2 Trial Violations

All eight patients completed the study and attended all trial visits. There were no major protocol violations that affected the study endpoints. One patient underwent surgical resection 32 days post-TACE. Surgery was initially planned 13 days post TACE, but due to lack of ITU beds surgery was delayed.

2.4.3 TACE and surgery treatment details

All patients underwent successful treatment with BTG-002814. Six patients (75%) received the full volume of beads (1 ml), whilst one patient received 0.4 ml and one patient 0.9 ml due to early stasis. Treatment was delivered over a median of 2 infusions (range 1-3) over a total time of 22 mins (range 8-64 minutes). Vasospasm occurred in two patients (25%) with embolisation outside of the intended treatment zone occurring in six patients (75%).

All patients underwent surgery as planned at median of 14.9 days (range, 7-32 days) following treatment with BTG-008214 (Table 4). A total of 13 lesions were resected, of which 10 had been treated with BTG-002814. All lesions were resected with an R0 margin.

Table 4: Type of liver surgery performed for each trial patient

Patient	Diagnosis	Surgery Procedure	Open vs Laparoscopic
1	HCC	Right anterior sectionectomy	Open
2	HCC	Segmentectomy VII	Open
3	mCRC	Segmentectomy VII	Open
4	mCRC	Segmentectomy IV	Open
5	mCRC	Right anterior sectionectomy & Segmentectomy IVa/VIII & II	Open
6	mCRC	Segmentectomy V	Open
7	mCRC	Segmentectomy V	Open
8	mCRC	Segmentectomy III, IV, V, VI, VII	Open

Abbreviations: HCC, hepatocellular carcinoma; mCRC, metastatic colorectal cancer.

2.4.4 Safety Results and Adverse Events

2.4.4.1 Summary of adverse events

Table 5 shows a summary of all adverse events that occurred during the trial.

Table 5: Summary of all adverse events

	Patients n (%)	Events n
All treatment emergent adverse events	8 (100.0%)	309
Adverse events within one day of treatment with BTG-002814	8 (100.0%)	71
Vandetanib-related adverse events prior to surgery	7 (87.5%)	57
TACE-related adverse events prior to surgery	7 (87.5%)	55
Adverse events following surgery up to end of follow-up	8 (100.0%)	177
All treatment emergent serious adverse events	4 (50.0%)	10
Serious adverse events within one day of treatment with BTG-002814	0 (0.0%)	0
Vandetanib-related serious adverse events prior to surgery	0 (0.0%)	0
TACE-related serious adverse events prior to surgery	0 (0.0%)	0
Serious adverse events following surgery up to end of follow-up	4 (50.0%)	9
Adverse events resulting in death	1 (12.5%)	1
Adverse events with CTCAE grade ≥ 3	5 (62.5%)	58

2.4.4.2 Adverse Events post-TACE (prior to surgery)

All eight patients (100%) had an AE following treatment with BTG-002814. There was one Grade 3 (G3) or higher AE; G3 hypertension in a patient with a known diagnosis of hypertension (G1 at baseline). This occurred post-treatment with BTG-002814 and returned to G1 without intervention. The most common G2 AEs due to treatment were dyspepsia (four ,50%), fatigue (four, 50%) and hypertension (three, 37.5%) (Tables 6-7). ECG prolongation was reported in two patients (G1). No patients had a G3 laboratory value pre-surgery. All patients were discharged home within 24-hours of treatment.

Table 6: Adverse events related to Vandetanib

Adverse event	CTCAE grade					
	CS	1	2	3	4	5
	n	n	n	n	n	n
ALT	.	1	0	0	0	0
Abdominal pain	.	0	2	0	0	0
Acute kidney injury	.	1	0	0	0	0
Anorexia	.	2	1	0	0	0
Bloating	.	0	1	0	0	0
Calculated GFR (mL/min)	1	0	0	0	0	0
Constipation	.	1	0	0	0	0
Cough	.	1	0	0	0	0
Dehydration	.	1	0	0	0	0
Dyspepsia	.	1	4	0	0	0
Electrocardiogram QT corrected interval prolonged	.	2	0	0	0	0
Fatigue	.	2	4	0	0	0
Flu like symptoms	.	1	0	0	0	0
Hypertension	.	2	2	1	0	0
Insomnia	.	0	1	0	0	0
Laryngeal inflammation	.	1	0	0	0	0
Myalgia	.	1	0	0	0	0
Nausea	.	1	1	0	0	0
Rash acneiform	.	1	0	0	0	0
Serum Creatinine (umol/L)	.	0	1	0	0	0
Sore throat	.	0	1	0	0	0
Tinnitus	.	1	1	0	0	0
Urea	1	1	0	0	0	0

Table 7: Adverse events related to TACE

Adverse event	CTCAE grade					
	CS	1	2	3	4	5
	n	n	n	n	n	n
ALT	.	1	0	0	0	0
Abdominal pain	.	0	2	0	0	0
Acute kidney injury	.	1	0	0	0	0
Anorexia	.	2	1	0	0	0
Back pain	.	1	1	0	0	0
Bloating	.	0	1	0	0	0
Calculated GFR (mL/min)	1	0	0	0	0	0
Cardiac disorders - Other: Bradycardia	.	0	1	0	0	0
Dyspepsia	.	1	3	0	0	0
Dyspnea	.	0	1	0	0	0
Fatigue	.	3	4	0	0	0
Flu like symptoms	.	1	0	0	0	0
Hematoma	.	1	0	0	0	0
Hypertension	.	2	1	0	0	0
Musculoskeletal and connective tissue disorder - Other: Groin pain	.	0	1	0	0	0
Myalgia	.	1	0	0	0	0
Nausea	.	1	1	0	0	0
Non-cardiac chest pain	.	0	1	0	0	0
Pain	.	2	0	0	0	0
Paresthesia	.	2	0	0	0	0
Presyncope	.	0	1	0	0	0
Serum Creatinine (umol/L)	.	0	1	0	0	0
Urea	1	1	0	0	0	0

Abbreviations: ALT, alanine transaminase; GFR, glomerular filtration rate.

2.4.4.3 Adverse events post-surgery

Overall, post-surgery there were 18 grade 3 or higher adverse events, of which seven were haematological.

Table 8: Adverse events post-surgery until last trial visit- patients

Adverse event	CTCAE grade					
	CS	1	2	3	4	5
	n	n	n	n	n	n
ALP (IU/L)	.	5	0	0	0	0
ALT	.	2	0	0	0	0
ANC (x10^9/L)	.	2	0	0	0	0
AST (IU/L)	.	2	0	0	0	0
Abdominal pain	.	1	7	0	0	0
Acute kidney injury	.	0	1	0	0	0
Albumin	.	0	2	1	0	0
Anorexia	.	0	1	1	0	0
Arthralgia	.	1	0	0	0	0
Ascites	.	0	1	0	0	0
Biliary anastomotic leak	.	0	0	1	0	0
Calcium (mmol/L)	.	2	0	0	0	0
Cardiac disorders - Other: Bradycardia	.	1	0	0	0	0
Constipation	.	3	2	0	0	0
Cough	.	1	0	0	0	0
Delirium	.	0	1	0	0	0
Dyspnea	.	1	0	0	0	0
Fatigue	.	0	6	0	0	0
Fever	.	2	0	0	0	0
GGT (U/L)	.	3	2	0	0	0
Gastritis	.	1	0	0	0	0
Gastrointestinal disorders - Other: Small bowel ileus	.	0	0	1	0	0
Haemoglobin	.	5	0	2	0	0
Hematoma	.	0	0	1	0	0
Hiccups	.	1	0	0	0	0
Hypotension	.	1	1	0	0	0
Lung infection	.	0	0	2	0	0
Magnesium (mmol/L)	.	1	0	0	0	0
Nausea	.	0	5	0	0	0
Other: CRP	.	0	0	1	0	0
Other: Creatinine	.	0	1	0	0	0
Other: Lactate	.	0	0	1	0	0
Other: Neutrophil Count	.	0	0	1	0	0
Platelet (x10^9/L)	.	1	0	0	0	0
Pruritus	.	0	1	0	0	0
Random glucose (mmol/L)	.	3	0	0	0	0
Sepsis	.	0	0	0	1	0
Small intestinal obstruction	.	0	0	1	0	0
TSH (mU/L)	.	1	0	0	0	0
Urate (umol/L)	.	3	0	0	0	0
Vomiting	.	2	0	0	0	0
WBC	.	1	0	1	0	0
Weight loss	.	1	2	0	0	0
Wound dehiscence	.	0	1	0	0	0
Wound infection	.	0	2	2	0	0

Abbreviations: ALP, alkaline phosphatase; ALT, alanine transaminase; ANC, absolute neutrophil count; AST, aspartate aminotransferase; GGT, Gamma-glutamyl transferase; CRP, C-reactive protein; TSH, thyroid stimulating hormone; WCC, white cell count.

Table 9 outlines all CTCAE grade ≥ 3 AEs that occurred during the trial, along with causality and time from treatment with BTG-002814. In total, there were 19 grade ≥ 3 AEs in five patients. Six were potentially related to treatment with BTG-002814.

Table 9: Listing of the first occurrence of each CTCAE grade ≥ 3 adverse events

Patient	Diagnosis	Event term	CTCAE grade	Days from treatment	Related to vandetanib	Related to TACE	Pre-treatment grade*
1	HCC	Wound infection	3	24	Not related	Not related	.
2	HCC	Lung infection	3	17	Related	Not related	.
		Upper gastrointestinal haemorrhage	5	102	Related	Related	.
4	mCRC	Hypertension	3	0	Related	Not related	1
7	mCRC	Albumin	3	48	Not related	Not related	.
		Biliary anastomotic leak	3	47	Not related	Related	.
		Haemoglobin	3	62	Not related	Not related	.
		CRP	3	47	Not related	Not related	.
		Lactate	3	47	Not related	Not related	.
		Neutrophil Count	3	49	Not related	Not related	.
		Sepsis	4	47	Not related	Related	.
		WBC	3	49	Not related	Not related	.
8	mCRC	Anorexia	3	17	Not related	Not related	.
		Small bowel ileus	3	11	Not related	Not related	.
		Haemoglobin	3	13	Not related	Not related	.
		Haematoma	3	14	Not related	Related	.
		Lung infection	3	10	Not related	Not related	.
		Small intestinal obstruction	3	14	Not related	Not related	.
		Wound infection	3	21	Not related	Not related	.

Notes: Patient 4 had CTCAE G1 hypertension pre-treatment which worsened to CTCAE G3 on the day of BTG-002814 treatment; this was considered causally related to vandetanib

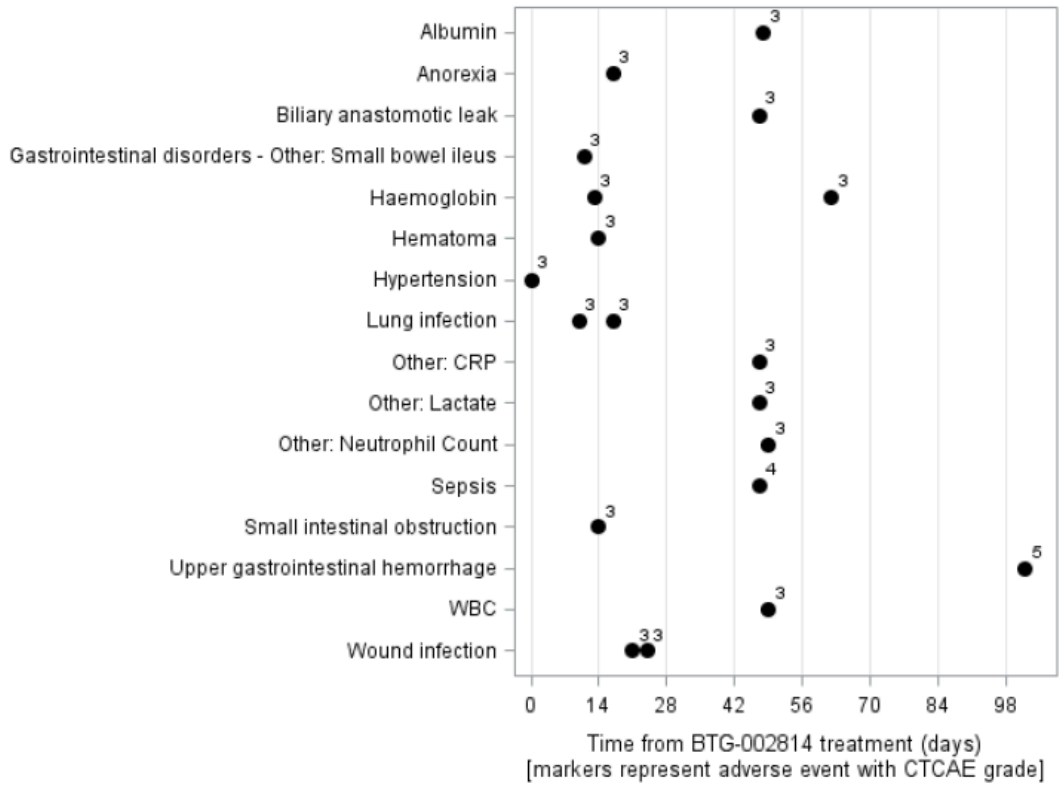

Figure 3: Time from BTG-002814 treatment to first occurrence of CTCAE grade ≥ 3 events. Abbreviations: 3, Grade 3 CTCAE event; 4, grade 4 CTCAE event; 5, grade 5 CTCAE event; CRP, C-reactive protein; WCC, white cell count.

2.4.4.4 Serious Adverse Events

There were no SAEs following treatment with BTG-002814 prior to surgery. Following surgery, SAEs were reported in four patients (50%): wound infection (two, 25%), wound dehiscence (one, 12.5%), small intestinal obstruction (one, 12.5%), biliary leak with associated sepsis and acute kidney injury (one, 12.5%), lung infection (one, 12.5%), and one death due to an upper gastrointestinal haemorrhage that occurred 102 days post-treatment with BTG-002814 (Table 10). Although the upper gastrointestinal haemorrhage in patient 2 occurred after the last trial visit, as the patient had an ongoing SAE (wound dehiscence) that had not resolved at the time of last trial visit, this SAE was recorded.

Table 10: Listing of all serious adverse events during the trial

Patient	Diagnosis	Event term	Grade	Days from treatment	Related to vandetanib	Related to TACE	Expected vandetanib	Expected TACE
1	HCC	Wound infection	3	24	Not related	Not related	Unexpected	Expected
2	HCC	Lung infection	3	17	Related	Not related	Expected	Expected
		Ascites	2	19	Not related	Not related*	Unexpected	Unexpected
		Wound dehiscence	2	19	Related	Not related	Unexpected	Unexpected
		Upper gastrointestinal hemorrhage	5	102	Related**	Related**	Expected	Unexpected
7	mCRC	Acute kidney injury	2	47	Not related	Not related	Unexpected	Unexpected
		Biliary anastomotic leak	3	47	Not related	Related**	Unexpected	Unexpected
		Sepsis	4	47	Not related	Related**	Expected	Expected
8	mCRC	Small intestinal obstruction	3	14	Not related	Not related	Unexpected	Unexpected
		Wound infection	3	21	Not related	Not related	Unexpected	Unexpected

* SAE Review: Sponsor Causality = “Related (reasonable possibility)”

** SAE Review: Sponsor Causality = “Not related (no reasonable possibility)”

Abbreviations; HCC, hepatocellular carcinoma; mCRC, metastatic colorectal cancer.

Patient 1 was admitted post-surgery with a G3 wound infection which was felt not to be related to TACE or vandetanib.

Patient 2 had a prolonged post-operative hospital admission. This patient developed a G3 lung infection post-operatively, which was felt possibly related to vandetanib, as a cough developed post-TACE. The patient also developed G2 ascites, possibly related to TACE, and G2 wound dehiscence, possibly related to vandetanib. Patient 2 died 3 months post-surgical resection of an upper gastrointestinal haemorrhage. This was felt possibly related to BTG-002814, although the patient was known to have a previous history of a duodenal ulcer.

Patient 7 was re-admitted to hospital post-surgical resection of a segment V lesion. The cause of readmission was a post-surgical biliary leak. This led to G4 sepsis and an acute kidney injury (G2). At the time of final trial follow-up, the sepsis and biliary leak were ongoing, although the acute kidney injury had resolved. The biliary leak was most likely due to damage to the biliary ducts at the time of surgery, although the TACE procedure may have contributed.

Patient 8 had a prolonged hospital admission post-surgical resection due to small bowel obstruction. This was due to abdominal adhesions from previous bowel surgery (resection of colorectal primary cancer) and not due to the TACE procedure or vandetanib. Following further abdominal surgery for adhesion, a wound infection did develop, which was not felt related to TACE or vandetanib.

2.5 DISCUSSION

The findings of this first-in human study show that BTG-002814 has an acceptable safety profile and is feasible to deliver prior to liver resection in patients with HCC and mCRC. This is an important advance in this field of research as it is the first time that a targeted anti-angiogenic agent has been successfully loaded on to DEBs and delivered directly into human liver tumours. The majority of BTG-002814 related AEs were mild and transient and considered to be associated with the known side effect profile of either vandetanib or the TACE procedure.

There was one transient G3 event (hypertension) that occurred following TACE prior to surgery that subsequently improved without treatment. Hypertension is a well-recognised side effect of anti-angiogenic agents, including vandetanib [13, 14]. Furthermore, there was one G3 groin haematoma that occurred following surgery that was related to the TACE treatment. This was initially a G1 haematoma post-TACE that progressed to a G3 after surgery, likely due to the use of anticoagulants in the post-operative period. G2 AEs related to BTG-002814 were expected and included dyspepsia (50%), fatigue (50%) and hypertension (37.5%). There were only two patients that experienced G1 prolongation in the QT interval seen on ECG monitoring. Although 19 ≥G3 AEs were reported, including SAEs in four patients, 18 AEs occurred following surgery with the majority unrelated to treatment with BTG-002814. Surgery was not delayed by TACE and post-operative morbidity reflected patients undergoing major open liver surgery and is in keeping with other published series [15-17].

A number of phase 1 dose escalation studies have been conducted in patients with mCRC to determine the maximum tolerated dose (MTD) of vandetanib in combination with different therapeutic agents and regimens. In a study of 21 patients with vandetanib 100 mg (n=11) and vandetanib 300 mg (n=10) combined with standard 14-day treatment cycles of FOLFIRI, the most commonly reported AEs were diarrhoea, fatigue and nausea. It was concluded that vandetanib at dose levels of both 100 mg and 300 mg daily was adequately tolerated in combination with standard 14-day cycles of FOLFIRI in patients with advanced colorectal cancer [18].

In one phase I study of vandetanib combined with cetuximab and irinotecan, 27 patients with mCRC were enrolled at four dose levels. Two dose-limiting toxicities (DLTs) (grade 3 QTc prolongation and diarrhoea) were detected at 300 mg vandetanib with cetuximab and irinotecan resulting in 200 mg being the MTD [19]. In another phase I study, 13 patients received vandetanib at doses of 100 mg and 300 mg daily in combination with capecitabine and oxaliplatin, which was well tolerated. However, the addition of bevacizumab resulted in severe diarrhoea in three out of four patients. Bevacizumab was not well tolerated with vandetanib and XELOX in combination [20].

In another study, 17 patients with advanced mCRC, vandetanib 100 mg (n=9) or 300 mg (n=8) was combined with mFOLFOX6 chemotherapy. The most commonly reported AEs were diarrhoea, lethargy and nausea. The CTCAE G3/4 events that were considered to be related to vandetanib were G3 diarrhoea in three patients (one patient in the 100 mg cohort and two patients in the 300 mg cohort) and G3 thrombocytopenia in one patient (300 mg cohort) [21].

In a further phase I study designed to assess the effect of vandetanib on vascular permeability in patients with advanced mCRC, 22 patients received the study drug; 10 received 100 mg and 12 received 300 mg. The most commonly reported AEs were diarrhoea, dry mouth, fatigue and nausea [22].

To date, there has been only one trial that has assessed the safety and efficacy of vandetanib in HCC patients. Again, this study, by Hsu *et* al, involved oral systemic administration rather than trans-arterial targeted therapy. Sixty-seven HCC patients were randomised to oral vandetanib 300 mg (n=19), oral vandetanib 100 mg (n=25) or placebo (n=23). Twenty-nine patients subsequently entered open-label treatment (300 mg/day). In both vandetanib treatment arms, tumour stabilisation rate was not significantly different from placebo. The most common AEs reported in the primary treatment phase were diarrhoea and rash, irrespective of randomised treatment. Twenty-three patients experienced CTCAE grade ≥ 3 AEs (six patients from each of the vandetanib arms and 11 patients in the placebo group). Seven patients in the vandetanib 300 mg group (36.8%) and four in the vandetanib 100 mg group (16.0%) either required dose interruption or dose reduction due to AEs. No dose interruption or reduction was reported for patients in the placebo group. Six patients discontinued treatment due to AEs: hepatic failure (100 mg group), diarrhoea and palmar-plantar erythrodysaesthesia syndrome (100 mg group); diarrhoea, upper gastrointestinal haemorrhage and hyperbilirubinaemia (placebo group). Of these, hepatic failure, palmar-plantar erythrodysaesthsia syndrome and upper gastrointestinal haemorrhage were considered to be related to study treatment. The safety profile for the secondary open-label phase was similar to that of the randomised phase, with diarrhoea and rash being the most common AEs. Nine patients (31.0%) required treatment interruption or dose reduction due to AEs. Two patients

discontinued treatment in the secondary phase due to AEs on the nervous system and hypertension [23].

Although the data on vandetanib in HCC and mCRC patients is limited to early phase clinical trials, oral vandetanib is already licensed for use in the treatment of medullary thyroid cancers. This was following the results of a randomised, double-blind, phase III study of 300 mg vandetanib versus placebo conducted to demonstrate safety and efficacy of vandetanib 300 mg. This study included 331 patients with unresectable locally advanced or metastatic MTC. The study met its primary objective of progression free survival prolongation with vandetanib versus placebo (hazard ratio [HR], 0.46; 95% CI, 0.31 to 0.69; $p< 0.001$). Statistically significant advantages for vandetanib were also seen for objective response rate ($p< 0.001$), disease control rate ($p< 0.001$), and biochemical response ($p< 0.001$) [13].

With regards to safety, 31 patients discontinued treatment during the randomised phase due to an AE: 28 (12%) receiving vandetanib and three (3%) receiving placebo. Adverse events such as diarrhoea, rash, nausea, and hypertension occurred in more than 30% of patients receiving vandetanib; AEs leading to discontinuation of vandetanib reported in more than 1% of patients were asthenia (1.7%) and rash (1.3%). More patients required dose reduction of vandetanib compared with placebo for AEs or QTc prolongation (35% v 3%). Nineteen patients (8%) developed protocol-defined QTc prolongation, but there were no reports of Torsades de pointes. Five patients on the vandetanib arm experienced AEs leading to death during the randomised phase; these were single instances of aspiration pneumonia, respiratory arrest, respiratory failure, staphylococcal sepsis, and arrhythmia and acute cardiac failure in one patient [13].

From the AEs reported in our cohort, 100 mg of vandetanib delivered via TACE is safe and well-tolerated prior to surgery. It was anticipated that a more tolerable side effect profile would be achieved when compared to oral administration due to the lower systemic concentrations of vandetanib as result of local delivery and the fact that a single 100 mg dose was delivered. It therefore appears safe to move forwards with this dose in further clinical trials. However, only dose level has been tested in this cohort of patients, as all patients (regardless of tumour

size) received a maximum of 1 ml of BTG-002814 (containing 100mg vandetanib). As 300 mg/day has been shown to be a safe oral daily dose, a dose-escalation trial (dependent on tumour size and the achievement of tumour vessel stasis) with increments in dose of vandetanib in patients with unresectable HCC and mCRC would be the next step. However, close monitoring for side effects such as hypertension, diarrhoea, fatigue, dyspepsia, prolongation of the QTc interval and skin reactions would be imperative.

There are limitations to this study. This is a small, phase 0, window-of-opportunity study and although the initial aim was to recruit 12 patients (six with HCC, six with mCRC), accrual was slower than anticipated. Although 166 patients were identified from MDTs as being potentially suitable, following initial screening in clinic only 43 patients were found to be suitable. Main reasons for ineligibility were high surgical risk, chemotherapy within 3-months (for mCRC patients) and the identification of other factors on review that meant that patients were no longer suitable for surgical resection. Of the 43 patients given a PIS, eight (19%) were consented onto the trial. Ten patients were later deemed not to meet all of the inclusion criteria, and 25 patients declined to take part. The main reasons that eligible patients declined recruitment into the clinical trial was due to the number of additional trial visits. Although patients were approached at the earliest opportunity, being their first surgical clinical attendance, there was often a short interval of just a few weeks from initial consultation to surgery date. With patients being informed at that consultation that the recovery period following liver surgery would be up to 3-months, to then be required to attend additional trial visits in the weeks preceding surgery was felt to be too much of a commitment for a number of patients.

Poor accrual to early phase clinical trials is well recognised. The NCI Cancer Therapy Evaluation Program recently analysed 19 months of corrective action plans (CAP) received for slow-accruing Phase 1 and 2 trials in order to identify reasons for slow accrual. Of the 135 CAPs analysed, 69 were for Phase 1 trials and 66 for Phase 2 trials. The authors report that primary reasons cited for slow accrual were safety/toxicity (Phase 1: 48%), design/protocol concerns (Phase 1: 42%, Phase 2: 33%), and eligibility criteria (Phase 1: 41%, Phase 2: 35%) [24]. Although safety concerns were not reported in our study, the concern of attending

for additional trial scans and trial visits was a major reason for patients not agreeing to enrol, which related to study design. With regards to meeting eligibility criteria, this was an issue with regards to prior chemotherapy and patients being deemed high-risk for surgery. However, strict eligibility criteria needed to be in place for this first-in human early phase clinical trial to ensure maximal safety in this cohort of patients prior to surgery. What can be taken forward from this trial, is the burden that additional trial visits have on patients, and this information should be taken into consideration in the design of the phase I/II trials of BTG-002814.

2.6 CONCLUSION

In conclusion, this first-in-human, phase 0, window-of-opportunity study has shown that vandetanib-eluting radiopaque beads (BTG-002814) can be safely delivered to patients with liver tumours prior to surgical resection. The ability to safely deliver vandetanib locally to liver tumours *via* TACE is a novel approach that warrants further exploration in future clinical trials in patients with intermediate-stage HCC and non-resectable CRC liver metastases.

2.7 REFERENCES

[1] Bruix J, Sherman M. Management of hepatocellular carcinoma: an update. Hepatology (Baltimore, Md). 2011;53:1020-2.
[2] EASL Clinical Practice Guidelines: Management of hepatocellular carcinoma. Journal of hepatology. 2018;69:182-236.
[3] Van Cutsem E, Cervantes A, Adam R, Sobrero A, Van Krieken JH, Aderka D, et al. ESMO consensus guidelines for the management of patients with metastatic colorectal cancer. Ann Oncol. 2016;27:1386-422.
[4] Park W, Chung YH, Kim JA, Jin YJ, Lee D, Shim JH, et al. Recurrences of hepatocellular carcinoma following complete remission by transarterial chemoembolization or radiofrequency therapy: Focused on the recurrence patterns. Hepatol Res. 2013;43:1304-12.
[5] Llovet JM, Real MI, Montana X, Planas R, Coll S, Aponte J, et al. Arterial embolisation or chemoembolisation versus symptomatic treatment in patients with unresectable hepatocellular carcinoma: a randomised controlled trial. Lancet (London, England). 2002;359:1734-9.
[6] Hagan A, Phillips GJ, Macfarlane WM, Lloyd AW, Czuczman P, Lewis AL. Preparation and characterisation of vandetanib-eluting radiopaque beads for locoregional treatment of hepatic malignancies. Eur J Pharm Sci. 2017;101:22-30.
[7] Denys A, Czuczman P, Grey D, Bascal Z, Whomsley R, Kilpatrick H, et al. Vandetanib-eluting Radiopaque Beads: In vivo Pharmacokinetics, Safety and Toxicity Evaluation following Swine Liver Embolization. Theranostics. 2017;7:2164-76.
[8] Lewis AL, Willis SL, Dreher MR, Tang Y, Ashrafi K, Wood BJ, et al. Bench-to-clinic development of imageable drug-eluting embolization beads: finding the balance. Future Oncol. 2018;14:2741-60.
[9] Levy EB, Krishnasamy VP, Lewis AL, Willis S, Macfarlane C, Anderson V, et al. First Human Experience with Directly Image-able Iodinated Embolization Microbeads. Cardiovasc Intervent Radiol. 2016;39:1177-86.
[10] Morabito A, Piccirillo MC, Falasconi F, De Feo G, Del Giudice A, Bryce J, et al. Vandetanib (ZD6474), a dual inhibitor of vascular endothelial growth factor receptor (VEGFR) and epidermal growth factor receptor (EGFR) tyrosine kinases: current status and future directions. Oncologist. 2009;14:378-90.

[11] Duran R, Namur J, Pascale F, Czuczman P, Bascal Z, Kilpatrick H, et al. Vandetanib-eluting Radiopaque Beads: Pharmacokinetics, Safety, and Efficacy in a Rabbit Model of Liver Cancer. Radiology. 2019;293:695-703.
[12] Beaton L, Tregidgo HFJ, Znati SA, Forsyth S, Clarkson MJ, Bandula S, et al. VEROnA Protocol: A Pilot, Open-Label, Single-Arm, Phase 0, Window-of-Opportunity Study of Vandetanib-Eluting Radiopaque Embolic Beads (BTG-002814) in Patients With Resectable Liver Malignancies. JMIR Res Protoc. 2019;8:e13696.
[13] Wells SA, Jr., Robinson BG, Gagel RF, Dralle H, Fagin JA, Santoro M, et al. Vandetanib in patients with locally advanced or metastatic medullary thyroid cancer: a randomized, double-blind phase III trial. J Clin Oncol. 2012;30:134-41.
[14] Qi WX, Shen Z, Lin F, Sun YJ, Min DL, Tang LN, et al. Incidence and risk of hypertension with vandetanib in cancer patients: a systematic review and meta-analysis of clinical trials. Br J Clin Pharmacol. 2013;75:919-30.
[15] Ito H, Are C, Gonen M, D'Angelica M, Dematteo RP, Kemeny NE, et al. Effect of postoperative morbidity on long-term survival after hepatic resection for metastatic colorectal cancer. Ann Surg. 2008;247:994-1002.
[16] Martin AN, Narayanan S, Turrentine FE, Bauer TW, Adams RB, Stukenborg GJ, et al. Clinical Factors and Postoperative Impact of Bile Leak After Liver Resection. J Gastrointest Surg. 2018;22:661-7.
[17] Sadamori H, Yagi T, Shinoura S, Umeda Y, Yoshida R, Satoh D, et al. Risk factors for major morbidity after liver resection for hepatocellular carcinoma. The British journal of surgery. 2013;100:122-9.
[18] Saunders MP, Wilson R, Peeters M, Smith R, Godwood A, Oliver S, et al. Vandetanib with FOLFIRI in patients with advanced colorectal adenocarcinoma: results from an open-label, multicentre Phase I study. Cancer Chemother Pharmacol. 2009;64:665-72.
[19] Meyerhardt JA, Ancukiewicz M, Abrams TA, Schrag D, Enzinger PC, Chan JA, et al. Phase I study of cetuximab, irinotecan, and vandetanib (ZD6474) as therapy for patients with previously treated metastastic colorectal cancer. PloS one. 2012;7:e38231.
[20] Cabebe EC, Fisher GA, Sikic BI. A phase I trial of vandetanib combined with capecitabine, oxaliplatin and bevacizumab for the first-line treatment of metastatic colorectal cancer. Investigational new drugs. 2012;30:1082-7.

[21] Michael M, Gibbs P, Smith R, Godwood A, Oliver S, Tebbutt N. Open-label phase I trial of vandetanib in combination with mFOLFOX6 in patients with advanced colorectal cancer. Investigational new drugs. 2009;27:253-61.
[22] Mross K, Fasol U, Frost A, Benkelmann R, Kuhlmann J, Buchert M, et al. DCE-MRI assessment of the effect of vandetanib on tumor vasculature in patients with advanced colorectal cancer and liver metastases: a randomized phase I study. Journal of angiogenesis research. 2009;1:5.
[23] Hsu C, Yang TS, Huo TI, Hsieh RK, Yu CW, Hwang WS, et al. Vandetanib in patients with inoperable hepatocellular carcinoma: a phase II, randomized, double-blind, placebo-controlled study. Journal of hepatology. 2012;56:1097-103.
[24] Massett HA, Mishkin G, Rubinstein L, Ivy SP, Denicoff A, Godwin E, et al. Challenges Facing Early Phase Trials Sponsored by the National Cancer Institute: An Analysis of Corrective Action Plans to Improve Accrual. Clin Cancer Res. 2016;22:5408-16.

3 PHARMACOKINETICS OF BTG-002814 IN THE VERONA CLINICAL TRIAL

3.1 INTRODUCTION

3.1.1. Vandetanib

Vandetanib (Caprelsa) (N-(4-bromo-2-fluorophenyl)-6-methoxy-7-[(1-methyl-piperidin-4-yl) methoxy] 9 quinazolin-4-amine) is an orally available tyrosine kinase inhibitor of vascular endothelial growth factor receptor (VEGFR) and endothelial growth factor receptor (EGFR) [1]. These tyrosine kinases act through a number of signalling pathways to promote cell proliferation, differentiation, migration, survival, and angiogenesis [2, 3]. Oral vandetanib has been approved for the treatment of advanced medullary thyroid cancers [4, 5]. Its use has also been investigated in the treatment of non-small cell lung cancer, as monotherapy and in combination with chemotherapy, and in the treatment of hepatocellular carcinoma (HCC) [6-8].

3.1.2 Pharmacokinetics of vandetanib

The pharmacokinetics of vandetanib have been studied in healthy individuals, in phase I clinical studies in patients with advanced solid tumours refractory to standard therapy, and in patients with renal or hepatic impairment [9-12].

Following single doses of 300-1200 mg of vandetanib to healthy volunteers, the absorption of vandetanib was found to be slow with the maximum concentration (C_{max}) achieved at a median time (T_{max}) of 6 hours (individual range 4 to 10 hours) [9]. Similarly, in patients following single doses of vandetanib of 50-600 mg median T_{max} ranged from 4.0-7.5 hours, followed by slow oral plasma clearance with a time of 100 to 120 hours [11, 12].

Vandetanib is metabolised by cytochrome P450 3A4 (CYP3A4) to N-desmethyl vandetanib and by monooxygenase enzymes FM01 and FM03 to vandetanib N-oxide. Gluronide conjugate is a minor metabolite (Figure 1). N-desmethyl-vandetanib is reported to circulate at a concentration of 7.0% to 17.1% of the parent compound and inhibits VEGFR and EGFR similarly to vandetanib. Vandetanib-N-oxide circulates at a concentration of 1.4-2.2% of vandetanib and is more than 50-fold less potent than the parent compound [13].

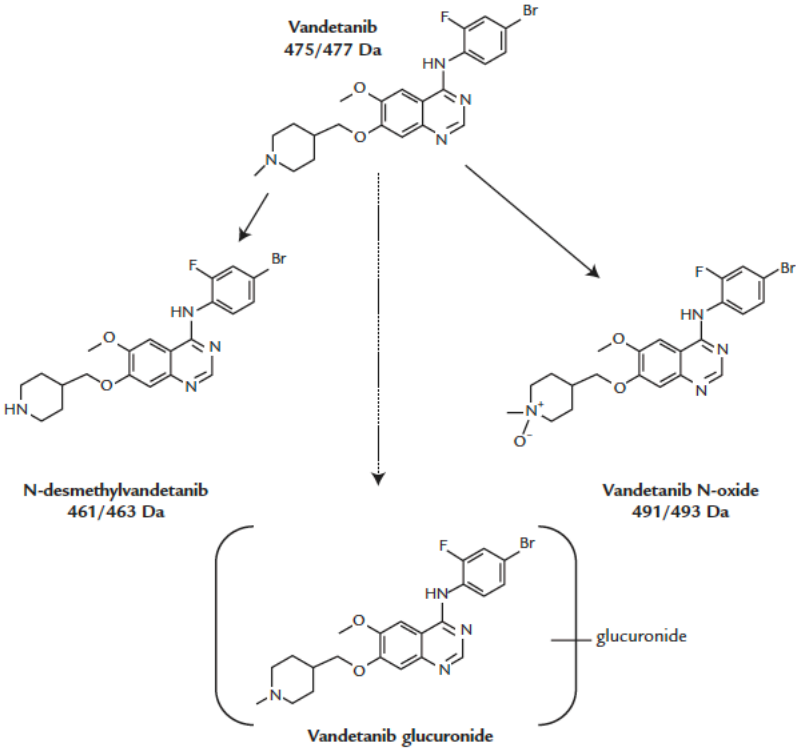

Figure 1: Metabolism of vandetanib [9]. Schema of the metabolism of vandetanib into three main metabolites.

Table 1. Overview of pharmacokinetics of oral vandetanib [13]

Absorption	T_{max} 6 hours (range 4-10 hours)
Distribution	Volume of distribution = 7450 L
	Protein binding 90% bound to α-l-acid-glycoprotein and serum albumin
Metabolism	Liver by CYP3A4, FM01 and FM03
	Metabolites: N-desmethyl vandetanib and vandetanib-N-oxide
Excretion	Total body clearance: 13.2 l/hr
	Excreted unchanged in urine and faeces
	Elimination half-life: 19 days

3.1.3 Drug-eluting beads (DEBs)

Drug-eluting beads (DEBs) are controlled release micro spherical devices that are used for sustained locoregional delivery of chemotherapeutic agents. Drug-eluting beads are frequently utilised in liver transarterial chemoembolisation (TACE). TACE is a minimally invasive, image guided procedure in which a

chemotherapeutic agent is injected via the hepatic artery into the tumour feeding blood vessels. This is followed by an embolic material which occludes the vessels, with the intention of starving the tumour of oxygen and nutrients. TACE is the standard of care for patients with intermediate stage HCC and a treatment option for liver-limited metastases from colorectal cancer (mCRC) [14, 15].

In DEB-TACE, the chemotherapeutic drug is loaded onto the bead prior to the procedure, and by virtue of its chemical structure, the bead sequesters the drug from solution allowing it be delivered as a drug-device combination [16]. Compared with systemic drug delivery, DEBs have been shown to decrease the systemic circulation of the chemotherapy agent, increase the drug concentration in target tissue and lead to an extended presence of the drug within the tumour [17, 18].

3.1.4 Pre-clinical studies of BTG-002814

BTG-002814 is a novel vandetanib-eluting radiopaque bead for use in TACE. To date, there has been one pharmacokinetic study of BTG-002814 in a porcine model of hepatic artery embolisation [17]. In this pre-clinical study, healthy swine were treated with intra-arterial vandetanib-eluting radiopaque beads, and blood and tissue samples taken to determine the pharmacokinetic properties of different doses over 30 days.

The peak plasma levels of vandetanib (C_{max}) released from the various doses of BTG-002814 ranged between 6.19-17.3 ng/mL indicating a low systemic burst release. The time to reach C_{max} (T_{max}) was approximately 1 hour following treatment. The plasma profile of vandetanib was found to consistent with a distribution phase up to 6 hours after administration, followed by elimination with a half-life of 20-23 hours. The AUC of vandetanib and its major metabolite N-desmethyl vandetanib was approximately linear with the dose strength of vandetanib beads. Vandetanib plasma levels were at or below limits of detection two weeks after administration.

In liver samples, vandetanib and N-desmethyl vandetanib were present in treated sections at 30 days after administration at levels above the in vitro IC50 for biological effectiveness. At 90 days both analytes were still present in the treated liver but were near or below the limit of quantification in untreated liver sections,

demonstrating sustained release from the beads. Furthermore, intra-arterial delivery resulted in low systemic exposure, with no obvious systemic toxicity [17].

3.2 OBJECTIVES

The objective of this study was to measure the concentrations of vandetanib and N-desmethyl metabolite in plasma and resected liver tissue following treatment with BTG-002814.

3.3 MATERIALS AND METHODS

3.3.1 Patient selection

All patients in this study were treated as part of the VEROnA clinical trial, which is outlined in detail in Chapter 2 (section 2.2)

3.3.2 Tissue and plasma vandetanib levels

3.3.2.1 Plasma vandetanib and N-desmethyl vandetanib levels

As part of the clinical trial protocol, plasma vandetanib and N-desmethyl vandetanib samples were collected at the following time points (Figure 2):

- 0 hours pre-treatment with BTG-002814
- 2 hours (+/- 15 minutes) post-treatment with BTG-002814
- 4 hours (+/- 15 minutes) post-treatment with BTG-002814
- 24 hours (+/- 1 hour) post-treatment with BTG-002814
- 7-21 days post-treatment with BTG-002814 (day prior to surgery)
- 28-32 days post-surgery

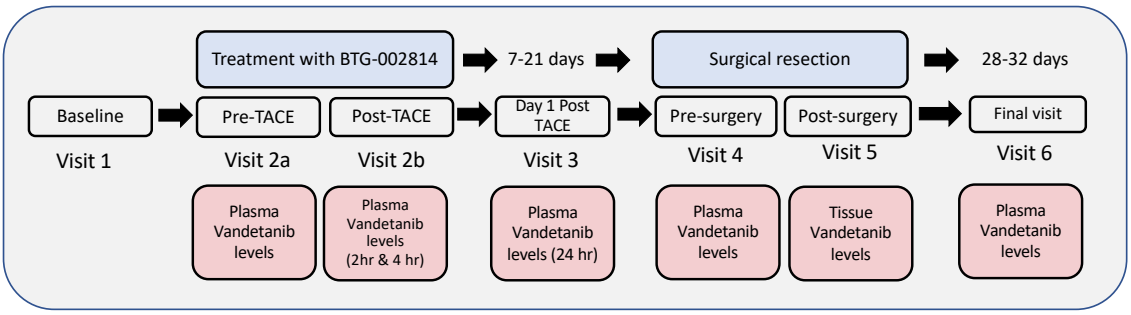

Figure 2: Trial schema overview for the VEROnA trial with pharmacokinetic sampling timepoints.

Time was measured from the start of the BTG-002814 infusion during the TACE procedure. At each time point for analyses, whole blood was collected into a 6 ml Vacutainer© tube containing lithium heparin. Immediately following collection, the blood tube was gently inverted multiple times to ensure that the anticoagulant had adequately mixed with the blood sample. Within 30 minutes of collection the sample was centrifuged at 1000 x g for 10 minutes at 4°C. 0.5 ml of the plasma was then pipetted into two labelled 1.8 ml cryovials. The cryovials were then stored at -70°C (or below) within 60 minutes of collection. Plasma vandetanib and N-desmethyl vandetanib concentrations were determined using solid phase extraction followed by liquid chromatography coupled to mass spectrometry. All analyses were performed by Andrew Wills and Niall Harvey at York Bioanalytical Solutions Ltd, York, United Kingdom.

In brief, cryovials of plasma were thawed to room temperature. 25 µl of each sample was pipetted into a 2 ml 96-well plate, along with control plasma, quality control (QC) samples and calibration standards. 50 µL of an internal standard was added to all wells (except blanks) which received 50 µL of methanol/water (MeOH:H20 30:70). The wells were mixed at 1000 rpm for 1 minute, and then 100 µL of formic acid (FA, 0.2%) in ammonium formate (10 mM) was added prior to repeat mixing.

An Oasis micro elution Hydrophilic-Lipophilic-Balanced (HLB) plate was conditioned with 200 µL of MeOH to activate the plate and equilibrated with 200 µL of water (to wash the methanol off). Plasma samples were then loaded onto the plate. The plate was then washed with 100 µl of MeOH:FA (0.2%) in ammonium formate (10mM), and samples eluted onto a 2 ml plate with 50 µl FA in acetonitrile(MECN):H20:ammonim formate (IM) (90:10:0.2). 250 µL of FA (0.2%) in MECN:H20: ammonium formate (1M) (90:10:0.2) was then added, mixed and submitted for analysis.

Separation was achieved using a 5 µL injection into a Thermo Accucore HILIC 50 x 3 mm 2.6 µm analytical column run at 40°C, using FA (0.2 %) in acetonitrile: water: ammonium formate (1 M) mobile phases at 0.6 ml/min. Vandetanib, N-desmethyl vandetanib and labelled analytical/internal standards were used as reference standards for the chromatography. Liquid chromatography was

coupled to tandem mass spectrometry (MDS API5000) using turbospray in positive ion, multiple reaction monitoring mode.

3.3.2.2 Liver tissue vandetanib levels

As part of the VEROnA study, 7-21 days after treatment with BTG-002814, all patients underwent surgical resection of the liver tumour(s). All liver resections were performed by the following surgeons: Professor Joerg-Matthias Pollok, Mr Dinesh Sharma and Professor Massimo Malago.

Following surgical resection, the liver specimen was immediately secured within a plastic bag and stored on ice in an insulated container before transfer to the pathologist (Dr Marnix Jansen) for sampling. Four samples were taken from each resected liver lesion from the following sites (Figure 3):

- Centre of tumour (1)
- In between centre and periphery (2)
- Periphery of the tumour (3)
- 1 cm away from tumour (normal liver tissue) (4)

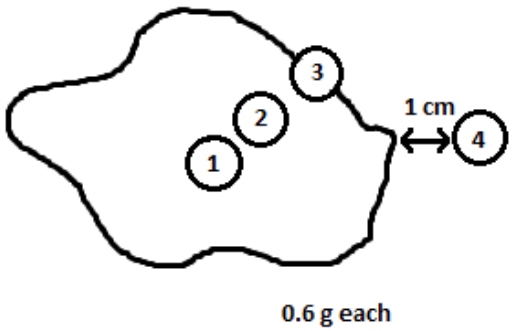

Figure 3. Location of samples taken for vandetanib levels from resected liver tumour. Centre of tumour (1), in between centre and periphery (2), periphery of the tumour (3) and 1 cm away from tumour (normal liver tissue) (4).

A minimum of 0.6 g of tissue per sample was required for each sample taken. Samples were immediately wrapped in foil and snap frozen into liquid nitrogen. The foiled samples were then stored at -80°C until transfer. Tissue vandetanib and N-desmethyl vandetanib were then determined using solid phase extraction followed by liquid chromatography coupled to mass spectrometry.

Prior to analysis, the liver tissue first needed to undergo homogenisation. This was performed by blending the thawed liver samples with dry ice until it formed a powder and allowing the dry ice to evaporate. A volume of methanol (in µl) corresponding to 100 times the weight of the liver (in g) was then added, followed by a volume of FA (0.2%) in MeOH-H2O 40:60 (an extractant agent) corresponding to 3 times the weight of the homogenised liver. The sample was then placed on an oscillator for 30 minutes at 300 rpm and centrifuged for 10 minutes at 3000 g at 4^0C.

The processed liver samples underwent solid phase extraction as previously outlined. In this case, 50 µl of the processed liver, QC samples, control liver and calibration standards were aliquoted onto a 2 ml 96-well plate. Each well was diluted with 600 µl of FA (0.2%) in ammonium formate (10mM) and mixed at 1000 rpm followed by centrifugation at 4000 rpm for 10 minutes at 4^0C. The Oasis micro-elution HLB plate was conditioned with 200 µl of MeOH and equilibrated with 200 µl FA (0.2%) in ammonium formate (10mM). After loading of the processed liver samples, the plates were washed with 100 µl of FA (0.2%) in ammonium formate (10mM) and then 100 µl of MeOH:FA (0.2%) in ammonium formate (10mM) 10:90 followed by a wash of 100 µl of MeOH:FA (0.2%) in ammonium formate (10mM) 30:70. Samples were then eluted onto a 1 ml plate with 2 x 100 µl FA (0.2%) in MeCN:H20:ammonium formate (1M) 90:10:0.2. Following a final vortex for 2 minutes at 600 rpm samples were submitted for analysis.

Separation was achieved using a 10 µL injection into a Thermo Accucore HILIC 50 x 3 mm 2.6 µm analytical column run at 50°C, using formic acid (0.2 %) in acetonitrile: water: ammonium formate (1 M) mobile phases at 0.6 ml/min. Vandetanib, N-desmethyl vandetanib and labelled analytical/internal standards were used as reference standards for the chromatography. Liquid

chromatography was coupled to tandem mass spectrometry (MDS API5000) using turbospray in positive ion, multiple reaction monitoring mode.

3.4 RESULTS

3.4.1 Patient selection

Eight patients were successfully treated with BTG-002814 as part of the VEROnA study, as outlined in full detail in Chapter 2 (Section 2.4). Plasma samples for vandetanib and N-desmethyl vandetanib were collected at all time points

3.4.2 Protocol violations on vandetanib plasma and tissue sampling

For patient 1, the post-treatment (visit 2) blood sample for vandetanib was taken one hour later than the protocol-specified 2 hours post-treatment timepoint, and 10 minutes later than the protocol specified 4 hours post-treatment timepoint. Furthermore, the visit 3 blood samples for vandetanib (24 hours after treatment) were taken 55 minutes early as the patient was unable to stay later. For patient 2, the post-treatment (visit 2) blood samples for vandetanib levels were taken 24 minutes later than the protocol-specified 2 hours post-treatment timepoint and 1 hour 20 minutes outside the protocol-specified window of 4 hours post-treatment due to poor venous access and clotting of the samples. For patient 7, surgical resection, and therefore tissue sampling for vandetanib, occurred 32 days post-treatment with BTG-002814, which was outside of the protocol-specified period of 7-21 days. This was due to non-availability of Intensive Treatment Unit beds.

3.4.3 Plasma VTB and N-VTB results

Plasma vandetanib and N-desmethyl vandetanib concentrations were measured for each patient at the following timepoints: pre-treatment, 2 hours, 4 hours, 24 hours, prior to surgery, and end-of-study (Table 2).

Table 2. Plasma vandetanib and N-desmethyl vandetanib levels

Patient	Timepoint	Vandetanib concentration (ng/mL)*	N-desmethyl vandetanib concentration (ng/ml)*
1	Pre-treatment	<LLOQ<(1.00)	<LLOQ<(1.00)
1	2 hours	18.3	<LLOQ<(1.00)
1	4 hours	17.7	<LLOQ<(1.00)
1	24 hours	17.0	<LLOQ<(1.00)
1	Prior to surgery	9.14	<LLOQ<(1.00)
1	End-of-study	1.77	<LLOQ<(1.00)
2	Pre-treatment	<LLOQ<(1.00)	<LLOQ<(1.00)
2	2 hours	33.2	1.81
2	4 hours	15.4	1.27
2	24 hours	14.4	1.09
2	Prior to surgery	6.51	<LLOQ<(1.00)
2	End of study	<LLOQ<(1.00)	<LLOQ<(1.00)
3	Pre-treatment	<LLOQ<(1.00)	<LLOQ<(1.00)
3	2 hours	25.6	1.59
3	4 hours	19.8	<LLOQ<(1.00)
3	24 hours	19.3	<LLOQ<(1.00)
3	Prior to surgery	8.44	<LLOQ<(1.00)
3	End-of-study	2.83	<LLOQ<(1.00)
4	Pre-treatment	<LLOQ<(1.00)	<LLOQ<(1.00)
4	2 hours	41.7	<LLOQ<(1.00)
4	4 hours	24.8	<LLOQ<(1.00)
4	24 hours	16.2	<LLOQ<(1.00)
4	Prior to surgery	18.1	<LLOQ<(1.00)
4	End-of-study	3.12	<LLOQ<(1.00)
5	Pre-treatment	<LLOQ<(1.00)	<LLOQ<(1.00)
5	2 hours	10.8	<LLOQ<(1.00)
5	4 hours	11.3	<LLOQ<(1.00)
5	24 hours	10.5	<LLOQ<(1.00)
5	Prior to surgery	12.5	<LLOQ<(1.00)
5	End-of-study	1.34	<LLOQ<(1.00)
6	Pre-treatment	<LLOQ<(1.00)	<LLOQ<(1.00)
6	2 hours	6.61	<LLOQ<(1.00)
6	4 hours	5.03	<LLOQ<(1.00)
6	24 hours	3.88	<LLOQ<(1.00)

Patient	Timepoint	Vandetanib concentration (ng/mL)*	N-desmethyl vandetanib concentration (ng/ml)*
6	Prior to surgery	2.07	<LLOQ<(1.00)
6	End-of-study	<LLOQ<(1.00)	<LLOQ<(1.00)
7	Pre-treatment	<LLOQ<(1.00)	<LLOQ<(1.00)
7	2 hours	12.4	<LLOQ<(1.00)
7	4 hours	13.0	<LLOQ<(1.00)
7	24 hours	11.2	<LLOQ<(1.00)
7	Prior to surgery	4.86	<LLOQ<(1.00)
7	Prior to surgery	1.84	<LLOQ<(1.00)
7	End-of-study	<LLOQ<(1.00)	<LLOQ<(1.00)
8	Pre-treatment	<LLOQ<(1.00)	<LLOQ<(1.00)
8	2 hours	43.3	1.30
8	4 hours	27.0	<LLOQ<(1.00)
8	24 hours	17.8	<LLOQ<(1.00)
8	Prior to surgery	17.5	1.12
8	End-of-study	1.84	<LLOQ<(1.00)

*Vandetanib and N-desmethyl vandetanib plasma levels are reported at each trial time point. For both vandetanib and N-desmethyl vandetanib the lower limit of quantification (LLOQ) was 1.00 ng/ml.

From this data, pharmacokinetic parameters C_{max} (maximum concentration), T_{max} (time to maximum concentration) and AUC_{EoS} (area under the curve until end of study) were derived. This analysis was performed by Samantha Ryan at BTG (Table 3).

Mean C_{max} of vandetanib for all patients was 24.3 ng/ml (SD 13.94) and was approximately the same for HCC and mCRC patients, 25.8 ng/mL and 23.8 ng/mL respectively. For the patients that did not receive the full planned dose of vandetanib, as stasis was achieved after administration of 40% and 90% of the dose, C_{max} was notably lower. For patient 6 this was 6.6 ng/ml (40% dose) and for patient 7.13 ng/ml (90% dose). Median T_{max} was 2 hours (range 2-192 hours). Although most patients reached T_{max} at the 2-hour or 4-hour timepoint, in patient 5, T_{max} was 192 hours. However, the plasma vandetanib level did not change considerably from 2 hours (10.8 ng/ml) to 192 hours (12.5 ng/ml) post-

treatment in this patient (Table 3). Vandetanib was present in the plasma of all patients at visit 4 (pre-surgery) and in six patients (75%) at the end-of-study visit. Overall, vandetanib remained measurable in the plasma for a median of 36 days (range 12-45 days).

Mean AUC_{EoS} values were similar for HCC and mCRC patients, 6827.4 ng/h/ml and 7030.0 ng/h/ml respectively. However, as anticipated, lower levels were seen in patients 6 and 7 who received 40% and 90% of the dose (Table 3). Plasma vandetanib concentration-over-time graphs for each patient are presented in Figure 4.

Table 3: Vandetanib plasma pharmacokinetic parameters

	Dose of BTG-002814 delivered (ml)	C_{max} (ng/mL)	T_{max} (hours)	AUC_{EoS} (ng*h/mL)
Patient 1 (HCC)	1.0	18.3	2.0	8093.1
Patient 2 (HCC)	1.0	33.2	2.0	5561.6
Patient 3 (mCRC)	1.0	25.6	2.0	9179.5
Patient 4 (mCRC)	1.0	41.7	2.0	10215.4
Patient 5 (mCRC)	1.0	12.5	1920	8161.8
Patient 6 (mCRC)	0.4	6.6	2.0	1684.5
Patient 7 (mCRC)	0.9	13.0	4.0	3105.1
Patient 8 (mCRC)	1.0	43.3	2.0	9833.5
HCC mean (SD)		25.8 (10.54)	2.0 (0.00)	6827.4 (1789.98)
HCC median		25.8	2.0	6827.4
HCC range		18.3 - 33.2	2.2	5561.64 - 8093.06
mCRC mean (SD)		23.8 (15.77)	34.0 (77.41)	7030.0 (3684.76)
mCRC median		19.3	2.0	8670.7
mCRC range		6.61, 43.3	2, 192	1684.51-10215.4
Overall mean (SD)		24.3 (13.94)	26.0 (67.08)	6979.3 (3188.21)
Overall median		22.0	2.0	8127.4
Overall range		6.61 - 43.3	2 -192	1684.51-10215.4

Notes: Vandetanib pharmacokinetic parameters are summarized for each patient. Where C_{max} occurred at more than one timepoint, the earliest timepoint was reported as T_{max}. For example, where the concentration was below LLOQ for all timepoints, T_{max} was reported as pre-treatment (the earliest timepoint).

Patient 1:

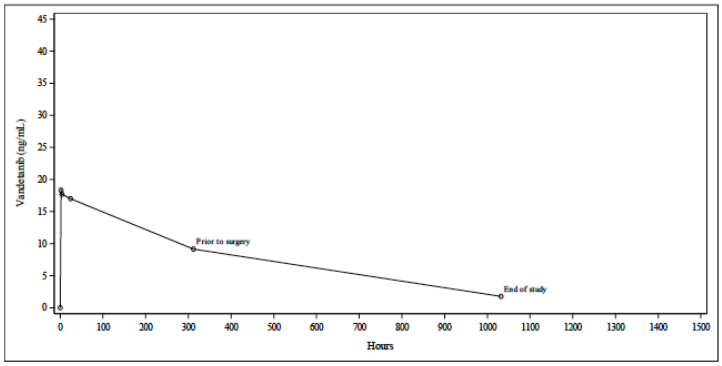

Patient 2:

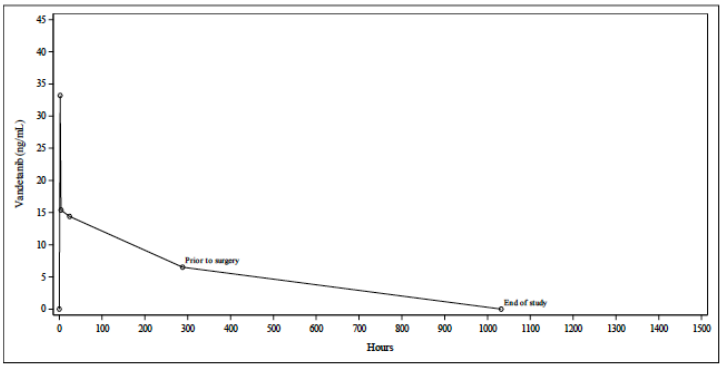

Patient 3

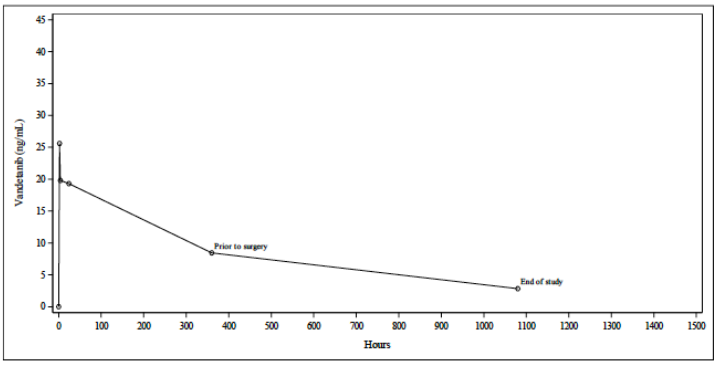

Figure 4a: Graphs of plasma vandetanib against time (hours) for each patient. Plasma vandetanib concentrations are plotted against time-of-sampling (hours) calculated from the start of the treatment with BTG-002814 (0 hours) to the end-of-study visit.

Patient 4:

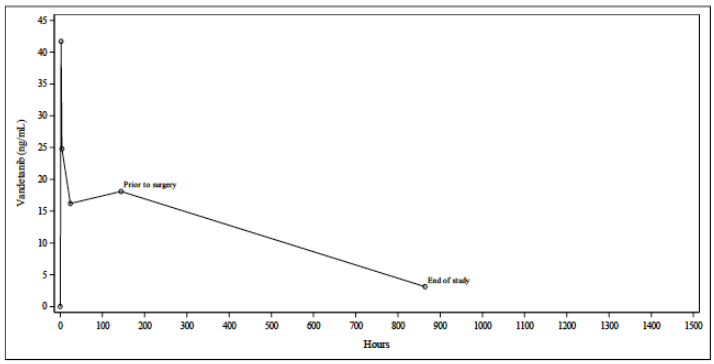

Patient 5:

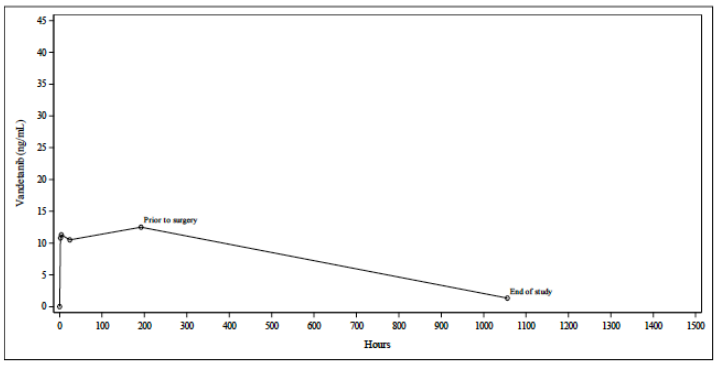

Patient 6:

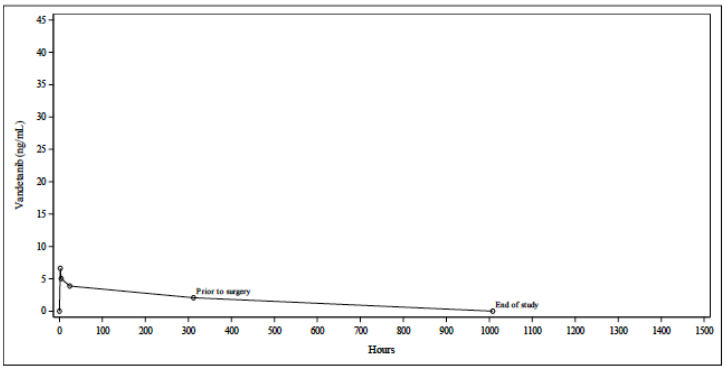

Figure 4b: Graphs of plasma vandetanib against time (hours) for each patient. Plasma vandetanib concentrations are plotted against time-of-sampling (hours) calculated from the start of the treatment with BTG-002814 (0 hours) to the end-of-study visit

Patient 7:

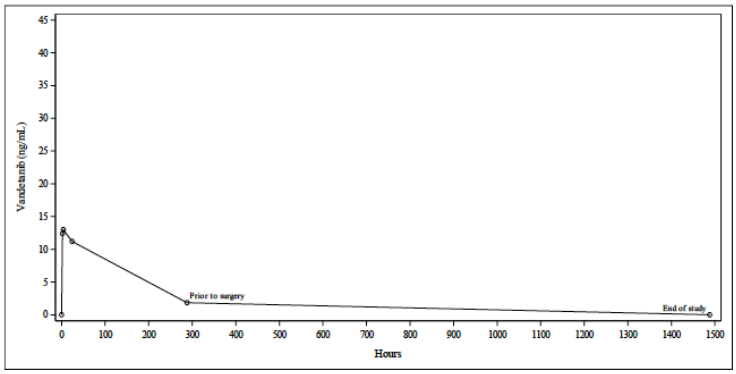

Patient 8:

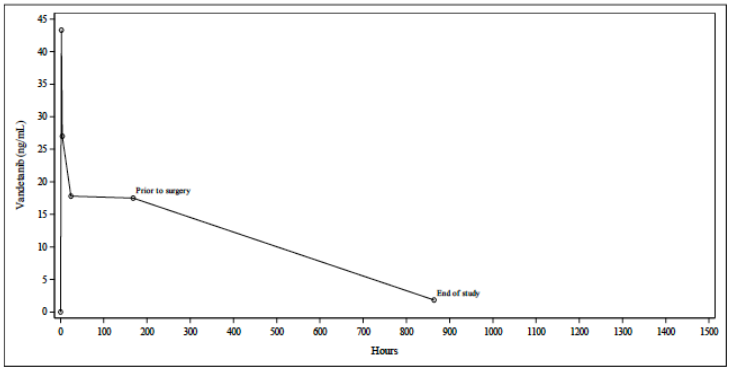

Figure 4c: Graphs of plasma vandetanib against time (hours) for each patient. Plasma vandetanib concentrations are plotted against time-of-sampling (hours) calculated from the start of the treatment with BTG-002814 (0 hours) to the end-of-study visit

In comparison to vandetanib levels, N-desmethyl vandetanib concentrations were low, with 5/8 (62.5%) patients having plasma concentrations below the lower level of quantification (LLOQ) at all time points. For those patients with measurable plasma concentrations the C_{max} values were similar, with a mean of 0.6 ng/ml (SD 0.82), and median T_{max} was 2 hours (range 0-2 hours) (Table 4). Plasma N-desmethyl vandetanib concentration-over-time graphs for those patients with measurable level (patients 2, 3 and 8) are presented in Figure 5.

Table 4: N-desmethyl vandetanib plasma PK levels for all patients

	Dose of BTG-002814 delivered (ml)	C_{max} (ng/mL)	T_{max} (hours)	AUC_{EoS} (ng*h/mL)
Patient 1 (HCC)	1.0	0.0	0.0	0.0
Patient 2 (HCC)	1.0	1.8	2.0	172.4
Patient 3 (mCRC)	1.0	1.6	2.0	3.2
Patient 4 (mCRC)	1.0	0.0	0.0	0.0
Patient 5 (mCRC)	1.0	0.0	0.0	0.0
Patient 6 (mCRC)[a]	0.4	0.0	0.0	0.0
Patient 7 (mCRC)[b]	0.9	0.0	0.0	0.0
Patient 8 (mCRC)	1.0	1.3	2.0	473.0
HCC mean (SD)		0.9 (1.28)	1.0 (1.41)	86.2 (121.88)
HCC median		0.9	1.0	82.2
HCC min, max		0, 1.81	0, 2	0, 172.37
mCRC mean (SD)		0.5 (0.75)	0.7 (1.03)	79.4 (192.85)
mCRC median		0.0	0.0	0.0
mCRC min, max		0, 1.59	0, 2	0, 473
Overall mean (SD)		0.6 (0.82)	0.8 (1.04)	81.1 (169.40)
Overall median		0.0	0.0	0.0
Overall min, max		0-1.81	0-2	0-473

Notes: N-desmethyl vandetanib pharmacokinetic parameters are summarized for each patient Where C_{max} occurred at more than one timepoint, the earliest timepoint was reported as T_{max}. For example, where the concentration was below LLOQ for all timepoints, T_{max} was reported as Pre-treatment (the earliest timepoint).

Patient 2:

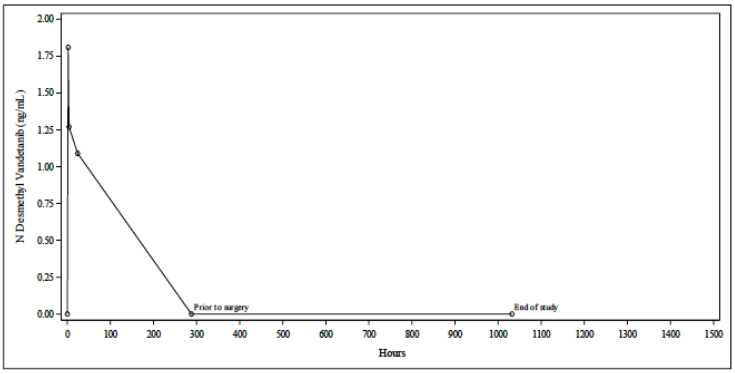

Patient 3:

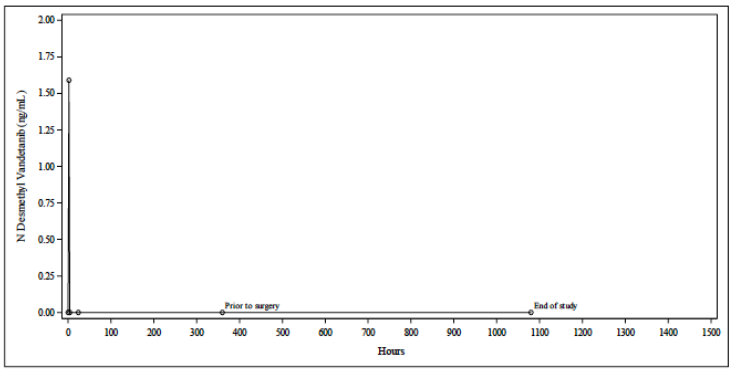

Patient 8:

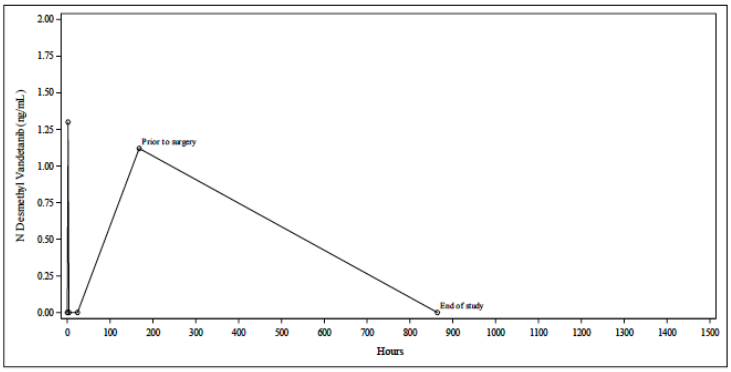

Figure 5: Graphs of plasma N-desmethyl vandetanib against time for patients 2, 3 and 8 (no levels recorded in patients 1, 4, 5, 6 and 7). Plasma vandetanib concentrations are plotted against time-of-sampling (hours) calculated from the start of the treatment with BTG-002814 (0 hours) to the end-of-study visit.

3.4.4 Tissue VTB and N-VTB results

Median time from treatment with BTG to liver resection was 14.0 days (range, 7-32 days). After resection, vandetanib and N-desmethyl vandetanib concentrations were measured at the centre, middle, and edge of the tumour, as well as in the normal tissue surrounding all treated tumour. Tissue vandetanib and N-desmethyl vandetanib levels were available for six of the eight patients in this study (75%). In one patient, samples were unavailable due to errors in fixating the sample (patient 2). For one patient, the resected tumour was too small to take additional trial samples (patient 4). Vandetanib tissue and N-desmethyl concentrations are shown in Figures 6 and 7 and Table 5 for the six patients (eight tumours) with results available.

For seven of the eight tumours assessed, vandetanib concentrations were highest in the tumour when compared to levels in the normal surrounding tissue (1 cm away from the tumour). Conversely, N-desmethyl vandetanib levels were highest in the normal tissue in six of the eight resected tumours. In the five patients with a single tumour, vandetanib concentrations were highest at the centre of the tumour in three patients (patients 1,6 and 7) and at the edge of tumour in two patients (patients 3 and 5). N-desmethyl vandetanib concentrations were highest in the middle of the tumour in two patients (patients 1 and 6), and in the surrounding normal tissue in two patients (patients 5 and 7). Patient 8 had liver data from three tumours treated with BTG-002814. The largest tumour (tumour 1) had the highest vandetanib and N-desmethyl vandetanib concentrations in the surrounding normal tissue as opposed to within the tumour. The second largest tumour (tumour 2) had the highest vandetanib concentration in the centre of the tumour, but values for the concentration at the centre and the normal surrounding tissue were close at 6180 ng/ml and 6010 ng/ml, respectively. N-desmethyl vandetanib concentrations for this tumour (tumour 2) were highest in the normal tissue. The smallest tumour (tumour 3) was 1 cm in diameter, so concentrations were measured for the entire lesion and 1 cm away from the lesion in the normal surrounding tissue. Vandetanib concentration was much higher in the lesion than the tissue 1 cm away, but the N-desmethyl concentration in the normal tissue was higher.

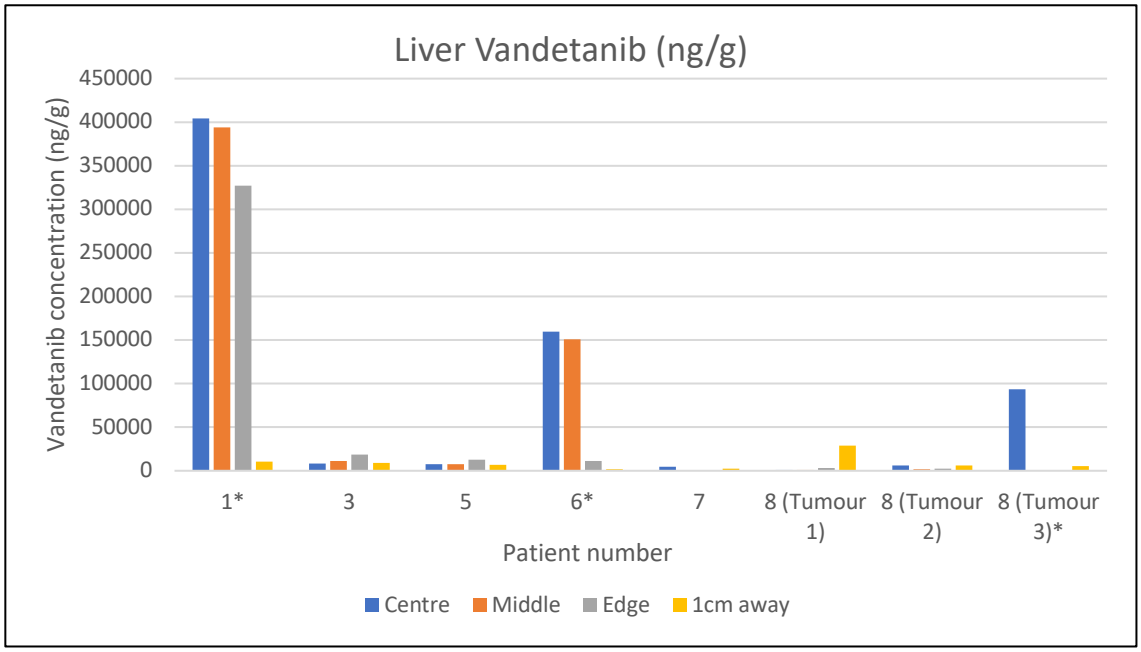

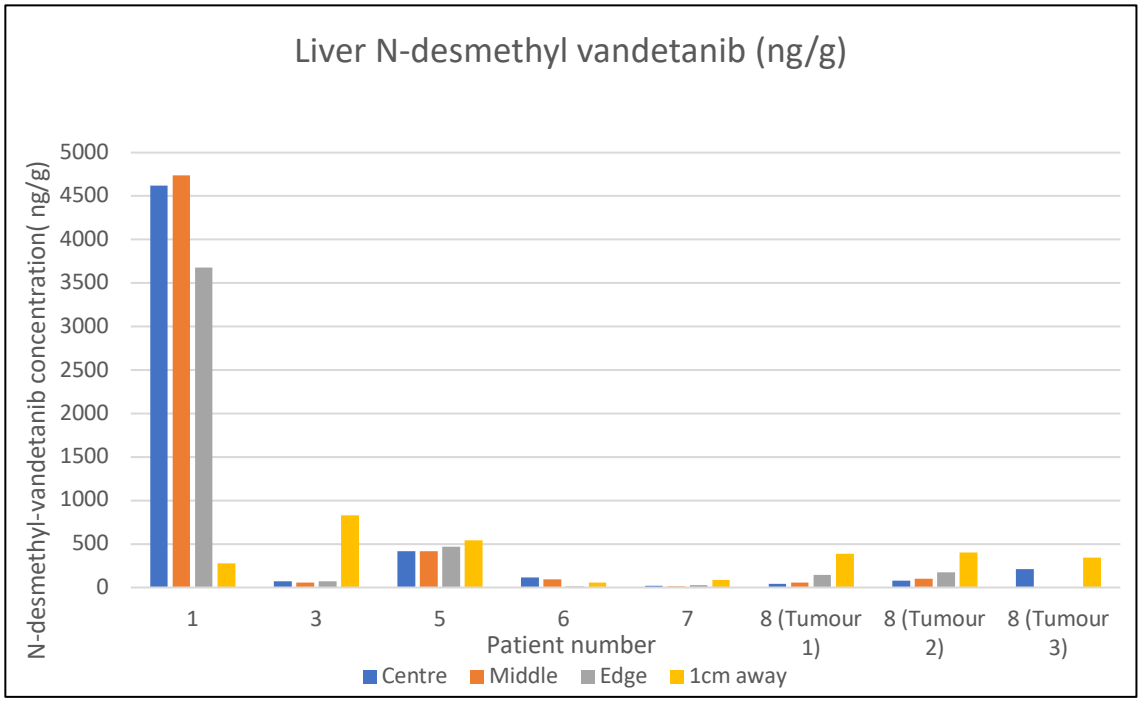

Figures 6a and b: Tissue levels of vandetanib and N-desmethyl vandetanib by patient. Levels of vandetanib and N-desmethyl vandetanib are shown for each patient by area of tumour sampled and compared on the same scale. Of note, patient 8 had three tumours sampled but due to the small size of tumour 3, samples were too small to separate out by location so the sample reflects the whole tumour. *Extrapolated value as levels above the upper limit of quantification (60000 ng/g).

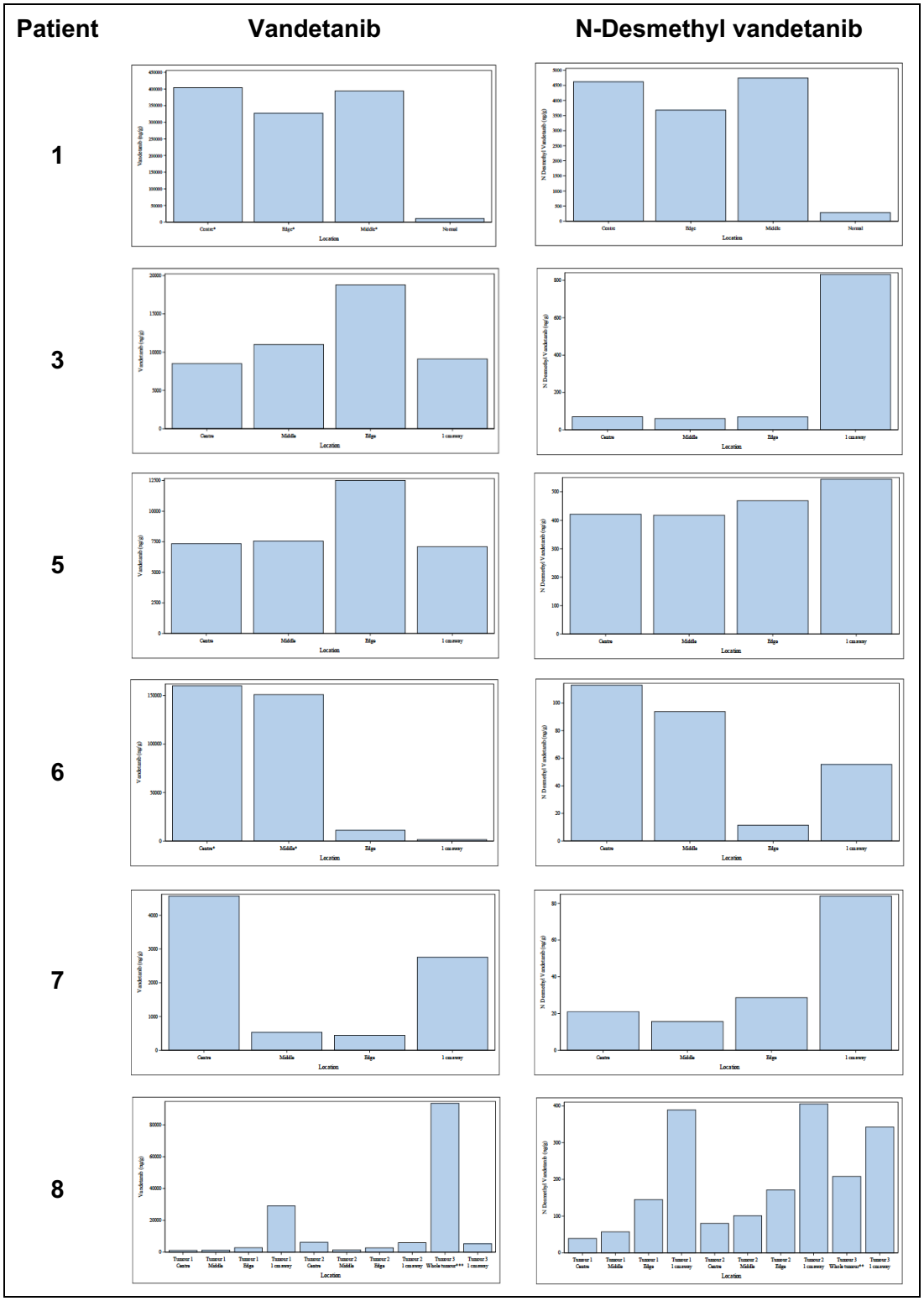

Figure 7: Variation in vandetanib and N-desmethyl vandetanib by location within tumour. Levels of vandetanib and N-desmethyl vandetanib are shown for each patient, and as a result are on different scales. Of note, patient 8 had three tumours sampled but due to the small size of tumour 3, samples were too small to separate out by location so the sample reflects the whole tumour. *Extrapolated value as levels above the upper limit of quantification.

Table 5. Tissue vandetanib and N-desmethyl vandetanib concentrations by location

Patient	Tumour number	Location	Vandetanib concentration (ng/g)	N-desmethyl vandetanib concentration (ng/g)
1	NA	Centre	404000*	4620
1	NA	Middle	394000*	4740
1	NA	Edge	327000*	3680
1	NA	1cm away	10800	280
2	NA	Centre	NR	NR
2	NA	Middle	NR	NR
2	NA	Edge	NR	NR
2	NA	1cm away	NR	NR
3	NA	Centre	8510	69.6
3	NA	Middle	11000	59.8
3	NA	Edge	18800	69.2
3	NA	1cm away	9120	831
4	NA	Centre	NS	NS
4	NA	Middle	NS	NS
4	NA	Edge	NS	NS
4	NA	1cm away	NS	NS
5	NA	Centre	7340	421
5	NA	Middle	7550	418
5	NA	Edge	12500	469
5	NA	1cm away	7090	544
6	NA	Centre	160000*	113
6	NA	Middle	151000*	93.9
6	NA	Edge	11100	11.4
6	NA	1cm away	1480	55.6
7	NA	Centre	4570	21.0
7	NA	Middle	531	15.7
7	NA	Edge	441	28.7
7	NA	1cm away	2760	84.0
8	1	Tumour Centre	1140	39.3
8	1	Middle	1240	57.1
8	1	Edge	2840	145

Patient	Tumour number	Location	Vandetanib concentration (ng/g)	N-desmethyl vandetanib concentration (ng/g)
8	1	1cm away	29100	389
8	2	Tumour Centre	6180	80.2
8	2	Middle	1440	101
8	2	Edge	2710	171
8	2	1cm away	6010	405
8	3	Whole tumour	93500*	208
8	3	1cm away	5350	342

Notes: Vandetanib and N-desmethyl vandetanib tissue levels are reported from four locations for each tumour. For both tissue vandetanib and N-desmethyl vandetanib levels the lower limit of quantification was 0.150 ng/g. The upper limit of validation for vandetanib was 60,000 ng/g. Therefore data is extrapolated for measurements in patients 1,6 and 8 (*).

3.5 DISCUSSION

In this first-in-human study of BTG-002814, vandetanib was detected in the plasma of all patients following treatment, at a median of 36 days (range 12-45 days). As the peak concentration of vandetanib was evident 2 hours after treatment, with a mean C_{max} of 24.3 ng/ml (SD 13.94), it appears as though there was a low burst release of vandetanib in the first few hours following administration. This was also seen in the pre-clinical porcine study of vandetanib-eluting beads, where a T_{max} of 1 hour was reported and C_{max} ranged from 6.19-17.3 ng/ml for the three doses of vandetanib studied (36 mg, 72 mg and 120 mg) [17].

In comparison to oral delivery, the systemic concentration of vandetanib is far lower when delivered by DEB-TACE. In a Phase 1 study of oral vandetanib in Japanese patients with advanced solid tumours, the mean C_{max} following a single dose of 100 mg vandetanib was 103 ng/mL (SD 42), and median T_{max} was 6 hours [12]. The difference in systemic concentration of vandetanib is, however, expected due to the different mechanisms between oral and DEB delivery of vandetanib. The design of DEBs means that the loaded vandetanib drug elutes from the bead slowly over time directly into the adjacent tumour cells. Although a peak is seen at 2 hours, assuming a blood volume of 5 litres and minimal

metabolism and elimination in the first 2 hours, the concentrations seen in the plasma represent around 0.12% of the loaded drug. As anticipated, following local delivery, minimal free drug enters the systemic circulation. These findings are in keeping with those of vandetanib-loaded beads in the porcine model in which <0.1% of the loaded drug was detected within the first hour [17]. Furthermore, studies of doxorubicin-loaded beads show a similar low burst release with 0.5-6% of the loaded dose being detectable in the plasma in the first few hours post-TACE [19]. This slow and sustained release system is highly desirable particularly when adverse effects of drugs are seen with oral delivery.

As a result of the local delivery and sustained drug release, vandetanib and its major metabolite, N-desmethyl vandetanib, were measurable in the resected liver tissue up to 32 days following treatment with BTG-002814. For all patients with tissue levels available (with the exception of one tumour for patient 8), the highest levels of vandetanib were seen located within the tumour (with variation from centre, mid and edge of tumour locations). In four of the six patients, the highest levels of N-desmethyl vandetanib were recorded 1 cm away from the tumour, in the normal surrounding tissue. For the other two patients, the highest N-desmethyl vandetanib levels were seen within the tumour itself, demonstrating that the drug is metabolised in normal liver as well as in tumours. As N-desmethyl vandetanib has a similar inhibitory activity against VEGFR-1, VEGFR-2, EGFR and FGFR-1 compared to vandetanib the presence of this metabolite in the target tissue up to 32 days post-surgery is useful from a locoregional efficacy perspective [17].

In addition to the variation of vandetanib concentrations between the tumour and normal liver, there is also considerable variation in the vandetanib concentrations between the patients in this trial, as shown in Figure 8. In particular high doses are seen in patient 1, patient 6 and in the smallest of the three tumours treated in patient 8. This is particularly interesting in the case of patient 6 in which just 40% of the dose was delivered. This variation in distribution and levels of vandetanib (and N-desmethyl vandetanib) may therefore not just reflect the dose of vandetanib delivered but also the proximity of the beads to the tumour, as although TACE involves depositing the beads in the vessels feeding the tumour, direct access into these vessels can vary depending on the size of the tumour

and underlying histology. For example, highly selective TACE is often possible with more hypervascular HCC tumours when compared to the more hypovascular metastases from colorectal cancer.

The variation in plasma N-desmethyl levels seen across the patients in this study is also interesting as plasma levels were only detectable in 3 patients. Although this is likely to reflect the limited amount of metabolised drug that enters the systemic circulation following local delivery, it may also reflect the fact that that N-desmethyl vandetanib is not in fact the major metabolite. N-desmethyl vandetanib was chosen, because it is known that N-desmethyl vandetanib is the major metabolite when vandetanib is given orally. It may be possible that N-oxide is the major metabolite following intra-arterial delivery, although this was not demonstrated in pre-clinical studies [17]. Furthermore, N-desmethyl vandetanib was detected in the liver specimen of all patients sampled. Pharmacokinetic studies in healthy volunteers have also shown that following oral absorption, excretion is via urine and faeces, underlying the importance of two routes of elimination. It may be that after intra-arterial administration some excretion is perhaps biliary and not entirely via the renal route.

We have shown in this study that vandetanib is delivered to the tumour following DEB-TACE delivery, but the question then arises as to whether the concentrations of vandetanib achieved in and around the tumour are high enough to induce the desired antitumoral effect. The activity of anti-neoplastic drugs is classically assessed in vitro in cell cultures, by measuring the concentration that gives a 50% decrease of cell proliferation (IC50). In vitro studies on human umbilical vein endothelial cell (HUVEC) proliferation have reported IC50 levels of 0.06 μM for VEGF and 0.17 μM for EGFR [1]. In comparison, concentration of vandetanib found in the liver tumours in this study ranged from 441 ng/g to 404,000 ng/g, equating to 0.928 μM to 850 μM. The average across all tumours is 155 μM which is higher than the levels seen in the porcine study, where at doses of 100 mg concentrations of 0.22 μM were reported [17].

There are limitations to note in this study. Firstly, this study was not designed with multiple time points for plasma sampling immediately after treatment with BTG-002814. As such we only have plasma levels at six time points, with just three of

them being in the first 24 hours post-treatment. As such, the time to maximum concentration may not have been sampled. It could have in fact been at 1 hour, as seen in the pre-clinical porcine model, whereas the earliest time point in this study was at 2 hours. Furthermore, there were violations in the collection of plasma samples for two patients that may have had some impact on these results. Although eight patients were enrolled into this study, tissue data was only available for six patients due to errors in sampling for one patient, and the tumour being too small to take trial samples in another. Furthermore, the underlying histology varied between patients, with two patients having a diagnosis of HCC (and underlying cirrhosis) and six patients of mCRC. This may have impacted blood flow to the tumour, and the resulting metabolism of vandetanib in the liver.

Finally, there was a variation in time between treatment with BTG-002814 and tissue sampling, which ranged from 7 to 32 days. Although in porcine studies, vandetanib was detected at 30 and 90 days following intra-arterial delivery, the levels of drug detected are likely to be affected by time. However, in this small cohort, no clear correlation was found between vandetanib levels in the tumour and time from treatment. This may however become apparent in larger clinical trials.

3.6 CONCLUSION

In conclusion, the pharmacokinetic studies of BTG-002814 in the VEROnA study showed a rapid absorption of vandetanib but lower plasma concentrations following transarterial administration when compared to oral delivery. Vandetanib and N-desmethyl vandetanib were present in all resected specimens, up to 32 days following treatment with BTG-002814, demonstrating sustained release from the loaded beads and metabolism within the liver. Levels of vandetanib are within range to provide efficacy.

3.7 REFERENCES

[1] Ryan AJ, Wedge SR. ZD6474--a novel inhibitor of VEGFR and EGFR tyrosine kinase activity. Br J Cancer. 2005;92 Suppl 1:S6-13.
[2] Ferrara N. Vascular endothelial growth factor as a target for anticancer therapy. Oncologist. 2004;9 Suppl 1:2-10.
[3] Kowanetz M, Ferrara N. Vascular endothelial growth factor signaling pathways: therapeutic perspective. Clin Cancer Res. 2006;12:5018-22.
[4] Wells SA, Jr., Robinson BG, Gagel RF, Dralle H, Fagin JA, Santoro M, et al. Vandetanib in patients with locally advanced or metastatic medullary thyroid cancer: a randomized, double-blind phase III trial. J Clin Oncol. 2012;30:134-41.
[5] Wells SA, Jr., Gosnell JE, Gagel RF, Moley J, Pfister D, Sosa JA, et al. Vandetanib for the treatment of patients with locally advanced or metastatic hereditary medullary thyroid cancer. J Clin Oncol. 2010;28:767-72.
[6] Natale RB, Thongprasert S, Greco FA, Thomas M, Tsai CM, Sunpaweravong P, et al. Phase III trial of vandetanib compared with erlotinib in patients with previously treated advanced non-small-cell lung cancer. J Clin Oncol. 2011;29:1059-66.
[7] Herbst RS, Sun Y, Eberhardt WE, Germonpre P, Saijo N, Zhou C, et al. Vandetanib plus docetaxel versus docetaxel as second-line treatment for patients with advanced non-small-cell lung cancer (ZODIAC): a double-blind, randomised, phase 3 trial. The Lancet Oncology. 2010;11:619-26.
[8] Hsu C, Yang TS, Huo TI, Hsieh RK, Yu CW, Hwang WS, et al. Vandetanib in patients with inoperable hepatocellular carcinoma: a phase II, randomized, double-blind, placebo-controlled study. Journal of hepatology. 2012;56:1097-103.
[9] Martin P, Oliver S, Kennedy SJ, Partridge E, Hutchison M, Clarke D, et al. Pharmacokinetics of vandetanib: three phase I studies in healthy subjects. Clin Ther. 2012;34:221-37.
[10] Weil A, Martin P, Smith R, Oliver S, Langmuir P, Read J, et al. Pharmacokinetics of vandetanib in subjects with renal or hepatic impairment. Clin Pharmacokinet. 2010;49:607-18.
[11] Holden SN, Eckhardt SG, Basser R, de Boer R, Rischin D, Green M, et al. Clinical evaluation of ZD6474, an orally active inhibitor of VEGF and EGF

receptor signaling, in patients with solid, malignant tumors. Ann Oncol. 2005;16:1391-7.
[12] Tamura T, Minami H, Yamada Y, Yamamoto N, Shimoyama T, Murakami H, et al. A phase I dose-escalation study of ZD6474 in Japanese patients with solid, malignant tumors. J Thorac Oncol. 2006;1:1002-9.
[13] Cooper MR, Yi SY, Alghamdi W, Shaheen DJ, Steinberg M. Vandetanib for the treatment of medullary thyroid carcinoma. Ann Pharmacother. 2014;48:387-94.
[14] EASL Clinical Practice Guidelines: Management of hepatocellular carcinoma. Journal of hepatology. 2018;69:182-236.
[15] Van Cutsem E, Cervantes A, Adam R, Sobrero A, Van Krieken JH, Aderka D, et al. ESMO consensus guidelines for the management of patients with metastatic colorectal cancer. Ann Oncol. 2016;27:1386-422.
[16] Lewis AL, Holden RR. DC Bead embolic drug-eluting bead: clinical application in the locoregional treatment of tumours. Expert Opin Drug Deliv. 2011;8:153-69.
[17] Denys A, Czuczman P, Grey D, Bascal Z, Whomsley R, Kilpatrick H, et al. Vandetanib-eluting Radiopaque Beads: In vivo Pharmacokinetics, Safety and Toxicity Evaluation following Swine Liver Embolization. Theranostics. 2017;7:2164-76.
[18] Varela M, Real MI, Burrel M, Forner A, Sala M, Brunet M, et al. Chemoembolization of hepatocellular carcinoma with drug eluting beads: efficacy and doxorubicin pharmacokinetics. Journal of hepatology. 2007;46:474-81.
[19] Lewis AL, Taylor RR, Hall B, Gonzalez MV, Willis SL, Stratford PW. Pharmacokinetic and safety study of doxorubicin-eluting beads in a porcine model of hepatic arterial embolization. Journal of vascular and interventional radiology : JVIR. 2006;17:1335-43.

4 HISTOPATHOLOGICAL AND CYTOKINE RESPONSE FOLLOWING TREATMENT WITH BTG-002815

4.1 INTRODUCTION

4.1.1 Mechanism of action of transarterial chemoembolisation (TACE)

Conventional TACE involves the delivery of a cytotoxic drug directly into the arteries supplying liver tumours followed by an embolic agent to block the tumour's major source of nutrients. To increase the intra-tumoral concentrations and lower systemic concentrations of the cytotoxic agent, drug-eluting bead (DEB-TACE) has been developed [1, 2]. The rationale behind TACE is that tumour cells are killed by a combination of the cytotoxic effects of the drug delivered directly to the tumour and the ischaemic effect of embolisation [3].

Despite advances and technical refinements of TACE, including the introduction of DEB-TACE, the long-term survival of patients managed with TACE is generally poor, mainly as a result of the high rates of tumour recurrence. Understanding the mechanisms behind tumour recurrence and TACE failure are important factors in improving clinical outcomes post-TACE delivery. Improving the technique used for DEB-TACE by being able to visualise the beads on CT scans and by developing the ability to load new anti-cancer molecularly targeted drugs on to the beads, specifically vandetanib, are two important approaches to potentially improving the efficacy of TACE for patients with liver tumours.

In order to understand the mechanism of action of this novel combination it is vital to be able to assess the degree of necrosis within the tumour in response to treatment, to map out the location of the beads in relation to the tumour and identify key cytokines that can act as markers of response. It is also important to understand whether it is the embolic agent, or the systemic agent that induces necrosis. Although TACE has been shown to improve overall survival when compared to best supportive care in hepatocellular carcinoma [4, 5], no prospective trial has shown that TACE is superior to bland embolisation with regards to overall survival [6, 7]. However, improved response rates have been reported with TACE [6, 8, 9].

4.1.2 Mechanism of action of vandetanib

Vandetanib is an ATP mimetic small molecule that is an inhibitor of the tyrosine kinase activity of VEGFR-2, an endothelial cell receptor for vascular endothelial growth factor (VEGF). It also possesses activity against the epithelial growth factor receptor (EGFR) and REarranged during Transfection (RET) tyrosine kinases [10, 11]. By targeting both angiogenesis and EGFR- and RET-dependent tumour cell growth, it is hypothesised that the growth of tumours will be controlled, with relative sparing of normal tissues.

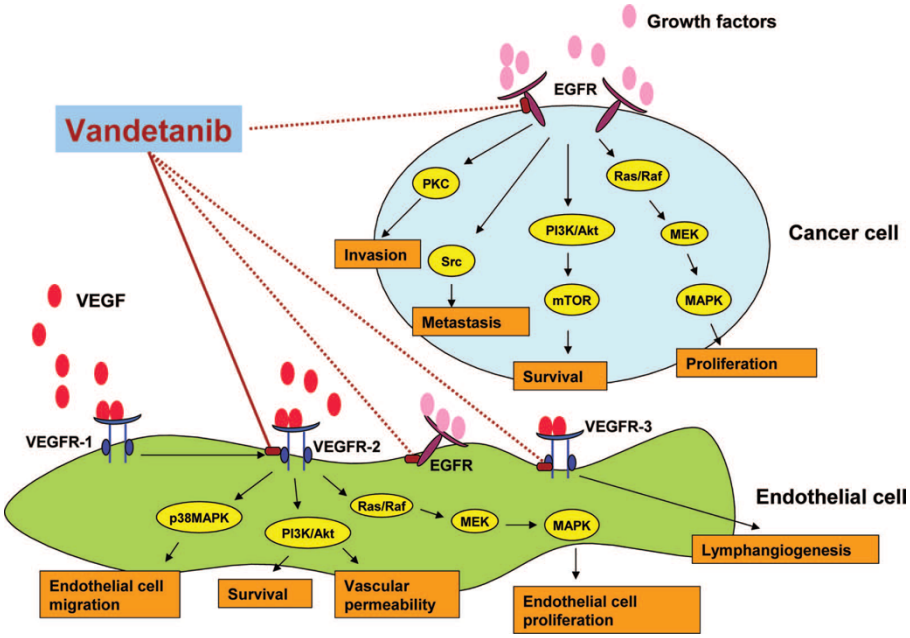

Figure 1: Mechanism of action of vandetanib [12]

Abbreviations: EGFR, epidermal growth factor receptor; MAPK, mitogen-activated protein kinase; MEK, MAPK/extracellular signal–related kinase; mTOR, mammalian target of rapamycin; PI3K, phosphatidylinositol 3 kinase; PKC, protein kinase C; VEGFR, vascular endothelial growth factor receptor.

4.1.2.1 VEGF pathway and angiogenesis

Vascular endothelial growth factor (VEGF/VEGF-A) belongs to the family of peptide growth factors. Other members of this family include VEGF-B, VEGF-C, VEGF-D and VEGF-E, in addition to placenta-derived growth factor (PlGF). There are three VEGF receptors, VEGFR-1, VEGFR-2 and VEGFR-3, each of which has intrinsic tyrosine kinase (TK) activity that is stimulated after ligand binding and receptor dimerisation. Following dimerisation, proteins that are active in

signal transduction cascades undergo phosphorylation. The actions of VEGF are mediated by binding to two of these receptors, VEGFR-1 and VEGFR-2 [13].

VEGFR-1 and VEGFR-2 are found predominantly on the surfaces of vascular endothelial cells, where they bind to VEGF with high affinity. The majority of angiogenic effects are attributed to the interaction of VEGF with VEGFR-2. VEGFR-1 is thought to function predominantly as a decoy receptor by regulating the amount of free VEGF available to activate VEGFR-2 because VEGFR-1 negatively regulates VEGF/VEGFR-2 interaction. A soluble form of VEGFR-1 (sVEGFR-1) can also bind with VEGF and subsequently inhibit VEGF-induced mitogenesis [13, 14]. VEGF-B and PlGF bind and activate VEGFR-1. VEGF-C and VEGF-D bind to VEGFR-3, located on lymphatic endothelium. Although binding to VEGFR-3 leads to the mediation of lymphangiogenesis, it is also recognised that VEGF-B and VEGF-C do show some activity toward VEGFR-2 [13-15]. The role of PlGF as a growth factor in angiogenesis remains controversial; however, gain- and loss-of-function experiments have shown that it may directly stimulate vessel growth and maturation and recruit pro-angiogenic bone marrow-derived progenitors and monocyte macrophage lineage cells [14].

Stimulation of the VEGF pathway ultimately leads to angiogenesis, the formation of new blood vessels. Pathogenic angiogenesis, the formation of new blood vessels within a tumour, is an essential process in cancer cell survival and tumour growth as, in order to grow, they require an ongoing supply of oxygen and nutrients. They can only maintain this supply by creating new blood vessels. This process therefore requires the recruitment of neighbouring blood vessels in addition to circulating endothelial precursor cells from the bone marrow to promote neovascularisation [13, 14].

Angiogenesis is regulated by a number of growth factors, such as VEGF and basic fibroblast growth factor (b-FGF) that are present in the microenvironment. Such factors can be produced by the tumours themselves, or by infiltrating macrophages and fibroblasts. The majority of activating compounds exert their actions through endothelial cell surface receptors, for which they serve as ligands, which ultimately leads to the secretion of additional angiogenic factors. Other factors such as hypoxia, mechanical stress and hypoglycaemia are also

recognised as triggers for angiogenesis. The entire process is complex and balanced by the production of antiangiogenic factors. The 'angiogenic switch', the process by which pro-angiogenic mechanisms overtake the negative regulators of angiogenesis, is well recognised as one of the hallmarks of cancer [16, 17].

Although a number of factors have been implicated in promoting angiogenesis, VEGF appears to play a vital role, due to its ability to regulate key steps in the angiogenesis cascade including inducing endothelial cell proliferation, migration, survival and capillary tube formation and increasing vascular permeability. Furthermore, high circulating plasma levels of VEGF have been shown to correlate with a poor prognosis in patients with a variety of solid malignancies [11]. The inhibition of angiogenesis by blocking VEGF receptors therefore represents a promising therapeutic approach to reducing tumour growth. The clinical importance of the VEGF signalling pathway in the development of solid cancers has already been demonstrated by the development and clinical use of the anti-VEGF monoclonal antibodies, such as bevacizumab. This has been demonstrated in patients with metastatic colorectal cancer, where the use of bevacizumab in combination with chemotherapy has led to an improvement in overall survival [18, 19]. Angiogenesis inhibition is particularly promising in the treatment of hepatocellular carcinoma (HCC), since HCC is characterised by hypervascularisation and neo-angiogenesis formation [20]. As such, sorafenib, an oral multi-tyrosine kinase inhibitor with anti-VEGF activity, is used as first-line systemic therapy after it was shown to prolong overall survival (OS) [21-23]. More recently, lenvatinib, an oral multi-kinase inhibitor that targets VEGF receptors 1–3, has been shown to be non-inferior to sorafenib with a median OS of 13.6 months (95% CI 12.1 – 14.9) [24].

4.1.2.2 EGFR pathway

Vandetanib also has an 'indirect' effect on angiogenesis by interfering with EGFR-induced production of angiogenic growth factors. EGFR is a transmembrane receptor tyrosine kinase that is frequently overexpressed or aberrantly activated in a number of the most common solid tumours, including colorectal cancer (CRC) [25]. The EGFR pathway is central to tumour progression.

There are four members of the EGFR family of receptors; EGFR (Erb1), ErbB2 (HER-2), ErbB3 and ErbB4. Each protein has an extra-cellular domain, single hydrophobic transmembrane domain and cytoplasmic TK containing domain. The receptors are activated following binding to peptide growth factors of the EGF family, including EGF, heparin-binding EGF (HB-EGF) and transforming growth factor alpha (TGF-α). On ligand binding, the receptors either form homo- or hetero-dimers, and auto- and transphosphorylation in the tyrosine residues of Erb receptors follows. Each EGFR member is able to recruit a variety of signalling molecules that bind to specific phosphorylation residues in the intracellular portion of the receptors. This ultimately leads to the stimulation of corresponding signalling cascades, which include the KRAS-BRAF-MEK-ERK pathway, phosphoinositide 3-kinase (PI3K), phospholipase C gamma protein pathway, the anti-apoptotic AKT kinase pathway and the STAT signalling pathway, which leads to cell proliferation, angiogenesis, migration, survival, and adhesion [25, 26].

As overexpression of EGFR and/or its ligands, transforming growth factor alpha (TGFα) and epidermal growth factor (EGF), is a common feature of many solid tumours, the EGFR pathway has already been highlighted as a key therapeutic target in the treatment for cancer. For example, the monoclonal anti-EGFR antibodies cetuximab and panitumumab have been shown to improve the clinical outcome of patients with metastatic CRC when combined with combination chemotherapy regimens in the first-line setting [27-33]. In HCC the role of erlotinib, a EGFR tyrosine kinase inhibitor, has been investigated, but in combination with sorafenib it was not found to improve OS [34].

4.1.3 Vandetanib in-vitro pharmacology

Vandetanib has been shown to be a potent inhibitor of VEGFR-2 tyrosine kinase activity with an IC50 value of 40 nM using recombinant enzyme essays. Furthermore, in isolated enzyme assays, vandetanib was found to be a sub-micromolar inhibitor of fms-like tyrosine kinase (Flt)-4 (VEGFR-3, the VEGF-C and –D receptor: IC50 =110 nM) and EGFR tyrosine kinases (IC50 = 500 nM) [11, 35]. In addition, vandetanib is a potent inhibitor of VEGF stimulated human umbilical vein endothelial cell (HUVEC) proliferation in vitro (IC50=60 nM) as well as an inhibitor of EGF stimulated HUVEC proliferation (IC50=170 nM) and b-FGF stimulated HUVEC proliferation (800 nM)[12, 35]. Evidence from in-vitro studies

also show that vandetanib can cause direct inhibition of tumour cell growth. Vandetanib has been shown to inhibit the growth of cell lines derived from various human cancers, including lung, breast, ovarian and colon cancer [11].

The direct effects of vandetanib on HCC cell proliferation, adhesion, migration and invasion in vitro, has also been investigated using an array of human HCC cell lines (Alexander, HepG2, SK-Hep1, HLF). Vandetanib was shown to inhibit HCC cell proliferation, adhesion, migration and invasion. Vandetanib also inhibited the expression of phosphorylated EGFR [20]. The effects of vandetanib on cell growth has been further investigated in a range of HCC cells (Sk-Hep-1, Alexander, HepG2, HLF, Chang). IC50 of vandetanib after 3 days exposure on different HCC cell lines is reported to range from 0.58 to 5 μM [36]. Vandetanib has also been shown to suppress phosphorylation of VEGFR-2 in HUVECs and EGFR in hepatoma cells [10].

4.1.4 Cytokines and blood biomarkers

Cytokines are secreted or membrane-bound proteins that regulate the growth, differentiation and activation of immune cells. They are released in response to a range of cellular stresses, including carcinogen-induced injury, infection and inflammation. Cytokines can bind to receptors, leading to the production of other types of cytokines, resulting in the accumulation of high concentrations not only in local tissues but also in the blood, serum or plasma [37, 38]. The ability to therefore measure the levels of cytokines has led to the exploration of using them as potential cancer biomarkers for use in the evaluation of anti-cancer therapies [39, 40].

As part of the VEROnA study, we explore a number of cytokines as potential indicators of response to treatment with BTG-002814. In choosing which cytokines to analyse as part of this trial, we focused on the mechanism of action of vandetanib, cytokines that have been shown to be released in response to TACE, and cytokines that have been shown to play an important role in the development of HCC and mCRC.

4.1.4.1 Cytokines in response to oral vandetanib

A number of studies have already assessed the impact of oral vandetanib on circulating cytokines and angiogenic factors in an attempt to identify key biomarkers that may indicate early response to treatment.

Hanrahan *et al* investigated patterns of change of cytokine and angiogenic factors following treatment with vandetanib. In this study, 35 cytokines and angiogenic factors were analysed from 123 patients with non-small cell lung cancer in a randomised phase II study [39]. Patients received either oral vandetanib, chemotherapy with carboplatin and paclitaxel, or a combination of the two. Changes in cytokine levels were assessed at days 8, 22 and 43 from baseline. The authors found that in the vandetanib monotherapy arm there was a significant increase in VEGF levels from baseline to day 43 (p=0.048) and a significant decrease in sVEGFR (p<0.001) over this same time period. There were also significant increases in IL-8 (a pro-angiogenic cytokine) (p=0.041) and granulocyte colony-stimulating factor (G-CSF), a haemopoetic growth factor, from baseline to day 8 (p=0.03), and in IL-17 levels at day 43 (p=0.045). When looking at correlation between cytokine levels and progression free survival (PFS) in patients treated with vandetanib alone, the authors found that patients with a greater than median increase in intercellular adhesion molecule 1 (ICAM-1) concentration at day 8 had a significantly improved PFS compared to those with a less than median increase (p=0.012). In the same cohort of patients, patients with a greater than median increase in VEGF were found to have an inferior PFS, compared to those with a less than median increase (p=0.054) [39].

In another study by Hsu *et al*, biomarkers were measured following oral vandetanib in 67 patients with locally advanced or metastatic inoperable HCC. In this study, patients were randomised 1:1:1 to receive vandetanib 300 mg/day, vandetanib 100 mg/day or placebo. Plasma samples were assessed at screening, at the end of weeks 4 and 8 of study treatment, and then every 8 weeks until objective progression of disease or withdrawal. A statistically significant increase in circulating VEGF was observed with both arms of the vandetanib treatment (V100, p=0.004 and V300 p=0.03) from baseline to week 4, which correlated with significant decreases in VEGFR-2 levels (p<0.01 in both groups). VEGFR-1 levels were unchanged but were found to be significantly

elevated in the placebo arm. Changes in other circulating angiogenic factors, including basic fibroblast growth factor (bFGF), angiopoietin-2 (Ang-2), Tie-2, and IL-8 were not consistent amongst treatment groups [41].

Mross *et al* investigated the effect of two doses of oral vandetanib (100 mg/day and 300 mg/day) in patients with metastatic CRC, and measured levels of VEGF, EGFR, sVEGFR-2, Tie2, bFGF and Ang1 and Ang2 at various time points following treatment. They reported that higher plasma levels of VEGF were detected at both vandetanib doses following multiple dosing, although large variability was observed. No consistent time- or dose-related changes from baseline were observed for sVEGFR-2, bFGF, EGFR, Tie-2, Ang1 or Ang2 [42].

4.1.4.2 Cytokines in response to TACE

In TACE, embolisation of the arterial vessels supplying the hepatic tumour leads to ischaemia, resulting in tumour necrosis. The creation of a hypoxic tumour environment can lead to the release of VEGF, in addition to other key cytokines that are involved in angiogenesis, cell growth and inflammation [43-45].

Chao *et al* report on cytokine changes in forty-one TACE naive HCC patients that underwent TACE [43]. They found that serum IL-6 increased rapidly and peaked on day 1 post-TACE. VEGF levels were found to rise more slowly, with peak levels seen on day 14. bFGF and TNF-alpha increased mildly and peaked in week 1 post-TACE. IL-8 and EGFR showed no significant change. EGF and TGF-ß1 levels decreased post-TACE, with levels being maintained up to day 14. Furthermore, ineffective TACE cases were found to have higher serum VEGF levels at day 14 compared to cases of effective TACE. The difference in VEGF from baseline and day 14 post-TACE was also found to predict for survival, with a difference of <500 pg/ml predicting a longer survival (22.1 vs 10.9 months p=0.013) [43].

Kim *et al* also report on changes of thirteen cytokines following TACE in 83 patients with HCC [40]. IL-6 was again reported to rise post-TACE, with peak levels on day 3, and decreasing levels after day 7. IL-10, along with IL-4 and IL-5, was seen to increase during the late phase, 2 months post-TACE, without any significant change in the immediate post-treatment period. IL-17A, however,

continued to decrease over time, reaching a significantly lower level 2 months post-TACE compared with baseline (p=0.014).

4.1.4.3 Biomarkers and cytokines in HCC

The development of HCC is a complex multistep process that usually occurs on the background of liver cirrhosis. Cirrhosis can develop as a result of chronic infection with Hepatitis B or C, or after regular insult with alcohol. Cirrhosis is characterised by a decrease in the growth of healthy liver cells (hepatocytes) and is due to the constant degeneration and regeneration of cells. It is the regeneration of cells that leads to an increase in fibrous scar tissue in the liver which then provides the environment for the malignant changes to occur [46].

Growth factors, such as EGF, TGF α/-β, insulin-like growth factor (IGF), and VEGF, are known to play a key role in liver regeneration after injury, while fibroblast growth factor (FGF) and the platelet-derived growth factor (PDGF) family are involved in liver fibrosis and HCC growth [47]. The MAPK, phosphoinositide 3-kinase (PI3K)/Akt/mTOR, c-MET, IGF, Wnt-β-catenin and Hedgehog signalling pathways, and the VEGFR and PDGF receptor (PDGFR) signalling cascades all show altered activity in HCC [47]. The importance of the VEGF pathway in angiogenesis has already been demonstrated. VEGF is known to be produced by hepatoma cells, hepatic stellate cells, and endothelial cells, and its expression level has been shown to be correlated with tumour growth. Hepatoma cells also produce EGF and TGF-a and express EGF receptor.

However, unlike with other solid tumours, there is no one clear pathway to target with HCC. As such, no one clear biomarker has been identified that can be used to predict response to treatment. However, a number of biomarkers are starting to show promise. Serum alpha-feto protein (AFP), a serum glycoprotein antigen, is commonly used for the diagnosis and surveillance of HCC [48]. More recently, there have been suggestions that AFP may also act as an independent indicator for prognosis [49, 50]. Other circulating factors such as Ang2, HGF, TGF-beta, and VEGF have also been shown to be independent factors for HCC prognosis [48, 49].

4.1.4.4 Biomarkers and cytokines in metastatic CRC

A large number of genetic alterations have already been identified that underlie the development of CRC, including those affecting the KRAS-, MYC-, Wnt-, mitogen-activated protein kinase (MAPK)-, or TGF-β/bone morphogenetic protein (BMP)- signalling pathways. More recently, it has been shown that immune infiltrates in the tumour microenvironment appear to differently modulate CRC development with initial studies reporting a correlation between the inflammatory cell pattern in CRC tumours and prognosis [51].

Carcinoembryonic antigen (CEA), a protein biomarker, is already utilised in clinical practice as a marker of clinical response and has been shown to be an independent prognostic factor [52]. Cytokines, such as tumour necrosis factor (TNF) and interleukin-6 (IL-6), are classically regarded as central players in CRC, driving activation of the key oncogenic transcription factors nuclear factor-κB (NF-κB) and signal transducer and activator of transcription 3 (STAT3), to promote proliferation and resistance to apoptosis. More recently, cytokines with similar biochemical functions, including IL-11, IL-17A and IL-22, have gained attention as facilitators of CRC [37]. Increased serum cytokine concentrations of TNF-a, IL-8, IL-6, and platelet-derived growth factor (PDGF) have been reported in CRC patients compared with healthy individuals, and certain cytokines and chemokines, such as IL-6 and VEGF, are considered to have prognostic value [53].

The serum levels of several cytokines, including TNF-alpha, IL-8 and IL-6, have been shown to be higher in CRC patients, and some studies have suggested that increased plasma levels of these cytokines may have a prognostic value. The level of IL-10 in serum has also been shown to be significantly increased in CRC patients when compared with healthy controls and may have potential diagnostic value for CRC. Furthermore, overexpression of MMP-2, -7 and -9 has been demonstrated in CRC patients [38].

The subsequent progression of CRC, and the development of liver metastases is a complex process, involving a number of complex interactions with the tumour microenvironment. It has been suggested that systemic inflammation, mediated by circulating cytokines, may increase the likelihood of metastatic deposits developing and progressing by similar mechanisms to those acting on the primary

tumour at the microenvironment [54]. As with HCC, the detection of cytokines that reflect this complex interactive process may help identify key biomarkers that indicate response to therapy.

4.1.4.5 Biomarkers selected for analysis in the VEROnA trial

Although previous studies have investigated a number of different cytokine and angiogenic factors in response to VEGF inhibitors, and following treatment with TACE, it is clear that this is an area that requires further exploration. We therefore had a novel window-of-opportunity to measure a number of these key biomarkers in response to treatment with vandetanib-eluting beads used for TACE as part of the VEROnA trial. The final list of selected biomarkers for analyses in the VEROnA trial is shown in Table 1.

Table 1: Biomarkers selected for analysis in the VEROnA study

Pro-angiogenic factors:	**Anti-angiogenic factors**	**Marker of endothelial function**
VEGF A	IP-10	sVEGFR-1
VEGF C	sIL-6a	sVEGFR-2
VEGF D	IL-12p40	sHER2
Basic FGF (FGF 2)	IL-12p70	sEGFR
EGF		
TNF-alpha	**Hypoxia markers**	**Other cytokines**
IL-6	Osteopontin	sCD40L
IL-8		IGFBP-1
MMP-9	**Other interleukins**	MMP-2
HGF	IL-2	Leptin
sTIE-2	IL=17A	sPECAM-1
Ang-2		suPAR
TGF-alpha	**Haemopoetic growth factors**	
PDGF	G-CSF	
PLGF		
Endoglin	**Inflammatory factors**	
TNF-beta	ICAM-1	
Follistatin	Interferon gamma	
HB-EGF		

4.2 OBJECTIVES

BTG-002814 is a novel RO vandetanib-eluting bead for use in TACE. In order to understand the mechanism of action of this novel combination the aim of this part of the study was to:

1. Evaluate the histopathological response in liver tumours following treatment with BTG-002814.
2. Evaluate the distribution of BTG-002814 on tumour vasculature using micro-CT images of the resected liver specimen.
3. Study blood biomarkers with the potential to identify patients likely to respond to BTG-002814.

4.3 MATERIALS AND METHODS

4.3.1 Patient selection

All patients in this study were treated as part of the VEROnA clinical trial, which is outlined in detail in Chapter 2 (section 2.2).

4.3.2 Histopathological analysis

Following surgical resection, standard haematoxylin and eosin stain sections were cut, and the extent of tumour necrosis, viable tumour and presence of vascular changes reported. This was performed by Dr Marnix Jansen.

4.3.3 Distribution of radiopaque beads following treatment

In order to assess the distribution of radiopaque (RO) beads following TACE treatment, a novel surface-based segment matching algorithm was used to register the pre-surgical non-contrast CT scan with an ex-vivo scan of the resected liver specimen. Following resection of the tumour, and prior to tissue sampling, the resected specimen was imaged on a Mediso nanoScan Positron Emission Tomography/CT. Embolised vasculature were then aligned between the two images on manually selected fiducial points. Using calibrated scans of the RO beads, volume of beads within the tumour, resection specimen and liver were calculated. This analysis was performed by Henry Tregidgo, Research Associate in Advanced Liver Imaging.

4.3.4 Measurement of serum tumour markers

Serum tumour markers were assessed at the following time points as part of the VEROnA trial:

- Baseline (Visit 1)
- 0-24 hours prior to treatment with BTG-002814 (Visit 2)
- 7-21 days post-treatment with BTG-002814 (Visit 4)

Patients with a diagnosis of HCC had serum AFP levels measured and patients with mCRC had CEA, CA 19-9, Ca 125 levels measured. Testing was performed at the local laboratory according to the laboratory's normal procedures.

4.3.5 Measurement of exploratory plasma biomarkers

Exploratory plasma biomarkers were assessed at the following time points:

- Baseline (visit 1)
- 0-24 hours prior to treatment with BTG-002814 (visit 2)
- Day 1 post-treatment with BTG-002814 (visit 3)
- 7-21 days post treatment with BTG-002814 (day prior to surgery) (visit 4)
- 28-32 days post-surgery (visit 6)

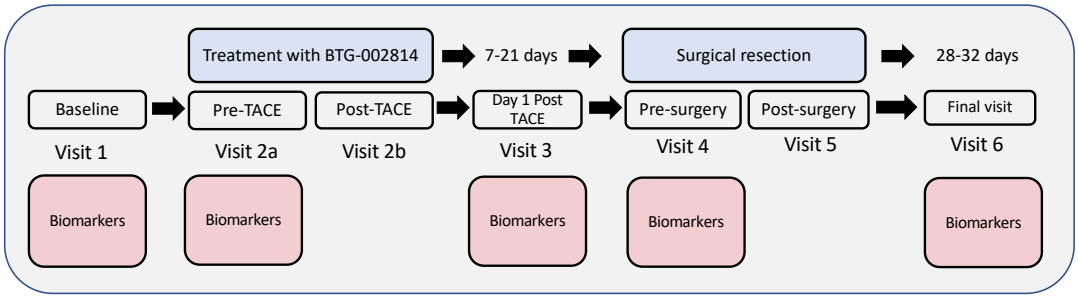

Figure 2: Sampling of exploratory biomarkers in the VEROnA trial

At each trial time point, approximately 4 ml of blood was collected into a 4 ml Vacutainer© EDTA tube. Within 30 minutes of collection the sample was then centrifuged at 1000 x g for 10 minutes at room temperature. Plasma was then pipetted as 100 µL aliquots into 6-8 labelled cryovials (Figure 3). Each cryovial was stored at –70°C or below. Once the last patient had completed all trial visits, measurement of each cytokine listed in Table 1 was performed using the Merck Milliplex kits for the Luminex 200 machine. Assays were conducted in accordance

to the protocol provided by the supplier Millipore (Merck, Darmstadt, Germany) (Figure 4).

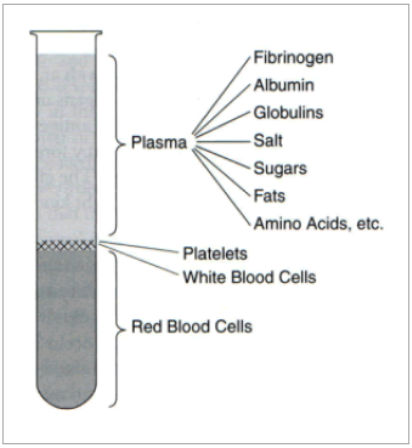

Figure 3: Plasma collection for exploratory cytokines. The blood sample was centrifuged at 1000 x g for 10 minutes at room temperature. After separation, samples from the top plasma layer were taken.

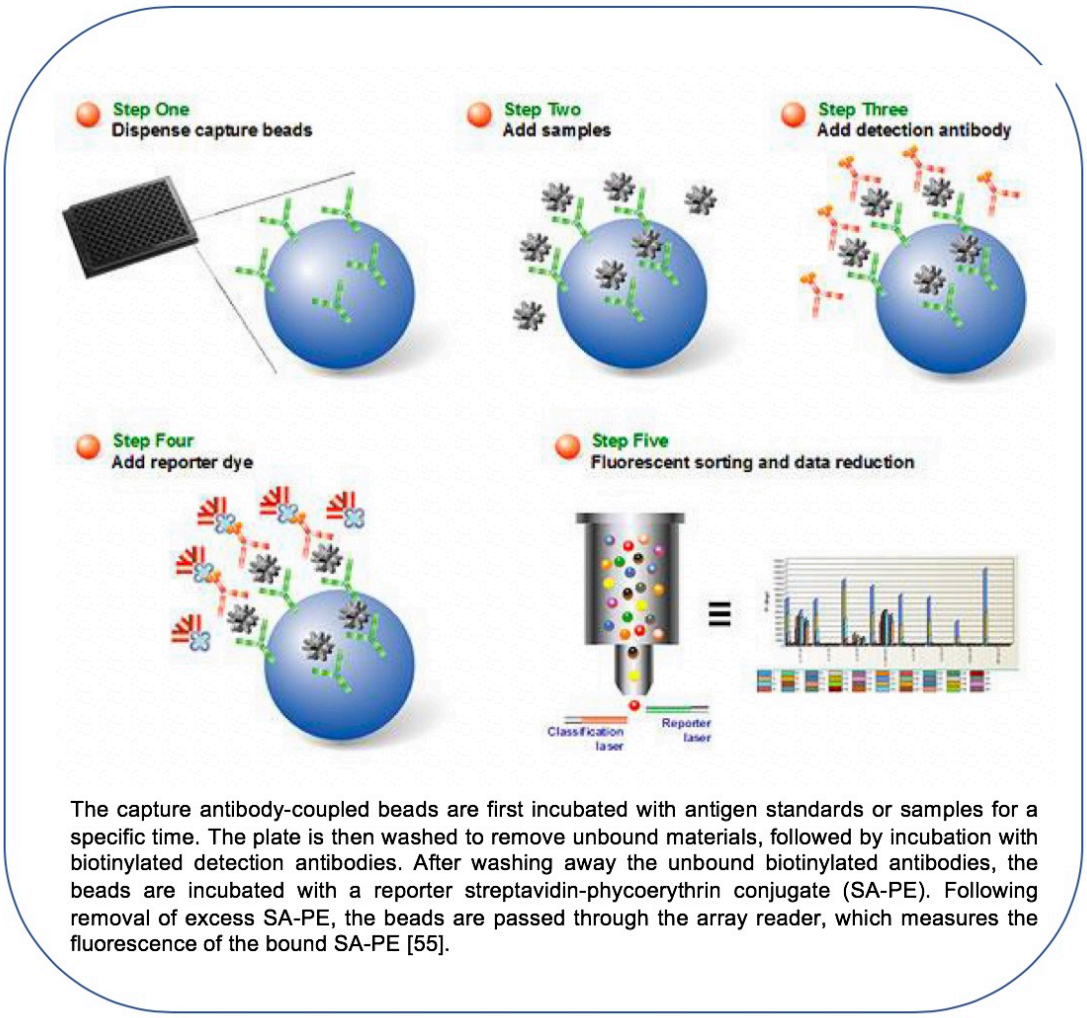

The capture antibody-coupled beads are first incubated with antigen standards or samples for a specific time. The plate is then washed to remove unbound materials, followed by incubation with biotinylated detection antibodies. After washing away the unbound biotinylated antibodies, the beads are incubated with a reporter streptavidin-phycoerythrin conjugate (SA-PE). Following removal of excess SA-PE, the beads are passed through the array reader, which measures the fluorescence of the bound SA-PE [55].

Figure 4: Overview of the Luminex xMAP technology

In brief, quality control and standards components were all rehydrated within the appropriate timeframe and diluted in accordance with the specific kit protocol and added to appropriate wells of the assay plate. Each patient's plasma sample was thawed on ice, then diluted to the appropriate dilution (as recommended by the specific kit protocol). Each time point for each patient sample was added in triplicate, to allow for calculations of coefficient of variation (%CV). Antibody-conjugated beads specific to the desired analytes and detection antibodies to quantify analyte-bead binding were then added to each sample. Samples were then incubated, and plates read on the Bio-Rad Bioplex multiplex immunoassay plate reader. Analytes were identified by specific bead colour and quantified in pg/ml by the amount of detection antibody binding. Assays were conducted according to the standard operating procedures produced by GCLP lab, which was written in accordance with the protocol provided by the supplier (Millipore)

(Appendix 1). However, each kit had slight differences in specific reagent dilutions and volumes. All analyses were performed by the UCL GCLP lab.

4.4 STATISTICAL ANALYSIS

Tumour necrosis and bead distribution parameters were summarised with descriptive statistics. Serum biomarkers were compared from baseline (visit 1) to post-treatment levels (visit 4) using Wilcoxon signed-rank test. For each exploratory biomarker measured a time-concentration plot was created for each patient. After a review of the time-concentration plots, a Wilcoxon signed-rank test was used to assess for statistical significance in those biomarkers with evidence of a large change. Statistical analysis was performed using SAS version 9.4 (SAS Institute, Cary NC).

4.5 RESULTS

4.5.1 Patient selection

Eight patients were successfully treated with BTG-002814 as part of the VEROnA study, as outlined in full detail in Chapter 2 (Section 2.4). All patients underwent surgery as planned at an average of 14.9 days (+/- 7.6 days) following treatment with BTG-008214. A total of 13 lesions were resected, of which 10 had been treated with BTG-002814.

4.5.2 Histopathological results

Tumour necrosis and viability were analysed for all treated tumours. Overall, the median percentage of tumour necrosis was 92.5% (range 5-100%). For patients with mCRC median tumour necrosis was 92.5% (range 20% -100%), and conversely median viability was 7.5% (range 0% to 80%). For the patients with HCC the results varied greatly, with one tumour being 100% necrotic (0% viable) and one being 5% necrotic (95% viable) (Table 4). Of note, the tumour with 5% necrosis measured 82 mm; the maximum volume of beads allowed in this feasibility study was 1 ml, regardless of tumour size. No vascular changes were observed in any of the tumours examined.

Table 2: Pathological tumour response following treatment with BTG-002814

Patient	Histo.	No. lesions	Tumour size, CT (mm)	Vol. BTG-002814 delivered (ml)	Time from TACE to surgery (days)	Pathological response (necrosis)
1	HCC	1	33	1	14	100%
2	HCC	1	82	1	13	5%
3	mCRC	1	21	1	16	90%
4	mCRC	1	8	1	7	100%
5	mCRC	2	12 (treated)	1	14	100%
			14 (untreated)	NA		NA
6	mCRC	1	40	0.6	14	95%
7	mCRC	1	24	0.9	32	20%
8	mCRC	5	42 + 29 +16 (treated)	1	8	50%
			22 + 24 (untreated)	NA		NA

Notes: Patient 5 had two tumours, one treated and one untreated. Patient 8 had five tumour, three treated and two untreated. Abbreviations: HCC, hepatocellular carcinoma; mCRC, metastatic colorectal cancer; NA, not assessed (untreated lesion).

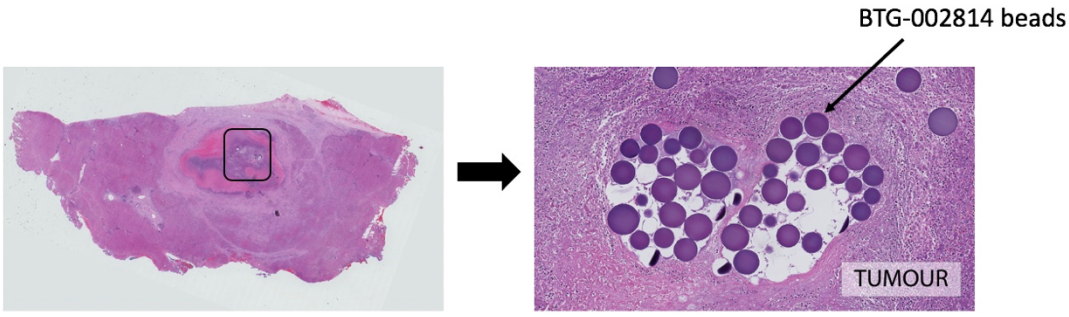

Figure 5: Photomicrographs of pathological resection specimen showing 100% necrosis after treatment with vandetanib-eluting beads (BTG-002814). Beads are shown stained as purple circles within the tumour with evidence of background tumour necrosis.

4.5.3 Bead distribution results

Analysis were performed for all patients expect one (patient 4), due to small tumour size. Assessment of bead quantification showed that “on target” bead delivery to the tumour varied from 0-78% across the 7 patients evaluated (median 1.36%) and was higher in HCC patients compared to those with mCRC (Table 3). When analysis included a 1 cm margin around the tumour target, bead delivery increased to 19.78% (range 1.61-80.78%) and with a 2 cm margin, median target bead delivery was 40.58% (range 8.99-85.0%).

Table 3: On target volume and percentage of beads in resected specimen and tumour

Patient	Volume of beads in liver (µL)	Volume of beads in resection (µL) (%)*	Volume of beads in tumour (µL) (%)*	Volume of beads in tumour + 1cm (µL) (%)*	Volume of beads in tumour + 2cm (µL) (%)*
1	928.83	399.27 (42.9%))	361.14 (38.88%)	393.79 (42.40%)	479.28 (51.60%)
2	764.69	**	596.78 (78.04%)	617.72 (80.78%)	649.97 (85.00%)
3	594.79	116.54 (19.59%)	0.32 (0.05%)	36.26 (6.10%)	108.85 (18.30%)
5	849.29	751.62 (88.50%)	0 .00 (0.00%)	15.26 (1.80%)	76.33 (8.99%)
6	202.56	148.09 (73.11%)	51.14 (25.25%)	115.39 (56.96%)	166.8 (82.35%)
7	720.78	103.82 (14.40%)	4.32 (0.60%)	75.43 (10.47%)	133.26 (18.49%)
8 (tumour 1)	693.73	422.37 (14.40%)	9.46 (1.36%)	137.23 (19.78%)	281.51 (40.58%)
8 (tumour 2)	693.73	422.37 (60.88%)	12.4 (1.79%)	171.12 (24.67%)	364.28 (52.51%)
8 (tumour 3)	693.73	422.37 (60.88%)	0.01 (0.00%)	11.16 (1.61%)	86.3 (12.44%)

Notes: On target volume and percentage of beads in resected specimen, tumour, and tumour with a margin of 1 cm and 2 cm for each patient. The volume of beads within the liver taken as 100% for each patient. **Patient 2 micro-CT artefacts prevented registration. No results available for patient 4 due to small tumour size.

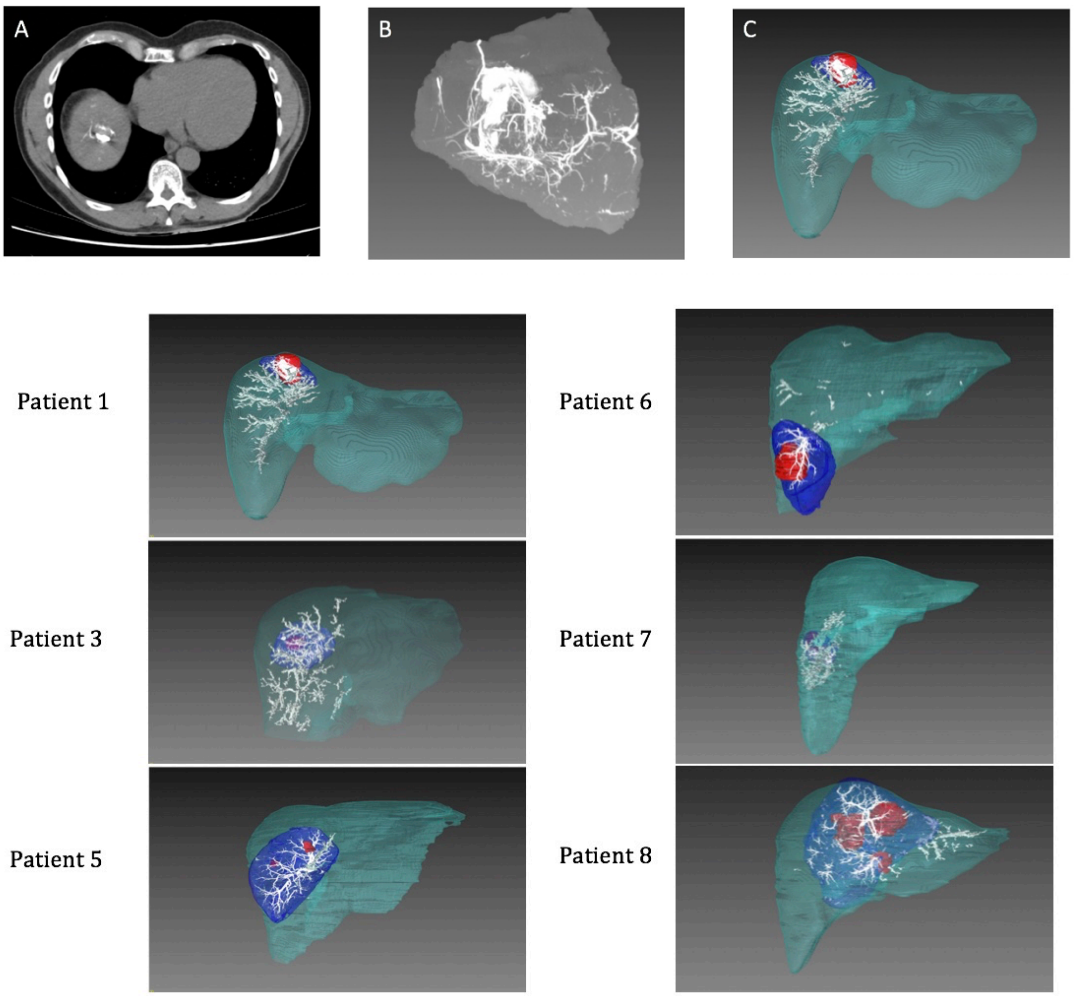

Figure 6: Distribution of radiopaque beads along the vasculature, with tumour and resection specimens registered from micro-CT images. A novel surface-based segment matching algorithm was used to register the pre-surgical non-contrast CT scan with an ex-vivo scan of the resected liver specimen. Embolised vasculature were then aligned between the two images on manually selected fiducial points. Using calibrated scans of the RO beads, volume of beads within the tumour, resection specimen and liver were calculated. *Code:* A: Pre-surgical non-contrast CT scan of a segment VIII HCC post-treatment with BTG-002814. B: Mediso nanoScan Positron Emission Tomography/CT (micro-CT) of the resected HCC specimen showing radiopacity along the tumour vasculature. C: Combined volume visualisation of the HCC tumour on CT scan and micro-CT scans. Images were not available for patient 2 due to micro-CT artefacts preventing registration and for patient 4 due to small tumour size. Inferior section of liver in patient 3 not imaged.

Code: Cyan, liver; Red, tumour; Blue, resected specimen; White, RO beads along liver vasculature.

Table 4: Summary table: Histology, tumour size, bead distribution and tumour necrosis

	Histology	Tumour size (mm)	Volume of beads in tumour (µl)	On target bead percentage (%)*	Bead volume in tumour µl/cm3	Tumour necrosis (%)
1	HCC	33	361.14	38.8	30.18	100%
2	HCC	82	596.78	78.04	2.69	5%
3	mCRC	21	0.32	0.05	0.10	90%
4	mCRC	8	**	**	**	100%
5	mCRC	12	0.00	0	0.00	100%
6	mCRC	40	51.14	25.25	3.93	95%
7	mCRC	24	4.32	0.60	0.70	20%
8	mCRC (tumour 1)	42	9.46	1.36	0.55	50%
8	mCRC (tumour 2)	29	12.4	1.79	0.88	50%
8	mCRC (tumour 3)	16	0.01	0	0.01	NA

*The on-target bead percentage is a percentage of the beads in the tumour with the volume of beads within the liver taken as 100% for each patient

1.3.4 Serum biomarker results

Median baseline AFP was 4.0 kU/L for HCC patients (range 3.9-4.1). For mCRC patients, median baseline CEA, CA19-9 and CA125 levels were 9.1 (range 2.0-201.0), 17.6 (range 9-195) and 9.0 (range 4012). No significant changes in tumour markers were observed from baseline (visit 1) to post-treatment with BTG-002814 (visit 4) which was on average 12.9 days (SD 7.3) later. However, by-patient measurements generally trended down from baseline to post-treatment with BTG-002814. AFP decreased in both patients with HCC at the visit 4 timepoint. CEA decreased at the visit 4 timepoint in 4/5 patients with available visit 4 data, and CA19-9 decreased in 3/5 patients with available visit 4 data (Table 5).

Table 5: Change in serum tumour markers

Tumour marker	Baseline median (range)	Post-treatment median (range)	Change from baseline median (range)	p value**
HCC patients (n=2)				
AFP (kU/L)	4.0 (3.9-4.1)	3.1	-0.9 (-0.6 to -1.2)	0.50
mCRC patients (n=5)*				
CEA (ug/L)	9.1 (2.0-201.0)	4.7 (1.1-139)	-1.9 (-62.0 to 0.2)	0.13
CA19-9 (kU/L)	17.6 (9-195)	20 (6-205)	-1 (-14 to 10)	0.88
CA125 (kU/L)	9.0 (4-12)	8 (3-16)	1 (-1 to 4)	0.75

Notes: Baseline (visit 1) and post-treatment (visit 4) levels are shown for each serum tumour marker measured during the trial. *One patient with mCRC had a value missing post-treatment. **Wilcoxon signed-rank test used for statistical analysis.

4.5.5 Exploratory biomarker results

All patients underwent sampling at all specified timepoints within the trial and as such there were no missing data points. Figure 7 outlines the time-concentration plots for each patient and each biomarker analysed. Exploratory biomarker analysis showed an overall trend towards an increase between baseline and the immediate post-TACE sample (visit 3) in endoglin, G-CSF, and leptin. An increase between baseline and visit 4 (pre-surgery) was seen in follistatin, IGFBP, osteopontin, sTie-2, sEGFR, VEGF-A, sVEGFR1, sVEGFR2, and suPAR. MMP2 showed an overall decrease at visit 4, with VEGF-D showing a decrease at visit 3. Angiopoietin showed an increase between baseline and visit 4 and continued to increase following surgery.

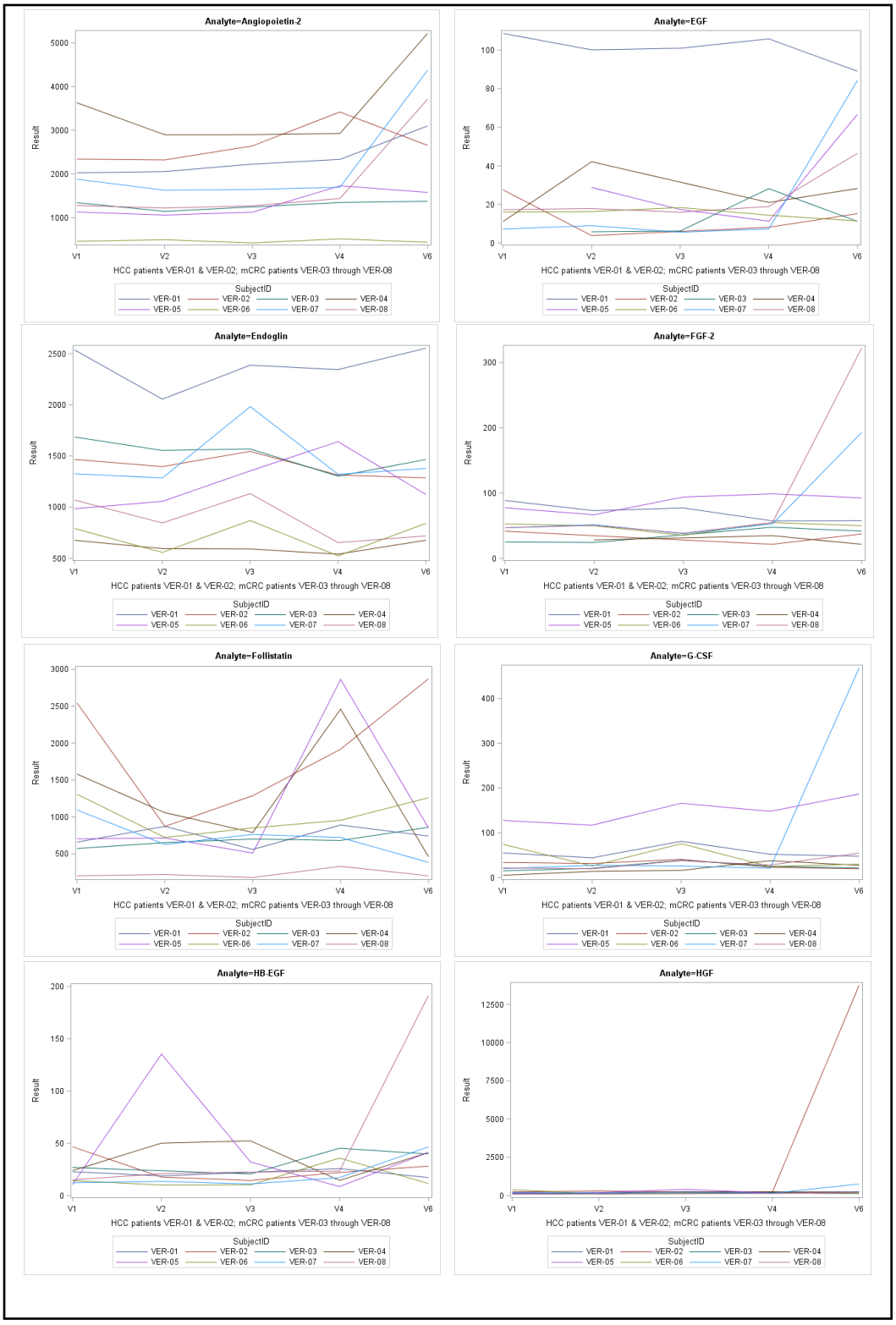

Figure 7 (a). Time-concentration plots for each biomarker analysed in the VEROnA trial. Each plot shows the level of each cytokine measured for each patient across the trial visits: visit 1 (baseline), visit 2 (immediately pre-BTG-002814), visit 3 (24 hours post-BTG-002814), visit 4 (pre-surgery) and visit 6 (28-32 days post-surgery). All 39 cytokines are shown in alphabetical order. Data is not shown when values were below the lower limit of quantification on each assay. As such, for some plots data for each patient is not shown. All results are pg/ml.

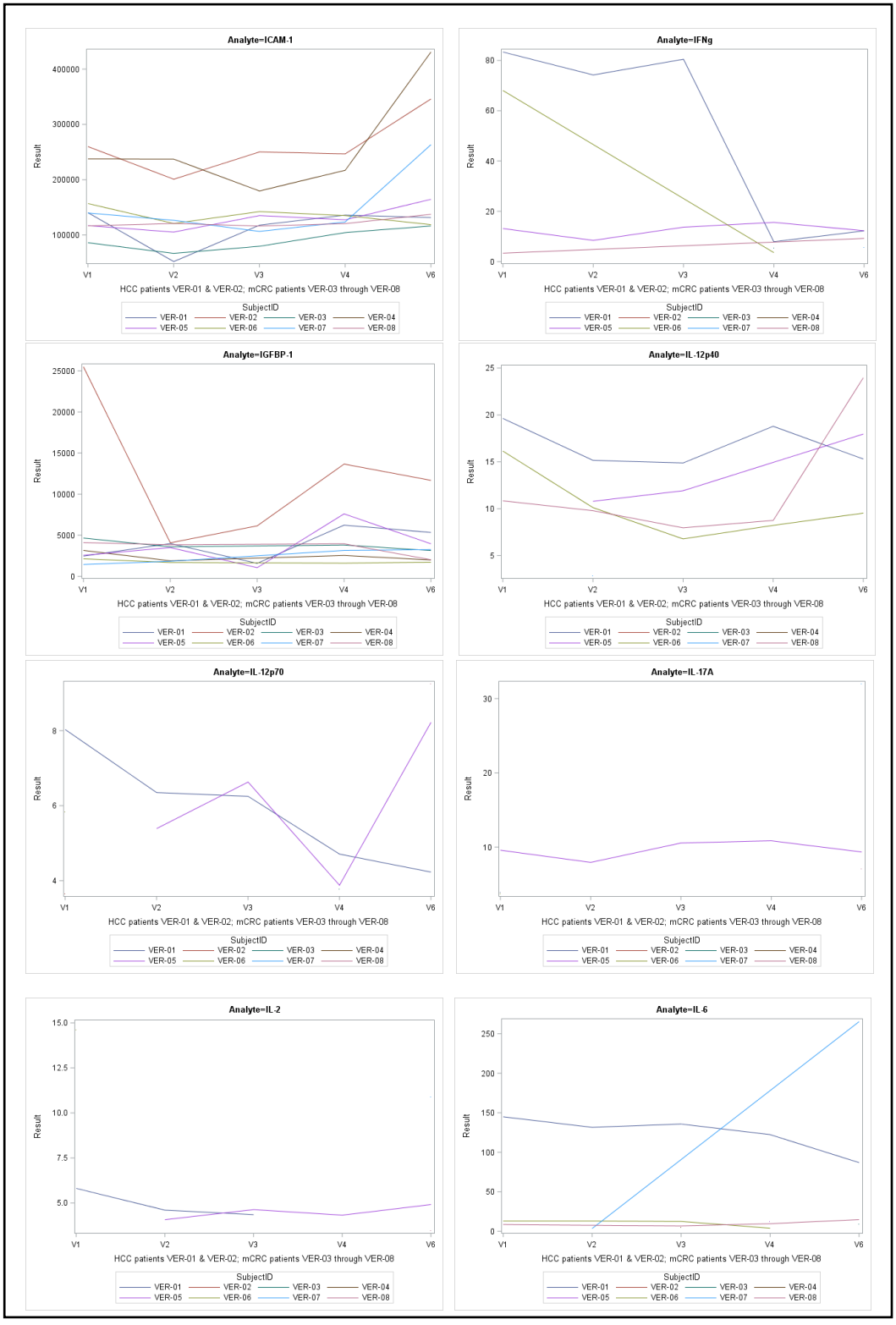

Figure 7 (b). Time-concentration plots for each biomarker analysed in the VEROnA trial. Each plot shows the level of each cytokine measured for each patient across the trial visits: visit 1 (baseline), visit 2 (immediately pre-BTG-002814), visit 3 (24 hours post-BTG-002814), visit 4 (pre-surgery) and visit 6 (28-32 days post-surgery). All 39 cytokines are shown in alphabetical order. Data is not shown when values were below the lower limit of quantification on each assay. As such, for some plots data for each patient is not shown. All results are pg/ml.

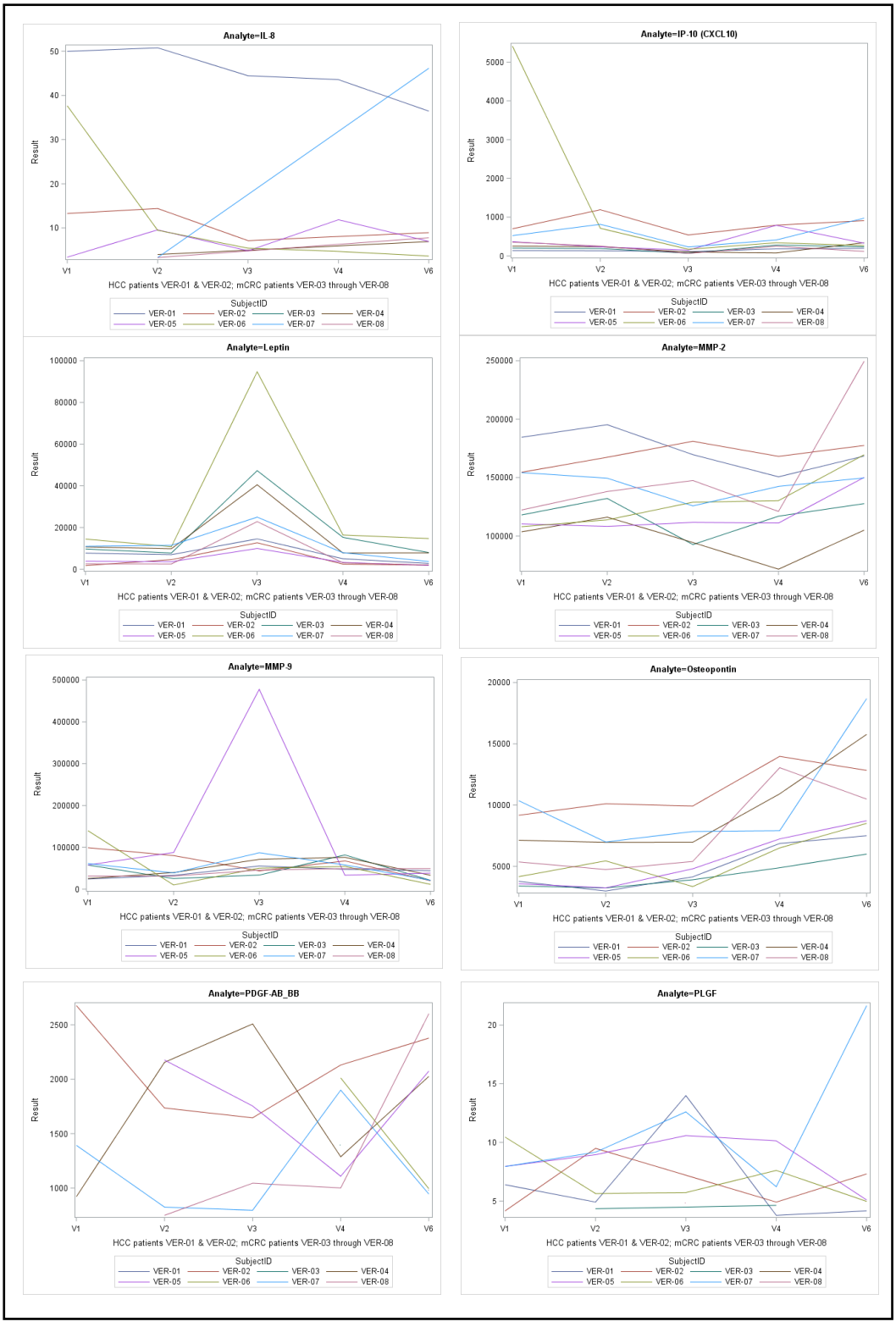

Figure 7 (c). Time-concentration plots for each biomarker analysed in the VEROnA trial. Each plot shows the level of each cytokine measured for each patient across the trial visits: visit 1 (baseline), visit 2 (immediately pre-BTG-002814), visit 3 (24 hours post-BTG-002814), visit 4 (pre-surgery) and visit 6 (28-32 days post-surgery). All 39 cytokines are shown in alphabetical order. Data is not shown when values were below the lower limit of quantification on each assay. As such, for some plots data for each patient is not shown. All results are pg/ml.

Figure 7 (d). Time-concentration plots for each biomarker analysed in the VEROnA trial. Each plot shows the level of each cytokine measured for each patient across the trial visits: visit 1 (baseline), visit 2 (immediately pre-BTG-002814), visit 3 (24 hours post-BTG-002814), visit 4 (pre-surgery) and visit 6 (28-32 days post-surgery). All 39 cytokines are shown in alphabetical order. Data is not shown when values were below the lower limit of quantification on each assay. As such, for some plots data for each patient is not shown. All results are pg/ml.

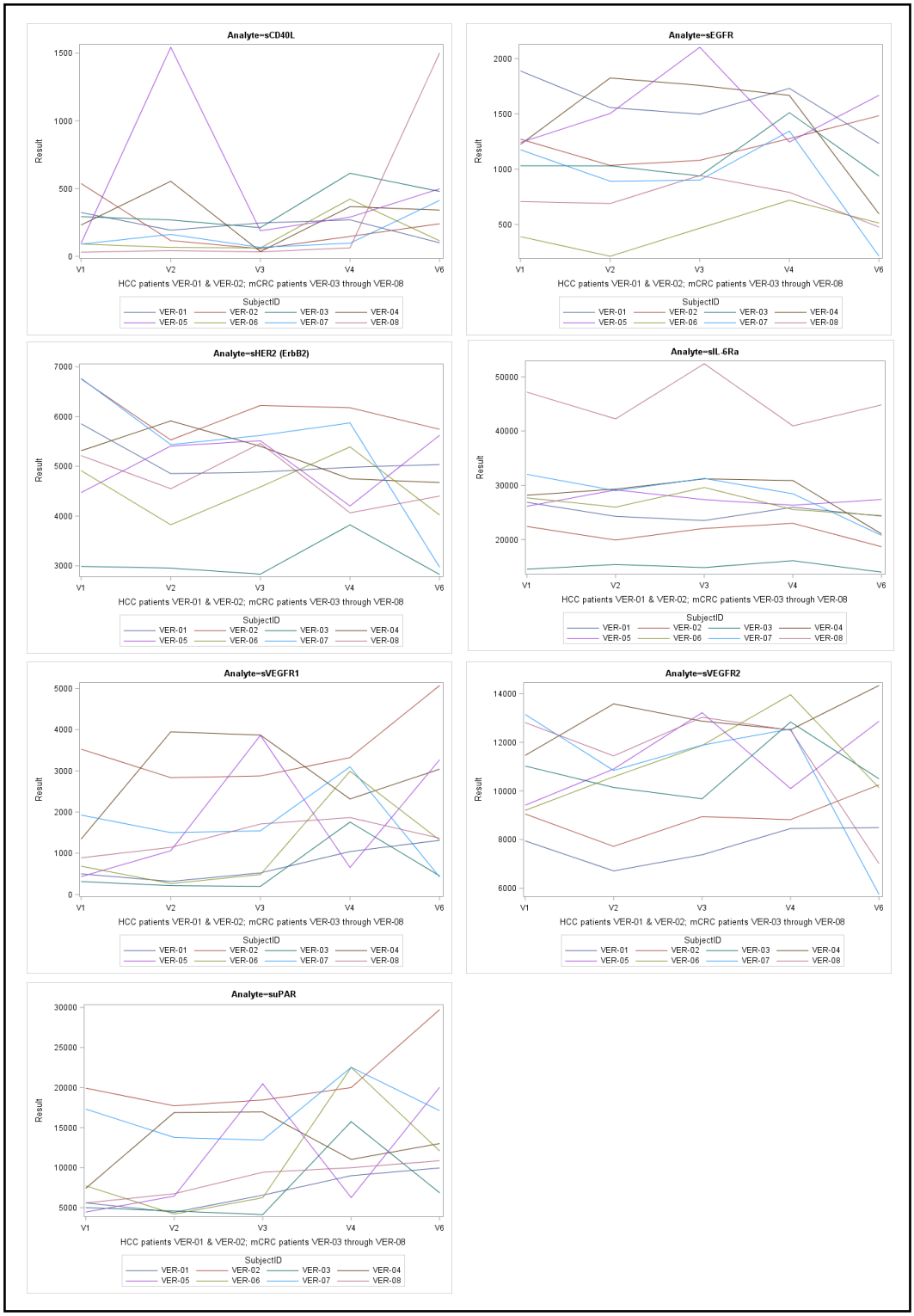

Figure 7 (e). Time-concentration plots for each biomarker analysed in the VEROnA trial. Each plot shows the level of each cytokine measured for each patient across the trial visits: visit 1 (baseline), visit 2 (immediately pre-BTG-002814), visit 3 (24 hours post-BTG-002814), visit 4 (pre-surgery) and visit 6 (28-32 days post-surgery). All 39 cytokines are shown in alphabetical order. Data is not shown when values were below the lower limit of quantification on each assay. As such, for some plots data for each patient is not shown. All results are pg/ml.

Table 6: Statistical analysis of cytokines that showed changes in the time-concentration plots after treatment with BTG-002814.

Biomarker	Observed trend from time-concentration plot	V1 vs V3	V2 vs V3	V1 vs V4	V2 vs V4	V3 vs V4	V1 vs V6	V2 vs V6	V3 vs V6	V4 vs V6
Angiopoietin	Increases at V4 and V6	*	*	0.38	0.01	*	0.02	0.02	*	0.31
Endoglin	Increases at V3	0.74	0.02	*	*	0.08	*	*	0.11	*
Follistatin	Increases at V4	*	*	0.74	0.01	*	*	*	*	0.55
G-CSF	Increase at V3	008	0.02	*	*	0.11	*	*	*	
IGFBP	Increase at V4	*	*	1.00	0.02	*	*	*	*	0.04
Leptin	Increase at V3	0.08	0.01	*	*	0.01	*	*	*	
MMP2	Decrease at V4	0.95	0.31	0.46	0.20	*	*	*	*	0.01
Osteopontin	Increase at V4	*	*	0.04	0.01	*	0.08	0.01	*	0.25
VEGF-A	Increase at V4	*	*	0.88	0.31	0.25	*	*	*	0.13
VEGF-D	Decrease at V3	0.08	0.01	*	*	0.01	*		0.03	*
sTie2	Increase at V4	*	*	0.02	0.01	*	0.08	0.02	*	*
sEGFR	Increase at V4	*	*	0.05	0.15	*	*	*	*	0.11
sVEGFR1	Increase at V4	*	*	0.02	0.20	0.46	*	*	*	0.95
sVEGFR2	Increase at V4	*	*	0.15	0.05		*	*	*	*
suPAR	Increase at V4	*	*	0.01	0.11	0.38	*	*	*	0.84

Notes: Selected visits are compared depending on the trend seen in the initial plots from Figure 7. Wilcoxon single-ranked analysis was used to generate p values for each comparison between visits as shown in each column. V1= visit1 (baseline), V2 = visit 2 (pre-treatment), V3 = visit 3 (24 hours post-treatment with BTG-002814), V4 = visit 4 (pre-surgery) and V6 = visit 6 (28-32 days post-surgery). Note, *p*-values are for information only and should not be interpreted as evidence of statistical significance given the small sample size and number of comparisons being made.

4.6 DISCUSSION

4.6.1 Histopathological results and correlation to bead location

Although efficacy was not a specific outcome of this study, the degree of tumour necrosis seen in our cohort appears favourable, with a median necrosis of 92.5% (5-100%). Furthermore, 5/8 (62.5%) of patients had greater than 90% necrosis following treatment with BTG-002814.

Published information on the pathological response to TACE is limited as TACE is rarely used prior to liver resection or transplant. The PARAGON II trial, a phase II study of neoadjuvant therapy using irinotecan beads in patients with resectable liver metastases from colorectal cancer, reported a median necrosis value of 50% (range 0-100%) and necrosis greater than 50% in 77% of patients [56]. In comparison, in our mCRC cohort, median necrosis was 92.5% (range 20-100%) with 66.7% of patients having necrosis greater than 50%. For HCC patients, in a cohort of 53 patients treated with conventional TACE with doxorubicin prior to liver transplant, mean necrosis was reported as 78.7% +/- 31.5% (range 0-100%) [57]. Our histopathological response rates are consistent with these published studies and further efficacy studies of BTG-002814 are therefore warranted.

The rationale behind TACE efficacy is that tumour cells are killed by a combination of the cytotoxic effects of the drug delivered directly to the tumour and the ischaemic effect of vessel embolisation [3]. In order to understand the mechanisms of TACE resistance it is vital to develop methodologies that can map the delivery of anticancer drugs in relation to liver tumours, and correlate bead location to tumour response. The innovative design of this window-of-opportunity study has allowed RO bead location to be correlated with the surgical resection specimen and enable a highly accurate calculation of on-target bead delivery. To our knowledge, this is the first study to report this correlation in humans [58]. In our cohort, it appears as though it is not just bead delivery to the tumour that is important, but also bead delivery to the surrounding 1-2 cm. In our cohort, median bead delivery to the tumour was just 1.36%. As expected, due the hypervascular nature of HCC lesions, and the ability to deliver super selective TACE, bead delivery was higher in HCC patients when compared to those with mCRC (median 58.46 vs 1.36%). When a 1 cm region around the tumour was included

in the analysis of bead distribution, median target bead delivery increased to 19.78% (range 0.49-80.78%), and with a 2 cm region around the tumour median target bead delivery was 40.58% (range 0.64-85.0%).

It is, however, important to highlight that in this study all patients received 1ml of BTG-002814 regardless of tumour size. As such, it is not entirely unexpected that the HCC patient with an 82 mm tumour had 5% pathological necrosis despite an on-target bead percentage of 78%. By the same rationale, 1 ml was delivered to three tumours in one patient, with a combined maximum dimension of 87 mm, resulting in 50% necrosis in two of the three tumours analysed. Table 7 summarises the percentage of on-target bead delivery, degree of tissue necrosis and bead volume in each tumour normalised to tumour volume (µl/cm^3). As anticipated, the volume of beads per cm^3 is far lower in the large HCC tumour (patient 2) at 2.69 µl/cm^3, which is not reflected by just analysing the on-target bead delivery percentage. This may certainly explain the far lower level of necrosis seen in this tumour despite the high on target bead percentage when compared to the smaller HCC tumour with 100% necrosis, in which bead volume per cm^3 was 30.18 ul/cm^3. As already mentioned, for the mCRC tumours on-target bead percentage was low due to the more hypovascular nature of mCRC tumours resulting in a more lobar distribution of beads during TACE when compared to the super selective bead delivery possible with hypervascular HCC tumours. Despite this bead distribution, tumour necrosis levels of more than 90% were seen in four mCRC patients (although beads distribution could not be analysed in one patient with 100% necrosis). Proximity of bead delivery to tumour is clearly vital in order to achieve tumour response, but as demonstrated in the mCRC cohort, this may not be the only factor to consider. How much of the necrosis is due to the beads blocking the main feeding tumour vessels compared to the action of the anti-angiogenic agent vandetanib on the tumour has yet to be elucidated.

4.6.2 Tissue vandetanib levels and correlation with necrosis and bead location

As discussed, it is likely that bead proximity to the tumour relates to pathological response. However, no clear correlation has been found in this small sample. For example, in the patient with 20% necrosis post-TACE, bead delivery to the tumour

was low (0.60%), which is the likely explanation for this poorer pathological response, yet patients with a better pathological response had similar bead levels. However, as outlined in detail in Chapter 3, in patient 7 we did see lower levels of vandetanib and N-desmethyl vandetanib within the tumour when compared to other patients (Table 7). This may indicate an underlying difference in the way that vandetanib is metabolised within certain tumours that then impacts pathological response. Further studies with larger numbers are therefore required to fully analyse the correlation between bead location, drug concentration across the whole treated tumour and pathological response

Table 7: Comparison of VTB and N-VTB concentrations, on target bead percentage and pathological response

	Histology	Tumour size	Maximum vandetanib concentration (ng/g)/location	Maximum N-desmethyl vandetanib concentration (ng/g)/location	On target bead percentage (%)	Bead volume in tumour µl/cm3	Tumour necrosis (%)
1	HCC	33	404000 (centre)	4740 (middle)	38.8	30.18	100%
2	HCC	82	*	*	78.04	2.69	5%
3	mCRC	21	18800 (edge)	831 (1cm away)	0.05	0.10	90%
4	mCRC	8	*	*	**	**	100%
5	mCRC	12	12500 (edge)	544 (1cm away)	0	0.00	100%
6	mCRC	40	160000 (centre)	113 (centre)	25.25	3.93	95%
7	mCRC	24	4570 (centre)	84 (1cm away)	0.60	0.70	20%
8	mCRC (tumour 1)	42	29100 (1cm away)	389 (1cm away)	1.36	0.55	50%
8	mCRC (tumour 2)	29	6180 (centre)	405 (1cm away)	1.79	0.88	50%
8	mCRC (tumour 3)	16	93500 (whole tumour)	208 (centre)	0	0.01	NA

4.6.3 Serum biomarkers

Although significant changes in mean tumour markers were not seen, by-patient measurements generally trended down from baseline to post-treatment with BTG-002814. Several studies have however reported changes in the AFP levels following TACE [59, 60] and anti-angiogenic therapy [61]. However, in these studies patients typically had baseline AFP levels >20. In contrast, the two HCC patients in our cohort had baseline AFP levels of 3.9 and 4.1 kU/L.

CEA responses have also been seen post-TACE in mCRC patients, but typically at the 3-month time point following treatment [62]. It may be that in our cohort, samples were taken too early to see this response in tumour markers.

4.6.4 Exploratory Cytokines

In this study, we explored the changes in 39 cytokines in response to TACE with BTG-002814. Leptin was seen to increase at visit 3 (24 hours post-TACE) and then fall back to near baseline levels in all patients (Figure 7). The main function of leptin is regulation of energy consumption and appetite, but it has been reported that leptin stimulates the proliferation of different malignant cells. Furthermore, there is evidence that leptin has an important role in tumour invasion, metastasis, angiogenesis and refractoriness to chemotherapy [63, 64]. However, the effect of TACE or vandetanib on leptin has so far not been investigated. As leptin is known to have key role in inflammation, it is likely that this is released immediately post-TACE due to the local inflammation caused by the procedure, and the reason for the rise seen in our cohort at visit 3.

Osteopontin is an integrin-binding glycophosphoprotein with an important role in immune responses and vascular remodelling. It is produced by various tissues including macrophages, activated lymphocytes and Kupffer cells. Its expression has been found to be up regulated in HCC tumours and especially in metastatic HCC tumours. As a result, osteopontin has been associated with advanced disease, portal vein and lymph node invasion and early metastasis [65]. In one study of 46 HCC patients, low baseline osteopontin levels and their decrease (> 10%) 4-weeks post-TACE, was correlated to better response to treatment and better cumulative survival. Nevertheless, when evaluated in a multivariate analysis, this relationship was not statistically significant [66]. Osteopontin levels in this study were found to increase at visit 4 which occurred on average 13.1 days (+/- 7.9 days) post-TAC. This increase is likely due to the early liver damage following TACE and the resulting upregulation of osteopontin at this time point. It does not appear to correlate with tumour response metrics such as necrosis and is most likely not indicative of a poor or better prognosis post-TACE in our cohort.

It has been shown that the VEGF receptor pathway and the Tie-2 receptor pathway are two independent processes essential for in-vivo angiogenesis. Higher levels of Tie-2 have been associated with development of metastases [67]. Tie-2 is cleaved by VEGF, resulting in the production of soluble Tie-2 (sTie-2) [68]. Additionally, Tie-2 is up-regulated in capillaries as a function of neovascularization during wound healing [69]. In our study, the rise in sTie-2 at visit 4 is likely to be as a result of this process occurring after the necrosis caused by TACE. Two studies have previously investigated the change in sTie-2 following treatment with oral vandetanib but report no consistent changes [41, 42].

Although general trends were seen in other biomarkers (Table 4) the variation between the two baseline visits (visits 1 and 2), which were both prior to treatment with BTG-002814, meant that these changes were not consistent and may have been due to overall variation in cytokine levels as opposed to a direct changes as a result of treatment. However, given the small cohort of this study, they may be worth further exploration in future clinical studies and certainly warrant further consideration. Of particular interest are the trends seen post-treatment with BTG-002814 in VEGF-A, sVEGFR2, sEGFR1 and sEGFR2, angiopoietin, endoglin, follistatin, G-CSF, IGFBP, MMP2, and suPAR.

Increases in VEGF and decreases in soluble VEGF receptor 2 (sVEGFR-2) have been commonly reported in phase I and II studies of VEGFR tyrosine kinase inhibitors (TKIs). In particular, in the study by Hanrahan *et al,* lung cancer patients treated in the vandetanib monotherapy arm had significant increase in VEGF levels from baseline to day 43 and a significant decrease in sVEGFR-2 over this same time period [39]. In HCC patients treated with oral vandetanib, an approximate two to threefold increase in VEGF levels was observed which correlated with significant decreases in VEGFR- 2 levels [41]. Furthermore, serum VEGF levels have been reported to peak 14 days post-TACE in HCC patients, with ineffective cases showing higher serum VEGF levels on day 14 compared to effective cases [43]. With regards to sVEGFR-2 post-TACE, in one study serum VEGFR-2 concentrations were shown to decrease in 26.0% of patients at week 4 post-TACE and those that had a sVEFGR-2 response at week 4 had a longer median survival than those who did not have a VEGFR-2 decrease

[70]. In our cohort, VEGF was seen to rise post-TACE at visit 4 in 3/5 (60%) patients with recordable levels. For three patients, VEGF levels were unrecordable at all visits from baseline to visit 4. However, a decrease in sVEGFR-2 was not seen in our cohort post-TACE.

sEGFR is a circulating soluble growth factor receptor derived from its EGFR membrane counterpart. Previous studies have shown that following treatment with vandetanib, changes in sEGFR have not been reported [42]. Furthermore, changes have not been seen post-TACE [43]. Although there was a trend of sEGFR levels increasing at visit 4, this was not consistent. As stated in previous trials, vandetanib is a relatively weak EGFR inhibitor and it remains unclear, in HCC, patients whether vandetanib results in the dual inhibition of VEGFR and EGFR [41].

In our cohort angiopoetin-2 levels generally increased post-TACE, but a more dramatic increase is seen post-surgery (visit 6). Angiopoetin-2 is an upstream ligand of Tie-2 and has a role in angiogenesis with VEGF. In studies of oral vandetanib, angiopoetin-2 levels have not changed in response to treatment [41, 42]. However, levels have been shown to increase 7 days post-TACE [71], and, furthermore, have been shown to be upregulated in CRC in response to hypoxia [72].

Endoglin is an endothelial cell membrane receptor that is highly expressed on tumour vasculature. Endoglin is essential for angiogenesis and its expression has been shown to be upregulated by hypoxia and vascular endothelial growth factor (VEGF) inhibition [73]. Previous studies have not investigated the effect of vandetanib or TACE on endoglin levels.

Follistatin is known to be a secretory protein and several reports have shown that it regulates a variety of processes of angiogenesis, metastasis, and cell apoptosis. It has been suggested that follistatin, in combination with VEGF, may advance the creation of new blood vessels by stimulating the production of MMP-2, a proteolytic enzyme that has been implicated in tumour angiogenesis. A significant decrease of MMP-2 levels have been reported 1 and 3 months post-TACE [74], whilst vandetanib has been shown to down regulate MMP-2 in HCC

cell lines [36]. In our cohort, MMP-2 levels were shown to decrease post-TACE whilst follistatin levels increased at visit 4.

4.6.5 Limitations of this study

In this study, we have been able to assess the location of novel RO vandetanib-eluting beads and relate this to histopathological response. Furthermore, the window-of-opportunity design has allowed the response of 39 cytokines to be assessed in response to treatment with BTG-002814. However, there are limitations.

Firstly, is that this is a small cohort with a mixture of patients with HCC and mCRC. As such, this limits the extent of detailed analysis with regards to histopathological and cytokine analysis. Although our results are hypothesis generating, it results in the reporting of trends rather than clear observed changes. This is particularly apparent with regards to cytokine analysis.

Furthermore, the Milliplex assays utilised for cytokine analysis have not been validated for clinical use. Traditionally, methods such as the enzyme-linked immunosorbent assay (ELISA) have enabled the analysis of single cytokines, and although such techniques have been invaluable in our current understanding, this has limited research to focus on a few key targets. The Luminex assay has become an important tool in cytokine detection and quantification because of its capacity to measure multiple different cytokines simultaneously in a single run of the assay with small sample size requirement [75]. However, as with any biological assay, the potential of simultaneously analysing multiple analytes poses problems in terms of validation and standardisation, especially for use in clinical studies. Furthermore, one further limitation with this system, is the ability to detect low levels of samples, which was evident in this study particularly with the measurement of a number of inflammatory cytokines [76]. As such, key trends may not have been detected.

4.7 CONCLUSION

In conclusion, TACE with 1 ml of BTG-002814 results in significant tumour necrosis (median necrosis 90%, range 5-100%) unrelated to tumour size. The ability to quantitatively assess bead distribution around a tumour, and to be able to relate this to pathological response, furthers our understanding of the link between TACE delivery and treatment response. Despite this, a clear correlation has yet to be found. Furthermore, TACE with BTG-002814 has led to changes in the levels of a number of key cytokines. However, in view of our small cohort these cytokines warrant further investigation in larger clinical trials.

4.8 REFERENCES

[1] Varela M, Real MI, Burrel M, Forner A, Sala M, Brunet M, et al. Chemoembolization of hepatocellular carcinoma with drug eluting beads: efficacy and doxorubicin pharmacokinetics. Journal of hepatology. 2007;46:474-81.

[2] Poon RT, Tso WK, Pang RW, Ng KK, Woo R, Tai KS, et al. A phase I/II trial of chemoembolization for hepatocellular carcinoma using a novel intra-arterial drug-eluting bead. Clinical gastroenterology and hepatology : the official clinical practice journal of the American Gastroenterological Association. 2007;5:1100-8.

[3] Chung JW, Kim HC. Can CT Following Chemoembolization with Radiopaque Drug-Eluting Beads Tell Us How Much Drug We Deliver? Radiology. 2018;289:405-6.

[4] Llovet JM, Real MI, Montana X, Planas R, Coll S, Aponte J, et al. Arterial embolisation or chemoembolisation versus symptomatic treatment in patients with unresectable hepatocellular carcinoma: a randomised controlled trial. Lancet (London, England). 2002;359:1734-9.

[5] Lo CM, Ngan H, Tso WK, Liu CL, Lam CM, Poon RT, et al. Randomized controlled trial of transarterial lipiodol chemoembolization for unresectable hepatocellular carcinoma. Hepatology (Baltimore, Md). 2002;35:1164-71.

[6] Meyer T, Kirkwood A, Roughton M, Beare S, Tsochatzis E, Yu D, et al. A randomised phase II/III trial of 3-weekly cisplatin-based sequential transarterial chemoembolisation vs embolisation alone for hepatocellular carcinoma. Br J Cancer. 2013;108:1252-9.

[7] Brown KT, Do RK, Gonen M, Covey AM, Getrajdman GI, Sofocleous CT, et al. Randomized Trial of Hepatic Artery Embolization for Hepatocellular Carcinoma Using Doxorubicin-Eluting Microspheres Compared With Embolization With Microspheres Alone. J Clin Oncol. 2016;34:2046-53.

[8] Malagari K, Pomoni M, Kelekis A, Pomoni A, Dourakis S, Spyridopoulos T, et al. Prospective randomized comparison of chemoembolization with doxorubicin-eluting beads and bland embolization with BeadBlock for hepatocellular carcinoma. Cardiovasc Intervent Radiol. 2010;33:541-51.

[9] Nicolini A, Martinetti L, Crespi S, Maggioni M, Sangiovanni A. Transarterial chemoembolization with epirubicin-eluting beads versus transarterial

embolization before liver transplantation for hepatocellular carcinoma. Journal of vascular and interventional radiology : JVIR. 2010;21:327-32.
[10] Inoue K, Torimura T, Nakamura T, Iwamoto H, Masuda H, Abe M, et al. Vandetanib, an inhibitor of VEGF receptor-2 and EGF receptor, suppresses tumor development and improves prognosis of liver cancer in mice. Clin Cancer Res. 2012;18:3924-33.
[11] Ryan AJ, Wedge SR. ZD6474--a novel inhibitor of VEGFR and EGFR tyrosine kinase activity. Br J Cancer. 2005;92 Suppl 1:S6-13.
[12] Morabito A, Piccirillo MC, Falasconi F, De Feo G, Del Giudice A, Bryce J, et al. Vandetanib (ZD6474), a dual inhibitor of vascular endothelial growth factor receptor (VEGFR) and epidermal growth factor receptor (EGFR) tyrosine kinases: current status and future directions. Oncologist. 2009;14:378-90.
[13] Ferrara N. Vascular endothelial growth factor as a target for anticancer therapy. Oncologist. 2004;9 Suppl 1:2-10.
[14] Zhao Y, Adjei AA. Targeting Angiogenesis in Cancer Therapy: Moving Beyond Vascular Endothelial Growth Factor. Oncologist. 2015;20:660-73.
[15] Toi M, Matsumoto T, Bando H. Vascular endothelial growth factor: its prognostic, predictive, and therapeutic implications. The Lancet Oncology. 2001;2:667-73.
[16] Hicklin DJ, Ellis LM. Role of the vascular endothelial growth factor pathway in tumor growth and angiogenesis. J Clin Oncol. 2005;23:1011-27.
[17] Hanahan D, Weinberg RA. Hallmarks of cancer: the next generation. Cell. 2011;144:646-74.
[18] Hurwitz H, Fehrenbacher L, Novotny W, Cartwright T, Hainsworth J, Heim W, et al. Bevacizumab plus irinotecan, fluorouracil, and leucovorin for metastatic colorectal cancer. The New England journal of medicine. 2004;350:2335-42.
[19] Saltz LB, Clarke S, Diaz-Rubio E, Scheithauer W, Figer A, Wong R, et al. Bevacizumab in combination with oxaliplatin-based chemotherapy as first-line therapy in metastatic colorectal cancer: a randomized phase III study. J Clin Oncol. 2008;26:2013-9.
[20] Giannelli G, Azzariti A, Sgarra C, Porcelli L, Antonaci S, Paradiso A. ZD6474 inhibits proliferation and invasion of human hepatocellular carcinoma cells. Biochem Pharmacol. 2006;71:479-85.

[21] Llovet JM, Ricci S, Mazzaferro V, Hilgard P, Gane E, Blanc JF, et al. Sorafenib in advanced hepatocellular carcinoma. The New England journal of medicine. 2008;359:378-90.
[22] Abou-Alfa GK, Schwartz L, Ricci S, Amadori D, Santoro A, Figer A, et al. Phase II study of sorafenib in patients with advanced hepatocellular carcinoma. J Clin Oncol. 2006;24:4293-300.
[23] Cheng A-L, Kang Y-K, Chen Z, Tsao C-J, Qin S, Kim JS, et al. Efficacy and safety of sorafenib in patients in the Asia-Pacific region with advanced hepatocellular carcinoma: a phase III randomised, double-blind, placebo-controlled trial. The Lancet Oncology. 2009;10:25-34.
[24] Kudo M, Finn RS, Qin S, Han KH, Ikeda K, Piscaglia F, et al. Lenvatinib versus sorafenib in first-line treatment of patients with unresectable hepatocellular carcinoma: a randomised phase 3 non-inferiority trial. Lancet (London, England). 2018;391:1163-73.
[25] Vlahovic G, Crawford J. Activation of tyrosine kinases in cancer. Oncologist. 2003;8:531-8.
[26] Seshacharyulu P, Ponnusamy MP, Haridas D, Jain M, Ganti AK, Batra SK. Targeting the EGFR signaling pathway in cancer therapy. Expert Opin Ther Targets. 2012;16:15-31.
[27] Van Cutsem E, Kohne CH, Hitre E, Zaluski J, Chang Chien CR, Makhson A, et al. Cetuximab and chemotherapy as initial treatment for metastatic colorectal cancer. The New England journal of medicine. 2009;360:1408-17.
[28] Van Cutsem E, Kohne CH, Lang I, Folprecht G, Nowacki MP, Cascinu S, et al. Cetuximab plus irinotecan, fluorouracil, and leucovorin as first-line treatment for metastatic colorectal cancer: updated analysis of overall survival according to tumor KRAS and BRAF mutation status. J Clin Oncol. 2011;29:2011-9.
[29] Bokemeyer C, Bondarenko I, Hartmann JT, de Braud F, Schuch G, Zubel A, et al. Efficacy according to biomarker status of cetuximab plus FOLFOX-4 as first-line treatment for metastatic colorectal cancer: the OPUS study. Ann Oncol. 2011;22:1535-46.
[30] Douillard JY, Oliner KS, Siena S, Tabernero J, Burkes R, Barugel M, et al. Panitumumab-FOLFOX4 treatment and RAS mutations in colorectal cancer. The New England journal of medicine. 2013;369:1023-34.

[31] Van Cutsem E, Lenz HJ, Kohne CH, Heinemann V, Tejpar S, Melezinek I, et al. Fluorouracil, leucovorin, and irinotecan plus cetuximab treatment and RAS mutations in colorectal cancer. J Clin Oncol. 2015;33:692-700.
[32] Bokemeyer C, Kohne CH, Ciardiello F, Lenz HJ, Heinemann V, Klinkhardt U, et al. FOLFOX4 plus cetuximab treatment and RAS mutations in colorectal cancer. European journal of cancer (Oxford, England : 1990). 2015;51:1243-52.
[33] Douillard JY, Siena S, Cassidy J, Tabernero J, Burkes R, Barugel M, et al. Randomized, phase III trial of panitumumab with infusional fluorouracil, leucovorin, and oxaliplatin (FOLFOX4) versus FOLFOX4 alone as first-line treatment in patients with previously untreated metastatic colorectal cancer: the PRIME study. J Clin Oncol. 2010;28:4697-705.
[34] Zhu AX, Rosmorduc O, Evans TR, Ross PJ, Santoro A, Carrilho FJ, et al. SEARCH: a phase III, randomized, double-blind, placebo-controlled trial of sorafenib plus erlotinib in patients with advanced hepatocellular carcinoma. J Clin Oncol. 2015;33:559-66.
[35] Wedge SR, Ogilvie DJ, Dukes M, Kendrew J, Chester R, Jackson JA, et al. ZD6474 inhibits vascular endothelial growth factor signaling, angiogenesis, and tumor growth following oral administration. Cancer Res. 2002;62:4645-55.
[36] Giannelli G, Sgarra C, Porcelli L, Azzariti A, Antonaci S, Paradiso A. EGFR and VEGFR as potential target for biological therapies in HCC cells. Cancer Lett. 2008;262:257-64.
[37] West NR, McCuaig S, Franchini F, Powrie F. Emerging cytokine networks in colorectal cancer. Nat Rev Immunol. 2015;15:615-29.
[38] Pengjun Z, Xinyu W, Feng G, Xinxin D, Yulan L, Juan L, et al. Multiplexed cytokine profiling of serum for detection of colorectal cancer. Future Oncol. 2013;9:1017-27.
[39] Hanrahan EO, Lin HY, Kim ES, Yan S, Du DZ, McKee KS, et al. Distinct patterns of cytokine and angiogenic factor modulation and markers of benefit for vandetanib and/or chemotherapy in patients with non-small-cell lung cancer. J Clin Oncol. 2010;28:193-201.
[40] Kim MJ, Jang JW, Oh BS, Kwon JH, Chung KW, Jung HS, et al. Change in inflammatory cytokine profiles after transarterial chemotherapy in patients with hepatocellular carcinoma. Cytokine. 2013;64:516-22.
[41] Hsu C, Yang TS, Huo TI, Hsieh RK, Yu CW, Hwang WS, et al. Vandetanib in patients with inoperable hepatocellular carcinoma: a phase II, randomized,

double-blind, placebo-controlled study. Journal of hepatology. 2012;56:1097-103.
[42] Mross K, Fasol U, Frost A, Benkelmann R, Kuhlmann J, Buchert M, et al. DCE-MRI assessment of the effect of vandetanib on tumor vasculature in patients with advanced colorectal cancer and liver metastases: a randomized phase I study. Journal of angiogenesis research. 2009;1:5.
[43] Chao Y, Wu CY, Kuo CY, Wang JP, Luo JC, Kao CH, et al. Cytokines are associated with postembolization fever and survival in hepatocellular carcinoma patients receiving transcatheter arterial chemoembolization. Hepatol Int. 2013;7:883-92.
[44] Li X, Feng GS, Zheng CS, Zhuo CK, Liu X. Expression of plasma vascular endothelial growth factor in patients with hepatocellular carcinoma and effect of transcatheter arterial chemoembolization therapy on plasma vascular endothelial growth factor level. World J Gastroenterol. 2004;10:2878-82.
[45] Ranieri G, Ammendola M, Marech I, Laterza A, Abbate I, Oakley C, et al. Vascular endothelial growth factor and tryptase changes after chemoembolization in hepatocarcinoma patients. World J Gastroenterol. 2015;21:6018-25.
[46] Llovet JM, Zucman-Rossi J, Pikarsky E, Sangro B, Schwartz M, Sherman M, et al. Hepatocellular carcinoma. Nat Rev Dis Primers. 2016;2:16018.
[47] Kudo M. Signaling pathway/molecular targets and new targeted agents under development in hepatocellular carcinoma. World J Gastroenterol. 2012;18:6005-17.
[48] Zhu K, Dai Z, Zhou J. Biomarkers for hepatocellular carcinoma: progression in early diagnosis, prognosis, and personalized therapy. Biomark Res. 2013;1:10.
[49] Llovet JM, Pena CE, Lathia CD, Shan M, Meinhardt G, Bruix J, et al. Plasma biomarkers as predictors of outcome in patients with advanced hepatocellular carcinoma. Clin Cancer Res. 2012;18:2290-300.
[50] Wang Y, Chen Y, Ge N, Zhang L, Xie X, Zhang J, et al. Prognostic significance of alpha-fetoprotein status in the outcome of hepatocellular carcinoma after treatment of transarterial chemoembolization. Ann Surg Oncol. 2012;19:3540-6.
[51] Mager LF, Wasmer MH, Rau TT, Krebs P. Cytokine-Induced Modulation of Colorectal Cancer. Front Oncol. 2016;6:96.

[52] Thirunavukarasu P, Sukumar S, Sathaiah M, Mahan M, Pragatheeshwar KD, Pingpank JF, et al. C-stage in colon cancer: implications of carcinoembryonic antigen biomarker in staging, prognosis, and management. J Natl Cancer Inst. 2011;103:689-97.
[53] Kantola T, Klintrup K, Vayrynen JP, Vornanen J, Bloigu R, Karhu T, et al. Stage-dependent alterations of the serum cytokine pattern in colorectal carcinoma. Br J Cancer. 2012;107:1729-36.
[54] Gunawardene A, Dennett E, Larsen P. Prognostic value of multiple cytokine analysis in colorectal cancer: a systematic review. J Gastrointest Oncol. 2019;10:134-43.
[55] Bio-Rad. https://www.bio-rad.com/en-uk/applications-technologies/bio-plex-multiplex-immunoassays?ID=LUSM0ZMNI#2. Accessed April 2020.
[56] Jones RP, Malik HZ, Fenwick SW, Terlizzo M, O'Grady E, Stremitzer S, et al. PARAGON II - A single arm multicentre phase II study of neoadjuvant therapy using irinotecan bead in patients with resectable liver metastases from colorectal cancer. Eur J Surg Oncol. 2016;42:1866-72.
[57] Najmi Varzaneh F, Pandey A, Aliyari Ghasabeh M, Shao N, Khoshpouri P, Pandey P, et al. Prediction of post-TACE necrosis of hepatocellular carcinoma usingvolumetric enhancement on MRI and volumetric oil deposition on CT, with pathological correlation. Eur Radiol. 2018;28:3032-40.
[58] Mikhail AS, Pritchard WF, Negussie AH, Krishnasamy VP, Amchin DB, Thompson JG, et al. Mapping Drug Dose Distribution on CT Images Following Transarterial Chemoembolization with Radiopaque Drug-Eluting Beads in a Rabbit Tumor Model. Radiology. 2018;289:396-404.
[59] Lee YK, Kim SU, Kim DY, Ahn SH, Lee KH, Lee DY, et al. Prognostic value of alpha-fetoprotein and des-gamma-carboxy prothrombin responses in patients with hepatocellular carcinoma treated with transarterial chemoembolization. BMC cancer. 2013;13:5.
[60] Liu G, Ouyang Q, Xia F, Fan G, Yu J, Zhang C, et al. Alpha-fetoprotein response following transarterial chemoembolization indicates improved survival for intermediate-stage hepatocellular carcinoma. HPB (Oxford). 2019;21:107-13.
[61] Shao YY, Lin ZZ, Hsu C, Shen YC, Hsu CH, Cheng AL. Early alpha-fetoprotein response predicts treatment efficacy of antiangiogenic systemic

therapy in patients with advanced hepatocellular carcinoma. Cancer. 2010;116:4590-6.
[62] Martin RC, Joshi J, Robbins K, Tomalty D, O'Hara R, Tatum C. Transarterial Chemoembolization of Metastatic Colorectal Carcinoma with Drug-Eluting Beads, Irinotecan (DEBIRI): Multi-Institutional Registry. J Oncol. 2009;2009:539795.
[63] Milosevic VS, Vukmirovic FC, Krstic MS, Zindovic MM, Lj Stojanovic D, Jancic SA. Involvement of leptin receptors expression in proliferation and neoangiogenesis in colorectal carcinoma. J BUON. 2015;20:100-8.
[64] Sharma D, Saxena NK, Vertino PM, Anania FA. Leptin promotes the proliferative response and invasiveness in human endometrial cancer cells by activating multiple signal-transduction pathways. Endocr Relat Cancer. 2006;13:629-40.
[65] Tampaki M, Doumba PP, Deutsch M, Koskinas J. Circulating biomarkers of hepatocellular carcinoma response after locoregional treatments: New insights. World J Hepatol. 2015;7:1834-42.
[66] Kim SH, Chung YH, Yang SH, Kim JA, Jang MK, Kim SE, et al. Prognostic value of serum osteopontin in hepatocellular carcinoma patients treated with transarterial chemoembolization. Korean J Hepatol. 2009;15:320-30.
[67] Chin KF, Greenman J, Reusch P, Gardiner E, Marme D, Monson JR. Vascular endothelial growth factor and soluble Tie-2 receptor in colorectal cancer: associations with disease recurrence. Eur J Surg Oncol. 2003;29:497-505.
[68] Shoji H, Yoshio S, Mano Y, Doi H, Sugiyama M, Osawa Y, et al. Pro-angiogenic TIE-2-expressing monocytes/TEMs as a biomarker of the effect of sorafenib in patients with advanced hepatocellular carcinoma. Int J Cancer. 2017;141:1011-7.
[69] Tanaka S, Sugimachi K, Yamashita Yi Y, Ohga T, Shirabe K, Shimada M, et al. Tie2 vascular endothelial receptor expression and function in hepatocellular carcinoma. Hepatology (Baltimore, Md). 2002;35:861-7.
[70] Zheng YB, Meng QW, Zhao W, Liu B, Huang JW, He X, et al. Prognostic value of serum vascular endothelial growth factor receptor 2 response in patients with hepatocellular carcinoma undergoing transarterial chemoembolization. Med Oncol. 2014;31:843.

[71] Hsieh MY, Lin ZY, Chuang WL. Serial serum VEGF-A, angiopoietin-2, and endostatin measurements in cirrhotic patients with hepatocellular carcinoma treated by transcatheter arterial chemoembolization. Kaohsiung J Med Sci. 2011;27:314-22.
[72] Gu J, Yamamoto H, Ogawa M, Ngan CY, Danno K, Hemmi H, et al. Hypoxia-induced up-regulation of angiopoietin-2 in colorectal cancer. Oncol Rep. 2006;15:779-83.
[73] Li Y, Zhai Z, Liu D, Zhong X, Meng X, Yang Q, et al. CD105 promotes hepatocarcinoma cell invasion and metastasis through VEGF. Tumour Biol. 2015;36:737-45.
[74] Daniele A, Divella R, Quaranta M, Mattioli V, Casamassima P, Paradiso A, et al. Clinical and prognostic role of circulating MMP-2 and its inhibitor TIMP-2 in HCC patients prior to and after trans-hepatic arterial chemo-embolization. Clin Biochem. 2014;47:184-90.
[75] Khalifian S, Raimondi G, Brandacher G. The use of luminex assays to measure cytokines. J Invest Dermatol. 2015;135:1-5.
[76] Chowdhury F, Williams A, Johnson P. Validation and comparison of two multiplex technologies, Luminex and Mesoscale Discovery, for human cytokine profiling. J Immunol Methods. 2009;340:55-64.

5 PERFUSION IMAGING OF PRIMARY AND SECONDARY LIVER TUMOURS IN THE VERONA STUDY

5.1 INTRODUCTION

5.1.1 Overview of imaging in liver cancers

The ability to accurately image tumours is a vital component in the management of liver cancers. It enables accurate diagnoses, can circumvent the need for diagnostic testing, allows response to be monitored during and after a course of treatment, and furthermore detects for early evidence of disease recurrence. As our knowledge of certain disease pathways increases, so does our ability to develop targeted therapeutic agents directed against these key pathways. However, it is increasingly recognised that standard imaging techniques may not be sophisticated enough to detect tumour response following these novel treatments. There is therefore a need to explore novel imaging techniques and identify specific imaging biomarkers that can help predict which tumours are likely to respond to certain therapies and detect early changes in response to such treatments [1].

Currently, imaging of the liver is routinely performed using computerised tomography (CT) and magnetic resonance imaging (MRI). In the case of hepatocellular carcinoma (HCC), multiphasic CT scans are required for diagnosis, which produce a series of arterial, portal, and delayed contrast-enhanced images. If a liver lesion shows arterial hypervascularity, and washout of contrast on the venous or delayed phases, then a diagnosis of HCC can be made without the need for an invasive biopsy [2]. Liver metastases from colorectal cancer (mCRC) are often detected on routine CT imaging performed as part of a follow-up imaging schedule or following a rise in blood markers [3]. However, the enhancement of liver metastasis varies depending on the vascularity. For example, it has been shown that small mCRC liver lesions are often hyperattenuating during the hepatic arterial phase whereas larger lesions show a hyperattenuating rim during the hepatic arterial phase and a hypoattenuating centre. In contrast, larger lesions are often detected as hypoattenuating lesions during the portal venous phase [4]. Despite improvements in CT imaging for both HCC and mCRC, further imaging with contrast MRI scans is often required to provide further diagnostic clarification.

MRI is particularly useful in the case of mCRC lesions <10 mm and in the setting of liver cirrhosis to exclude regenerative nodules [2, 5].

5.1.2 Perfusion Computerised Tomography

Perfusion CT imaging involves the measurement of blood flow characteristics through dynamic CT acquisitions following the intravenous administration of a low molecular weight iodinated contrast agent. When administered as an intravenous bolus, tissue concentration is dependent on vascular flow and interstitial accumulation, resulting in differential attenuation on CT imaging, before recirculation and clearance of the agent by the kidneys. As tissue attenuation is directly proportional to the local concentration of contrast agent in the tissue, it is an indirect measure of tissue vascularity and assessment of tissue perfusion is possible [6].

Neovascularisation and hyperpermeability within the tumour vasculature results in a concentration curve that differs from that of healthy tissue, with a more rapid initial uptake of contrast, high peak enhancement and rapid washout [7]. Qualitative and semiquantitative evaluation and mapping of these data can improve tumour detection and differentiation of tumour tissue from healthy or treated tissues and detect changes in blood flow in response to local and systemic treatment [8]. More complex kinetic perfusion models can derive functional physiological parameters such as blood flow (BF), blood volume (BV), mean transit time (MTT), extracellular extravascular volume fraction, and permeability surface (PS) area product. Blood flow reflects the delivery of oxygen and other nutrients to tumour tissue, and is an indirect measure of hypoxia and angiogenesis, whereas the PS area product reflects the leakiness of tissue vasculature and interstitial pressure [9].

In general, there are two mathematic models most frequently used in the assessment of perfusion parameters, namely the compartmental model (one- or two-compartment model) and the distributed parameter model. The one-compartment model allows for estimates of BF or perfusion that is defined as the blood flow through the tissue of interest per unit of time (expressed as ml/min/100 ml). In comparison, the two compartment and distributed parameter models allow the following additional perfusion parameters to be obtained: BV, MTT and permeability. At present there is no real consensus regarding the best method for

liver perfusion imaging but the one-compartmental method has tended to dominate liver perfusion studies, partly due to its relatively simple underlying principle [10].

In order to obtain pCT images, sequential CT scanning of the same volume over time is required. Images are obtained prior to, during, and following the delivery of a contrast agent in order to trace the changes in CT attenuation in the liver over time. The liver is a unique organ to assess with perfusion studies due to its dual blood supply. The liver is predominantly supplied by the low-pressure portal vein (75%) and supplemented by the high-pressure hepatic artery (25%). As a result, the effective time-intensity curve obtained from liver tissue is a combination of both the arterial and the portal venous components. However, diseases such as liver cirrhosis as well as primary and secondary liver tumours can lead to perfusion changes resulting in increased hepatic arterial blood flow and decreased portal venous flow. In the case of liver tumours, the mechanism behind these changes is different depending on whether the tumour is a primary highly vascular HCC or a metastatic lesion from colorectal cancer. In HCC, the increase in hepatic flow is due to the development of new arteries that are not associated with portal vein branches (tumour neovascularisation). In liver metastasis, it is the proliferation of sinusoidal endothelial cells (assisted by VEGF expression) that results in the increase in the hepatic flow [11]. As a result, methods that allow a separation of the arterial and portal venous components are ideally required when assessing liver perfusion analysis [1].

The dual input maximum slope method is a one compartment-based model approach, which considers the intravascular and extra-vascular spaces as a single compartment. This model is based on Fick's principle, which calculates tissue perfusion based on conversion of mass within the system [8]. The dual input component takes into account the fact that the liver has a dual blood supply and therefore separates tumour perfusion into arterial and portal components. The time to peak splenic enhancement, defined as the end of the arterial phase and start of the portal phase of liver perfusion, is used for separating hepatic arterial perfusion and portal venous perfusion. The maximum slope of the liver time-intensity curve in both the arterial and portal venous phase is then divided by the peak aortic and portal enhancement to calculate the arterial and portal liver

perfusion parameters (in ml/min/100ml). The perfusion index (PI), defined as the ratio of the arterial perfusion to the total hepatic perfusion can then be calculated:

PI = arterial perfusion/ (arterial + portal perfusion)

The benefit of using a dual vascular input model for analysis of CT perfusion data is that it improves test-retest reproducibility [1, 12]. However, this method works on the assumption that there is no venous outflow, which means that a high injection rate is required, and it does not allow for calculation of other perfusion parameters.

5.1.2.1 Perfusion imaging in clinical trials

The role of perfusion CT imaging has been investigated in a number of clinical trials in primary HCC and liver metastases [6, 13-21]. Studies have shown that pCT parameters correlate well with the presence and extent of tumour vessels, which could be utilised in the earlier detection of liver tumours and response to treatment by acting as surrogates of tumour angiogenesis [1, 12]. It has also been suggested that the quantitative evaluation of hepatic perfusion on CT images is a more sensitive imaging biomarker than tumour size and tumour density for monitoring the anti-angiogenic treatment effects in HCC [22, 23]. Furthermore, it has been demonstrated that pCT as follow-up imaging modality post-TACE is feasible for early response assessment and detection of residual tumour 1 to 4 weeks post-treatment [16].

Change in perfusion parameters have also been linked to tumour response. Chen *et al* correlated TACE response by RECIST with change in perfusion parameters in 39 HCC patients 4 weeks after treatment. Only one case had a complete response by RECIST and the CT perfusion maps of post-treatment lesion displayed complete absence of signals. In the partial response group, hepatic artery perfusion (HAP), hepatic arterial fracture (HAF) and hepatic blood volume (HBV) of viable tumours post-TACE were reduced compared with pre-TACE. In the stable disease group, all CT perfusion parameters were not significantly different pre- and post-TACE. In the progressive disease group, HAP, HAF, portal vein perfusion (PVP) and hepatic blood flow (HBF) of viable tumours post-TACE were significantly increased compared with pre-TACE [14]. Lv *et al* also

correlated change in perfusion parameters with outcome in mCRC patients and found that the percentage change in HAP 1-month post treatment was the optimal predicting parameter (p = 0.003). The best cut-off value was -21.5% and patients who exhibited a ≥ 21.5% decrease in HAP had a significantly higher overall survival rate than those who exhibited a < 21.5% decrease (p < 0.001) [20].

5.1.3 Dynamic contrast-enhanced MRI

5.1.3.1 Overview

Perfusion imaging can also be performed with MRI. In this situation, sequential images are obtained by injecting a low molecular weight gadolinium chelated contrast into a vein at a constant rate. The contrast agent (CA) is carried by blood flow into tissue causing increased signal intensity (SI) of the T1 weighted images due to the shortening of the longitudinal relaxation time of the tissue [24]. As with pCT images, SI time curves can be deconvoluted by mathematical models to extract parameters that may reflect tumour angiogenesis.

As with pCT imaging there are a number of models that can be used in the mathematical calculation of perfusion parameters. For DCE-MRI, an initial conversion step of SI into CA concentration is required before concentration-time curves can be fitted using the selected model [24]. Here, we focus on the extended Tofts model [25] and the dual-input single-compartment (DISC) model [26].

The extended Tofts model uses a single arterial input function in a bi-compartmental model, accounting for the vessels and extravascular extracellular space (EES) [34]. Using this model, the following parameters can be calculated: K^{trans}, K_{ep}, V_e and V_p. K^{trans} is the forward volume transfer constant. This determines the flux of gadolinium from intravascular space to the EES, and as a result represents vascular permeability in high flow situation and blood flow into tissue in flow limited situations. K_{ep} represents the reverse flux flow rate constant. This parameter expresses the return process of the contrast agent from EES to intravascular space. V_e is the volume fraction of EES, an indirect measure

representing cellular density of the tissue, whilst V_p is the fractional plasma volume [24] (Figure 1).

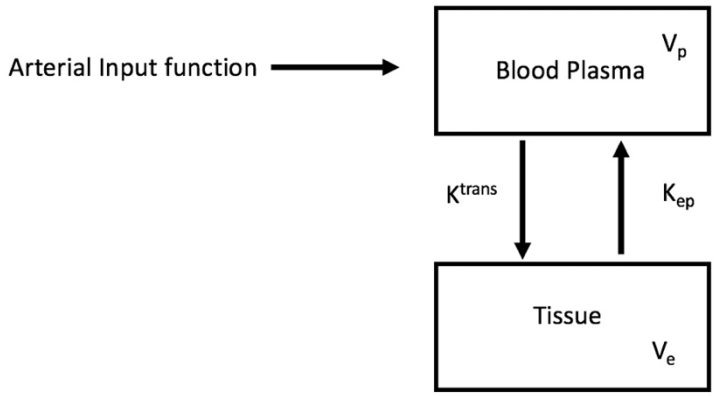

Figure 1: Extended Tofts Model.

Abbreviations: K_{ep} reverse flux flow rate constant; V_e, volume fraction of extravascular extracellular space; V_p fractional plasma volume

In comparison, the DISC model can be used to reflect the fact that the liver has a dual blood supply from both the hepatic artery and the portal vein, and therefore has two inflow rate constants. In this one-compartmental model the whole liver, including capillaries, extravascular space, and cells, is considered as a single functional compartment [27]. This model can be used to obtain parameters including arterial blood flow, portal blood flow, hepatic arterial fraction, distribution volume (DV) and MTT [24].

5.1.3.2 DCE-MRI in clinical trials

As with pCT imaging, DCE-MRI had already been used in a number of clinical trials in assessing response to anti-angiogenic agents [23, 28, 29]. Two studies in particular have assessed changes in response in oral vandetanib [30, 31], but there is limited data on changes in DCE-MRI perfusion parameters post-TACE. Clinical studies have mainly focused on K^{trans} as a parameter to reflect changes in blood flow following anti-angiogenic treatment but results from these studies have shown varying results [23, 28-32].

5.2 OBJECTIVES

The aim of this study was to assess changes in blood flow using DCE-MRI and pCT following treatment with a novel vandetanib-eluting radiopaque bead (BTG-002814) in order to identify potential imaging biomarkers that can predict response to treatment with BTG-002814.

As such, the following specific objectives were set:

1. To evaluate the inter-reader variation of perfusion parameters between radiologists
2. To evaluate the within-patient reproducibility of perfusion parameters
3. To evaluate the changes in perfusion parameters following treatment with BTG-002814

5.3 MATERIALS AND METHODS

5.3.1. Study design and patient population

All patients in this study were treated as part of the VEROnA clinical trial, which is outlined in detail in Chapter 2 (section 2.2) As part of the trial protocol, patients underwent imaging with pCT and DCE-MRI at baseline, prior to treatment with BTG-002814 (as a second baseline scan) and 7-21 days post-treatment with BTG-002814 (day prior to surgical resection) (Figure 2). At each time point, CT scanning was performed before, or at least 90 minutes after, the MRI scan to prevent CT image contamination with gadolinium contrast.

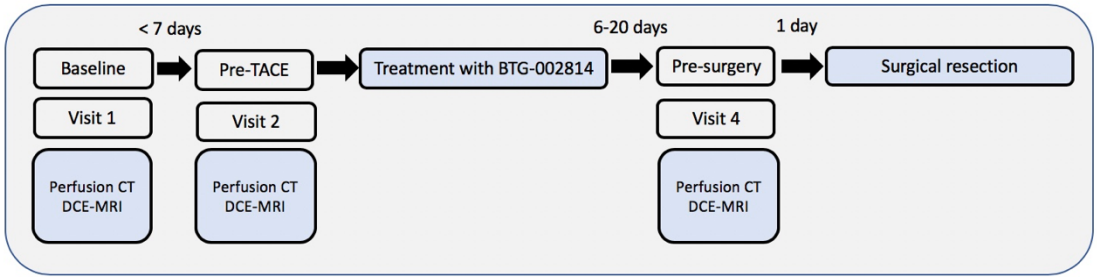

Figure 2: Overview of imaging schedule in the VEROnA study

Abbreviations: CT, computed tomography; MRI, magnetic resonance imaging, DCE, dynamic contrast enhanced.

5.3.2 Image acquisition and post-processing

5.3.2.1 Perfusion CT

All pCT studies were performed on a 320-detector row CT scanner (Aquilion ONE; Toshiba Medical Systems, Ohtaware, Japan). Initially, a non-contrast study of the upper abdomen was performed in order to locate the tumour. After the area to be covered had been selected, a bolus of 0.5 ml/kg of iodinated contrast (300 mg/mL) was administered at an injection rate of 5 ml/s through an antecubital vein. A low dose perfusion scan protocol was used, with intermittent scanning over 90 seconds at 100 kV, with a slice thickness of 0.5 mm. Shallow breathing or breath-hold was advised for the pCT. The cranio-caudal coverage for the perfusion sequence was 160 mm. The pCT data were post-processed using a commercially available software (Vitrea, Body perfusion, Canon/Toshiba Medical Systems) installed on a multimodality workstation. This software program automatically corrects the motion between dynamic volumes using a non-rigid deformable registration technique [19]. To avoid measurement errors due to compact embolisation material, and to ensure only soft tissue was loaded into the perfusion software, an upper threshold was set at 150 Hounsfield units (HU), and the lower threshold was defined as −80 HU [16].

Regions of interest (ROI) were placed on the abdominal aorta, main portal vein, normal liver parenchyma and spleen to generate respective time-density curves (TDC) (Figure 3). The generated TDCs represented the hepatic artery input function and the portal vein input function respectively. The time of maximum enhancement within a splenic ROI was used to separate arterial and portal venous phases of hepatic enhancement. Finally, quantitative maps of liver perfusion were created and displayed by means of a colour scale. Colour maps represented arterial liver perfusion (ml/100 ml/min), portal liver perfusion (ml/100 ml/min), and hepatic PI (%) (Figure 3). All maps were created by the Clinical Research Fellow (LB) and reviewed by a Consultant Radiologist (JH). A second analysis was planned based on the Patlak method; a single-input dual-compartment model available on the Vitrea Body System [12]. However, due to lack of reproducibility with the creation of the Patlak plot this data was not analysed.

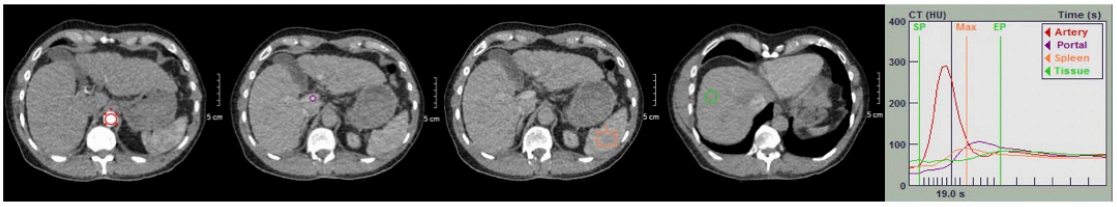

Figure 3: Region of interest inputs and time-density curves. Perfusion CT images showing regions of interest and generated time-density curves: aorta (red), portal vein (purple), spleen (orange) and normal liver parenchyma (green).

For perfusion measurements, tumour ROIs were contoured by two independent readers, both Consultant Radiologists with experience of perfusion scanning and 19 and 20 years of experience in radiology. Tumour ROIs were contoured by each reader independently on the axial slice with the largest tumour diameter, using diagnostic CT and MRI sequences to ensure accurate contouring. The entire tumour was carefully contoured and perfusion parameters calculated. For analysis of normal liver parenchyma, one radiologist contoured an ROI in the liver, measuring 4-5 cm^2, in an area away from the tumour avoiding large blood vessels. For each tumour and normal parenchyma the following perfusion parameters were obtained: arterial blood flow (AF; mL/min/100 mL), portal venous blood flow (PF; mL/min/100 mL), and the perfusion index (PI; AF/(AF + PF); %) which represents the percentage of total liver blood flow from arterial origin (Figure 4).

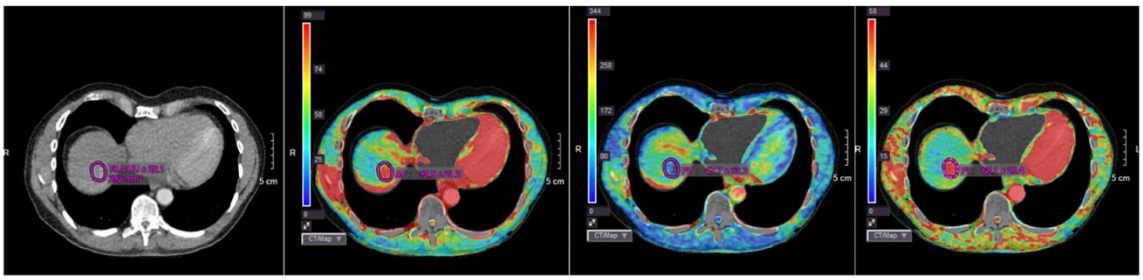

Figure 4: Tumour regions of interest and perfusion parameters. Perfusion maps with tumour contoured showing: A, tumour area and tumour density in HU; B, tumour arterial blood flow (AF; mL/min/100 mL); C, tumour portal venous blood flow (PF; mL/min/100 mL); D, tumour perfusion index (PI; AF / (AF + PF); %).

5.3.2.2 Dynamic-Contrast Enhanced MRI

MRI was performed using a 3.0 T scanner (Achieva, Philips Healthcare, Best, Netherlands) with a 16-channel body coil (SENSE XL-Torso, Philips Healthcare, Best, Netherlands). Standard clinical liver sequences were initially acquired which included a T2 weighted TSE axial plane, axial and coronal mDixon based sequences and diffusion weighted imaging with 8 b-values. T1 mapping was performed using three-dimensional (3D) volumetric gradient echo imaging with varying flip angles. A series of T1–weighted 3D volumetric images were acquired at baseline and sequentially during administration of a bolus of intravenous paramagnetic MR contrast agent Gd-DOTA (gadoterate dimeglumine, Dotarem®, Guerbet, Roissy, France) (10ml Gd-DOTA mixed with 10ml normal saline injected at a rate of 4 mL/s followed by a 20ml saline flush). Each acquisition took approximately 5 seconds during which time patients are asked to hold their breath in full expiration or if necessary to breathe in a shallow fashion. The MRI protocol finished with a final T1 map at 5 minutes post-contrast (Appendix A).

DCE-MRI image analysis was performed by one radiologist (MC) with 11 years' experience of abdominal MRI. Post-processing steps were performed using in-house developed Matlab code (MathWorks, Natick, USA). DCE-MRI volumes were initially reviewed and volumes with significant motion artefact removed (Figure 4). In order to select these volumes, a single representative slice was reviewed across time. Removed volumes were then replaced with interpolated data and all volumes underwent a registration process to remove motion artefact. The DCE-series was then registered with the T1 weighted volumes acquired at six separate flip angles. The registered T1 multiple flip angle (MFA) volumes and B1 data were used to generate a T1 map. Five representative slices centred on the main tumour volume were selected for data analysis, with contouring of the liver for regional analysis. T1 mapping data was used for pixel wise conversion of post-contrast SI data into CA concentration for each of the 5 slices.

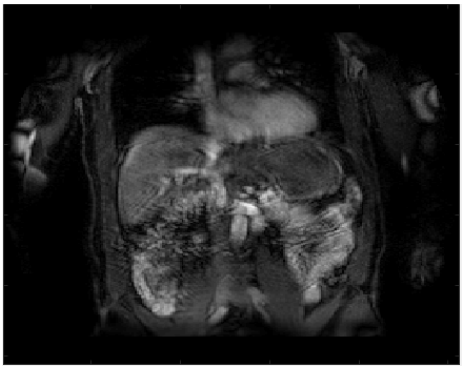

Figure 5. Example of DCE-MRI frame with motion artefact

Tumour and liver parenchyma ROIs were all contoured by one Consultant Radiologist (JH) and SI curves used to calculate the following tissue parameters using Tofts model: K^{trans} (volume transfer constant between plasma and extravascular extracellular space, min^{-1}); K_{ep} (volume transfer constant between extravascular extracellular space and plasma, min^{-1}): V_e (volume of extravascular extracellular space per unit volume of tissue,%). DISC modelling was undertaken using an in-house developed Matlab code [26]. Inflow and outflow constants were used to derive estimates of portal vein perfusion (PV) (ml/min/100 g), total liver blood flow (TLBF, sum of hepatic artery and portal vein perfusion, ml/min/100 g), hepatic artery fraction (HA, %), distribution volume (DV, %) and mean transit time (MTT, secs). Semi-quantitative analysis was performed in order to obtain the following parameters: time-to-peak (TTP, secs), area under curve at 60 and 90 seconds (AUC mmol/L.s), and peak gadolinium concentrations C_{peak} (mmol/L).

5.4 STATISTICAL ANALYSIS

Log transformed values have been utilised in a number of previous studies that have evaluated variability in DCE-MRI and pCT perfusion parameters. This transformation is based on the assumption that perfusion parameters follow log-normal distributions, as is typical of biologic systems [30, 33, 34]. Therefore, based on this assumption, along with our small sample size and after a statistical review of the spread of the data, this was the approach taken in our study. As such, all pCT and DCE-MRI parameters were transformed to the logarithmic scale prior to analyses of variation.

For pCT analysis, as tumour ROIs were contoured by two independent radiologists, inter-reader agreement was first evaluated using the intraclass correlation coefficient (ICC) for each parameter, with 95% confidence intervals; the value of ICC lies between 0 and 1, with ICC = 0 indicating no reproducibility between observers and ICC = 1 perfect reproducibility [35].

To measure the repeatability of DCE-MRI and pCT parameters, coefficients of variation were calculated between the baseline visits. Bland-Altman plots, with bias and 95% limits-of agreement, were produced for each parameter to assess baseline agreement. Exploratory analyses of the within group treatment effect, comparing $\log_e$-transformed variables pre- and post-TACE, was assessed using descriptive statistics and Wilcoxon signed-rank tests. Statistical analysis was performed by Nicholas Counsell (Trial Statistician) using SAS software version 9.4 (SAS Institute Inc., Cary, NC, USA) and GraphPAD Prism version 6.07 for Windows (GraphPad Software, La Jolla, California, USA).

5.5 RESULTS

5.5.1 Study patients

Eight patients were successfully treated with BTG-002814 as part of the VEROnA study, as outlined in full detail in Chapter 2 (Section 2.4). As per protocol, all subjects underwent baseline imaging (mean 4.3 ± 2.3 days) prior to treatment, with repeat imaging within the 24 hours prior to TACE with BTG-002814. Mean time between visit 1 and visit 2 scans was 3.9 days (SD 2.2 days). Post-treatment imaging was 12.9 +/- 7.3 days following treatment on the day prior to surgical resection (Figure 2). Six patients (75%) received the full volume (1 ml), whilst one patient received 0.4 ml and one patient 0.9 ml due to early stasis. One subject was excluded from the final pCT and DCE-MRI analysis as the tumour was not visible on the perfusion sequences due to its small size (patient 4). One patient (patient 7) underwent a repeat visit 4 scan due a delay in surgery and a requirement of the protocol to repeat all imaging. Baseline patient and tumour characteristics are outlined in Table 1.

Table 1: Patient tumour, treatment and pathological response details

Patient	Diagnosis	No. lesions	Size (mm)	Liver segment	Volume of BTG-002814 delivered (mL)	Time from TACE to imaging	Pathological response (necrosis)
1	HCC	1	33	VIII	1	13	100%
2	HCC	1	82	VII	1	12	5%
3	mCRC	1	21	VII	1	15	90%
4	mCRC	1	8	II/IVa	1	6	100%
5	mCRC	2	12 (treated)	VII	1	8	100%
			14 (untreated)	VIII	NA		NA
6	mCRC	1	40	V	0.6	13	95%
7	mCRC	1	24	V	0.9	29	20%
8	mCRC	5	42 + 29 +16 (treated)	IV	1	7	50%
			22 + 24 (untreated)		NA		NA

Abbreviations: HCC, hepatocellular carcinoma; mCRC, metastatic colorectal cancer; NA, result not available.

5.5.2 Perfusion CT Results

5.5.2.1 Overview

All pCT scans were performed according to the protocol and uploaded successfully for post-processing. However, after review, visit 2 scans were excluded from further analysis for three patients (one HCC, two mCRC) due to significant motion issues that impacted perfusion parameter readings. For one patient (patient 1) the tumour was at the dome of liver, and significant motion across the perfusion image sequence meant that lung tissue was inadvertently included in perfusion analysis. This was also the case for a second patient (patient 3) whereby the tumour was located at the edge of the liver. For the third patient (patient 5), breathing motion significantly affected the position of the portal vein which impacted the accuracy of the time-density curves.

5.5.2.2 Interobserver variation for pCT parameters

Agreement analysis between the two readers on pCT imaging for all lesions are shown in Table 2. Inter-reader agreement was high for all parameters across all

three visits, with ICC values of 0.871-0.950. Therefore, the values of one reader were taken for further analysis.

Table 2: Intraclass correlation coefficients for pCT parameters

Perfusion CT Parameter	Visit	N	Intraclass Correlation Coefficient (parameter on log scale)	Coefficient of Variation (parameter on log scale)
Max_slope_AF	V1	12	0.871 (95% CI: 0.612-0.961)	11.4% (95%CI: 6.7-16.3)
Max_slope_AF	V2	8	0.955 (95% CI: 0.793-0.991)	7.1% (95%CI: 3.6-10.8)
Max_slope_AF	V4	13	0.856 (95% CI: 0.595-0.954)	16.9% (95%CI: 10.1-24.1)
Max_slope_HPI	V1	12	0.924 (95% CI: 0.759-0.978)	10.8% (95%CI: 6.4-15.5)
Max_slope_HPI	V2	8	0.918 (95% CI: 0.646-0.983)	6.3% (95%CI: 3.2-9.5)
Max_slope_HPI	V4	13	0.913 (95% CI: 0.741-0.973)	11.1% (95%CI: 6.7-15.7)
Max_slope_PF	V1	12	0.881 (95% CI: 0.640-0.964)	14.8% (95%CI: 8.6-21.3)
Max_slope_PF	V2	8	0.950 (95% CI: 0.774-0.990)	5.8% (95%CI: 2.9-8.8)
Max_slope_PF	V4	13	0.906 (95% CI: 0.720-0.970)	13.7% (95%CI: 8.2-19.5)

Notes: Patient 5 had data for two tumours (one treated) and patient 8 data for 5 tumours (three treated). Patients 1,3 and 5 had data excluded from visit 2 due to significant motion. There were two visit 4 scans for patient 7 due to a delay in surgery. Patient 4 has no data at any visit.

5.5.2.3 Variation between pCT baseline visits

Table 3 summarises the variation in pCT parameters in both tumour and liver parenchyma between the two baseline visits (visits 1 and 2). For all patients variation was 11.2% for the arterial flow (AF), 29.8% for portal flow (PF) and 17.7% for the hepatic perfusion index (HPI) in the contoured liver tumours. For mCRC patients only, variation was 12.0% for AF, 30.6% for PF and 17.7% for HPI (Table 4).

Table 3: Variation in tumour and normal liver parameters between baseline visits (all patients)

Perfusion CT Parameter	Tumour / Normal liver	N	Coefficient of Variation (parameter on log scale)
Max_slope_AF	Tumour	8	11.2% (95%CI: 5.5-17.1)
Max_slope_HPI	Tumour	8	17.7% (95%CI: 8.7-27.5)
Max_slope_PF	Tumour	8	29.8% (95%CI: 14.2-47.5)
Max_slope_AF	Parenchyma	6	35.6% (95%CI: 14.1-61.1)
Max_slope_HPI	Parenchyma	6	67.5% (95%CI: 25.1-124.4)
Max_slope_PF	Parenchyma	6	86.6% (95%CI: 31.1-165.6)

Notes: Patient 5 had data for two tumours (one treated) and patient 8 data for 5 tumours (three treated). Patient 7 had data from 2 post-TACE scans. Patients 1,3 and 5 had tumour data excluded from visit 2 due to significant motion. Of the eight patients for liver parenchyma, patient 4 has no data at any visit and patient 5 has no data at visit 2.

Table 4. Variation in tumour and normal liver parameters between baseline visits (mCRC patients only)

Perfusion CT Parameter	Tumour / Normal liver	N	Coefficient of Variation (parameter on log scale)
Max_slope_AF	Tumour	7	12.0% (95%CI: 5.5-18.8)
Max_slope_HPI	Tumour	7	17.7% (95%CI: 8.1-28.2)
Max_slope_PF	Tumour	7	30.6% (95%CI: 13.5-50.2)
Max_slope_AF	Parenchyma	4	44.4% (95%CI: 11.9-86.2)
Max_slope_HPI	Parenchyma	4	34.7% (95%CI: 9.6-65.5)
Max_slope_PF	Parenchyma	4	43.7% (95%CI: 11.8-84.6)

Notes: Patient 5 had data for two tumours (one treated) and patient 8 data for 5 tumours (three treated). Patient 7 had data from 2 post-TACE scans. Patients 3 and 5 had tumour data excluded from visit 2 due to significant motion. Of the seven patients for liver parenchyma, patient 4 has no data at any visit and patient 5 has no data at visit 2.

5.5.2.4 Change in parameters post-treatment with BTG-002814

As Bland Altman analysis showed minimal variation in perfusion parameters (AF and HPI) between visits 1 and 2, and as data for visit 2 for three patients was not available, parameters from visit 1 were taken as baseline for all patients. Table 5 outlines tumour and parenchyma values pre and post-treatment with BTG-002814.

Figure 6 represents the percentage change in each parameter (log_e) for each patient included in the analysis. For the two HCC patients (patients 1 and 2), AF and HPI decreased, whilst PF increased. For the mCRC patients (3-8), in 4/7 tumours AF increased. PF increased in 5/7 tumours, whilst HPI decreased in 4 tumours.

Table 5: Change in tumour parameters in response to treatment with BTG-002814

	HCC patients			mCRC patients		
	Pre-treatment (absolute values)	**Post-treatment (absolute values)**	**Change (absolute values)**	**Pre-treatment Median (range)**	**Post-treatment Median (range)**	**Change Median (range)**
Tumour						
AF (ml/min/100ml)	73.8 & 102.4	69.8 & 83.6	-18.8 & -4.0	47.6 (31.3 to 61.7)	51.5 (31.9 to 88.1)	4.7 (-13.6 to 27.5)
PF (ml/min/100ml)	53.4 & 109.5	132.8 & 218.4	23.3 & 165.0	108.9 (88.5 to 190.1)	112.6 (56.0 to 230.4)	15.0 (-95.8 to 74.2)
HPI (%)	49.0 & 68.4	29.1 & 39.2	-39.3 & -9.8	30.8 (20.3 to 41.3)	27.6 (22.3 to 56.6)	-2.5 (-10.2 to 25.8)
Liver Parenchyma						
AF (ml/min/100ml)	28.2 & 33.0	35.8 & 36.1	3.1 & 7.6	46.7 (26.5 to 99.4)	30.9 (30.7 to 53.9)	-16.0 (-68.5 to 27.4)
PF (ml/min/100ml)	25.9 & 131.2	128.4 & 139.8	8.6 & 102.5	147.6 (127.0 to 324.4)	163.8 (148.7 to 197.2)	16.2 (-175.7 to 70.2)
HPI (%)	18.3 & 70.2	20.1 & 22.7	47.5 & 1.8	23.7 (15.2 to 27.2)	17.2 (14.2 to 24.9)	-6.5 (-13.0 to 9.7)

Notes: Pre-treatment values are taken from visit 1 scans for all patients. Absolute values are given for HCC patients and median (range) for mCRC patients.

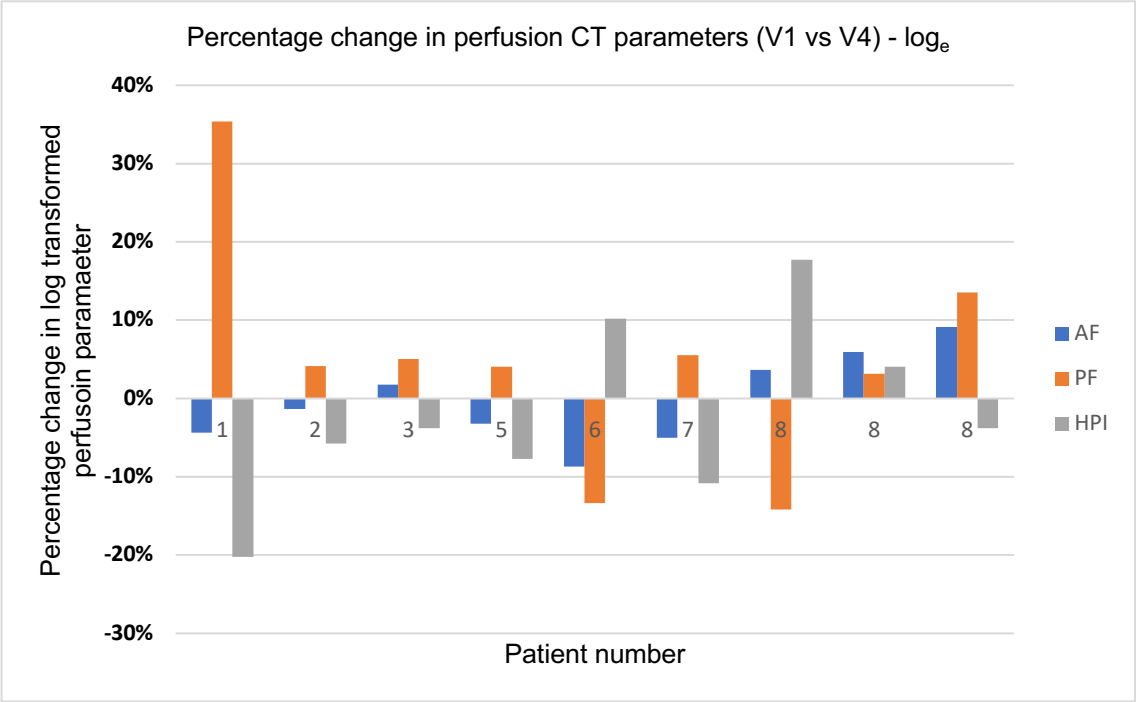

Figure 6: Bar graph showing the variation in perfusion CT parameters between visits 1 (baseline) and 4 (after treatment) for each patient. Log transformed values are reported for each perfusion parameter and the percentage difference between baseline (visit 1) and post-treatment (visit 4) is shown. Patients 1 and 2 had HCC. Patients 3-8 had mCRC. Three treated tumours were analysed for patient 8. *Abbreviations*: AF, arterial flow; PF, portal flow; HPI, hepatic perfusion index.

For statistical analysis, as the plan was to compare each group separately (HCC and mCRC), only results for the mCRC patients are reported in Table 6. As there were only 2 HCC patients, statistical analysis was not performed on this group. Using Wilcoxon signed-rank test and $\log_e$ transformed values, there was no statistically significant change in any parameter assessed in the mCRC cohort between baseline and post-treatment with BTG-002814.

Figure 7 outlines the change in perfusion parameters for the three mCRC tumours in two patients that were not treated with BTG-002814.

Table 6: Wilcoxon signed rank-test between baseline visit (V1) and post-treatment (V4) parameters for mCRC patients only

pCT parameter	n	Absolute change median (range)	Wilcoxon signed-rank test statistic (p-value)
Parenchyma: Max_slope_AF	5	0.1 (-1.2 to 0.7)	S=-0.5 (p=1.00)
Parenchyma: Max_slope_HPI	5	-0.0 (-0.6 to 0.5)	S=-1.5 (p=0.81)
Parenchyma: Max_slope_PF	5	0.1 (-0.8 to 0.4)	S=2.5 (p=0.63)
Treated Tumour: Max_slope_AF	7	0.1 (-0.3 to 0.4)	S=4.0 (p=0.58)
Treated Tumour: Max_slope_HPI	7	-0.1 (-0.4 to 0.6)	S=2.0 (p=0.81)
Treated Tumour: Max_slope_PF	7	0.1 (-0.7 to 0.6)	S=1.0 (p=0.94)
Untreated Tumour: Max_slope_AF	3	0.1 (-0.1 to 0.2)	S=1.0 (p=0.75)
Untreated Tumour: Max_slope_HPI	3	0.1 (-0.1 to 0.4)	S=2.0 (p=0.50)
Untreated Tumour: Max_slope_PF	3	0.0 (-0.2 to 0.2)	S=1.0 (p=0.75)

Notes: Log_e transformed values are compared for each perfusion parameter. Data is also provided for the three non-treated tumours.

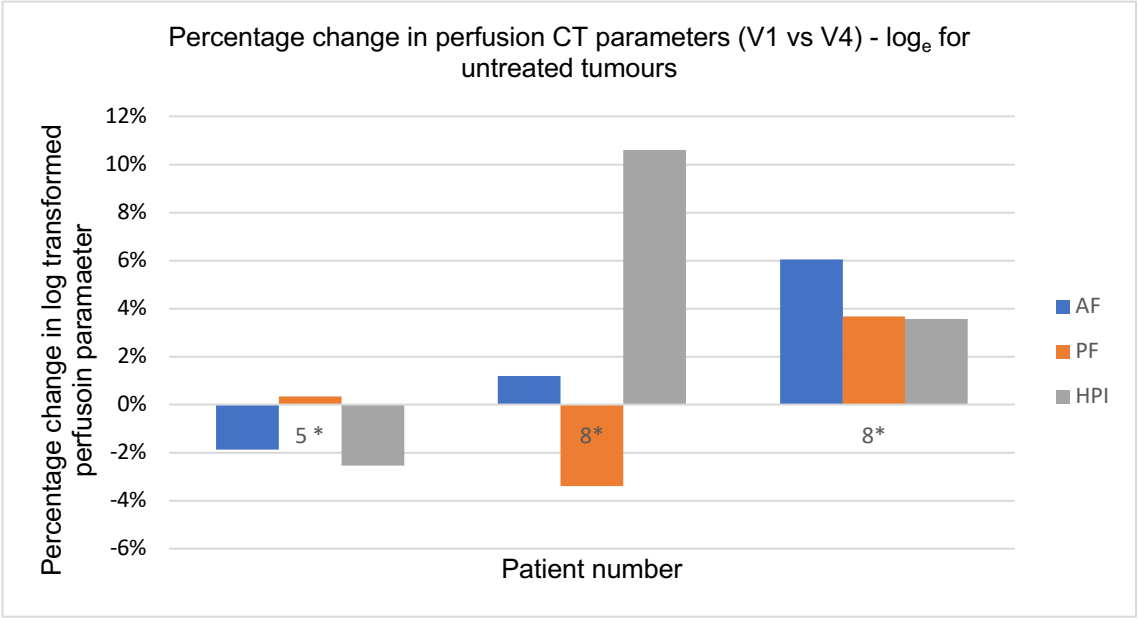

Figure 7: Bar graph showing the variation in perfusion CT parameters between visits 1 (baseline) and 4 (post-TACE) for untreated tumours. Log transformed values are reported for each perfusion parameter and the percentage difference between baseline (visit 1) and post-treatment (visit 4) is shown.* Data is shown for three untreated tumours, one in patient 5 and two in patient 8. *Abbreviations*: AF, arterial flow; PF, portal flow; HPI, hepatic perfusion index.

5.5.3 DCE-MRI Results

5.5.3.1 Overview

Although the protocol for the DCE-MRI sequences was set up on the scanner, there were minor deviations from the protocol during the trial. Firstly, the DCE-MRI scans for patient 1 and visit 1 of patient 2 were acquired as 30 slice volumes whilst all successive scans were acquired as 60 slice volumes. Furthermore, due to a software upgrade prior to patient 6, there were no B1 maps for this patient. The lack of a B1 map meant that the T1 volume reconstructions are likely to be less accurate for this patient but the methodology was consistent between all trial visits. Finally, due to the small nature of the tumour in patient 4 contouring was not possible and therefore this patient was excluded from further analysis. For patient 5, although two tumours were present (one treated and one untreated), DCE-MRI analysis was performed only on the treated tumour. This was the same for patient 8 in whom there were five tumours, three of which were treated with BTG-002814. DCE-MRI analysis was possible on the two largest tumours in this case.

5.5.3.2 Variation between DCE-MRI baseline visits

Table 9 summarises the variation in DCE-MRI parameters in both tumour and liver parenchyma between the two baseline visits (visits 1 and 2) using Tofts and the DISC model.

Variation in tumour perfusion parameters ranged from 19.9% (DV) to 234.9% (V_p). For the frequently used K^{trans} parameter, variation between baseline visits for the contoured tumour was 115.3% (95% CI 47.9-213.5%).

Table 7: DCE-MRI variation between baseline visits (all patients)

DCE-MRI Parameter	Tumour / Normal liver	N	Coefficient of Variation (parameter on log scale)
DISC_DV	Tumour	8	21.4% (95%CI: 10.4-33.5)
DISC_HAfrac	Tumour	8	68.5% (95%CI: 30.5-117.7)
DISC_HAperf	Tumour	8	96.6% (95%CI: 41.2-173.8)
DISC_MTT	Tumour	8	50.3% (95%CI: 23.1-83.5)
DISC_PVperf	Tumour	8	65.5% (95%CI: 29.3-111.9)
DISC_TLperf	Tumour	8	55.3% (95%CI: 25.2-92.7)
SemiQ_GAD_AUC60	Tumour	8	42.6% (95%CI: 19.8-69.6)
SemiQ_GAD_AUC90	Tumour	8	35.8% (95%CI: 16.9-57.8)
SemiQ_SI_AUC60	Tumour	8	26.8% (95%CI: 12.9-42.4)
SemiQ_SI_AUC90	Tumour	8	19.9% (95%CI: 9.7-31.1)
SemiQ_TTP	Tumour	8	72.5% (95%CI: 32.1-125.4)
SemiQ_upslope	Tumour	8	91.3% (95%CI: 39.2-163.0)
Tofts_Kep	Tumour	8	292.6% (95%CI: 100.9-667.5)
Tofts_Ktrans	Tumour	8	115.3% (95%CI: 47.9-213.5)
Tofts_Ve	Tumour	8	87.4% (95%CI: 37.8-154.9)
Tofts_Vp	Tumour	8	234.9% (95%CI: 85.2-505.5)
DISC_DV	Parenchyma	8	28.8% (95%CI: 13.8-45.8)
DISC_HAfrac	Parenchyma	8	195.8% (95%CI: 73.9-403.3)
DISC_HAperf	Parenchyma	8	164.4% (95%CI: 64.2-325.7)
DISC_MTT	Parenchyma	8	152.2% (95%CI: 60.3-296.8)
DISC_PVperf	Parenchyma	8	375.4% (95%CI: 121.5-920.4)
DISC_TLperf	Parenchyma	8	169.7% (95%CI: 65.9-338.5)
SemiQ_GAD_AUC60	Parenchyma	8	35.0% (95%CI: 16.5-56.3)
SemiQ_GAD_AUC90	Parenchyma	8	39.4% (95%CI: 18.4-64.0)
SemiQ_SI_AUC60	Parenchyma	8	24.9% (95%CI: 12.0-39.3)
SemiQ_SI_AUC90	Parenchyma	8	28.1% (95%CI: 13.4-44.6)
SemiQ_TTP	Parenchyma	8	39.9% (95%CI: 18.7-64.9)
SemiQ_upslope	Parenchyma	8	34.9% (95%CI: 16.5-56.2)
Tofts_Kep	Parenchyma	8	218.4% (95%CI: 80.5-461.5)
Tofts_Ktrans	Parenchyma	8	137.2% (95%CI: 55.4-262.2)
Tofts_Ve	Parenchyma	8	67.2% (95%CI: 30.0-115.0)
Tofts_Vp	Parenchyma	8	225.8% (95%CI: 82.7-481.2)

When analysis included just the mCRC patients (five patients with seven treated tumours), coefficients of variation improved for some variables, namely tumour hepatic artery fraction, hepatic artery perfusion and MTT from the DISC model, and K_{trans}, V_e and V_p from the Tofts model (Table 8). Despite this, the variation between baseline visits in K^{trans} remained high at 32.3% (95% CI 12.9-54.9%).

Table 8: DCE-MRI Variation between baseline visits (mCRC patients)

DCE-MRI Parameter	Tumour / Normal liver	N	Coefficient of Variation (parameter on log scale)
DISC_DV	Tumour	6	25.1% (95%CI: 10.2-42.0)
DISC_HAfrac	Tumour	6	39.7% (95%CI: 15.6-68.7)
DISC_HAperf	Tumour	6	36.6% (95%CI: 14.5-63.0)
DISC_MTT	Tumour	6	27.3% (95%CI: 11.1-46.0)
DISC_PVperf	Tumour	6	53.4% (95%CI: 20.4-95.4)
DISC_TLperf	Tumour	6	36.1% (95%CI: 14.3-62.0)
SemiQ_GAD_AUC60	Tumour	6	35.2% (95%CI: 14.0-60.3)
SemiQ_GAD_AUC90	Tumour	6	29.0% (95%CI: 11.7-49.0)
SemiQ_SI_AUC60	Tumour	6	20.9% (95%CI: 8.6-34.6)
SemiQ_SI_AUC90	Tumour	6	15.7% (95%CI: 6.6-25.7)
SemiQ_TTP	Tumour	6	77.5% (95%CI: 28.3-145.7)
SemiQ_upslope	Tumour	6	90.8% (95%CI: 32.4-175.1)
Tofts_Kep	Tumour	6	33.3% (95%CI: 13.3-56.8)
Tofts_Ktrans	Tumour	6	32.3% (95%CI: 12.9-54.9)
Tofts_Ve	Tumour	6	13.3% (95%CI: 5.6-21.7)
Tofts_Vp	Tumour	6	292.9% (95%CI: 81.1-752.1)
DISC_DV	Parenchyma	6	33.9% (95%CI: 13.5-57.9)
DISC_HAfrac	Parenchyma	6	130.2% (95%CI: 43.6-269.0)
DISC_HAperf	Parenchyma	6	56.7% (95%CI: 21.5-102.1)
DISC_MTT	Parenchyma	6	70.8% (95%CI: 26.2-131.1)
DISC_PVperf	Parenchyma	6	347.4% (95%CI: 91.7-944.4)
DISC_TLperf	Parenchyma	6	96.2% (95%CI: 34.0-187.3)
SemiQ_GAD_AUC60	Parenchyma	6	32.3% (95%CI: 12.9-55.0)
SemiQ_GAD_AUC90	Parenchyma	6	36.3% (95%CI: 14.4-62.4)
SemiQ_SI_AUC60	Parenchyma	6	25.6% (95%CI: 10.4-42.9)
SemiQ_SI_AUC90	Parenchyma	6	29.5% (95%CI: 11.9-50.0)
SemiQ_TTP	Parenchyma	6	36.4% (95%CI: 14.4-62.5)
SemiQ_upslope	Parenchyma	6	31.4% (95%CI: 12.6-53.3)
Tofts_Kep	Parenchyma	6	133.0% (95%CI: 44.4-275.9)
Tofts_Ktrans	Parenchyma	6	123.9% (95%CI: 41.9-253.3)
Tofts_Ve	Parenchyma	6	44.9% (95%CI: 17.5-78.8)
Tofts_Vp	Parenchyma	6	217.2% (95%CI: 65.1-509.4)

5.5.3.3 Change in parameters post-treatment with BTG-002814

Although there was a large variation in DCE-MRI parameters between the baseline visits, further analysis between pre- and post-treatment values was performed. In keeping with the pCT data, parameters from visit 1 were taken as baseline for all patients. Table 9 outlines tumour and parenchyma values pre- and post-treatment with BTG-002814.

Table 9: Change in tumour parameters in response to treatment with BTG-002814

	HCC patients			mCRC patients		
	Pre-treatment (absolute values)	Post-treatment (absolute values)	Change (absolute values)	Pre-treatment Median (range)	Post-treatment Median (range)	Change Median (range)
DISC model						
DV	97.6 & 99.7	100.0 & 100.0	0.3 & 2.4	63.3 (46.8 to 100.0)	53.6 (25.3 to 94.0)	-14.5 (-37.0 to 28.2)
HA_{fract}	13.8 & 21.5	2.8 & 50.6	-18.7 & 36.8	36.4 (24.5 to 76.9)	43.9 (34.9 to 71.5)	13.4 (-33.9 to 41.5)
HA_{perf}	1147.7 & 2039.1	5.6 & 135.6	-2033.6 & -1012.0	53.1 (15.8 to 77.0)	27.9 (3.5 to 61.2)	-21.3 (-52.9 to 17.9)
MTT	0.8 & 1.0	29.8 & 40.2	28.9 & 39.4	44.3 (32.6 to 106.0)	71.8 (36.8 to 616.8)	31.4 (-8.4 to 510.8)
PV_{perf}	7196.3 & 7436.8	132.4 & 193.3	-7243.5 & -7063.9	62.2 (23.1 to 133.9)	23.3 (4.9 to 75.7)	-39.6 (-93.3 to 8.8)
TL_{perf}	8343.9 & 9476.0	198.9 & 268.1	-9277.1 & -8075.9	110.7 (45.1 to 177.2)	49.5 (8.3 to 137.0)	-42.2 (-130.2 to -28.0)
Tofts						
K^{trans}	0.2 & 0.4	0.0 & 0.0	-0.4 & -0.2	0.0 (0.0 to 0.0)	0.0 (0.0 to 0.0)	0.0 (0.0 to 0.0)
K_{ep}	3.4 & 4.9	0.0 & 0.0	4.8 & -3.4	0.0 (0.0 to 0.0)	0.0 (0.0 to 0.0)	0.0 (0.0 to 0.0)
V_e	0.1 & 0.1	0.9 & 0.9	0.8 & 0.8	0.5 (0.4 to 0.8)	0.4 (0.2 to 1.0)	-0.2 (-0.4 to 0.3)
Semi-quantitative analysis						
GAD AUC 60	103.7 & 131.0	20.4 & 39.1	-110.6 & -64.5	17.7 (13.6 to 24.8)	11.5 (4.7 to 20.2)	-5.2 (-15.7 to 1.7)
GAD AUC 90	155.5 & 187.7	36.7 & 63.0	-151.1 & -92.4	29.2 (22.4 to 39.3)	20.8 (8.5 to 31.5)	-7.0 (-23.7 to -0.8)
SI AUC 60	110.0 & 114.5	29.1 & 81.1	-85.4 & -28.9	53.2 (31.7 to 85.8)	43.2 (26.1 to 54.8)	-18.7 (-31.0 to 12.9)
SI AUC 90	170.5 & 171.8	52.4 & 130.7	-119.4 & -39.8	87.8 (57.6 to 135.3)	71.3 (47.3 to 93.9)	-26.2 (-41.4 to 11.9)
TTP	16.8 & 25.2	32.3 & 46.3	15.4 & 21.1	44.6 (29.3 to 164.1)	81.6 (20.5 to 205.2)	24.7 (-96.2 to 55.7)
Upslope	0.1 & 0.1	0.0 & 0.1	-0.1 & -0.1	0.0 (0.0 to 0.0)	0.0 (0.0 to 0.0)	0.0 (0.0 to 0.0)

As with the pCT analysis, as the statistical plan was to compare each group separately (HCC and mCRC) only results for the mCRC patients are reported in Table 10. As there were only 2 HCC patients, statistical analysis was not performed on this group. Using Wilcoxon signed-rank test and $\log_e$ transformed values, there was a statistically significant change seen in the gadolinium AUC at 90 seconds (GAD AUC 90) and in the total liver perfusion (TL_{perf}) between baseline and post treatment with BTG-002814.

Table 10. Wilcoxon signed rank-test between baseline visit (V1) and post-treatment (V4) parameters for DCE-MRI parameters for mCRC patients

DCE-MRI parameter	n	Absolute change median (range)	Wilcoxon signed-rank test statistic (p-value)
Parenchyma: DISC_DV	6	-0.5 (-1.0 to 0.0)	S=-10.5 (p=0.03)
Parenchyma: DISC_HAfrac	6	0.1 (-1.3 to 1.4)	S=1.5 (p=0.84)
Parenchyma: DISC_HAperf	6	-0.5 (-1.5 to 0.2)	S=-8.5 (p=0.09)
Parenchyma: DISC_MTT	6	0.5 (-1.9 to 1.9)	S=1.5 (p=0.84)
Parenchyma: DISC_PVperf	6	-1.2 (-2.4 to 1.8)	S=-3.5 (p=0.56)
Parenchyma: DISC_TLperf	6	-0.9 (-2.1 to 0.9)	S=-5.5 (p=0.31)
Parenchyma: SemiQ_GAD_AUC60	6	-0.5 (-0.8 to 0.3)	S=-8.5 (p=0.09)
Parenchyma: SemiQ_GAD_AUC90	6	-0.6 (-0.7 to 0.3)	S=-8.5 (p=0.09)
Parenchyma: SemiQ_SI_AUC60	6	0.0 (-0.2 to 0.3)	S=3.5 (p=0.56)
Parenchyma: SemiQ_SI_AUC90	6	0.0 (-0.5 to 0.3)	S=1.5 (p=0.84)
Parenchyma: SemiQ_TTP	6	-0.3 (-1.0 to 0.1)	S=-6.5 (p=0.22)
Parenchyma: SemiQ_upslope	6	0.1 (-0.3 to 0.9)	S=3.5 (p=0.56)
Parenchyma: Tofts_Kep	6	-0.3 (-0.6 to 2.2)	S=0.5 (p=1.00)
Parenchyma: Tofts_Ktrans	6	-0.3 (-1.3 to 1.6)	S=-1.5 (p=0.84)
Parenchyma: Tofts_Ve	6	-0.6 (-1.4 to 0.4)	S=-8.5 (p=0.09)
Parenchyma: Tofts_Vp	6	-0.5 (-2.8 to 2.0)	S=-4.5 (p=0.44)
Tumour: DISC_DV	6	-0.3 (-0.9 to 0.4)	S=-5.5 (p=0.31)
Tumour: DISC_HAfrac	6	0.4 (-0.6 to 0.9)	S=4.5 (p=0.44)
Tumour: DISC_HAperf	6	-0.7 (-1.5 to 0.3)	S=-8.5 (p=0.09)
Tumour: DISC_MTT	6	0.6 (-0.2 to 1.8)	S=8.5 (p=0.09)
Tumour: DISC_PVperf	6	-1.2 (-2.0 to 0.3)	S=-7.5 (p=0.16)
Tumour: DISC_TLperf	6	-0.7 (-1.7 to -0.3)	S=-10.5 (p=0.03)
Tumour: SemiQ_GAD_AUC60	6	-0.4 (-1.3 to 0.1)	S=-8.5 (p=0.09)
Tumour: SemiQ_GAD_AUC90	6	-0.3 (-1.1 to 0.0)	S=-10.5 (p=0.03)
Tumour: SemiQ_SI_AUC60	6	-0.3 (-0.7 to 0.3)	S=-6.5 (p=0.22)
Tumour: SemiQ_SI_AUC90	6	-0.3 (-0.6 to 0.2)	S=-7.5 (p=0.16)
Tumour: SemiQ_TTP	6	0.4 (-0.9 to 1.1)	S=3.5 (p=0.44)
Tumour: SemiQ_upslope	6	-0.6 (-1.4 to 0.8)	S=-6.5 (p=0.22)
Tumour: Tofts_Kep	6	-0.1 (-0.8 to 1.2)	S=1.5 (p=0.84)
Tumour: Tofts_Ktrans	6	-0.3 (-0.8 to 0.3)	S=-6.5 (p=0.22)
Tumour: Tofts_Ve	6	-0.4 (-1.2 to 0.4)	S=-7.5 (p=0.16)
Tumour: Tofts_Vp	6	-1.6 (-4.4 to 1.1)	S=-6.5 (p=0.22)

Notes: $\log_e$ transformed values are compared for each perfusion parameter.

5.6 DISCUSSION

5.6.1 Role of functional imaging in early phase clinical trials and clinical practice

In this phase 0, first-in human clinical trial of BTG-002814 we have utilised two novel perfusion imaging techniques and shown that the incorporation of both pCT and DCE-MRI is feasible in early phase clinical trials. Furthermore, to the best of our knowledge, this is the first trial to utilise both perfusion modalities in the setting of TACE treatment.

5.6.2 Perfusion CT imaging

Perfusion CT imaging has been assessed in a number of clinical trials in the assessment of treatment with both anti-angiogenic agents and TACE [6, 15, 16, 19, 22]. It is a feasible method to implement with commercial packages available for post-processing. In this clinical trial we utilised the Vitrea body perfusion software from Canon/Toshiba Medical Systems and utilised the maximum slope method as it is more frequently utilised in perfusion liver studies due to the fact that it takes the dual input supply of the liver into account [10].

Using this commercial system and mathematical model, we have demonstrated that inter-reader agreement was high in our cohort for all parameters across all visits. Other studies have also reported on inter-reader agreement using commercial software for pCT imaging and found varying results. In a study by Ippolito *et al,* the pCT scans of 16 patients with HCC (nine untreated, five recurrence/residual disease after TACE, and two after radiofrequency ablation treatment) were assessed by two readers. They report that inter-reader agreement was low and moderate for arterial perfusion (AP) and HPI in both untreated lesions (ICC, 0.31 and 0.52) and treated lesions (ICC, 0.29 and 0.48). In comparison Morsbach *et al* reported on inter-reader agreement in 40 patients with liver metastasis following treatment with transarterial radioembolisation (TARE). They report on AP as a parameter and showed that inter-reader agreement was high with an ICC of 0.972 (95 % CI: 0.952-0.983). It is important to note that these two studies used different commercial packages to each other, and to that used in our study, which may in part lead to the variation in ICC seen. The reproducibility of perfusion parameters in normal livers has been compared

between two commercial software packages and demonstrated that at best there was only moderate agreement between the two packages, and that AP measurements were the most reproducible parameter [10].

In this study, we were also able to report on the reproducibility of pCT imaging which, along with inter-reader agreement, is vital for its use in both the clinical and research settings. On comparison of pCT between visit 1 and visit 2, we found that variation was 11.2% for AF, 29.8% for PF and 17.7% for HPI in the contoured liver tumours. The greater variation in PF may be due to variation in contouring of the portal vein when compared to the aorta, especially when motion across the perfusion sequence is taken into account.

These results are in keeping with other studies that have also assessed variation in pCT parameters between baseline scans. Ng *et al* evaluated the variation in parameters from pCT scans that were performed 2-7 days apart in seven patients with liver tumours. They measured BF, BV, MTT, and PS for tumours and normal liver. The pCT studies were obtained in two phases: phase 1 (cine acquisition during a breath hold) and phase 2 (six further cine scans acquired during free breathing). For tumours, BF, BV, MTT, and PS values and reproducibility varied by analytical method, the former by up to 11%, 23%, 21%, and 138%, respectively. The best overall reproducibility was obtained with rigidly registered phase 1 and phase 2 images, with within-patient CVs for BF, BV, MTT, and PS of 11.2%, 14.4%, 5.5% and 12.1%, respectively [34].

With regards to change in perfusion parameters post-treatment with BTG-002814, we did not see a significant change in any parameter. Previous studies assessing parameters post-TACE have however found significant results. Tamandl *et al* evaluated pCT parameters on 16 HCC patients before and one day post-TACE with doxorubicin and found that all perfusion parameters (BF, BV, AP, PVP and HPI) showed a significant change from baseline. BF, BV, AP and HPI were all reduced whilst PVP increased [15]. In comparison, Wimmer *et al* evaluated 15 patients with HCC who underwent pCT imaging prior to and 4-7 days post TACE. They found no statistically significant difference between pre- and post-TACE arterial flow and portal venous flow, whereas HPI was significantly lower after TACE [16]. Yang *et al* assessed 24 patients with HCC

post-TACE and reported significant decreases in HAP and HPI four weeks post-TACE [17].

In mCRC patients, Lv *et al* evaluated the performance of pCT in predicting response to TACE with lipiodol in 61 patients before and one-month post-treatment. They found that the HBF, HBV, PS, HAF, and HAP values of the target lesions significantly decreased following treatment. By contrast, the mean MTT value significantly increased relative to its value before TACE. No statistical difference was observed in the PVP value [20].

Perfusion CT has also been used to evaluate the response to anti-angiogenic agents in HCC patients. In a study of 22 patients with advanced HCC, pCT scans were performed before and two months after sorafenib treatment. The group that responded to sorafenib (n=17) showed a significant reduction in hepatic perfusion (HP) and arterial perfusion in HCC target lesions after therapy in comparison with the non-responder group (n = 5) that demonstrated no significant variation before and after treatment in HP [6].

Although we did not see a statistical change in any pCT parameter, it is important to note that statistical analysis was only performed on the mCRC cohort, and that only two patients in this study had a diagnosis of HCC. In the two HCC patients, we did see an increase in AF and decrease in PF and HPI in keeping with previous studies (Table 1). If we had recruited more HCC patients into this trial, then we may have been able to identify more significant trends in perfusion parameters following treatment.

In contrast, for the seven mCRC tumours analysed, AF increased in 4 tumours whilst PF decreased in 5 and HPI decreased in 4. However, these changes were non-significant and it is likely that the small increase in AF seen in four tumours is due to variation between scans and not in fact a real trend. For example, variation in perfusion parameters for the three non-treated tumours were also seen, as shown in Figure 8. Further pCT studies in both HCC and mCRC patients in response to TACE and anti-angiogenic agents are clearly required, as are variation studies that can help identify levels of variation above which a change is considered to be clinically relevant.

In summary, there are several reasons that may account for the lack of predictive parameters identified in this study to measure vascular response after TACE with vandetanib. As already mentioned, this is a small cohort with just two HCC patients and five mCRC patients which limits our statistical analysis. Furthermore, although previous studies have shown significant changes as early as 1-day post-TACE, others have shown changes 1-2 months post-TACE. It may be that our scans performed on average 12.9 days post-TACE were not performed at the optimal time point. It is interesting that for patient 7, in whom two pCT scans were acquired post-TACE (due to a delay in surgery), there was a larger difference in parameters at the first time point (12 days post-TACE) when compared to the second (29 days post-TACE). This is shown in Figure 9. However, as yet it remains unclear as to what the optimal time for response is.

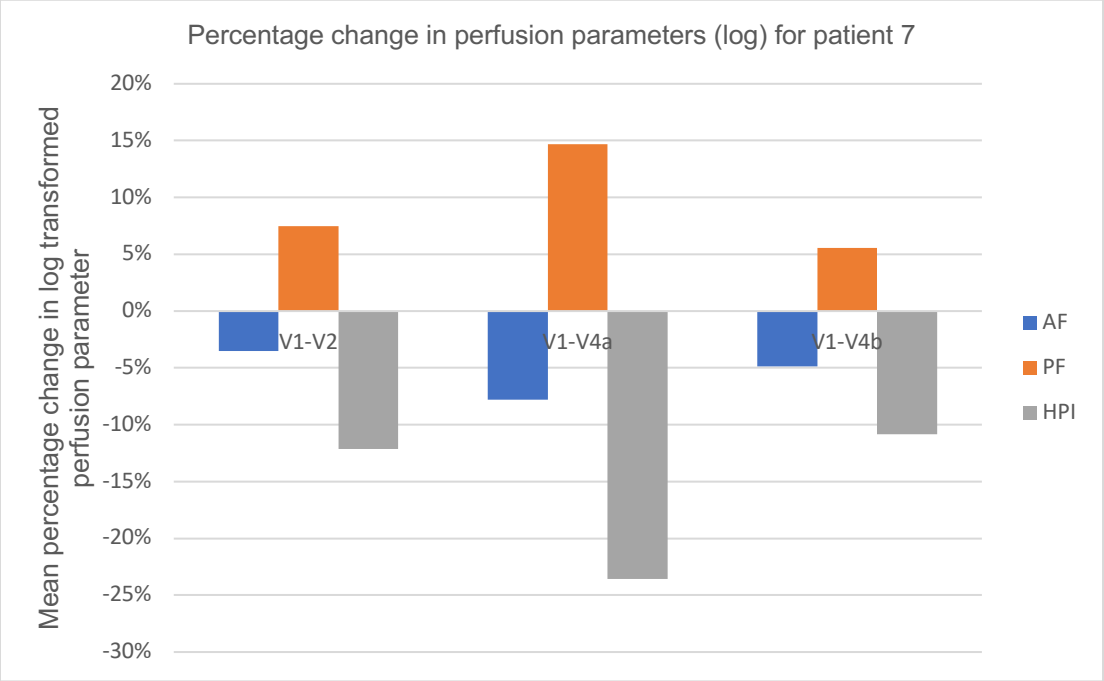

Figure 8: Bar graph showing the variation in perfusion CT parameters for patient 7. Log transformed values are reported for each perfusion parameter and the percentage difference shown. Changes between baseline visits (visit 1 and visit 2), visit 1 and visit 4a (12 days post-TACE) and visit 4b (29 days post-TACE) are shown. *Abbreviations*: AF, arterial flow; PF, portal flow; HPI, hepatic perfusion index.

In terms of tumour contouring, we have also only sampled the perfusion changes in each tumour on a single axial slice. It may be that this does not in fact give a true representation of the changes in perfusion across the whole tumour post-TACE. One way of overcoming this in future clinical trials would be to sample multiple slices across the tumour and take a mean perfusion value in the axial, coronal and sagittal planes. An alternative approach would be to create a 3D tumour volume that can be analysed; this function was not available in the software used in this trial. Finally, with regards to tumour delineation, the tumour was contoured separately on the pre- and post-TACE scans. As such, a change in size of the tumour may have impacted the change in perfusion parameters. One way of overcoming this would be to transfer the original tumour contour onto all subsequent scans, but again this was not possible with our software.

5.6.3 DCE-MRI

Like pCT imaging, DCE-MRI has been used in a number of clinical trials that have assessed response to ant-angiogenic drugs as well as TACE. Although feasible, it is important to highlight that there a number of additional factors to consider when compared to pCT imaging. Although it has the benefit of no ionising radiation, as shown in this study, DCE-MRI does involve far more complex post-processing steps. Furthermore, it has been shown the reproducibility of perfusion parameters can be variable.

Ng *et al* have reported on the variation in DCE-MRI parameters in 11 patients with liver tumours that underwent imaging 2-7 days apart without any intervening therapy. Using a two-compartment model, within-patient CoV was 8.9% for K^{trans}. Furthermore, they concluded that estimates of confidence that changes observed in a given patient were due to intervening therapy, rather than variability of the technique, ranged from 71% to 87% if a 20% reduction in a parameter was observed [39]. Mross *et al* assessed variation in parameters in 22 patients with mCRC and found that baseline measurements of AUC60 and K^{trans} were reproducible, with low intra-patient CoV (11% and 24%, respectively). As in our study, $\log_e$ transformed values were used for statistical analysis. Chouhan *et al* however found far greater levels of variation. In their study, reproducibility was assessed in nine normal volunteers with a 7-day interval between scans with

DISC modelling. They report CoV ranging from 64.1-71.8% for PV, 81.7-145.3% for HA fraction, 60.8-65.6% for MTT and 23.8-27.8% for DV depending on the vascular input function delay method used [26] .

In our cohort, we only saw a significant change in total liver perfusion and gadolinium (GAD) AUC 90 post-TACE with BTG-002814. However, due to our high baseline variation when compared to the literature, these results could not be reliably interpreted. Other studies of other VEGFR-2 tyrosine kinase inhibitors have demonstrated reductions in AUC in patients with advanced cancer [28, 30], but data on these changes in AUC post-TACE is currently lacking.

As vandetanib is expected to reduce capillary permeability via its antiangiogenic effects, it was anticipated that K^{trans} would drop following treatment (which reflects the permeability-surface area product, blood flow and intracellular uptake rate)[18]. For this reason, K^{trans} has been the main parameter investigated to date in response to vandetanib. In the study by Mross *et al,* 22 mCRC patients received oral vandetanib (n=10, 100mg/day; n=12, 300mg/day). DCE-MRI was used to assess tumour perfusion and vascular permeability at days 2, 8, 29 and 57, and changes in K^{trans} reported. Estimates of mean percentage changes from baseline were -4.6% (100 mg) and -2.7% (300 mg) for K^{trans}. AUC60 was also reported, with mean percentage changes of -3.4% (100 mg) and -4.6% (300 mg). Of note, a more than 40% threshold change was predefined as a significant change for this trial, as this cut off had been used previously for detection of anti-vascular activity by DCE-MRI [36]. One patient in each cohort showed > 40% reduction from baseline in AUC60 at least once, and four patients in each cohort a comparable decrease of >40% in K^{trans} at least once [30]. Hsu *et al* also used K^{trans} as a measure of response to oral vandetanib in HCC patients using DCE-MRI, with images taken at baseline and 7 days after start of treatment. In this study, patients were randomised to receive either 100mg, 300mg or placebo and a vascular response was defined by a decrease in K^{trans} of 30% or greater after 7 days of study treatment. Again, no significant change was seen in this parameter following treatment at this time point [29].

There is however rather limited data on the change in perfusion parameters post TACE. Saito *et al* assessed response to TACE and sorafenib (given 4 days post-

TACE) in 11 HCC patients. DCE-MRI scans were performed at baseline, and 3- and 10-days post TACE. In this study DV and K^{trans} were calculated and patients grouped by mRECIST after one month or more into responders (complete response, partial response) and non-responders (stable disease, progressive disease). In this study, DV was significantly reduced in all patients after initial TACE ($p < 0.001$) whilst K^{trans} was significantly reduced in the responder group ($p = 0.002$) [32]. Taouli *et al* report on three HCC patients treated with TACE, and on comparison of perfusion parameters pre- and post-TACE, there was a reported decrease in arterial fraction, arterial blood flow and DV, and an increase in portal venous blood flow (although values were not presented for this subset) [37].

As with pCT imaging, there are several reasons that may account for the lack of predictive parameters identified in this study to measure vascular response after TACE with vandetanib. Firstly, this a small cohort with just two HCC patients and five mCRC patients. As highlighted by previous negative studies, the vascular features of advanced HCC are heterogeneous due to tumour necrosis and arterio-venous shunting within the tumours may preclude reliable MRI measurement and comparison [31]. Secondly, as seen in other studies, the anti-angiogenic effects of vandetanib may not be detected by DCE-MRI [30, 31]. However, from the histopathological results in this study it is clear that TACE with BTG-002814 has had an impact, as the median percentage of tumour necrosis was 90% (range 5-100%) across all patients.

As highlighted with the pCT imaging, there are also limitations with our contouring methodology. A single measurement across the tumour (in this case a coronal slice) may not provide a true reflection of the changes within the whole tumour and change in tumour size post-TACE may impact perfusion parameters. Finally, DCE-MRI is complicated by the non-linear relationship between CA concentration and SI, and its dependence on scan parameters such as flip angle, repetition time and pre-contrast signal. As a result, quantitation can be complex, and one of the main limitations in the application of these perfusion methods in clinical practice is the poor reproducibility between different imaging techniques and different operators [13, 38]. As such, direct comparison with other clinical studies is limited due to variations in institutional DCE-MRI protocols and different patient

populations [30]. Further studies are necessary to explore the full potential of DCE-MRI and other functional imaging modalities in molecular targeted therapy for HCC.

5.6.4 Limitations

Although a clear strength of this study is the incorporation of two novel imaging modalities into an early phase clinical trial, there are limitations with both techniques. As stated, this a small mixed cohort of patients. As such, statistical analysis is limited and, as a result, it is difficult to reach any definitive conclusions for either cohort. It may be that in a larger study changes in parameters may reach statistical significance. Furthermore, with regards to the pCT scans, three scans from visit 2 had to be excluded due to motion issues. This does, however, highlight the importance of motion mitigation during perfusion scanning, how this can vary depending on the location of the lesion within the tumour, and how this can impact perfusion results.

For pCT post-processing we used one commercial software package and report on one mathematical model – the dual-input maximum slope method. Initially, at trial design, we did plan to also analyse tumour perfusion using the Patlak model, a single-input dual-compartment model. However, due to issues in the creation and reproducibility of the Patlak plot at the post-processing stage further detailed analysis was required to ensure the validity of these results. Although Patlak is not frequently used in liver perfusion studies, this does again highlight the issue of multiple models being available on commercial software and how this makes it increasingly difficult to reliably compare results between different studies. This is also relevant to DCE-MRI parameters, as each DCE-MRI study has used different scan acquisition parameters and different complex post-processing steps.

It also important to highlight that for both pCT and DCE-MRI parameters we did see significant variation in the parameters for normal liver parenchyma. Although this is partly due to the reproducibility between scans, this variation more likely reflects the fact that the exact normal liver ROI was not reproduced on each scan. Although attempts were made to contour in the same area at each visit, unlike for tumour contouring, there was no clear structure to outline in this case. Issues in

tumour contouring for both pCT and DCE-MRI have already been highlighted. Our original plan was to create 3D volumes for analysis and to transfer baseline tumour contours on to subsequent visits for each modality, but due to the software utilised in this study these approaches were not possible. However, future clinical trials would benefit from utilising this approach.

5.7 CONCLUSION

In conclusion, the incorporation of pCT and DCE-MRI into early phase liver clinical trials of new forms of TACE is feasible. Although there are limitations to their use, particularly with intra-individual variation in DCE-MRI, there does appear to be a role of pCT and DCE-MRI to assess response to anti-angiogenic and TACE procedures in the research setting. However, further larger scale studies that assess variation in addition to treatment response are required. Furthermore, methods of analysis need to be compared in both pCT and DCE-MRI in order to find the most robust dataset that can identify the optimal imaging biomarker. Finally, in a larger clinical trial setting, the correlation between change in perfusion parameters, bead distribution and tumour response should be assessed, particularly in hypervascular HCC tumours.

5.8 REFERENCES

[1] Kim SH, Kamaya A, Willmann JK. CT perfusion of the liver: principles and applications in oncology. Radiology. 2014;272:322-44.
[2] Galle PR. EASL Clinical Practice Guidelines: Management of hepatocellular carcinoma. Journal of hepatology. 2018;69:182-236.
[3] Van Cutsem E, Cervantes A, Adam R, Sobrero A, Van Krieken JH, Aderka D, et al. ESMO consensus guidelines for the management of patients with metastatic colorectal cancer. Ann Oncol. 2016;27:1386-422.
[4] Xu LH, Cai SJ, Cai GX, Peng WJ. Imaging diagnosis of colorectal liver metastases. World J Gastroenterol. 2011;17:4654-9.
[5] Zech CJ, Korpraphong P, Huppertz A, Denecke T, Kim MJ, Tanomkiat W, et al. Randomized multicentre trial of gadoxetic acid-enhanced MRI versus conventional MRI or CT in the staging of colorectal cancer liver metastases. The British journal of surgery. 2014;101:613-21.
[6] Ippolito D, Querques G, Okolicsanyi S, Franzesi CT, Strazzabosco M, Sironi S. Diagnostic value of dynamic contrast-enhanced CT with perfusion imaging in the quantitative assessment of tumor response to sorafenib in patients with advanced hepatocellular carcinoma: A feasibility study. Eur J Radiol. 2017;90:34-41.
[7] Goh V, Glynne-Jones R. Perfusion CT imaging of colorectal cancer. Br J Radiol. 2014;87:20130811.
[8] Sahani DV, Holalkere NS, Mueller PR, Zhu AX. Advanced hepatocellular carcinoma: CT perfusion of liver and tumor tissue--initial experience. Radiology. 2007;243:736-43.
[9] Beaton L, Bandula S, Gaze MN, Sharma RA. How rapid advances in imaging are defining the future of precision radiation oncology. Br J Cancer. 2019;120:779-90.
[10] Bretas EAS, Torres US, Torres LR, Bekhor D, Saito Filho CF, Racy DJ, et al. Is liver perfusion CT reproducible? A study on intra- and interobserver agreement of normal hepatic haemodynamic parameters obtained with two different software packages. Br J Radiol. 2017;90:20170214.

[11] Takeda A, Stoeltzing O, Ahmad SA, Reinmuth N, Liu W, Parikh A, et al. Role of angiogenesis in the development and growth of liver metastasis. Ann Surg Oncol. 2002;9:610-6.
[12] Miles KA, Lee TY, Goh V, Klotz E, Cuenod C, Bisdas S, et al. Current status and guidelines for the assessment of tumour vascular support with dynamic contrast-enhanced computed tomography. Eur Radiol. 2012;22:1430-41.
[13] Ippolito D, Fior D, Bonaffini PA, Capraro C, Leni D, Corso R, et al. Quantitative evaluation of CT-perfusion map as indicator of tumor response to transarterial chemoembolization and radiofrequency ablation in HCC patients. Eur J Radiol. 2014;83:1665-71.
[14] Chen G, Ma DQ, He W, Zhang BF, Zhao LQ. Computed tomography perfusion in evaluating the therapeutic effect of transarterial chemoembolization for hepatocellular carcinoma. World J Gastroenterol. 2008;14:5738-43.
[15] Tamandl D, Waneck F, Sieghart W, Unterhumer S, Kolblinger C, Baltzer P, et al. Early response evaluation using CT-perfusion one day after transarterial chemoembolization for HCC predicts treatment response and long-term disease control. Eur J Radiol. 2017;90:73-80.
[16] Wimmer T, Steiner J, Talakic E, Stauber R, Quehenberger F, Portugaller RH, et al. Computed Tomography Perfusion Following Transarterial Chemoembolization of Hepatocellular Carcinoma: A Feasibility Study in the Early Period. J Comput Assist Tomogr. 2017;41:708-12.
[17] Yang L, Zhang XM, Tan BX, Liu M, Dong GL, Zhai ZH. Computed tomographic perfusion imaging for the therapeutic response of chemoembolization for hepatocellular carcinoma. J Comput Assist Tomogr. 2012;36:226-30.
[18] Hayano K, Lee SH, Yoshida H, Zhu AX, Sahani DV. Fractal analysis of CT perfusion images for evaluation of antiangiogenic treatment and survival in hepatocellular carcinoma. Acad Radiol. 2014;21:654-60.
[19] Nakamura Y, Kawaoka T, Higaki T, Fukumoto W, Honda Y, Iida M, et al. Hepatocellular carcinoma treated with sorafenib: Arterial tumor perfusion in dynamic contrast-enhanced CT as early imaging biomarkers for survival. Eur J Radiol. 2018;98:41-9.

[20] Lv WF, Han JK, Cheng DL, Zhou CZ, Ni M, Lu D. CT Perfusion Imaging Can Predict Patients' Survival and Early Response to Transarterial Chemo-Lipiodol Infusion for Liver Metastases from Colorectal Cancers. Korean J Radiol. 2015;16:810-20.
[21] Detsky JS, Milot L, Ko Y-J, Munoz-Schuffenegger P, Chu W, Czarnota G, et al. Perfusion imaging of colorectal liver metastases treated with bevacizumab and stereotactic body radiotherapy. Physics and Imaging in Radiation Oncology. 2018;5:9-12.
[22] Jiang T, Kambadakone A, Kulkarni NM, Zhu AX, Sahani DV. Monitoring response to antiangiogenic treatment and predicting outcomes in advanced hepatocellular carcinoma using image biomarkers, CT perfusion, tumor density, and tumor size (RECIST). Invest Radiol. 2012;47:11-7.
[23] Zhu AX, Holalkere NS, Muzikansky A, Horgan K, Sahani DV. Early antiangiogenic activity of bevacizumab evaluated by computed tomography perfusion scan in patients with advanced hepatocellular carcinoma. Oncologist. 2008;13:120-5.
[24] Chen BB, Shih TT. DCE-MRI in hepatocellular carcinoma-clinical and therapeutic image biomarker. World J Gastroenterol. 2014;20:3125-34.
[25] Tofts PS, Kermode AG. Measurement of the blood-brain barrier permeability and leakage space using dynamic MR imaging. 1. Fundamental concepts. Magn Reson Med. 1991;17:357-67.
[26] Chouhan MD, Bainbridge A, Atkinson D, Punwani S, Mookerjee RP, Lythgoe MF, et al. Estimation of contrast agent bolus arrival delays for improved reproducibility of liver DCE MRI. Phys Med Biol. 2016;61:6905-18.
[27] Materne R, Smith AM, Peeters F, Dehoux JP, Keyeux A, Horsmans Y, et al. Assessment of hepatic perfusion parameters with dynamic MRI. Magn Reson Med. 2002;47:135-42.
[28] Yopp AC, Schwartz LH, Kemeny N, Gultekin DH, Gonen M, Bamboat Z, et al. Antiangiogenic therapy for primary liver cancer: correlation of changes in dynamic contrast-enhanced magnetic resonance imaging with tissue hypoxia markers and clinical response. Ann Surg Oncol. 2011;18:2192-9.
[29] Hsu CY, Shen YC, Yu CW, Hsu C, Hu FC, Hsu CH, et al. Dynamic contrast-enhanced magnetic resonance imaging biomarkers predict survival

and response in hepatocellular carcinoma patients treated with sorafenib and metronomic tegafur/uracil. Journal of hepatology. 2011;55:858-65.
[30] Mross K, Fasol U, Frost A, Benkelmann R, Kuhlmann J, Buchert M, et al. DCE-MRI assessment of the effect of vandetanib on tumor vasculature in patients with advanced colorectal cancer and liver metastases: a randomized phase I study. Journal of angiogenesis research. 2009;1:5.
[31] Hsu C, Yang TS, Huo TI, Hsieh RK, Yu CW, Hwang WS, et al. Vandetanib in patients with inoperable hepatocellular carcinoma: a phase II, randomized, double-blind, placebo-controlled study. Journal of hepatology. 2012;56:1097-103.
[32] Saito K, Ledsam J, Sugimoto K, Sourbron S, Araki Y, Tokuuye K. DCE-MRI for Early Prediction of Response in Hepatocellular Carcinoma after TACE and Sorafenib Therapy: A Pilot Study. J Belg Soc Radiol. 2018;102:40.
[33] Ng CS, Raunig DL, Jackson EF, Ashton EA, Kelcz F, Kim KB, et al. Reproducibility of perfusion parameters in dynamic contrast-enhanced MRI of lung and liver tumors: effect on estimates of patient sample size in clinical trials and on individual patient responses. AJR Am J Roentgenol. 2010;194:W134-40.
[34] Ng CS, Chandler AG, Wei W, Herron DH, Anderson EF, Kurzrock R, et al. Reproducibility of CT perfusion parameters in liver tumors and normal liver. Radiology. 2011;260:762-70.
[35] Ippolito D, Casiraghi AS, Talei Franzesi C, Bonaffini PA, Fior D, Sironi S. Intraobserver and Interobserver Agreement in the Evaluation of Tumor Vascularization With Computed Tomography Perfusion in Cirrhotic Patients With Hepatocellular Carcinoma. J Comput Assist Tomogr. 2016;40:152-9.
[36] Drevs J, Siegert P, Medinger M, Mross K, Strecker R, Zirrgiebel U, et al. Phase I clinical study of AZD2171, an oral vascular endothelial growth factor signaling inhibitor, in patients with advanced solid tumors. J Clin Oncol. 2007;25:3045-54.
[37] Taouli B, Johnson RS, Hajdu CH, Oei MT, Merad M, Yee H, et al. Hepatocellular carcinoma: perfusion quantification with dynamic contrast-enhanced MRI. AJR Am J Roentgenol. 2013;201:795-800.
[38] Kim H. Variability in Quantitative DCE-MRI: Sources and Solutions. J Nat Sci. 2018;4.

6 STEREOTACTIC BODY RADIOTHERAPY FOR HEPATOCELLULAR CARCINOMA

6.1 INTRODUCTION

Hepatocellular carcinoma (HCC) is the sixth most common cancer and the fourth leading cause of cancer related death worldwide [1]. Surveillance is recommended in high-risk groups to detect tumours at an early stage when curative treatments, such as liver transplantation, surgical resection and ablation, can provide 5-year survival rates up to 70% [2, 3]. However, at diagnosis, fewer than 30% of patients are suitable for curative treatment due to poor baseline liver function, underlying co-morbidities, vascular invasion, or large tumour burden, with over a third of patients presenting with tumours >5 cm [2, 4, 5].

Although transarterial chemoembolisation (TACE) is the standard of care for HCC patients with intermediate-stage disease [3], it is not curative and tumours ultimately become resistant to treatment [6-8]. For tumours >5 cm, local recurrence rates post-TACE are reported at 67%, with a median time to progression of 4 months [7]. In patients who progress, or for those unsuitable for TACE, sorafenib, a multi-kinase inhibitor, can prolong median overall survival (OS) from 7.9 to 10.7 months, provided there is preserved liver function (Child-Pugh A) [9-11]. As a result, sorafenib is the standard of care in many countries. Selective internal radiotherapy (SIRT) with yttrium-90 (Y^{90}) has recently been proposed as an alternative treatment option for patients with locally-advanced HCC. However, recent studies have failed to demonstrate a significant OS benefit from SIRT and systemic therapy, and sorafenib remains standard of care [12, 13].

Stereotactic body radiotherapy (SBRT) has recently emerged as a feasible and safe treatment option for patients with HCC ineligible for other local treatments, with local control (LC) rates comparable to that of radiofrequency ablation (RFA) [14-24]. For tumours ≥2 cm SBRT may offer superior LC when compared to RFA [24]. However, due to the risk of radiation induced liver disease (RILD), limited

data exist on the efficacy and safety of SBRT in patients with large tumours. In this chapter we evaluate the role of SBRT in the treatment of small (≤5 cm) and large (>5 cm) HCC tumours using data from one retrospective and one prospective series from a single institution.

6.2 OBJECTIVES

1. To report on the clinical outcomes and toxicities of patients with small (≤5 cm) HCCs treated with SBRT.
2. To investigate the efficacy and toxicity of SBRT in patients with large unresectable HCCs (>5 cm) who were not eligible for, or who had failed, previous liver-directed therapies (LDTs).

6.3 MATERIALS AND METHODS

6.3.1 Part 1: Stereotactic body radiotherapy for small unresectable hepatocellular carcinomas: A retrospective study

6.3.1.1 Patient Population

This retrospective, single institution study included the first 31 HCC patients with small tumours (≤5 cm) treated with SBRT at British Columbia (BC) Cancer from March 2011-July 2015. Eligibility criteria included patients with fewer than five synchronous lesions with none >5 cm, Child-Pugh score (CPS) A/B, no evidence of extra-hepatic disease, and an Eastern Cooperative Oncology Group (ECOG) score ≤ 2. Patients that had received prior LDTs were included. Treatment decisions were made at the discretion of the institutional multidisciplinary liver tumour board, following National Comprehensive Cancer Network (NCCN) guidelines. RFA was typically used as first choice for small tumours (<3 cm) whilst SBRT was reserved for patients ineligible or unsuitable for other local treatments, due to liver function, tumour position or progression after TACE/RFA. A diagnosis of HCC was established by biopsy or by meeting radiological criteria according to the American Association for the Study of Liver Disease [3]. Pre-treatment evaluation of all patients included clinical examination, multiphasic computed tomography (CT) scan and/or magnetic resonance imaging (MRI), baseline full

blood count (FBC), liver function tests (LFTs), liver enzymes and alpha fetoprotein (AFP). Approval for this study was obtained from the BC Cancer Research Ethics board.

6.3.1.2 SBRT Treatment

At least three gold fiducial markers were implanted in proximity to the tumour(s) under ultrasound guidance prior to radiotherapy planning, unless previous implanted markers such as surgical clips, bile duct stents or lipiodol were deemed adequate for tumour targeting. At time of simulation, liver motion during respiration was evaluated on fluoroscopy to determine if the patient would be best suited for gated treatments. Patients with a ≥2 cm cranial-caudal movement of fiducials and adequate correlation between the external respiratory marker block and fiducials were gated to reduce treatment volume. For patients unsuitable for gated treatments, a standard contrast-enhanced helical CT simulation scan and free-breathing four-dimensional CT (4DCT) scan were obtained. For gated patients, a contrast-enhanced CT scan during expiratory breath hold (ExBH) was obtained in place of a helical CT scan. In addition, a 4DCT scan was obtained to evaluate motion within the gating window. All patients were simulated supine in a customized Vac-Lok for immobilisation. Abdominal compression was not used.

Post-fiducial placement, pre-treatment diagnostic multiphasic CT and MRI scans were fused with the radiation planning CT scans to aid in tumour delineation in gated and non-gated patients. Scans were fused using rigid deformation, matched to fiducials, with priority given to the fiducial closest to the tumour. Gross tumour volume (GTV) was defined as the arterial enhancing lesion(s) with washout on delayed phase of the co-registered diagnostic scan. The clinical target volume (CTV) was an isotropic 5 mm margin around the GTV, but not extending outside of liver parenchyma.

For patients not suitable for respiratory-gating, an internal target volume (ITV) was generated using a 4DCT dataset, using implanted fiducial motion as a surrogate. Fiducials were contoured in all phases of the 4DCT and a ‘fiducial ITV’ created to guide daily patient set-up. No ITV was created for gated patients. Planning target volume (PTV) corresponded to the CTV (or ITV) with a 3-5 mm

isotropic margin. PTV margins were determined based on the accuracy of the fusion between diagnostic and planning CT scans, as well as size and visibility of the target lesion on the planning CT.

Organs at risk (OAR) were contoured on the helical planning CT for non-gated patients and the ExBH CT for gated patients. These included: spinal cord, liver, stomach, duodenum, small bowel, large bowel, skin, kidneys, great vessels and chest/abdominal wall. American Association of Physicists in Medicine Task Group (AAPM TG) 101 dose constraint guidelines were followed [25] (Table 1). Liver dose constraints were based on liver minus GTV volume.

Table 1. Summary of organ at risk tissue dose constraints [25]

		Three fractions		Five fractions	
Organ	Maximum critical volume above threshold	Threshold dose (Gy)	Max point dose[a] (Gy)	Threshold dose (Gy)	Max point dose[a] (Gy)
Spinal cord	<0.35 cc	18	21.9	23	30
Liver[b]	700cc	15	NAc	18	NAc
Oesophagus	< 5 cc	17.7	25.2	19.5	35
Heart/pericardium	< 15 cc	24	30	32	38
Great vessels	< 10 cc	39	45	47	53
Stomach	< 10 cc	16.5	22.2	18	32
Duodenum	< 5 cc	16.5	22.2	18	32
Large bowel	< 20 cc	24	28.2	25	38

[a] 'Point' defined as 0.035 cc or less

[b] Minimum critical volumes estimates: ≥ 700 cc of normal liver (liver-GTV) to receive ≤ 15 Gy in 3 fractions and ≤ 18 Gy in 5 fractions

[c] NA: Not applicable as parallel tissue.

Treatment was delivered using volumetric arc radiotherapy (VMAT) with 6 or 10 MV photon energy on a Varian TrueBeam™ linear accelerator. Treatment doses were individualised based on location of tumour in relation to the tolerance of nearby OAR. Planning aim was to cover 95% of the PTV by the prescription dose

and 99% of the PTV by at least 90% of the prescription dose. The dose prescribed to the PTV ranged from 40-55 Gy in 3-5 fractions. Dose constraints to OAR were placed as higher priority than PTV coverage and as such, PTV under-coverage was allowed. Daily image guidance with cone-beam CT scan was performed to localise the target before treatment delivery for non-gated patients, while orthogonal fluoroscopy prior to and during treatment delivery was used for gated patients.

6.3.1.3 Follow-up

Patients were evaluated every three months for the first year after treatment, and every 6 months thereafter. Clinical examination, blood work, and either multiphasic CT scan or contrast-enhanced MRI were performed at each follow-up visit. Toxicities were graded according to the Common Terminology Criteria for Adverse Events (CTCAE) v.4.0 and measured from the end date of radiotherapy and censored at time of disease progression, upon delivery of other LDT, or at last follow-up. Classic RILD was defined as anicteric hepatomegaly and ascites, typically occurring between 2 weeks and 3 months after therapy, with an elevated alkaline phosphatase (more than twice the upper limit of normal or baseline value) [26]. Response Evaluation Criteria in Solid Tumours (RECIST) was used to assess local tumour response [27]. Progression was defined either as local failure (occurring within the PTV), regional failure (occurring within the liver but outside of the PTV) or metastatic progression.

.

6.3.1.4 Statistical Analysis

Quantitative variables were reported by median and range, and qualitative variables by frequency and percentage. LC, progression free survival (PFS), and OS were calculated from the end of radiotherapy, and analysed using Kaplan-Meier survival analyses with log-rank testing. Univariate analysis was performed to explore the impact of patient, tumour and treatment related factors on outcomes. *P* values of <0.05 were considered statistically significant. Results were analysed with SAS Version 9.3 for Microsoft Windows (SAS Institute Inc., Cary, NC).

6.3.2 Part 2: Stereotactic body radiotherapy for large unresectable hepatocellular carcinomas- a single institution phase II study

6.3.2.1 Patient population

This single-institution prospective phase II study was approved by the BC Cancer Research Ethics board (NCT01850316). Patients with fewer than five HCCs, measuring >5 cm , but <15 cm, with at least 700cc of normal liver and no evidence of extra-hepatic disease were eligible. Histopathological confirmation of HCC was not required provided the lesion(s) satisfied radiological diagnostic criteria [3]. Patients were discussed at institutional multidisciplinary meetings and deemed ineligible for LDT (including surgery, liver transplantation, RFA, or TACE) due to liver function, tumour size, tumour position or progression after TACE/RFA. Other eligibility criteria included: age >18 years, ECOG score ≤ 2, and CPS ≤ B7. Patients were required to have a haemoglobin ≥ 90 g/L, absolute neutrophil count ≥ 1.0 bil/L, platelets ≥ 50 bil/L, and AST/ALT not to exceed three-times the upper limit of normal. Patients who had received prior LDTs were eligible provided there was documented recurrence or lack of complete response from treatment on cross-sectional imaging. A minimum of 4-weeks was required between TACE and SBRT. Exclusion criteria included: pregnancy, previous external beam radiotherapy to the upper abdomen, gastric/duodenal/variceal bleed within the past 2-months or evidence of distant disease or extrahepatic nodal metastases. All patients signed written consent forms prior to enrolment. All suitable patients were considered for sorafenib if they developed progressive disease on study. Accrual and toxicity data were reviewed by the Data and Safety Monitoring Committee on a 6-monthly basis.

6.3.2.2 Baseline assessments

Pre-treatment evaluation included clinical examination, multiphasic CT scan and/or contrast-enhanced MRI, within 8-weeks prior to radiation planning, FBC, LFTs and AFP. Baseline quality of life (QoL) assessment was scored using two validated patient-reported instruments: the EORTC Quality of Life Questionnaire Core-30 (QLQ-C30) version 3.0 and Functional Assessment of Cancer Therapy-Hepatobiliary version 4 (FACT-HEP) [28-31].

6.3.2.3 SBRT treatment

Radiotherapy was delivered as previously described (section 6.3.1.2). Dose prescribed to the PTV ranged from 40-45 Gy in five fractions delivered on alternate days. Prescribed dose was individualised based on tumour location in relation to the tolerance of nearby OARs (Table 2). Planning aim was to cover 95% of PTV by the prescription dose and 99% of PTV by at least 90% of the prescription dose (Figure 1). Dose constraints for OARs were placed as higher priority than PTV coverage. As such, under-coverage of the PTV was allowed. Daily imaging was performed as previously outlined. All patients were pre-medicated with ondansetron 8 mg orally 30-minutes prior to each treatment fraction.

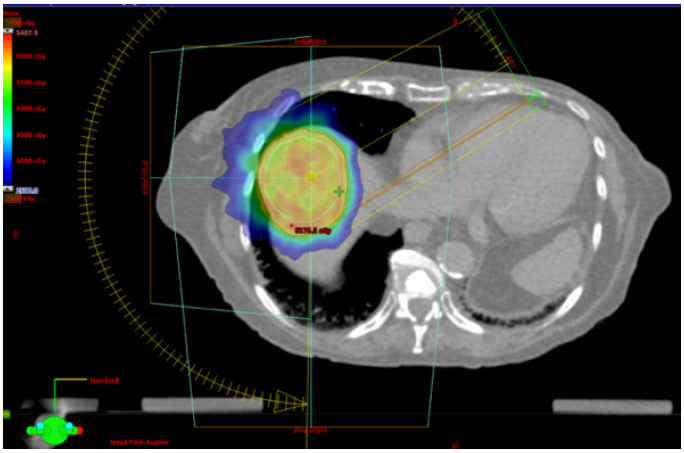

Figure 1: Stereotactic body radiotherapy plan for a large hepatocellular carcinoma. VMAT arc demonstrated along with the dose distribution (in colour wash) around the liver tumour. Planning target volume represented by red contour line.

Table 2. Normal tissue dose constraints for five fractions used in large HCC trial

Structure	Constraints	
	Threshold Volume	Max Dose point
Spinal Canal		28
Oesophagus		30
Stomach		30
Small Bowel bag		30
Large Bowel bag		30
Liver-GTV (>700cc)	As low as possible < 17 Gy (Mean Dose)	-
Kidneys (combined)	V17.5 Gy <70%	-
Heart		38
Major Vessels		53
Skin		30
Chest wall/Ribs		43

6.3.2.4 Evaluation and End Points

Patients were reviewed at 1, 6 and 12 weeks post-SBRT, then every 3 months thereafter. Toxicity assessment and laboratory tests were performed at each visit. A multiphasic contrast-enhanced CT scan/MRI was performed at each follow-up visit beginning at week 12. A masked independent review of imaging was performed by two radiologists (CM and CYH) using the modified RECIST (mRECIST) version 1.1 [32]. Progression was defined as either 'local' (occurring within the PTV), 'regional' (occurring within the liver but outside of the PTV) or metastatic. Primary endpoints were: objective response rate (defined as complete response (CR) and partial response (PR)) and overall response rate (CR, PR and stable disease (SD)) of the treated lesion(s) at 3 months. Secondary endpoints were 1-year LC, time-to-local progression (TTP), 1-year PFS, OS, toxicity and proportion of patients with a clinically significant change in QoL at 3 months. Toxicity was evaluated using the CTCAE v4.0 and censored at time of disease progression, transplant or death. QoL assessments were completed at

3, 6, 9, and 12-month visits using the EORTC QLQ-C30 and FACT-HEP questionnaires [28-31].

6.3.2.5 Statistical Analysis

TTP was measured from date of study-specific imaging immediately prior to SBRT to date of local failure. PFS and OS were calculated from date of first SBRT fraction to date of progression, death or date of censoring. Patients were censored at time of death if they died before evidence of progression, date of transplant, or last follow-up (if still alive). TTP, PFS and OS were analysed using Kaplan-Meier analyses. Wilcoxon Signed-Rank test was used to compare QoL scores from baseline to 3-months. The minimal clinically important difference (MID) on a QoL score was defined as upper bounds of published estimates; for QLQ-C30 this was defined as a change of ≥ 10 points, and ≥ 9 points for the FACT-HEP [33-35]. Statistical computation was performed using SAS Version 9.3 for Microsoft Windows (SAS Institute Inc., Cary, NC).

6.4 RESULTS

6.4.1 Small HCC tumours

6.4.1.1 Patient and Treatment Characteristics

Thirty-four separate hepatomas in 31 patients were treated, with a median size of 3.3 cm (range: 1.3-5.0 cm). Baseline patient and treatment demographics are outlined in Table 3. The most common cirrhosis aetiologies were Hepatitis B and C (52% and 29% respectively). Thirty patients (97%) had a pre-treatment CPS of ≤B7; one patient had a baseline CPS of B8. Twenty-six patients (84%) had received LDT prior to SBRT. In total, there were 50 previous LDTs in these 26 patients (median 2, range: 0-4).

Treatment factors are shown in Table 4. Radiotherapy prescription doses ranged from 40-55 Gy in 3-5 fractions, with 88% of lesions receiving 45 Gy in 3 or 5 fractions. Four patients (13%) were treated with a gated plan. Biological equivalent doses (BED), assuming an α/β of 10 (BED_{10}), were calculated and

reported in light of the heterogeneous prescription doses. Twenty-four (71%) lesions were treated with a BED_{10} prescription dose ≥100 Gy_{10}. Median BED_{10} to 95% of the PTV (D95) was 104.8 Gy_{10} (range: 45.0-116.5Gy_{10}). BED_{10} D95 for the PTV was ≥100 Gy_{10} in 20 patients (59%) and ≥80 Gy_{10} in 27 patients (79%).

Table 3. Baseline patient and prior treatment characteristics

Characteristics	All Patients (n=31) n (%)
Age, years	
Median	64
Range	48-88
Gender	
Male	24 (77.4%)
Female	7 (22.6%)
ECOG status	
ECOG ≤1	28 (90.3%)
ECOG 2	3 (9.7%)
Cirrhosis Aetiology	
Unknown	2 (6.5%)
Hepatitis C	9 (29.0%)
Hepatitis B	16 (51.6%)
Alcohol	0 (0%)
Combination	4 (12.9%)
Pre-treatment Child-Pugh Score	
A5	19 (61.3%)
A6	9 (29.0%)
B7	2 (6.5%)
B8	1 (3.3%)
Portal Venous Thrombosis	3 (9.7%)
Baseline AFP	
Median	18
Range	1.3-6100
Baseline ALBI score	
Grade 1	16 (51.6%)
Grade 2	13 (41.9%)
Grade 3	2 (6.5%)
Previous Treatment	
None	5 (16.1%)
Any*	26 (83.9%)
Previous TACE	15 (48.4 %)
Previous RFA	17 (55%)
Previous PEI	3 (9.7%)
Previous Surgery	14 (45.2%)
Previous Y-90	1 (3.2%)

Abbreviations: AFP, alpha fetoprotein; ALBI, albumin-bilirubin score; ECOG, Eastern Cooperative Oncology Group; TACE, transarterial embolisation; RFA, radiofrequency ablation: PEI, percutaneous ethanol injection: Y-90, yttrium-90.

* Includes TACE, RFA, PEI, surgery and Y-90.

Table 4. Tumour and dosimetric parameters of treated hepatomas

Characteristics	All Tumours (n=34) n (%)
Tumour size (cm)	
Median	3.3
Range	1.3-5.0
Prescription Dose (n, %)	
55Gy/3#	1 (2.9%)
45Gy/3#	22 (64.7%)
50Gy/5#	1 (2.9%)
48Gy/5#	1 (2.9%)
45Gy/5#	8 (23.5%)
40Gy/5#	1 (2.9%)
Prescription $BED_{10} \geq 100Gy_{10}$[a]	24 (70.6%)
Gated Plan	4 (11.8%)
PTV volume (cm^3)	
Median	82.0
Range	22.4-252
PTV V100%	
Median	93
Range[b]	64-99
PTV V95	
Median	98
Range[b]	70-100
D95 BED_{10}, Gy_{10}	
Median	104.8
Range	45.0-116.5
D95[c] BED_{10} (Gy) $\geq 80Gy_{10}$	27 (79.4%)
D95 [c] BED_{10} (Gy) $\geq 100Gy_{10}$	20 (58.8%)
Liver minus GTV mean dose, Gy	
Median	10.1
Range	3.7-20.1

[a] Biological equivalent dose assuming $\alpha/\beta = 10$

[b] PTV Vx= planning treatment volume receiving x% of prescribed dose

[c] Minimum dose delivered to 95% of the PTV

6.4.1.2 Treatment Outcomes

Median follow-up was 18.3 months (range: 2.1-50.1 months); at time of last follow-up, 20 patients (65%) were alive. LC was 94% at both 1- and 2-years (Figure 2A). PFS at 1- and 2-years was 49% and 37%, while OS was 84% at 1-year and 74% at 2-years (Figure 2B and 2C respectively).

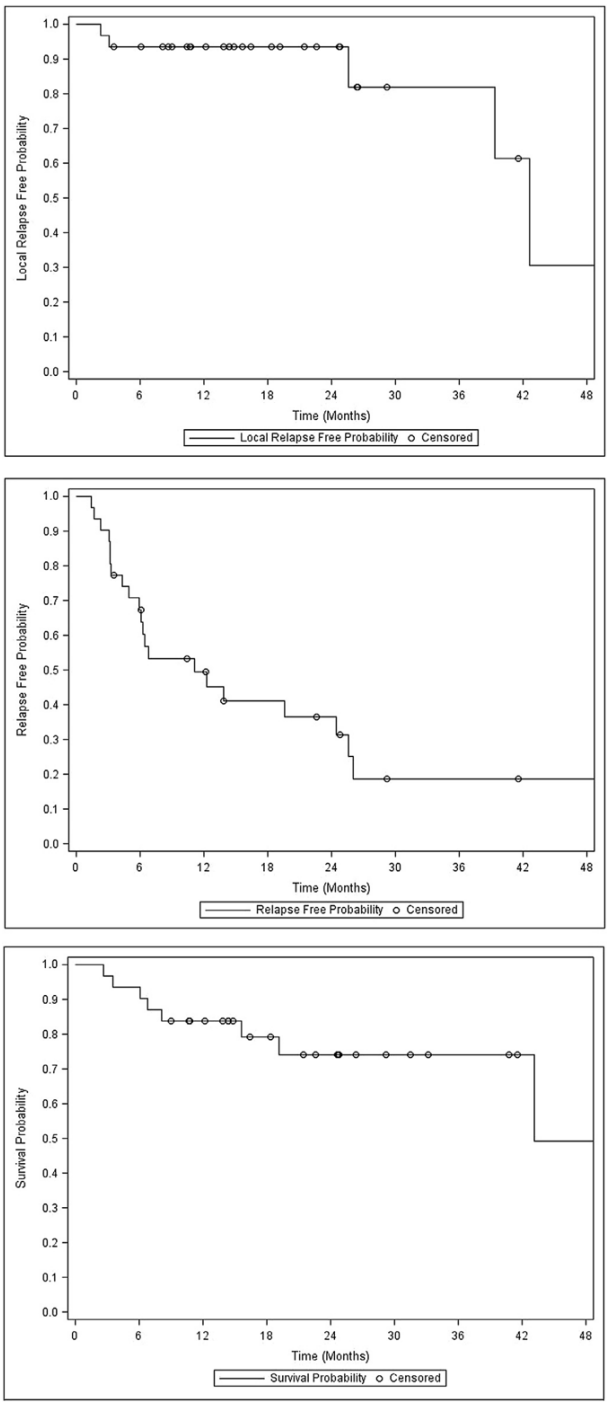

Figure 2: Kaplan-Meier curve of: (A) local control, (B) progression-free survival, (C), overall survival (small HCC patients)

Twenty-one patients (68%) had developed disease progression at time of analysis; 16 patients developed regional failure (occurring within the liver but outside of the PTV), three local failure at the same time as regional failure, whilst two patients developed distance relapse as first presentation of disease progression (Table 5). Two patients died prior to radiological evidence of relapse, whilst eight patients had no evidence of disease progression at time of analysis. Of the three patients that developed local failure, two had tumour progression within the 95% isodose line, whilst one patient had progression within the 50% isodose line.

Table 5: Sites of first recurrence

Site of initial recurrence	Number of patients	Time to first recurrence (months) Median (10^{th}, 90^{th} percentile)
Regional*	16	6.4 (1.6, 24.4)
Local**and regional	3	3.1 (2.3, 25.6)
Distant relapse	2	4.7 (4.4, 5.0)

*Within the liver but outside of the PTV. ** Within the PTV

Seventeen (81%) patients with disease progression went on to receive further HCC therapy. Three patients received sorafenib, whilst fourteen patients had further LDT for disease progressing within the liver outside of the SBRT site, including three patients who underwent liver transplantation. Four patients did not receive further treatment after progression due to advanced disease, decline in performance status, or markedly worsening liver function.

Two of the three patients who underwent liver transplantation had radiographic documentation of disease progression outside of the SBRT site. Pathology showed mostly necrosis within the treated volume with viable tumour elsewhere. The third patient who underwent transplant had worsening liver function without evidence of residual disease or disease progression on imaging. Pathology at time of transplant, however, revealed residual disease at the site of SBRT.

No patient, tumour or treatment factors including age, presence of portal vein thrombosis, baseline CP score or change in CPS, tumour size pre-treatment AFP, prescription dose or PTV coverage were predictive of improved LC on univariate analysis (UVA). For PFS, only a higher baseline albumin-bilirubin (ALBI score) [36], analysed as a continuous variable, predicted for a worse outcome (p=0.02). For OS, larger tumour size, analysed as a continuous variable, was associated with worse outcome (p=0.01), while prescription BED_{10} dose ≥100 Gy_{10} approached significance for improved survival (p=0.06) (Table 6). Baseline CP score ≥B7, an increase in CPS at three months by ≥ 2 points, and a higher baseline ALBI score were not predictive of worse OS (p=0.18, p=0.30 and p=0.27, respectively). Due to low cohort numbers, multivariate analysis was not performed.

Table 6: Univariate analysis of factors associated with overall survival

Variables	Hazard ratio	95% confidence interval	P-Value
Age at SBRT[a]	1.0	1.0-1.1	0.23
ECOG (2 vs 0-1)	1.7	0.2-14.3	0.62
Previous treatment	1.1	0.2-5.3	0.92
Tumour Size[a]	**3.3**	**1.3-8.3**	**0.01**
Pre-treatment AFP[a]	1.3	0.7-2.4	0.42
Pre-treatment CPS ≥ B7	2.4	0.7-9.1	0.18
Pre-treatment ALBI score[a]	1.82	0.6-5.2	0.27
Prescription BED_{10} ≥ 100 Gy_{10}[b]	0.3	0.1-1.1	0.06
D95[c] BED_{10} ≥ 80Gy_{10}	0.3	0.1-1.2	0.08
D95[c] BED_{10} ≥ 100Gy_{10}	0.5	0.1-1.8	0.28
CP Score Change post SBRT (≥2 vs < 2)	2.1	0.5-8.9	0.30
Post SBRT Treatment	0.8	0.5-1.3	0.41

[a] Analysed as continuous variables
[b] Biological equivalent dose assuming α/β = 10
[c] Minimum dose delivered to 95% of the PTV

6.4.1.3 Toxicity

There were no reported cases of classic RILD during follow-up. Six patients (19%) had worsened CPS by ≥ 2 points, which occurred at a median follow up of 3 months following SBRT. This was associated with disease progression in two patients. Of the four patients that did not progress, two A6 patients worsened to B8, one to a B9, and one to C12 (secondary to hepatitis reactivation). CPS worsening was transient for two patients but persistent in the remaining two.

Overall, ten patients (32%) had documented Grade 3 (G3) or higher toxicity during follow-up post SBRT. In 7/10 patients, the G3+ toxicity occurred within 3-months post-treatment. Three of these patients had elevation in gamma-glutamyltransferase (GGT), one had elevation in bilirubin and one had aspartate aminotransferase (AST) elevation. Three patients with G3 elevated liver function tests (one with hyperbilirubinemia and two with elevated GGT) had progressive regional liver disease at first follow-up and this may have contributed to their laboratory values. Toxicity was transient in the one patient with raised AST, whilst one patient had a G3 elevation of GGT at baseline that did not change post SBRT.

There was one acute G3 gastrointestinal bleed; this patient did require hospital admission due to melaena but did not require transfusion. Endoscopy revealed a 1.5cm non-metastatic duodenal ulcer, but no deterioration of oesophageal varices. This patient received 40 Gy in 5 fractions and maximum dose to the duodenum was 31.0 Gy, lower than the accepted dose tolerance of 32 Gy published in literature [25]. One patient developed acute G4 toxicity due to liver failure and elevation of bilirubin. This occurred 3 months after SBRT, but was felt secondary to decompensation of underlying liver cirrhosis from hepatitis C. The patient had a baseline CP score of A6 which increased to a score of C12 at 3 months. The patient had received previous TACE and RFA procedures and was treated with a dose of 45 Gy in 3 fractions to a 3.6 cm diameter hepatoma. Mean liver dose was 7.9 Gy and 1116 cc of liver received < 15 Gy, meeting acceptable liver dose tolerances [26]. The patient passed away 3.5 months after SBRT.

Three patients developed late toxicity, occurring more than 3-months after treatment. In one patient this was a transient thrombocytopenia, and in another a transient elevation in GGT. Overall, only one patient had irreversible G3 toxicity (hyperbilirubinemia) without evidence of disease progression that occurred 8 months post-treatment.

6.4.2 Large HCC tumours

6.4.2.1 Patient and treatment characteristics

Between November 2013 and February 2016, 16 hepatomas were treated in 13 patients. Nine patients (69%) had a baseline CPS of A5/6, and four (31%) B7. Eight patients (62%) were treatment-naive, five (38%) had received previous LDTs. Nine patients (69.2%) had underlying hepatitis B, two (15.4%) hepatitis C, and two (15.4%) alcohol-related cirrhosis. Baseline patient characteristics are summarised in Table 7.

All patients completed SBRT as planned. Median tumour size (based on sum of tumours in each patient) was 7.5 cm (range: 5.1-9.7 cm). Eleven patients had solitary tumours; in the two patients with multiple lesions, these were included in a single treatment volume. Three patients (23%) were treated with a respiratory-gated plan. Median prescribed dose was 45 Gy (range: 40-45 Gy) in five fractions. BED, assuming an α/β of 10 (BED10), was calculated and reported in light of the heterogeneous prescription doses. The median BED10 to 95% of the PTV (D95) was 74.9 Gy10 (range: 33.0-87.2 Gy10); underdosage was due to the intentional under-coverage of the PTV in order to meet OAR constraints. Median volume of liver receiving $\leq$15 Gy was 1669.6 cc (range: 882.3-2884.2 cc) and median mean liver dose (liver minus GTV) was 14.3 Gy (range: 9.9-17 Gy) (Table 8).

Table 7. Baseline patient characteristics

Characteristics	Patients n = 13 (%)
Age [Median (range)]	68 (53 – 88)
Gender	
Male	10 (76.9)
Female	3 (23.1)
ECOG status	
0	7 (53.8)
1	6 (46.2)
Baseline AFP [Median (range)]	66 (1.3-9400)
Baseline bilirubin [Median (range)]	15 (8-26)
Baseline platelets [Median (range)]	140 (52-225)
Baseline ALBI score	
Grade 1	2 (15.4)
Grade 2	10 (76.9)
Grade 3	1 (7.7)
Baseline Child Pugh score	
A5	6 (46.2)
A6	3 (23.1)
B7	4 (30.8)
Cirrhosis	
Yes	12 (92.3)
No	0 (0)
Unknown	1 (7.7)
Cirrhosis aetiology	
Hepatitis B	9 (69.2)
Hepatitis C	2 (15.4)
Alcohol-related	2 (15.4)
Previous liver-directed treatment	
TACE	2 (15.4)
Combination (TACE + other[a])	3 (23.1)
None	8 (61.5)

[a]RFA, microwave ablation or surgery

Abbreviations: TACE, transarterial embolisation; RFA, radiofrequency ablation

Table 8: Tumour and dosimetric parameters of treated hepatocellular carcinomas

Characteristics	Patients, n = 13 (%)
Tumour Size, cm (sum of tumours)	
Median (Range)	7.5 (5.1-9.7)
Prescription Dose	
45 Gy/5#	9 (69.2)
42.5 Gy/5#	3 (23.1)
40 Gy/5#	1 (7.7)
Energy	
6 MV FFF	7 (53.8)
10MV FFF	6 (46.2)
Gated Plan	
Yes	3 (23.1)
No	10 (76.9)
GTV volume (cm^3)	
Median (Range)	69.3 (26.5-487.8)
PTV volume (cm^3)	
Median (Range)	294.6 (137.4-1153.8)
GTV V95%	
Median (Range)	99.9 (48-100)
PTV V95%	
Median (Range)	94.2 (23.2–99.9)
D95 PTV (Gy)	
Median (Range)	41.1 (22.7-45.6)
D95 BED_{10} (Gy_{10})	
Median (Range)	74.9 (33.0-87.2)
Liver minus GTV (or ITV) volume (cm^3)	1669 (882-2884)
Median (Range)	
Liver minus GTV Dmean (Gy)	
Median (Range)	14.3 (9.9-17)
Volume of Liver spared 15 Gy (cm^3)	
Median (Range)	1105.1 (659.3-1486.3)

Abbreviations**:** GTV V95%, gross tumour volume receiving 95% of prescribed dose; PTV V95, planning target volume receiving 95% of prescribed dose; D95, minimum dose delivered to 95% of the planning target volume; D95 BED, minimum dose delivered to 95% of the PTV as a biological equivalent dose, assuming $\alpha/\beta = 10$.

6.4.2.2 Tumour Response

Median follow-up was 17.7 months. Objective response rate of the treated lesion(s) by mRECIST was achieved in 31% of patients at 3 months (CR=0, PR=4) with an overall response rate of 100% (PR=4, SD=9). Of note, two patients had tumours that were hypovascular and non-enhancing at baseline and on follow-up scans. In these cases, a PET/CT scan performed at the same time was used to assist with baseline and follow-up study measurements, and RECIST criteria was used for tumour size.

At 3 months there was one local failure; the treated lesion showed PR, but a new lesion developed at the edge of the PTV. One-year LC rate was 92% (95% CI, 56-99%) (Figure 3a). Median TTP was not reached. Four patients (31%) were downstaged to transplant criteria, and three underwent liver transplantation. One transplant patient had regional progression based on imaging (and ultimately pathology) 3-months post-SBRT; however, the treated lesion showed complete pathological response at time of transplant. The second transplant patient had a complete pathological response, while the third had 90% tumour necrosis at the treated site. The fourth patient died of hepatic failure prior to transplant.

6.4.2.3 Overall and Progression Free Survival

Median OS was 17.7 months (95% CI:5.8–23.9) and 1-year OS was 62% (95% CI: 31-82%) (Figure 3c). Eight patients experienced disease recurrence during study follow-up: seven developed regional failure (one together with local failure) and one patient distant failure along with regional failure. Median PFS (any progression) was 5.9 months (95% CI: 3.42 – not estimable) and 1-year PFS 46% (95% CI, 19%-70%). In addition to the three transplant patients, two further patients underwent treatment after regional failure post-SBRT; one received RFA followed by sorafenib, and the second patient sorafenib alone. Two additional patients were offered treatment at time of progression (TACE/RFA) but declined. At time of last review, ten patients had died, and three remained alive with a median time from SBRT of 48 months. Of the three patients alive, two had

received liver transplantation post-SBRT and one showed ongoing response post-SBRT without further treatment.

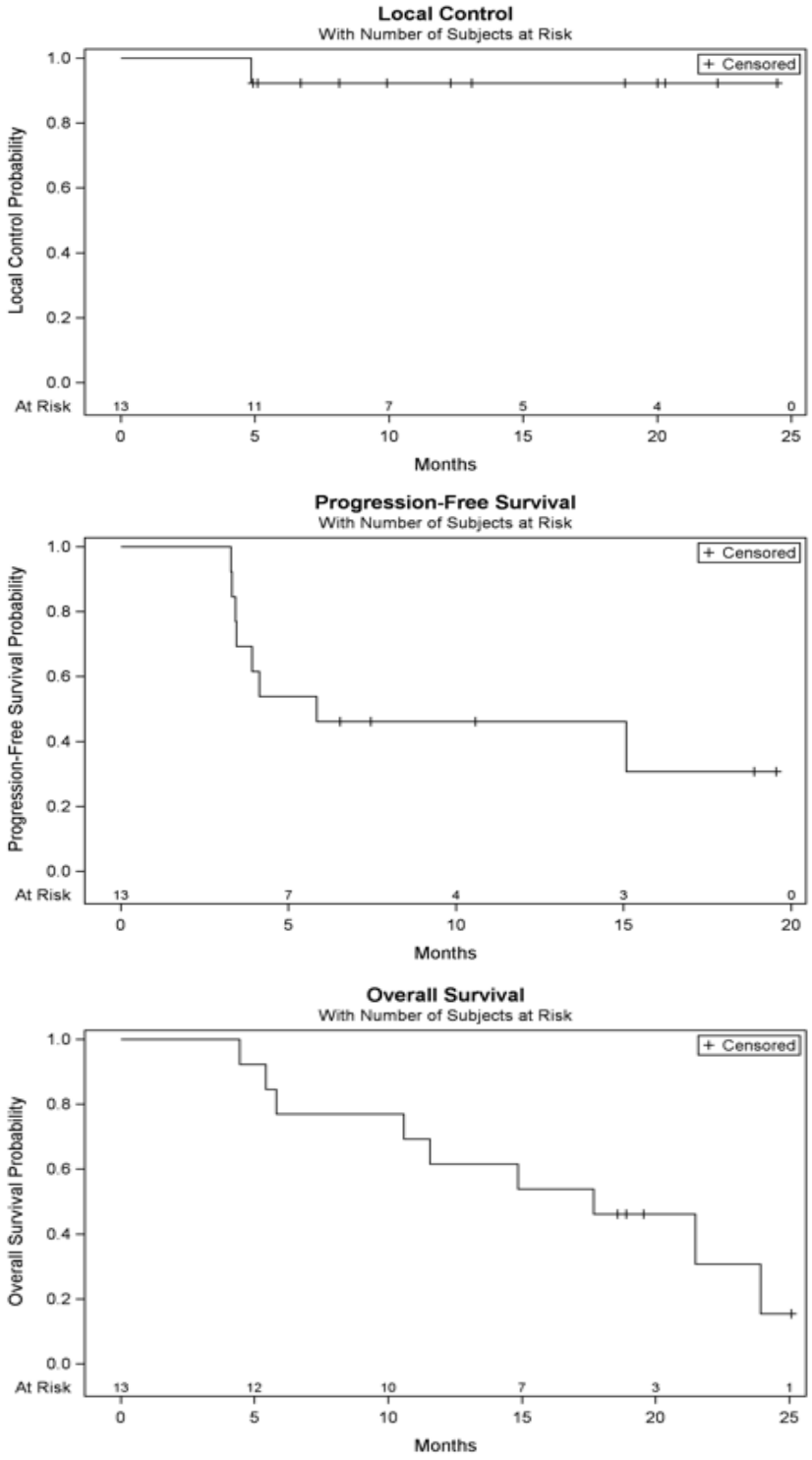

Figure 3. Kaplan Meier curves of: (A) local control, (B) progression-free survival, and (C) overall survival (Large HCC patients)

6.4.2.4 Toxicity and Child-Pugh Score

Cumulative acute and late toxicities are outlined in Table 9. Acute toxicity was defined as occurring within 3 months of treatment, and late toxicity after this. There were ten G3 acute toxicities (six haematological) in seven patients, of which three had CP B7 cirrhosis at baseline. The patients with CP B7 cirrhosis had acute G3 GGT dysfunction; however, two had G3 dysfunction at baseline that remained stable, and the third, a G2 GGT that worsened to G3 at 3 months. Three patients had acute G3 platelet abnormalities, of which two had baseline G2 dysfunction. One patient developed G3 oesophageal haemorrhage 6-weeks post-SBRT, due to varices that were subsequently banded. On review, no dose was delivered to the oesophagus. There were no acute G4/G5 toxicities and no cases of classic RILD.

There were six $\geq$ G3 late toxicities recorded during follow-up in three patients (23%), one with CP B7 cirrhosis and two with CP A5-6 cirrhosis. The most common G3 late toxicity was thrombocytopenia, occurring in two patients with baseline G2 platelet dysfunction. The G4 toxicity was a hepatic haemorrhage 12-months post-treatment, thought secondary to disease progression rather than SBRT. There was one G5 hepatic failure.

Overall, five patients (38%) had an increase in CPS by $\geq$ 2 points, 3-months post-SBRT. In three of these cases CP decline was due to disease progression. Of the two cases not attributed to progression, one patient (who progressed from CP A6 to B8) further deteriorated to CP C10 9-months post-SBRT and was placed on the transplant list. This patient subsequently died of hepatic failure 11-months post-SBRT (G5 hepatic failure). The second patient, whose pre-treatment CP increased from B7 to B9, recovered to pre-treatment CP 6-months post-SBRT.

Table 9. Cumulative acute and late toxicities

Toxicity	Grade 2 N (%)	Grade 3 N (%)	Grade 4 N (%)	Grade 5 N (%)
Acute (≤ 3 months)				
Fatigue	4	1	0	0
Diarrhoea	1	0	0	0
Pain	4	0	0	0
Nausea	0	1	0	0
Platelets	2	3	0	0
Haemoglobin	4	0	0	0
Neutrophils	0	1	0	0
Gamma GT	3	3	0	0
AST	1	0	0	0
Oesophageal varices haemorrhage	0	1	0	0
Vomiting	1	0	0	0
Acute total	**20**	**10**	**0**	**0**
Late (> 3months)				
Fatigue	3	1	0	0
Pain	3	0	0	0
Diarrhoea	1	0	0	0
Platelets	0	2	0	0
Neutrophils	1	0	0	0
AST	1	0	0	0
Gamma GT	1	1	0	0
Hepatic Necrosis	0	0	1	0
Hepatic failure	0	0	0	1
Late total	**10**	**4**	**1**	**1**

Abbreviations: AST, aspartate aminotransferase; Gamma GT, gamma-glutamyl transferase.

6.4.2.5 Quality of Life Assessment

Overall there was a decline in mean FACT-HEP score from baseline to 3-months of 9.7 points (95% CI: 1.5-17.9 points). Although an overall decline was also seen in the QLQ-C30 Global Health Score (GHS), this did not the reach the MID

threshold of 10-points (Table 10). However, QoL remained clinically stable or improved at 3 months in 61.5% and 53.8% of patients based on the QLQ-C30 GHS and FACT-HEP score respectively.

Table 10: Quality of life assessments: change from baseline to 3 months post-SBRT

	Mean score at baseline (SD)	Mean score at 3 months (SD)	Mean change (95% CI)	p-value
FACT-PWB	21.5 (6.4)	18.9 (7.4)	-1.54 (-4.75, -0.34)	0.049
FACT-SWB	22.6 (5.7)	20.6 (6.7)	-0.52 (-2.44, 1.40)	0.695
FACT-EWB	17.1 (4.1)	17.1 (5.3)	0 (-1.69, 1.69)	0.504
FACT-FWB	17.9 (6.4)	15.5 (7.1)	-2.39 (-5.19, 0.41)	0.079
FACT-HEP	128.6 (30.9)	118.9 (36.8)	**-9.69 (-17.91, -1.48)**	**0.025**
EORTC-GHS	68.6 (19.9)	59.6 (33.5)	-8.97 (-25.48, 7.53)	0.334

Notes: Minimally clinically important difference (MID) is ≥ 9 points for FACT-HEP and ≥ 10 points for EORTC global health score (GHS). *Abbreviations*: FACT, Functional Assessment of Cancer Therapy, -PWB, physical well-being, -SWB, social/family well-being, -EWB, emotional well-being, -FWB, functional well-being, -HEP, hepatobiliary

6.5 DISCUSSION

6.5.1 Overview

There is a growing body of literature supporting the use of SBRT in the treatment of HCC, with recent studies showing LC rates comparable to RFA, and improved LC rates when compared to TACE [24, 37]. As a result, the 2018 NCCN guidelines state that SBRT can be used as an alternative to RFA/TACE in inoperable HCC [38]. In contrast, the 2018 European Association for the Study of Liver Cancer (EASL) guidelines state that at present there is no robust evidence to support this therapeutic approach. These studies therefore contribute to the literature, by demonstrating that SBRT is well tolerated and offers excellent LC rates for patients not suitable, or refractory, to other LDTs.

The management of patients with unresectable, large HCCs remains a particular challenge. Current guidelines state that for patients with intermediate-stage disease, TACE is standard-of-care [3]. Although TACE can be repeated several times, tumours can eventually become resistant to treatment [6, 7, 39]. For these patients, further LDTs are limited, and systemic therapy is often the only remaining option. SBRT for large HCCs does present a significant challenge due to limited normal liver volume, liver dose constraints, and poor underlying liver function. Clinical experience on the safe delivery and efficacy of SBRT as a salvage treatment in this cohort is understandably limited. This study on the role of HCC in large tumours is therefore an important contribution to the evidence base, demonstrating both the safety and efficacy of SBRT in patients with large unresectable HCCs, not eligible for, or who have failed previous LDTs.

6.5.2 Small HCC tumours

The 1- and 2-year LC rates of 94% compare in this study favourably to the 70-100% LC rates reported in most studies on SBRT, including one of the largest reported series by Sanuki *et al* [14, 16, 18, 20, 21]. In our study, treatment dose and fractionation was individualised based on location of tumour in relation to tolerance of nearby OAR. Despite this, PTV coverage was good, with median D95 BED_{10} dose coverage of 104.8 Gy_{10} (range: 45.0-116.5 Gy_{10}). In the study

by Sanuki *et al*, the outcomes of 185 patients with tumours <5 cm treated with 35 or 40 Gy in 5 fractions were analysed. The 2-year LC was 93% and was not different between the two dose fractionations, suggesting that a lower dose than prescribed in our current institution may be equally effective in providing adequate LC [21]. In contrast, Bujold *et al* analysed the outcomes of 102 patients treated with doses ranging from 24-54 Gy (in 6 fractions) and showed that increased dose was associated with increased LC on UVA [20].

Overall survival in our study was 84% at 1 year and 74% at 2 years, which also is in line with published literature [14-16, 18, 21, 22, 24, 39]. On UVA, smaller tumour size was predictive of improved OS, while prescription BED_{10} dose ≥100 Gy_{10} approached significance. In our series, tumour size and prescription dose may be inter-related, as larger tumours were more likely to have been prescribed a lower prescription dose to meet liver constraints. As with LC, there are conflicting reports on whether prescription BED_{10} and tumour size are prognostic for OS. This may be due to the use of variable size and dose criteria for analyses in published studies, as clinically relevant values are not known. In our study, tumour size was analysed as a continuous variable due to small cohort numbers. In a retrospective study by Scorsetti *et al,* a BED_{10} >100 Gy_{10} and GTV <5 cm predicted for improved OS in tumours <6 cm treated in 3 or 6 fractions [22]. Similarly, Huang *et al* demonstrated that tumours <4 cm were predictive of improved OS in recurrent HCC patients treated with 37 Gy in 4-5 fractions [40]. Interestingly, BED_{10} >100 Gy_{10} and tumour size <3 cm were not predictive of OS in a large Japanese retrospective study of 79 HCC patients [15]. Clearly, to definitively answer what dose is desired for best LC and OS, larger sample sizes with more congruent BED dose and tumour size datasets are needed.

Our 1- and 2-year PFS rates were 49% and 38% respectively. Our reported PFS rates are low, but are in line with other published literature, indicating a high probability of progressive disease elsewhere in liver by 2-years, despite excellent LC [16, 22]. The lower PFS rates likely reflect the population being studied, as the majority (84%) of patients in our cohort received prior treatment with other modalities and therefore have already demonstrated a propensity for disease recurrence within the liver. Furthermore, as SBRT is often used later in a patient's

disease course, PFS and OS after SBRT may appear shorter than other local modalities which are commonly used at first disease presentation. The low PFS rate provides a rationale for investigating combination therapy with SBRT, including systemic therapies and TACE.

In our cohort, 84% of patients received LDT prior to SBRT, which is higher than most recent studies [17, 18, 20, 23, 41] . Liver-directed therapies can decrease the functional capacity of the liver, particularly in those with underlying liver disease, and increase the risk of adverse events from irradiation. Despite this, SBRT was well tolerated in our study, with no patients experiencing classic RILD and only six patients (19%) having a worsened CPS by $\geq$ 2 points. This decline in CPS is consistent with previous studies. For example, Andolino *et al* report a 20% deterioration post-SBRT whilst Bujold *et al* report a 29% decline (in those without disease progression) [18, 20]. Although we report that overall ten patients (32%) experienced G3+ toxicity during follow-up, seven patients (23%) developed toxicity within 3-months post-treatment. The remaining three patients experienced late toxicity. Furthermore, the majority of toxicities were haematological and transient in nature. Our acute toxicity rates are in keeping with comparable studies; Weiner *et al* recently reported on a cohort of patients with CPS <8 treated with SBRT and report 23% acute G3+ toxicities [42], whilst Andolino *et al* report that 36.7% of patients developed G3+ haematological toxicities post-SBRT[18]. Sanuki *et al* reports 24% G3+ toxicities, primarily thrombocytopenia [21].

Our relatively low toxicity rates are therefore reassuring, particularly in our cohort of heavily pre-treated patients. This may help explain the large number of patients who went on to receive further liver-directed treatments after SBRT, despite their initial ineligibility for other treatments. SBRT provided excellent LC to tumours that could not be readily targeted by other therapies due to a variety of factors including location, prior recurrence or tumour size. As patients frequently progressed outside of the SBRT treated areas, the low toxicities and well-maintained CPS after radiotherapy allowed patients to remain candidates for other local therapies. This provides strong evidence that SBRT can be added safely into the HCC treatment algorithm in conjunction with other therapies and

leads us to ask whether SBRT should now be considered earlier in the treatment pathway.

Although SBRT was not specifically used to downstage prior to transplant, it is interesting that three patients in our cohort underwent liver transplantation after receiving radiotherapy. Several studies have suggested a role for SBRT as a bridge to transplant, as it is well tolerated, and can result in a complete pathologic response [43-46]. Although beyond the scope of this study, the role of SBRT in bridging to transplant is intriguing and certainly warrants future investigation.

This study has the inherent limitations of a retrospective study from a single institution. Our patient population may therefore be individual to British Columbia; for example, none of our HCC cases were due to alcohol, whereas in North America and Europe alcohol accounts for 30-40% of cases [47]. Furthermore, as with most liver SBRT studies, the radiation dose was not homogenous. This common scenario reflects real-life practice where prescription dose is individualized to not exceed OAR dose tolerances. In general, our patient cohort received prescription doses in line with comparative studies. BED_{10} doses have also been reported to allow for comparison of outcomes to past and future studies.

6.5.3 Large HCC tumours

In this study, we report 1-year LC rates of 92%, 1-year OS rates of 62% and a median OS of 17.7 months for patients with tumours >5 cm, which is comparable with the published literature [20, 48, 49]. Bujold et al assessed 102 HCC patients with a median GTV of 7.2 cm treated with a BED10 of 56-102.6 Gy10. They report 1-year LC rates of 87%, a 1-year survival rate of 55% with a median survival of 17 months. In their cohort, they reported seven G5 toxicities (5 liver failures, 1 cholangitis, 1 gastrointestinal bleed) without classic RILD, and a decline in CP class in 29% of patients without progressive disease [20]. Kuo et al retrospectively analysed the impact of tumour size on 141 HCC patients treated with a BED10 of 48.6-89.70 Gy10 using Cyberknife [48]. For the 55 patients in the 'intermediate' group (> 4 cm to < 10 cm), an objective response rate of 90.9% was reported with 1-year LC and OS rates of 83.5% and 60.1% respectively. The

authors conclude that acute toxicity was not affected by tumour size, with three patients in the 'small' (<4 cm), and four patients in the 'intermediate' group experiencing ≥ G3 acute liver toxicity.

The safe delivery of SBRT to a large tumour often necessitates lower prescription doses which can impact the probability of tumour control. By using an individualised dose allocation, whereby OAR constraints, in particular liver constraints, were placed as a higher priority than PTV dose, we were able to safely deliver a median BED10 D95 to the PTV of 74.9 (range: 33.0-87.2 Gy10). Although five patients in our cohort did have an increase in CPS by ≥ two points 3-months post-SBRT, there were only two patients (15%) in which this occurred without disease progression, one of which was self-limiting. This suggests that our liver dose constraint, ensuring that ≥700 cm3 of uninvolved liver receives <17 Gy, is associated with favourable hepatic toxicity outcomes [50]. This is in keeping with the study by Son et al, which elicited a relationship between the volume of liver spared by 18 Gy and a decline in CP class, recommending that >800 cm3 of normal liver is spared [51].

Although our delivered dose is slightly lower than that reported by Bujold et al, it is consistent with the doses utilised by Kuo et al [20, 48]. Furthermore, our approach of allocating dose based on liver constraints is in keeping with current guidelines and clinical trials [52, 53]. While there are alternative approaches to treating large tumours, including hypofractionated regimens with a BED10 100 Gy in 15-25 fractions [54], our approach ensured that we were able to safely deliver SBRT with acceptable toxicities, and has demonstrated that this dose can provide good LC in this cohort of patients. As we develop the technical abilities to treat larger liver tumours, it becomes increasingly important to understand the relationship between dose and LC, and to balance this against the risk of toxicity, which includes death. Although dose escalation has always been the aim, it is now well recognised that HCC is a radiosensitive tumour. As a result, we may not need to deliver doses as high as once thought. A recent review of the current clinical data has shown that for doses between 53–84 Gy EQD2 (63.6–100 Gy BED10), LC rates increase from 50–90 %. Going beyond 84 Gy (100 Gy BED10) the degree of incremental LC improvement was shown to decrease with a

continued increase in toxicity [55]. However, it is important to correctly interpret dose delivered in the published literature as not all studies provide detailed dose-volume histogram (DVH) data, including mean, maximum, and minimum dose points of OARs, and the conversion of physical doses to BED. This is why there is now a recommendation for minimum standard reporting of achieved dose-metrics to be reported in future clinical studies. This will allow for robust normal tissue complication models to be developed and ultimately improve our understanding on the relationship between dose, tumour control and toxicity [56].

As well as providing evidence of good LC, our study also demonstrates that SBRT can be used safely in patients with large tumours that have previously received LDTs. There is a growing interest in combining SBRT with TACE, with a recent meta-analysis showing that TACE plus radiotherapy is associated with superior LC and disease-free survival compared to TACE alone [57]. On review of 25 trials (11 RCTs) involving 2577 patients, patients receiving TACE and radiotherapy showed significantly better 1-year survival (OR, 1.36 [95% CI, 1.19-1.54]) and complete response (OR, 2.73 [95% CI, 1.95-3.81]) compared with TACE alone. Although not a specific study outcome, our results also suggest that SBRT could be used to downstage patients to liver transplant criteria. In our cohort, four patients (31%) were successfully downstaged with SBRT. Three of these patients underwent subsequent transplantation, with one showing 90% necrosis at the treated site, and two showing complete pathological response. These findings are in keeping with a number of recent studies showing that SBRT is a feasible, well-tolerated treatment before transplantation, and can provide excellent responses [43-46]. SBRT may therefore have a role not only in combination with TACE, but also in downstaging large tumours that do not meet transplant criteria at initial presentation.

Despite excellent LC rates after SBRT, out-of-field hepatic progression remained problematic in our cohort, with 62% of patients developing regional failure. Apart from the single local failure, all other sites of regional progression were outside of the 50% isodose line. There is therefore a rationale to consider combining SBRT with systemic treatments to improve disease control and ultimately OS rates in these patients. The RTOG 1112 phase III randomised control trial is

already exploring this concept by comparing sorafenib to SBRT followed by sorafenib in patients with intermediate and advanced stage HCC [53].

In the interim, outside the context of a clinical trial, the treatment options for patients with large unresectable HCCs, ineligible for further LDTs, are limited. Sorafenib remains the standard-of-care in many countries for those with CPA, offering 1-year OS rates of 29-44% and a median OS of 6.5-10.7 months [9, 11]. In other countries, lenvatinib is now used in the first line setting following the results of the recent REFLECT trial where it was shown to be non-inferior to sorafenib with a medial OS of 13.6 months [58]. This study's 1-year OS rate of 62% and median survival of 17.7 months therefore compares favourably, and suggests that SBRT, a well-tolerated, non-invasive, local treatment, could be an alternative option to systemic therapy for patients with non-metastatic HCC measuring >5 cm and CPS $\leq$ B7. Alternative options that have been utilised include proton beam therapy (PBT) and SIRT. Although PBT is promising for large tumours, with studies reporting 2-year LC rates of 87% and 2-year OS rates of 36-52.4%, the wider penumbra due to lateral scatter means that it may not be the best option for tumours close to critical structures [54, 59, 60]. Furthermore, access to PBT is currently limited when compared to SBRT. In comparison, SIRT with Y90 has been used in patients with intermediate-stage HCC, with studies reporting a median OS of 16.9 months; for patients who have failed previous TACE, median OS is 13.6 months [61]. The exact role for SIRT, PBT and SBRT within the treatment algorithm for HCC, however, is unclear, and further studies are warranted to explore these options in this challenging cohort.

There are limitations inherent to this study. Although this is a prospective phase II study, it is restricted by its small cohort and single-institution nature. The initial plan was to recruit 20 patients, but due to slow accrual a decision was made to prematurely close the trial in July 2016. This was due to the opening of a competitor TheraSphere study for unresectable HCC patients (NCT01556490) in 2014 at our institution. This trial was also for HCC patients unsuitable for further local therapies, including TACE, and randomised patients between standard of care sorafenib and Y90. As such, this led to difficulty in patient recruitment, and ultimately early closure of the study before reaching our target of 20 patients. The

small number of patients therefore limits our ability to provide further statistical analyses. In the absence of international standardised criteria for assessing tumour response post-SBRT, we decided to use mRECIST reporting to keep in line with current clinical trials and international recommendations [3, 62]. However, there are limitations of using this approach. Although mRECIST was developed to take into account tumour necrosis and intra-tumoral vascularisation, non-enhancing tumours are not measurable using this criteria, thus preventing complete evaluation of response [32]. Furthermore, tumours with pre-existing high signal within a lesion, such as following TACE with lipiodol treatment, or as a result of haemorrhage, cannot be identified as target lesions due to the masking of any residual arterial enhancement. In 2/13 cases in our cohort, the tumours were non-enhancing and as such did not meet criteria for a target lesion. In these cases, the PET-CT scan performed at the same time was used to assist with baseline and follow-up study measurements, and RECIST criteria used for tumour size. As this was the case at baseline, and on all follow-up imaging, the same methodology was used across all study scans in these two patients. However, this does highlight the difficulties of solely using mRECIST criteria in reporting responses in HCC patients post-SBRT. Given the low sensitivity of both methods for determining response, it is now recommended that the reporting of both mRECIST and RECIST is utilised in clinical trials [3].

6.6 CONCLUSIONS

In conclusion, SBRT to small inoperable HCC provides high LC rates with acceptable toxicities, even in patients who have received prior LDT. Although, overall, 32% of patients experienced ≥ G3 + toxicities (23% acute), and 19% had a deterioration in CPS of ≥2 points, these changes were mainly transient with minimal clinical impact. Despite excellent LC, disease progression outside of the irradiated site remains prominent. This study demonstrates that SBRT can be delivered safely even after previous LDTs and that further liver therapies can follow treatment with SBRT. However, the exact positioning of SBRT within the HCC treatment algorithm remains uncertain and further studies are warranted to examine the role for SBRT in combination with other modalities to maximise disease control in the liver.

The large HCC study also demonstrates that SBRT can provide excellent LC with acceptable toxicities to patients with unresectable large HCCs not suitable for further LDTs. However, regional recurrence remains the major cause of disease progression. Large prospective clinical studies are required to further explore the role of SBRT in large HCCs, in combination with other treatment modalities, to maximise disease control in this challenging group of patients with limited or no alternative treatment options.

6.7 REFERENCES

[1] Bray F, Ferlay J, Soerjomataram I, Siegel RL, Torre LA, Jemal A. Global cancer statistics 2018: GLOBOCAN estimates of incidence and mortality worldwide for 36 cancers in 185 countries. CA Cancer J Clin. 2018;68:394-424.

[2] Bruix J, Sherman M. Management of hepatocellular carcinoma: an update. Hepatology (Baltimore, Md). 2011;53:1020-2.

[3] EASL Clinical Practice Guidelines: Management of hepatocellular carcinoma. Journal of hepatology. 2018;69:182-236.

[4] Tsoulfas G, Mekras A, Agorastou P, Kiskinis D. Surgical treatment for large hepatocellular carcinoma: does size matter? ANZ journal of surgery. 2012;82:510-7.

[5] Pawlik TM, Poon RT, Abdalla EK, Zorzi D, Ikai I, Curley SA, et al. Critical appraisal of the clinical and pathologic predictors of survival after resection of large hepatocellular carcinoma. Archives of surgery (Chicago, Ill : 1960). 2005;140:450-7; discussion 7-8.

[6] Park W, Chung YH, Kim JA, Jin YJ, Lee D, Shim JH, et al. Recurrences of hepatocellular carcinoma following complete remission by transarterial chemoembolization or radiofrequency therapy: Focused on the recurrence patterns. Hepatol Res. 2013;43:1304-12.

[7] Llovet JM, Real MI, Montana X, Planas R, Coll S, Aponte J, et al. Arterial embolisation or chemoembolisation versus symptomatic treatment in patients with unresectable hepatocellular carcinoma: a randomised controlled trial. Lancet (London, England). 2002;359:1734-9.

[8] Golfieri R, Renzulli M, Mosconi C, Forlani L, Giampalma E, Piscaglia F, et al. Hepatocellular carcinoma responding to superselective transarterial chemoembolization: an issue of nodule dimension? Journal of vascular and interventional radiology : JVIR. 2013;24:509-17.

[9] Llovet JM, Ricci S, Mazzaferro V, Hilgard P, Gane E, Blanc JF, et al. Sorafenib in advanced hepatocellular carcinoma. The New England journal of medicine. 2008;359:378-90.

[10] Abou-Alfa GK, Schwartz L, Ricci S, Amadori D, Santoro A, Figer A, et al. Phase II study of sorafenib in patients with advanced hepatocellular carcinoma.

Journal of clinical oncology : official journal of the American Society of Clinical Oncology. 2006;24:4293-300.
[11] Cheng A-L, Kang Y-K, Chen Z, Tsao C-J, Qin S, Kim JS, et al. Efficacy and safety of sorafenib in patients in the Asia-Pacific region with advanced hepatocellular carcinoma: a phase III randomised, double-blind, placebo-controlled trial. The Lancet Oncology. 2009;10:25-34.
[12] Chow PKH, Gandhi M, Tan SB, Khin MW, Khasbazar A, Ong J, et al. SIRveNIB: Selective Internal Radiation Therapy Versus Sorafenib in Asia-Pacific Patients With Hepatocellular Carcinoma. Journal of clinical oncology : official journal of the American Society of Clinical Oncology. 2018;36:1913-21.
[13] Vilgrain V, Pereira H, Assenat E, Guiu B, Ilonca AD, Pageaux G-P, et al. Efficacy and safety of selective internal radiotherapy with yttrium-90 resin microspheres compared with sorafenib in locally advanced and inoperable hepatocellular carcinoma (SARAH): an open-label randomised controlled phase 3 trial. The Lancet Oncology. 2017;18:1624-36.
[14] Cardenes HR, Price TR, Perkins SM, Maluccio M, Kwo P, Breen TE, et al. Phase I feasibility trial of stereotactic body radiation therapy for primary hepatocellular carcinoma. Clinical & translational oncology : official publication of the Federation of Spanish Oncology Societies and of the National Cancer Institute of Mexico. 2010;12:218-25.
[15] Yamashita H, Onishi H, Murakami N, Matsumoto Y, Matsuo Y, Nomiya T, et al. Survival outcomes after stereotactic body radiotherapy for 79 Japanese patients with hepatocellular carcinoma. J Radiat Res. 2015;56:561-7.
[16] Huertas A, Baumann AS, Saunier-Kubs F, Salleron J, Oldrini G, Croise-Laurent V, et al. Stereotactic body radiation therapy as an ablative treatment for inoperable hepatocellular carcinoma. Radiother Oncol. 2015;115:211-6.
[17] Tse RV, Hawkins M, Lockwood G, Kim JJ, Cummings B, Knox J, et al. Phase I study of individualized stereotactic body radiotherapy for hepatocellular carcinoma and intrahepatic cholangiocarcinoma. Journal of clinical oncology : official journal of the American Society of Clinical Oncology. 2008;26:657-64.
[18] Andolino DL, Johnson CS, Maluccio M, Kwo P, Tector AJ, Zook J, et al. Stereotactic Body Radiotherapy for Primary Hepatocellular Carcinoma. International Journal of Radiation Oncology*Biology*Physics. 2011;81:e447-e53.

[19] Kang JK, Kim MS, Cho CK, Yang KM, Yoo HJ, Kim JH, et al. Stereotactic body radiation therapy for inoperable hepatocellular carcinoma as a local salvage treatment after incomplete transarterial chemoembolization. Cancer. 2012;118:5424-31.
[20] Bujold A, Massey CA, Kim JJ, Brierley J, Cho C, Wong RK, et al. Sequential phase I and II trials of stereotactic body radiotherapy for locally advanced hepatocellular carcinoma. Journal of clinical oncology : official journal of the American Society of Clinical Oncology. 2013;31:1631-9.
[21] Sanuki N, Takeda A, Oku Y, Mizuno T, Aoki Y, Eriguchi T, et al. Stereotactic body radiotherapy for small hepatocellular carcinoma: a retrospective outcome analysis in 185 patients. Acta Oncol. 2014;53:399-404.
[22] Scorsetti M, Comito T, Cozzi L, Clerici E, Tozzi A, Franzese C, et al. The challenge of inoperable hepatocellular carcinoma (HCC): results of a single-institutional experience on stereotactic body radiation therapy (SBRT). Journal of cancer research and clinical oncology. 2015;141:1301-9.
[23] Lasley FD, Mannina EM, Johnson CS, Perkins SM, Althouse S, Maluccio M, et al. Treatment variables related to liver toxicity in patients with hepatocellular carcinoma, Child-Pugh class A and B enrolled in a phase 1-2 trial of stereotactic body radiation therapy. Pract Radiat Oncol. 2015;5:e443-e9.
[24] Wahl DR, Stenmark MH, Tao Y, Pollom EL, Caoili EM, Lawrence TS, et al. Outcomes After Stereotactic Body Radiotherapy or Radiofrequency Ablation for Hepatocellular Carcinoma. Journal of clinical oncology : official journal of the American Society of Clinical Oncology. 2016;34:452-9.
[25] Benedict SH, Yenice KM, Followill D, Galvin JM, Hinson W, Kavanagh B, et al. Stereotactic body radiation therapy: the report of AAPM Task Group 101. Medical physics. 2010;37:4078-101.
[26] Pan CC, Kavanagh BD, Dawson LA, Li XA, Das SK, Miften M, et al. Radiation-associated liver injury. International journal of radiation oncology, biology, physics. 2010;76:S94-100.
[27] Eisenhauer EA, Therasse P, Bogaerts J, Schwartz LH, Sargent D, Ford R, et al. New response evaluation criteria in solid tumours: revised RECIST guideline (version 1.1). European journal of cancer (Oxford, England : 1990). 2009;45:228-47.

[28] Heffernan N, Cella D, Webster K, Odom L, Martone M, Passik S, et al. Measuring health-related quality of life in patients with hepatobiliary cancers: the functional assessment of cancer therapy-hepatobiliary questionnaire. Journal of clinical oncology : official journal of the American Society of Clinical Oncology. 2002;20:2229-39.
[29] Groenvold M, Klee MC, Sprangers MA, Aaronson NK. Validation of the EORTC QLQ-C30 quality of life questionnaire through combined qualitative and quantitative assessment of patient-observer agreement. Journal of clinical epidemiology. 1997;50:441-50.
[30] Fayers P, Aaronson, N. K., Bjordal, K., Groenvold, M., Curran, D., & Bottomley, A. EORTC QLQ-C30 Scoring Manual (3rd edition). . Brussels: European Organisation for Research and Treatment of Cancer; 2001.
[31] FACIT. FACT-Hep (version 4).
[32] Lencioni R, Llovet JM. Modified RECIST (mRECIST) assessment for hepatocellular carcinoma. Seminars in liver disease. 2010;30:52-60.
[33] Osoba D, Rodrigues G, Myles J, Zee B, Pater J. Interpreting the significance of changes in health-related quality-of-life scores. Journal of clinical oncology : official journal of the American Society of Clinical Oncology. 1998;16:139-44.
[34] Maringwa JT, Quinten C, King M, Ringash J, Osoba D, Coens C, et al. Minimal important differences for interpreting health-related quality of life scores from the EORTC QLQ-C30 in lung cancer patients participating in randomized controlled trials. Supportive care in cancer : official journal of the Multinational Association of Supportive Care in Cancer. 2011;19:1753-60.
[35] Steel JL, Eton DT, Cella D, Olek MC, Carr BI. Clinically meaningful changes in health-related quality of life in patients diagnosed with hepatobiliary carcinoma. Ann Oncol. 2006;17:304-12.
[36] Johnson PJ, Berhane S, Kagebayashi C, Satomura S, Teng M, Reeves HL, et al. Assessment of liver function in patients with hepatocellular carcinoma: a new evidence-based approach-the ALBI grade. Journal of clinical oncology : official journal of the American Society of Clinical Oncology. 2015;33:550-8.
[37] Sapir E, Tao Y, Schipper MJ, Bazzi L, Novelli PM, Devlin P, et al. Stereotactic Body Radiation Therapy as an Alternative to Transarterial Chemoembolization for Hepatocellular Carcinoma. International Journal of Radiation Oncology*Biology*Physics. 2018;100:122-30.

[38] Network NCC. Hepatobiliary cancers (version 2.2018). 2018.
[39] Seo YS, Kim MS, Yoo SY, Cho CK, Choi CW, Kim JH, et al. Preliminary result of stereotactic body radiotherapy as a local salvage treatment for inoperable hepatocellular carcinoma. J Surg Oncol. 2010;102:209-14.
[40] Huang WY, Jen YM, Lee MS, Chang LP, Chen CM, Ko KH, et al. Stereotactic body radiation therapy in recurrent hepatocellular carcinoma. International journal of radiation oncology, biology, physics. 2012;84:355-61.
[41] Moon DH, Wang AZ, Tepper JE. A prospective study of the safety and efficacy of liver stereotactic body radiotherapy in patients with and without prior liver-directed therapy. Radiother Oncol. 2018;126:527-33.
[42] Weiner AA, Olsen J, Ma D, Dyk P, DeWees T, Myerson RJ, et al. Stereotactic body radiotherapy for primary hepatic malignancies - Report of a phase I/II institutional study. Radiother Oncol. 2016;121:79-85.
[43] O'Connor JK, Trotter J, Davis GL, Dempster J, Klintmalm GB, Goldstein RM. Long-term outcomes of stereotactic body radiation therapy in the treatment of hepatocellular cancer as a bridge to transplantation. Liver transplantation : official publication of the American Association for the Study of Liver Diseases and the International Liver Transplantation Society. 2012;18:949-54.
[44] Facciuto ME, Singh MK, Rochon C, Sharma J, Gimenez C, Katta U, et al. Stereotactic body radiation therapy in hepatocellular carcinoma and cirrhosis: evaluation of radiological and pathological response. J Surg Oncol. 2012;105:692-8.
[45] Moore A, Cohen-Naftaly M, Tobar A, Kundel Y, Benjaminov O, Braun M, et al. Stereotactic body radiation therapy (SBRT) for definitive treatment and as a bridge to liver transplantation in early stage inoperable Hepatocellular carcinoma. Radiation oncology (London, England). 2017;12:163.
[46] Sapisochin G, Barry A, Doherty M, Fischer S, Goldaracena N, Rosales R, et al. Stereotactic body radiotherapy vs. TACE or RFA as a bridge to transplant in patients with hepatocellular carcinoma. An intention-to-treat analysis. Journal of hepatology. 2017;67:92-9.
[47] Global Burden of Disease Liver Cancer C, Akinyemiju T, Abera S, Ahmed M, Alam N, Alemayohu MA, et al. The Burden of Primary Liver Cancer and Underlying Etiologies From 1990 to 2015 at the Global, Regional, and National

Level: Results From the Global Burden of Disease Study 2015. JAMA Oncol. 2017;3:1683-91.
[48] Kuo HT, Que J, Lin LC, Yang CC, Koay LB, Lin CH. Impact of tumor size on outcome after stereotactic body radiation therapy for inoperable hepatocellular carcinoma. Medicine (Baltimore). 2017;96:e9249.
[49] Gkika E, Schultheiss M, Bettinger D, Maruschke L, Neeff HP, Schulenburg M, et al. Excellent local control and tolerance profile after stereotactic body radiotherapy of advanced hepatocellular carcinoma. Radiation oncology (London, England). 2017;12:116.
[50] Loewen SK, Vollans E, Crumley C, Sahota H, Kosztyla R, Liu M, et al. Liver dosimetric evaluation in biologically based stereotactic body radiotherapy for large inoperable hepatocellular carcinoma. Journal of Radiation Oncology. 2015;4:177-84.
[51] Son SH, Choi BO, Ryu MR, Kang YN, Jang JS, Bae SH, et al. Stereotactic body radiotherapy for patients with unresectable primary hepatocellular carcinoma: dose-volumetric parameters predicting the hepatic complication. International journal of radiation oncology, biology, physics. 2010;78:1073-80.
[52] UK SABR Consortium. Stereotactic Ablatice Body Radiation Therapy (SABR): A Resource. . 2019;Version 6.1
https://www.sabr.org.uk/wp-content/uploads/2019/04/SABRconsortium-guidelines-2019-v6.1.0.pdf. Accessed Apri 2020.
[53] Sorafenib Tosylate With or Without Stereotactic Body Radiation Therapy in Treating Patients With Liver Cancer. https://clinicaltrials.gov/ct2/show/NCT01730937. Accessed April 2020.
[54] Crane CH, Koay EJ. Solutions that enable ablative radiotherapy for large liver tumors: Fractionated dose painting, simultaneous integrated protection, motion management, and computed tomography image guidance. Cancer. 2016;122:1974-86.
[55] Schaub SK, Hartvigson PE, Lock MI, Hoyer M, Brunner TB, Cardenes HR, et al. Stereotactic Body Radiation Therapy for Hepatocellular Carcinoma: Current Trends and Controversies. Technol Cancer Res Treat. 2018;17:1533033818790217.

[56] Miften M, Vinogradskiy Y, Moiseenko V, Grimm J, Yorke E, Jackson A, et al. Radiation Dose-Volume Effects for Liver SBRT. International journal of radiation oncology, biology, physics. 2018.
[57] Huo YR, Eslick GD. Transcatheter Arterial Chemoembolization Plus Radiotherapy Compared With Chemoembolization Alone for Hepatocellular Carcinoma: A Systematic Review and Meta-analysis. JAMA Oncol. 2015;1:756-65.
[58] Kudo M, Finn RS, Qin S, Han KH, Ikeda K, Piscaglia F, et al. Lenvatinib versus sorafenib in first-line treatment of patients with unresectable hepatocellular carcinoma: a randomised phase 3 non-inferiority trial. Lancet (London, England). 2018;391:1163-73.
[59] Kimura K, Nakamura T, Ono T, Azami Y, Suzuki M, Wada H, et al. Clinical results of proton beam therapy for hepatocellular carcinoma over 5 cm. Hepatol Res. 2017;47:1368-74.
[60] Sugahara S, Oshiro Y, Nakayama H, Fukuda K, Mizumoto M, Abei M, et al. Proton beam therapy for large hepatocellular carcinoma. International journal of radiation oncology, biology, physics. 2010;76:460-6.
[61] Sangro B, Carpanese L, Cianni R, Golfieri R, Gasparini D, Ezziddin S, et al. Survival after yttrium-90 resin microsphere radioembolization of hepatocellular carcinoma across Barcelona clinic liver cancer stages: a European evaluation. Hepatology (Baltimore, Md). 2011;54:868-78.
[62] Vincenzi B, Di Maio M, Silletta M, D'Onofrio L, Spoto C, Piccirillo MC, et al. Prognostic Relevance of Objective Response According to EASL Criteria and mRECIST Criteria in Hepatocellular Carcinoma Patients Treated with Loco-Regional Therapies: A Literature-Based Meta-Analysis. PLoS One. 2015;10:e0133488.

7 RADIOPAQUE BEADS AS POTENTIAL FIDUCIAL MARKERS FOR LIVER STEREOTACTIC BODY RADIOTHERAPY

7.1 BACKGROUND

7.1.1 Stereotactic body radiotherapy

Stereotactic body radiotherapy (SBRT) is a feasible and safe therapeutic option for patients with hepatocellular carcinoma (HCC) ineligible for other local treatments [1-9]. SBRT is also an effective treatment option for patients with liver oligometastases from colorectal cancer, with encouraging LC and survival rates [10, 11].

Although transarterial chemoembolisation (TACE) remains the standard of care for intermediate-stage HCC, recent studies have shown that SBRT can be used safely in the adjuvant setting and as a salvage treatment post-TACE failure [12-14]. It has been shown that patients who have received SBRT following incomplete TACE had a 2-year survival rate that was significantly higher compared to those that received repeat TACE alone (36.8 % vs. 14.3%, p=0.001) [15]. Furthermore, there is now a phase III randomised control study currently recruiting that is comparing the efficacy of TACE vs TACE combined with SBRT as a primary treatment for unresectable HCC (NCT03338647) [16].

7.1.2 Fiducial markers and image-guided SBRT

Target accuracy is crucial for liver SBRT due to the radiosensitive nature of the liver, proximity of tumours to small bowel and significant liver motion with respiration. However, liver tumours are often difficult to visualise on CT and cone-beam CT (CBCT) imaging without the use of contrast. Image-guidance radiotherapy (IGRT) is therefore typically accomplished through visualisation of a surrogate to the tumour. The surrogate can be the whole liver, the diaphragm or an implanted fiducial marker. Fiducial markers implanted close to a liver tumour have been shown to be a better surrogate of tumour position than anatomical landmarks [17]. Fiducials are typically made of a biologically inert metal with a high atomic number, most commonly gold. These can be designed specifically for radiotherapy, can be devices in off label use (such as coils) or

simple non-commercial materials [18]. Lipiodol, an embolic agent used in TACE, has already been shown to be a feasible surrogate for liver position during liver SBRT [19, 20].

Fiducial markers need to be visible at radiotherapy treatment planning, and in the modalities used for image-guided treatment. They must produce minimal imaging artefact, have minimal perturbation of the therapeutic dose to the target volume, be easy to insert, and show stability with negligible migration [21]. With regards to liver SBRT, three fiducials are typically placed in, or within, close proximity to the tumour to ensure movement with respiration is along the same plane as the tumour. Small gold fiducials are commonly placed under ultrasound or CT guidance, prior to radiotherapy planning.

7.1.3 Novel radio-opaque beads

The recent development of radiopaque (RO) beads used in TACE delivery, which can be visualised on CT [22], has the advantage of providing intra- and post-procedure visualisation of the tumour vasculature. Furthermore, the durable radiopacity of the beads means that beads are visible on x-ray-based imaging after treatment advantage [23, 24]. The retention of RO beads within the tumour vasculature means that RO beads could potentially act as a natural surrogate for direct image-guided tumour targeting [20].

7.2 AIMS AND OBJECTIVES

The overall aim of this study is to determine the feasibility of using RO beads as fiducial markers for liver IGRT on a gantry based linear accelerator.

The ability of RO beads to meet this objective is assessed in two parts:

- Part 1: Radiotherapy study using novel RO beads in the VEROnA trial
- Part 2: Assessment of RO beads in a phantom model

7.2.1 Part 1: Radiotherapy study using novel radiopaque beads in the VEROnA trial

The first part of this study focusses on the radiotherapy images acquired following treatment with BTG-002814 in patients treated in the VEROnA study.

In particular, part one assesses:

1. The ability to visualise the RO beads on 4D-CT scans post-treatment with BTG-002814
2. The ability to match the 4D-CT scans to the CBCT scans based on the RO beads
3. The stability of the RO bead position following treatment with BTG-002814

7.2.2. Part 2: Assessment of radiopaque beads in a phantom model

In the second part of this study, an in-house phantom model is used to assess the visibility of the RO beads in a number of additional IGRT imaging modalities, including kV, MV, 4D-CT and CBCT images with and without motion.

7.3 MATERIALS AND METHODS

7.3.1 4D-CT and CBCT imaging of the radiopaque beads in the VEROnA trial

7.3.1.1 Patient selection

All patients in this study were treated as part of the VEROnA clinical trial, which is outlined in detail in Chapter 2 (section 2.2) As part of this clinical trial all patients underwent imaging in the radiotherapy department with 4D-CT and CBCT 24 hours following treatment with BTG-002814. Patients also underwent imaging with CT and magnetic resonance imaging (MRI) at baseline and post-TACE, on the day prior to surgery.

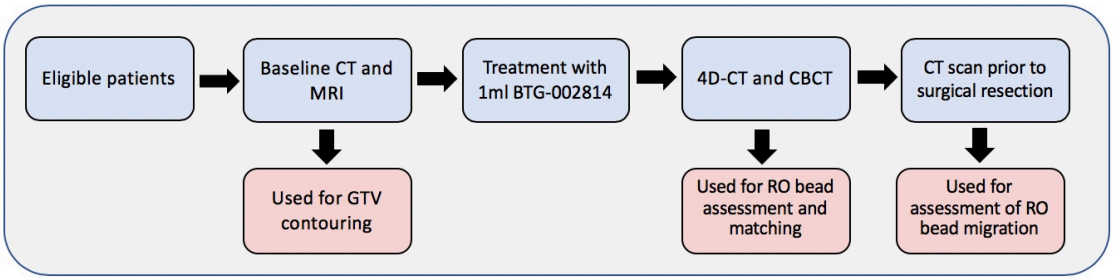

Figure 1: Overview of trial schema for radiopaque bead assessment. All eligible patients are treated with 1 ml of BTG-002814 via transarterial catheterization (TACE). Prior to treatment all patients underwent imaging with CT and MRI. On the day following TACE patients underwent 4D-CT and cone-beam CT imaging. 6-20 days post-TACE patients underwent repeat CT and MRI imaging.

7.3.1.2 4D-CT and CBCT acquisition details

For 4D-CT acquisition all patients were positioned supine, with arms up on a wing board and immobilised using a commercial immobilisation system (Combifix™). Patients were instructed to breathe freely, and abdominal compression was not used. For each patient, 1.25 mm slice thickness 4D-CT images (120kV, 100mA) were acquired on a GE Lightspeed CT scanner (Chicago, Illinois) and phase-sorted into ten bins of equal time share of the respiratory cycle. Following this, each patient was set-up in the same position, using reference skin marks and a three-point laser system on a TrueBeam linear accelerator (Varian Medical Systems, Palo Alto, CA). A free-breathing CBCT scan was acquired using the on-board imaging system (125kV, 60mA, 20ms, 1080mAs). The reconstructed volume was 17 cm along cranio-caudal axis and 45 cm in the axial plane. A reconstructed slice thickness of 2.5 mm was used. It is important to highlight that patients in the VEROnA study did not go undergo radiotherapy treatment.

7.3.1.3 Radiopaque bead evaluation

In order for RO beads to be used as fiducial markers for liver SBRT they need to be:

1. Visible at radiotherapy treatment planning (4D-CT)
2. Visible on the CBCT (used for treatment verification)

3. Have the same shape and size (volume) on 4D CT and CBCT and have the same spatial separation in order to allow reliable matching
4. Show stability with negligible migration

Furthermore, in keeping with current recommendations, it was decided that the following criteria should apply:

1. The volume of the RO fiducial needed to be >0.1 cm^3 (based on size of commercial fiducials)
2. The RO bead fiducial needed to be within 4 cm of the GTV [17]
3. A minimum of three RO beads fiducials would be identified

As RO beads must first and foremost be visible on the imaging method used for IGRT, areas of RO beads were initially contoured on the CBCT scan. As RO beads are aligned along liver blood-vessels and are not a discrete area of high density, as seen with commercial fiducials or lipiodol, the automated thresholding function in the Eclipse treatment planning system (Varian Medical Systems, Paolo Alto, CA) was utilised for contouring to avoid inter-observer variation. Automated thresholding automatically detects areas above a set Hounsfield unit (HU) threshold (Figure 2).

Firstly, a lower HU threshold limit was selected. To define this lower limit, the CBCT was reviewed, and three regions visible as discrete areas selected. The mean HU of these volumes was chosen as the initial HU threshold and increments then based on the areas that were contoured as a result. Automated thresholding was subsequently used to detect all areas with a HU value greater than the lower limit. Using the HU thresholds from the CBCT data, the same contouring approach was then applied to the average intensity projection (AVE-IP) scan of the 4D-CT, which was used as the primary data set. Gross tumour volume (GTV) was contoured for each treated tumour, using fused baseline MRI and CT scans taken prior to treatment. All RO bead areas > 4 cm from the GTV were excluded [17]. Any discrete volumes measuring <0.1 cm^3 were removed (Figure 3).

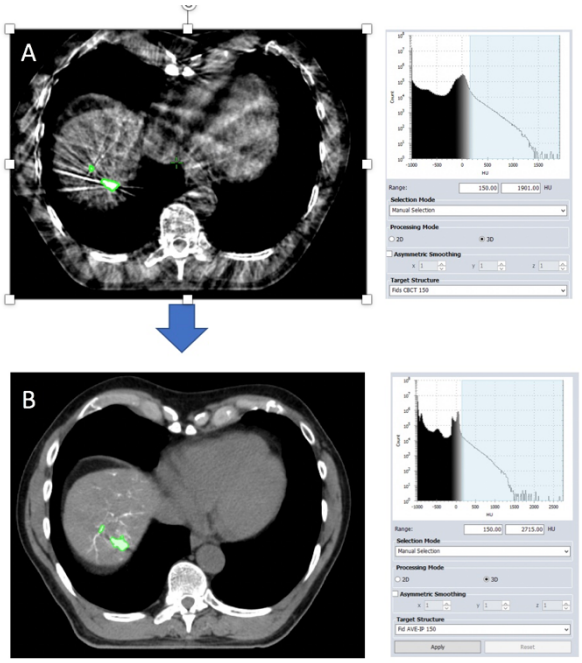

Figure 2: Automated threshold contouring on the CBCT and AVE-IP scan. Areas of beads with a denisty above 150 HU are automatically contoured on the cone-beam CT (CBCT) scan (image A) and average-intensity CT (AVE-IP) scans (image B)

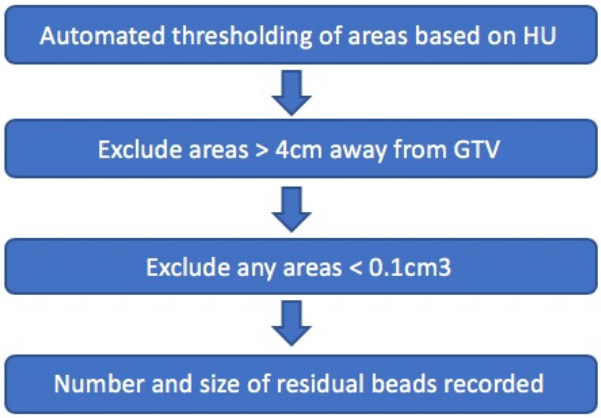

Figure 3: Flow diagram of contouring methodology

For each automated contour the following details were recorded:

1. The number of discrete visible areas detected
2. The volume of each area
3. The geometric distance between areas in the x, y and z positions.

The same thresholding and contouring approach was applied to the AVE-IP of the 4D-CT (Figure 2). Finally, for visual comparison this was repeated on the maximum intensity projection (MIP) sequence from the 4D-CT images.

7.3.1.4 Matching of RO beads on 4D-CT to CBCT

In keeping with our departmental practice for online matching between the CBCT and AVE-IP scans, the following steps were applied offline using Varian Offline Review: firstly, an anatomical auto-match was applied in the region-of-interest using grayscale recognition (Figure 4a). This was visually reviewed by a radiation therapist (MD) and radiation oncologist (LB) and corrected as required to ensure that the vertebral bodies were aligned; secondly, an auto-match to the liver edge was performed (Figure 4b). Finally, a manual match was performed based on the RO beads contoured on the AVE-IP plan using grayscale blending, split windows, and contour overlay matching (Figure 4c). Following matching based on the RO beads, the centre of mass (CoM) for each RO bead area was compared between CBCT and AVE-IP in the mediolateral (ML), anteroposterior (AP) and cranio-caudal (CC) directions, and difference in CoM position recorded. An absolute mean difference for each patient was calculated from all of the contoured RO bead areas.

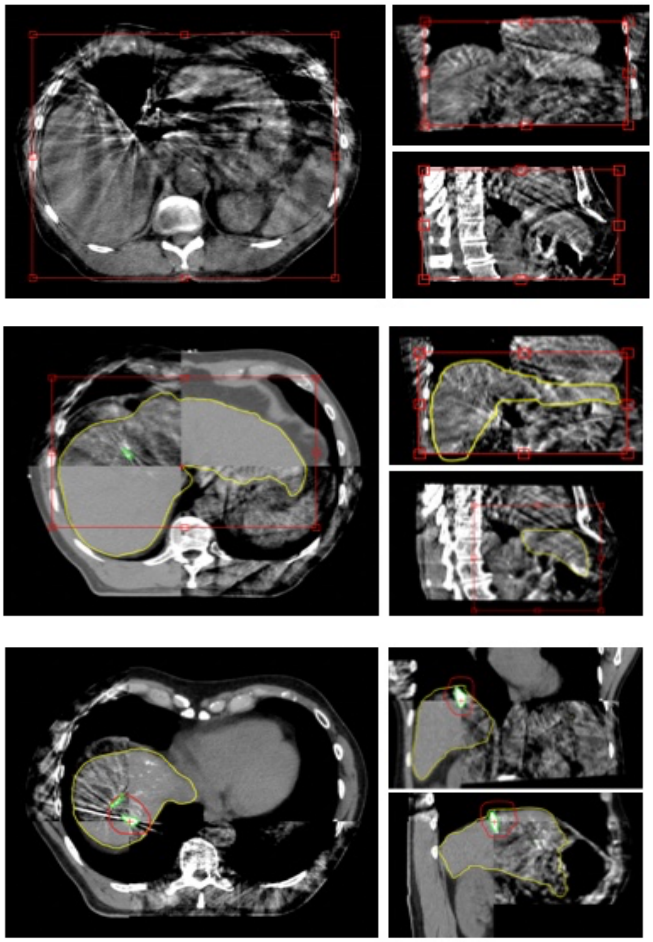

Figure 4: Offline matching between AVE-IP and CBCT image. A) Vertebral matching with grayscale, B) Liver contour matching, C) RO bead matching

As a formal motion management system was not utilised during image acquisition for the 4D-CT scans and CBCT, matching of RO beads was also assessed using a second method. Although liver position may vary between the 4D-CT and CBCT scans, the difference between each RO bead contour relative to the other should be comparable (geometric position without matching) if the same area of beads is contoured on each imaging modality (Figure 5). Therefore, the co-ordinates of the CoM for each fiducial was recorded for the CBCT and the distance between each fiducial CoM calculated. This was repeated for the AVE-IP scan, and distances compared. This approach aimed to negate the effect of motion, and the difference in the liver position between the two scans.

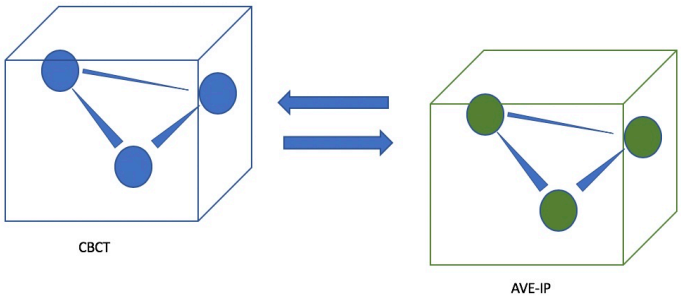

Figure 5: Geometrical positioning between cone beam CT and AVE-IP scans

7.3.1.5 Position of RO beads after placement.

In order to compare RO bead position over a period of time, the bead position on 4D-CT was compared to bead position on diagnostic CT imaging 6-20 days later. The AVE-IP and CT50 scans for each patient were matched to the diagnostic CT scan using an in-house rigid registration method. In brief, the RO beads were contoured on MATLAB® using automatic thresholding set to 2 SD above the mean liver region (HU). Segmentation was then refined with a local threshold (2 SD of background above the mean) limited to the 5 mm region around the vasculature and small connected components were filtered out to produce final segmentations of the embolised vasculature. Surface meshes were generated for each segmentation and nodes of these surfaces registered to each other using the globally-optimal iterative closest point algorithm [25]. This process was performed by Henry Tregidgo. Research Associate in Advanced Liver Imaging.

7.3.2 RO beads in a phantom model

As patients did not undergo treatment with SBRT as part of the VEROnA trial, the only radiotherapy images acquired were the 4D-CT and CBCT for each patient. In order to obtain further imaging details on the RO beads for use in radiotherapy, an in-house phantom was created for further evaluation.

7.3.2.1 RO bead phantom model creation

A simple phantom was created by filling a 2-litre plastic box with 2.5% liquid agar. The 2.5% agar provided a background HU range closest to that of liver on CT imaging [26]. A 4 cm circular sponge was placed into the middle of the liquid agar to create a structure that could represent tumour vasculature and retain the RO beads. The circular sponge was first filled with agar in a cylindrical shell. Once solidified, this was placed into a box filled with liquid agar (Figure 6). Utilising a 22 G catheter and three-way tap to avoid bead clumping, 1 ml of the RO beads (unloaded) mixed in 9 ml of phosphate-buffered saline was injected into the sponge whilst the agar was in a semi-solid state to prevent the development of air gaps. This approach was in keeping with the clinical trial, in which 1 ml of RO beads was mixed in 9 ml of Omnipaque prior to transarterial delivery via a catheter attached to a three-way tap. The phantom was then left to cool and solidify prior to imaging (Figure 7).

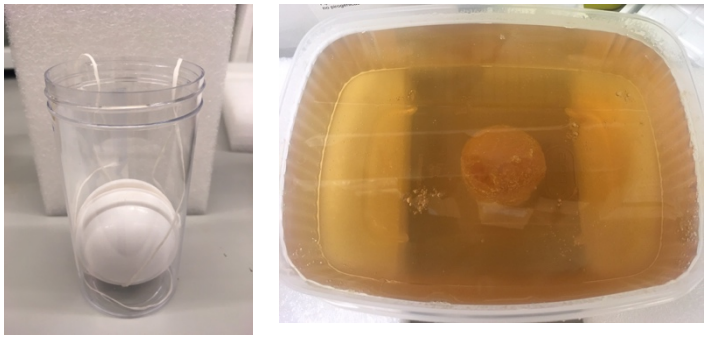

Figure 6. Creation of a radiopaque bead phantom. A: Agar filled sponge placed within a circular shell in order to create a 4 cm tumour B: 4 cm tumour placed within a box filled with liquid agar.

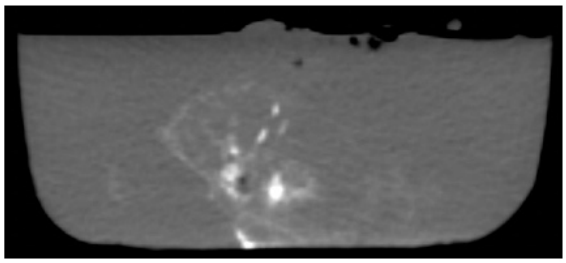

Figure 7: Helical CT image of phantom with RO beads inserted around a central sponge.

7.3.2.2 Assessment of RO beads in a phantom

Static images were first acquired to represent the RO beads in an end-exhalation phase, which included helical CT, kV, MV and CBCT scans. To replicate breathing motion, the phantom was placed onto the QUASAR™ Respiratory Motion Phantom (ModusQA, London, Ontario). This consists of two moving platforms: one platform represented internal respiratory motion in the superior-inferior (SI) directions, and the other stimulated the motion of the thoracic wall in the anterior-posterior (AP) direction. The AP motion was detected by the VARIAN RPM, and used as a surrogate for internal respiration during the non-static helical scans, 4DCT and treatment simulations (Figure 8). The QUASAR™ phantom was set to a breathing cycle of 5 seconds, with 10 mm amplitude and the following obtained: helical CT scan, 4DCT, kV, MV, and CBCT images. RO bead contouring was performed using the same method as for the clinical scans.

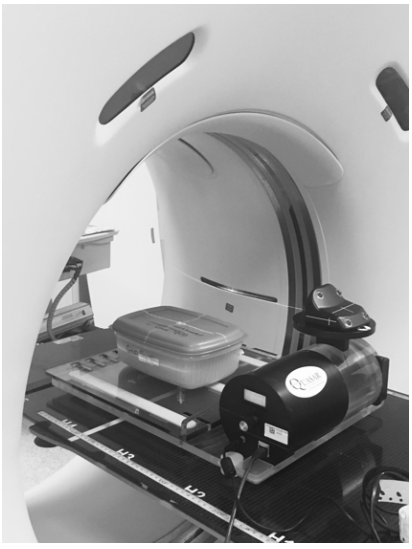

Figure 8: QUASAR™ respiratory phantom

7.4 RESULTS

7.4.1 Radiotherapy study using novel radiopaque beads in the VEROnA trial

Eight patients were successfully treated with BTG-002814 as part of the VEROnA study, as outlined in full detail in Chapter 2 (Section 2.4). 4D-CT and CBCT scans were acquired for all eight patients the day following treatment. For one patient, the primary series was selected as the MIP as opposed to the AVE-IP, which subsequently excluded this patient from the matching analysis. Patient, tumour and treatment details are outlined in Table 1.

Table 1: Baseline tumour, treatment and liver motion details

Patient	Diagnosis	Number of lesions treated	Size of treated lesion (mm)	Liver segment	Volume of BTG-002814 delivered (mL)	Liver motion (mm)*
1	HCC	1	33	VIII	1	11
2	HCC	1	82	VII	1	12
3	mCRC	1	21	VII	1	14
4	mCRC	1	8	II/IVa	1	9
5	mCRC	1	12	VII	1	22
6	mCRC	1	40	V	0.4	14
7	mCRC	1	24	V	0.9	15
8	mCRC	3	42 + 29 +16	IV	1	12

*Liver motion during imaging is measured in the cranio-caudal direction based on the mid-dome of the liver on coronal slices of the 4D-CT images.

7.4.1.1 Creation of fiducials from areas of RO beads

RO beads were visible for all patients on 4D-CT and CBCT imaging. Areas of RO beads were successfully contoured for all patients at 150 and 200 HU on 4D-CT and CBCT; below a threshold of 150 HU, areas of artefact were contoured by the automated thresholding. For two patients, areas of RO beads on the CBCT were unable to be separated into discrete areas due to the distribution of the beads. In these cases, the whole area was contoured for matching purposes. Median number of contoured RO bead areas on the CBCT at 150 HU was 3 (range 1-4), and 1.5 (range 0-4) at 200 HU. For the AVE-IP images, median number of

contoured RO bead areas at 150 HU was 3 (range 0-7), and at 200 HU 1.5 (range 0-4) (Table 2).

Table 2: Contoured RO bead areas on CBCT and AVE-IP images

	Patient number							
	1	2	3	4	5	6	7	8
CBCT 150 HU								
Number of areas	3	3	1	3	1*	3	1*	4
Total volume (cm^3)	1.9	0.2	0.2	1.6		0.8		
Volume of each area (cm^3)	1.7 0.1 0.1	0.1 0.1 0.1		0.8 0.1 0.7		0.1 0.2 0.5		1.1 3.1 0.5 0.1
CBCT 200 HU								
Number of areas	1	0	0	2	1	2	4	3
Total volume (cm^3)	1.45			0.5	0.5	0.1	0.7	2.0
Volume of each area (cm^3)	1.45			0.3 0.2		0.1	0.1 0.1 0.4 0.1	0.4 1.4 0.2
AVE-IP 150								
Number of areas	5	7	3	3	1*	3	5	3
Total volume (cm^3)	2.4	0.9	0.5	2.3		2.7	1.5	1.0
Volume of each area (cm^3)	3.0 0.13 0.1 0.13 0.1	0.1 0.1 0.1 0.3 0.1 0.1 0.1	0.2 0.1 0.2	1.2 0.2 0.9		0.2 1.4 1.1	0.1 0.7 0.1 0.5 0.1	0.1 0.8 0.1
AVE-IP 200								
Number of areas	1	1	0	3	4	2	2	1
Total volume (cm^3)	1.6	0.1		0.8	0.8	0.4	0.5	0.8
Volume of each area (cm^3)	1.6	0.1		0.5 0.1 0.2	0.1 0.3 0.1 0.3	0.3 0.1	0.4 0.1	0.8

*For patients 5 and 7 only one area of RO bead is contoured due to an inability to separate the RO beads into discrete areas.

7.4.1.2 Matching of RO beads

Matching CBCT to 4D-CT AVE-IP images using areas of contoured RO beads was successful in all patients (Figure 9). Due to the number of fiducials contoured for each patient using a threshold of 150 HU on CBCT and 4D-CT, these contours were used for final matching analysis. Although streak artefacts were observed in most of the CBCT images, this did not impact RO bead visibility or matching. Matching was performed using six degrees of freedom. The difference in couch shifts between RO beads and bony anatomy (vertebral bodies) and RO beads and liver edge ranged from 1.9-4.0 mm (Table 3).

Table 3: Couch shifts from fiducials for bony and liver edge matching

	Bony match		**Liver Edge**	
	Absolute Mean shift	**SD**	**Absolute Mean shift**	**SD**
Mediolateral (mm)	1.9	1.2	2.0	0.8
Anteroposterior (mm)	3.8	3.3	3.3	2.0
Craniocaudal (mm)	3.2	2.7	4.0	3.3
Pitch^0	1.24	1.55	1.67	1.65
Roll^0	2.63	2.92	2.61	2.76
Rotation^0	2.59	1.60	2.36	1.21

After matching on RO beads, the absolute mean change in CoM from CBCT to AVE-IP was 2.0 mm (SD 1.1) ML, 1.7 mm (SD 1.3) AP, and 3.5 mm (SD 2.4) in the CC direction (Table 4). Figure 9 shows the final matching of AVE-IP to CBCT, and MIP to CBCT for all patients.

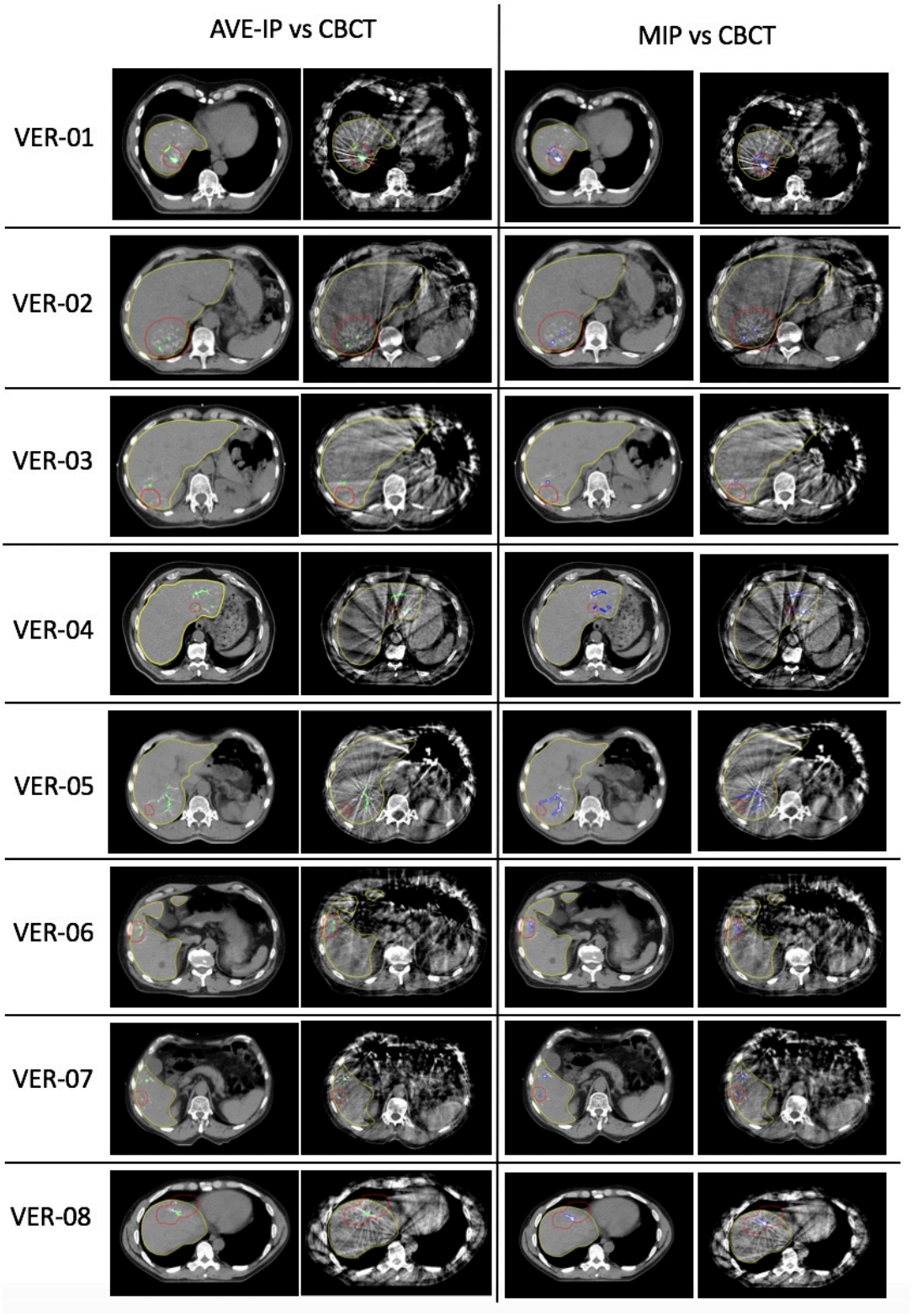

Figure 9: Matching of RO beads on AVE-IP, MIP and CBCT. Code: Red, planning target volume; Yellow, liver contour; Green, RO beads contoured on AVE-IP at 150 HU and matched to CBCT; Blue, RO beads contoured on MIP at 250 HU and matched to CBCT.

Table 4: Absolute mean change in centre of mass of fiducials from CBCT to AVE-IP post matching

	1	2	3	5	6	7	8	Absolute Mean (SD)
Change in volume (cm^3)	0.10	0.10	0.00	0.3	0.67	0.3	1.20	0. 34 (0.41)
Mediolateral (mm)	2.7	0.3	1.1	2.8	2.8	0.9	3.4	2.0 (1.1)
Anteroposterior, (mm)	1.2	0.4	0.8	2.6	0.8	2.0	4.3	1.7 (1.3)
Craniocaudal, (mm)	1.5	2.5	0.00	7.3	5.5	5.3	2.5	3.5 (2.4)

On assessment of the change in distance between fiducials relative to each other between CBCT and AVE-IP scans, mean change was 3.9 mm (SD 2.8) ML, 1.8 mm (SD 0.4) AP direction, and 3.5 mm (SD 1.7) in the CC directions (Table 5).

Table 5: Absolute change in distance between centre of mass of fiducials between CBCT and AVE-IP scans

	1	2	6	7	8	Absolute mean (SD)
Mediolateral (mm)	3.0	1.8	3.6	2.5	8.8	3.9 (2.8)
Anteroposterior (mm)	2.1	2.1	1.3	1.4	1.9	1.8 (0.4)
Craniocaudal (mm)	2.5	1,4	5.9	3.6	3.9	3.5 (1.7)

Notes: As only one fiducial area was contoured for patients 3 and 5 these patients do not have results.

7.4.1.3 Stability of RO bead position

RO bead position was compared between the AVE-IP and CT-50 images to the position on the visit 4 CT scans taken at a median 12.5 days (range 6-29 days) post-TACE with BTG-002814. Comparison of bead position on 4D-CT scans with post-TACE CT scans showed good alignment of beads along tumour vasculature up to 29 days later (Figure 10).

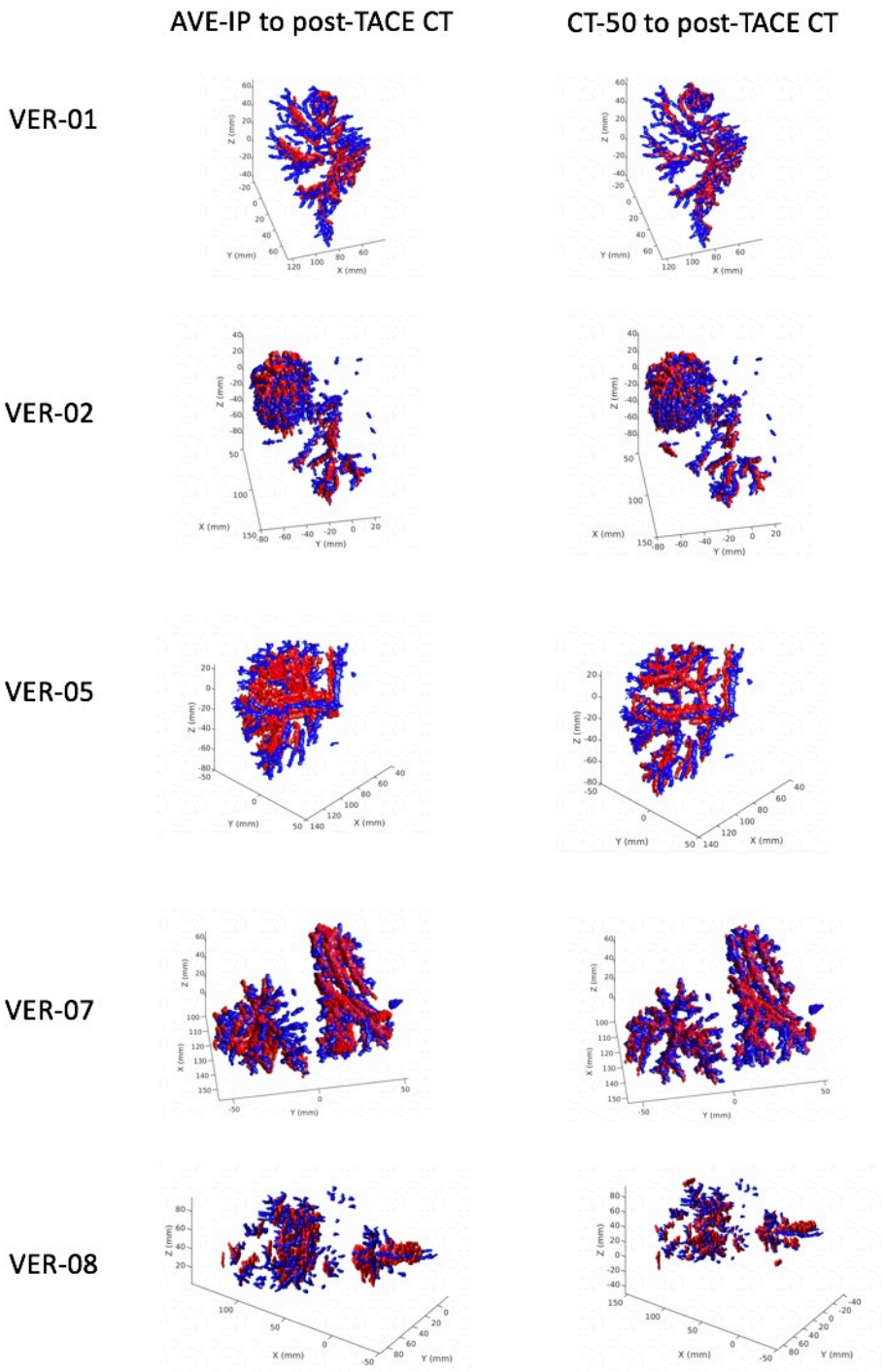

Figure 10. Comparison of bead position between 4D-CT images taken 1 day after treatment and CT scans taken 6-29 days post-TACE. AVE-IP and CT-50 scans are registered to the visit 4 CT scan using a Go-ICP algorithm. Red areas are the beads contoured on the 4D-CT scans (AVE-IP and CT50) and blue areas are the beads contoured on the visit 4 CT scans.

7.4.2 Part 2: Results from the phantom model

RO beads were visible on all imaging modalities in both the static and moving phantom (Figure 11). Using automated threshold contouring at 150 HU, five discrete areas of RO beads with a mean volume of 0.12 cm^3 were contoured on the CBCT images and three, with a mean volume of 0.1 cm^3, on the AVE-IP images.

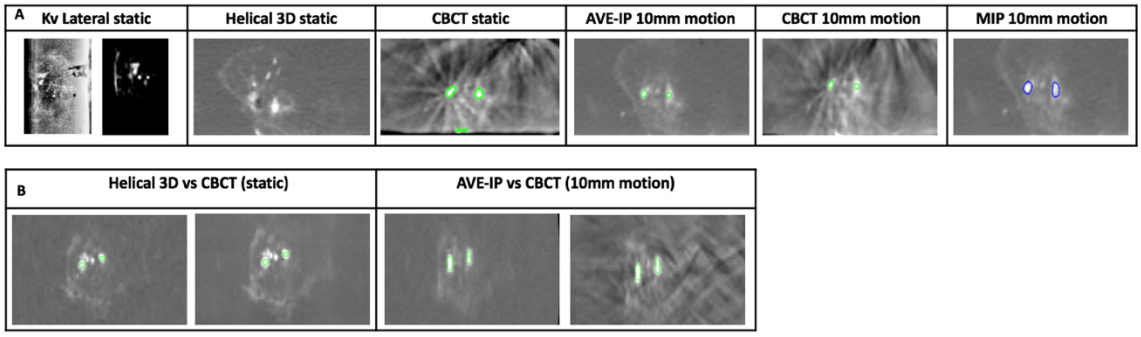

Figure 11: Radiopaque beads in phantom model. A: Comparison of RO beads visibility on different imaging modalities. B: Change in shape of RO beads between static and motion images.

Absolute mean difference in CoM between areas of RO beads on static CBCT and AVE-IP images were 0.5 mm (SD 0.2) ML, 0.4 mm (SD 0.2) AP and 0.6 mm (SD 0.6) in the CC direction. When 10 mm of cranio-caudal motion was applied, translational errors were 7.4 mm (SD 1.7), 5.6 mm (SD 0.8) and 5.1 mm (SD 3.3) in the ML, AP and CC directions (Table 6).

Table 6. Absolute translational shifts in centre of mass between CBCT and AVE-IP scan

	Fid 1	Fid 2	Fid 3	Mean (SD)
Static phantom				
Mediolateral, z (mm)	0.5	0.2	0.8	0.5 (0.2)
Anteroposterior, y(mm)	0.7	0.5	0.1	0.4 (0.2)
Craniocaudal, z(mm)	0.2	0.2	1.55	0.6 (0.6)
Phantom with 10 mm motion				
Mediolateral, z (mm)	6.3	6.6	9.3	7.4 (1.7)
Anteroposterior, y(mm)	6.4	5.5	4.9	5.6 (0.8)
Craniocaudal, z(mm)	3.0	3.5	9.0	5.1 (3.3)

7.5 DISCUSSION

Drug-eluting beads are an effective combined anti-cancer drug and embolisation treatment delivered directly to liver tumours during TACE treatment. The development of a novel RO bead, with durable radiopacity on CT scans, optimises the delivery technique by providing confirmation of bead location during and after the embolisation procedure [23, 24]. With TACE combined with SBRT likely to become a therapeutic option, this study indicates that RO beads can function as potential surrogates of liver tumour targeting for IGRT.

In this study, we have demonstrated that RO beads are visible on the imaging modalities required for IGRT, including CBCT, 4D-CT, KV and MV. Furthermore, we have shown that on-treatment matching can be performed using the RO beads between radiotherapy planning and CBCT scans. Due to size of the RO beads, and their varied clumping and distribution along tumour vasculature, the shape and size of high-density regions in and around a tumour is not uniform. It is also apparent that there is a difference between the distribution of beads between HCC and mCRC tumours.

As predicted, highly selective TACE delivery is possible with hypervascular HCC tumours, whereas mCRC tumours tend to be less vascular in nature, leading to

a more lobar distribution of beads during TACE delivery. Despite this, using an automated contouring method based on HU thresholding, distinct areas of RO beads can be contoured on radiotherapy planning scans and accurately matched to areas of RO beads on CBCT imaging for both types of liver tumours. Without any formal motion mitigation, matching on CoM of contoured areas was possible within 3.5mm. It is likely that with the application of motion mitigation methods, as used in standard clinical practice, this translational shift will be reduced further.

As shown in the phantom study using static images, matching between CBCT and AVE-IP scans is possible within 0.6 mm. However, the impact of motion on the shape, and therefore CoM of an irregular shaped object is evident (Figure 11b). When utilising 4D-CT for RT planning, patient-specific internal target volumes (ITV) can be created to minimise intrafraction errors. As with tumour contouring, in which the ITV is created by combining tumour volumes from all respiratory phases, this approach can also be applied to the RO beads, and a 'fiducial ITV' created that can be utilised for matching. The ability to match on CBCT, whether this is with an end-expiration phase, or AVE-IP, shows that RO beads can function as a surrogate for liver position in these approaches.

Although artefact streaking was present on CBCT, this did not impact RO bead visibility or the ability to match. Artefact streaking is a particular problem with commercial fiducials that can distort tumour contouring [21]. Although artefact was present, when visually compared, it was comparable to that produced by commercially available fiducials (Figure 12). Furthermore, artefact did not distort the ability to visualise or contour the tumour and for HCC patients, in which RO beads were located within the tumour vasculature, tumour contouring was felt to be enhanced.

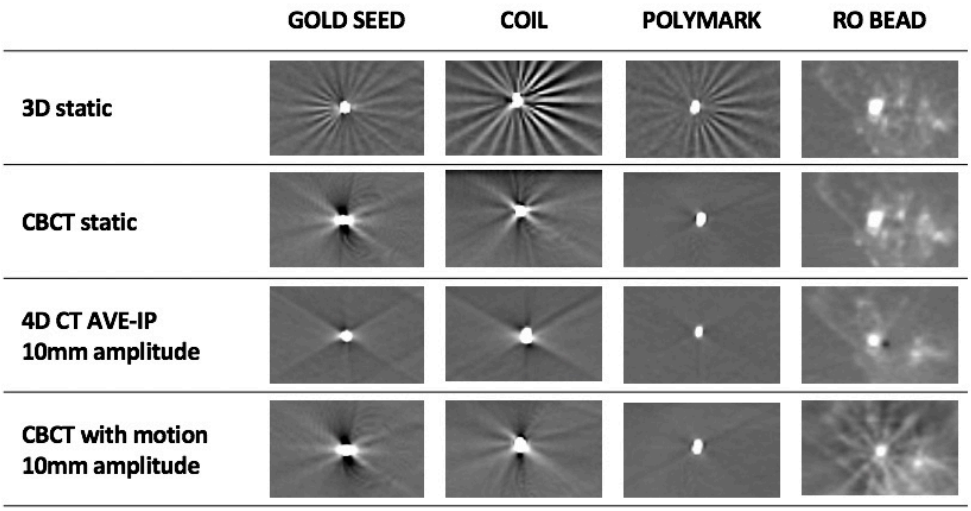

Figure 12: A comparison between RO beads and three commercial fiducial markers. Three commercial CIVCO™ fiducial markers were inserted into an identical phantom and IGRT images acquired.

When RO bead matching was compared to matching based on liver edge or bony structures, difference in translational shifts up to 4.0 mm were seen (Table 3). These findings suggest that bony anatomy and liver edge may be sub-optimal surrogates for tumour positioning in imaged guided RT. This is in keeping with the findings by Yue *et al*, where on comparison of matching on lipiodol and bony anatomy, difference in three-dimensional distances were 0.9-2.6 mm (maximum 3.8 mm) in the ML direction, 1.1-2.9 mm (maximum 4.3 mm) in the AP direction, and 1.2- 3.9 mm (maximum 5.5 mm) in the in the CC direction [19].

In this study, we have demonstrated that RO beads also show stability in position over time. On comparison of RO bead position immediately following insertion and 7-21 days later, bead position was stable. There is a necessary time delay between radiotherapy planning scans and treatment, and for RO beads to function as surrogates of tumour position, their position needs to remain stable during this time period, which can be up to 2 weeks. By showing that the RO beads are feasible as fiducial markers, this limits the necessity for the additional invasive procedures required for fiducial insertion.

There are limitations to this study and in the potential use of RO beads as fiducial markers. Firstly, this was a first-in-human clinical trial and, as such, our patient

numbers are small and include just two patients with HCC. Furthermore, as patients did not undergo SBRT in this proof-of-principle study, radiotherapy imaging was limited to 4D-CT scans and CBCT images, and patients did not have any motion mitigation. As shown with the phantom model, translational errors and matching accuracy is improved with reduced motion. We also used an automated contouring method to contour RO beads. Although this approach was taken to reduce variation in contouring, this may not be available on all radiotherapy planning systems. However, areas of beads can be contoured manually without this approach. The development of advanced radiotherapy techniques that can enable adaptive RT planning may also offer their own thresholding solutions. In this study, we only evaluated an approach that would clinically be consistent with motion mitigation (for example with abdominal compression). With the phantom model we did initially aim to assess triggered imaging and auto-beam hold (Varian TrueBeam) but due to the non-uniform shape and size of the RO bead areas this was not feasible. Further analysis of the beads in clinical trials may enable further input data that could enable this approach in the future, and furthermore explore the thresholding of beads on adaptive planning systems.

The use of RO beads as fiducials may also increase the complexity of RT planning and treatment delivery. Experience in contouring and matching on small areas of high intensity may take additional time. A final limitation of this study was that it did not specifically look at the impact of RO beads on dosimetry. Given the small volume of the high-density regions, it is anticipated that this will be negligible, but further evaluation would be required in a larger clinical study.

7.6 CONCLUSION

In conclusion, this study has shown that RO beads are visible on IGRT imaging modalities required for liver SBRT, show minimal artefact, can be reliably contoured, can be used for on-set matching with CBCT, and remain stable positionally within the liver vasculature. As such, their role as fiducial markers is feasible and warrants further exploration in combination studies of TACE followed by SBRT for liver tumours.

7.7 REFERENCES

[1] Sanuki N, Takeda A, Oku Y, Mizuno T, Aoki Y, Eriguchi T, et al. Stereotactic body radiotherapy for small hepatocellular carcinoma: a retrospective outcome analysis in 185 patients. Acta Oncol. 2014;53:399-404.

[2] Cardenes HR, Price TR, Perkins SM, Maluccio M, Kwo P, Breen TE, et al. Phase I feasibility trial of stereotactic body radiation therapy for primary hepatocellular carcinoma. Clinical & translational oncology : official publication of the Federation of Spanish Oncology Societies and of the National Cancer Institute of Mexico. 2010;12:218-25.

[3] Huertas A, Baumann AS, Saunier-Kubs F, Salleron J, Oldrini G, Croise-Laurent V, et al. Stereotactic body radiation therapy as an ablative treatment for inoperable hepatocellular carcinoma. Radiother Oncol. 2015;115:211-6.

[4] Yamashita H, Onishi H, Murakami N, Matsumoto Y, Matsuo Y, Nomiya T, et al. Survival outcomes after stereotactic body radiotherapy for 79 Japanese patients with hepatocellular carcinoma. J Radiat Res. 2015;56:561-7.

[5] Tse RV, Hawkins M, Lockwood G, Kim JJ, Cummings B, Knox J, et al. Phase I study of individualized stereotactic body radiotherapy for hepatocellular carcinoma and intrahepatic cholangiocarcinoma. J Clin Oncol. 2008;26:657-64.

[6] Andolino DL, Johnson CS, Maluccio M, Kwo P, Tector AJ, Zook J, et al. Stereotactic Body Radiotherapy for Primary Hepatocellular Carcinoma. International Journal of Radiation Oncology*Biology*Physics. 2011;81:e447-e53.

[7] Bujold A, Massey CA, Kim JJ, Brierley J, Cho C, Wong RK, et al. Sequential phase I and II trials of stereotactic body radiotherapy for locally advanced hepatocellular carcinoma. J Clin Oncol. 2013;31:1631-9.

[8] Wahl DR, Stenmark MH, Tao Y, Pollom EL, Caoili EM, Lawrence TS, et al. Outcomes After Stereotactic Body Radiotherapy or Radiofrequency Ablation for Hepatocellular Carcinoma. J Clin Oncol. 2016;34:452-9.

[9] Yeung R, Beaton L, Rackley T, Weber B, Hamm J, Lee R, et al. Stereotactic Body Radiotherapy for Small Unresectable Hepatocellular Carcinomas. Clinical Oncology.

[10] Petrelli F, Comito T, Barni S, Pancera G, Scorsetti M, Ghidini A, et al. Stereotactic body radiotherapy for colorectal cancer liver metastases: A systematic review. Radiother Oncol. 2018;129:427-34.

[11] Hoyer M, Swaminath A, Bydder S, Lock M, Mendez Romero A, Kavanagh B, et al. Radiotherapy for liver metastases: a review of evidence. Int J Radiat Oncol Biol Phys. 2012;82:1047-57.
[12] Jacob R, Turley F, Redden DT, Saddekni S, Aal AK, Keene K, et al. Adjuvant stereotactic body radiotherapy following transarterial chemoembolization in patients with non-resectable hepatocellular carcinoma tumours of >/= 3 cm. HPB (Oxford). 2015;17:140-9.
[13] Kang JK, Kim MS, Cho CK, Yang KM, Yoo HJ, Kim JH, et al. Stereotactic body radiation therapy for inoperable hepatocellular carcinoma as a local salvage treatment after incomplete transarterial chemoembolization. Cancer. 2012;118:5424-31.
[14] Paik EK, Kim MS, Jang WI, Seo YS, Cho CK, Yoo HJ, et al. Benefits of stereotactic ablative radiotherapy combined with incomplete transcatheter arterial chemoembolization in hepatocellular carcinoma. Radiation oncology (London, England). 2016;11:22.
[15] Shim SJ, Seong J, Han KH, Chon CY, Suh CO, Lee JT. Local radiotherapy as a complement to incomplete transcatheter arterial chemoembolization in locally advanced hepatocellular carcinoma. Liver Int. 2005;25:1189-96.
[16] ClinicalTrials.gov. SBRT or TACE for Advanced HCC.
[17] Seppenwoolde Y, Wunderink W, Wunderink-van Veen SR, Storchi P, Mendez Romero A, Heijmen BJ. Treatment precision of image-guided liver SBRT using implanted fiducial markers depends on marker-tumour distance. Phys Med Biol. 2011;56:5445-68.
[18] Valentine K, Cabrera T, Roberge D. Implanting metal fiducials to guide stereotactic liver radiation: McGill experience and review of current devices, techniques and complications. Technol Cancer Res Treat. 2014;13:253-8.
[19] Yue J, Sun X, Cai J, Yin FF, Yin Y, Zhu J, et al. Lipiodol: a potential direct surrogate for cone-beam computed tomography image guidance in radiotherapy of liver tumor. Int J Radiat Oncol Biol Phys. 2012;82:834-41.
[20] Chan MK, Lee V, Chiang CL, Lee FA, Law G, Sin NY, et al. Lipiodol versus diaphragm in 4D-CBCT-guided stereotactic radiotherapy of hepatocellular carcinomas. Strahlenther Onkol. 2016;192:92-101.

[21] Habermehl D, Henkner K, Ecker S, Jakel O, Debus J, Combs SE. Evaluation of different fiducial markers for image-guided radiotherapy and particle therapy. J Radiat Res. 2013;54 Suppl 1:i61-8.
[22] Lewis AL, Willis SL, Dreher MR, Tang Y, Ashrafi K, Wood BJ, et al. Bench-to-clinic development of imageable drug-eluting embolization beads: finding the balance. Future Oncol. 2018;14:2741-60.
[23] Levy EB, Krishnasamy VP, Lewis AL, Willis S, Macfarlane C, Anderson V, et al. First Human Experience with Directly Image-able Iodinated Embolization Microbeads. Cardiovasc Intervent Radiol. 2016;39:1177-86.
[24] Reicher J, Mafeld S, Priona G, Reeves HL, Manas DM, Jackson R, et al. Early Experience of Trans-arterial Chemo-Embolisation for Hepatocellular Carcinoma with a Novel Radiopaque Bead. Cardiovasc Intervent Radiol. 2019;42:1563-70.
[25] Yang J, Li H, Campbell D, Jia Y. Go-ICP: A Globally Optimal Solution to 3D ICP Point-Set Registration. IEEE Trans Pattern Anal Mach Intell. 2016;38:2241-54.
[26] Zeb I, Li D, Nasir K, Katz R, Larijani VN, Budoff MJ. Computed tomography scans in the evaluation of fatty liver disease in a population based study: the multi-ethnic study of atherosclerosis. Acad Radiol. 2012;19:811-8.

8 GENERAL DISCUSSION AND FUTURE DIRECTIONS

8.1 GENERAL DISCUSSION

8.1.1 Overview

In order to improve clinical outcome for patients with unresectable primary and secondary liver cancers, local directed therapies need to be optimised. Although transarterial chemoembolisation (TACE) provides a survival advantage over best supportive care in patients with intermediate-stage HCC [1], local recurrence rates can be up to 61.8% post-treatment due to persistence of viable tumour cells [2]. For patients with liver-limited metastases from colorectal cancer (mCRC), drug-eluting bead (DEB)-TACE is also a treatment option, with an average response rate of 56.2% [3]. Given the high recurrence rates post-TACE in both HCC and mCRC, new anti-cancer drugs that can be delivered directly to the tumour on pre-loaded beads are required. As TACE enhances the production of anti-angiogenic factors such as VEGF, combining TACE with anti-angiogenic agents may provide a mechanism for improving outcomes. Furthermore, the combination of TACE with stereotactic radiotherapy (SBRT) may further improve clinical outcomes for patients with unresectable HCC.

8.1.2 Summary of thesis results

In the VEROnA clinical trial, we investigated the feasibility of delivering a novel radiopaque bead (RO) loaded with vandetanib (BTG-002814) directly into liver tumours. In this phase 0, first-in-human study, we have demonstrated that BTG-002814 has an acceptable safety profile and is feasible to deliver prior to liver resection in patients with both HCC and mCRC. In comparison, an early phase clinical trial of oral vandetanib in HCC patients reported dose-limiting toxicities of hepatic failure, diarrhoea, palmar-plantar erythrodysaesthesia syndrome and hypertension [4]. Our data therefore demonstrates that there is a much more favourable safety profile following hepatic arterial administration, as transient hypertension was the only Grade 3 adverse event reported following treatment with BTG-002814 prior to surgery.

Although this study was not set up as a formal pharmacokinetic study, we have shown that the systemic concentrations of vandetanib are far lower following intra-arterial delivery when compared to oral dosing, which explains the well tolerated side effect profile. In our study the peak concentration of vandetanib was evident two hours post-treatment, with a mean C_{max} of 24.3 ng/ml demonstrating a low burst release of vandetanib in the first few hours following administration. However, as discussed in Chapter 3, the concentrations seen in the plasma represent around 0.12% of the loaded drug. As anticipated, following local delivery minimal free drug enters the systemic circulation.

As a co-primary endpoint of the study, we demonstrate that vandetanib and its metabolite, N-desmethyl vandetanib, were measurable in the resected liver tissue up to 32 days post-treatment, demonstrating sustained release from the loaded beads and metabolism within both the tumour and normal liver. This slow and sustained release system is particularly beneficial given the adverse effects of vandetanib when delivered orally. Furthermore, the concentration of vandetanib found in the liver tumours ranged from 441 ng/g to 404,000 ng/g, equating to 0.928-850 μM, which is higher than the IC50 of vandetanib for VEGF from in-vitro studies [5]. This study therefore provides evidence that therapeutic levels of vandetanib are maintained in the liver over a median period of 14 days, and up to 32 days post-TACE. An inevitable consequence of TACE is the de novo formation of hypoxic regions within a tumour. The sustained delivery of vandetanib to these hypoxic areas may therefore be more efficacious and combat the emergence of hypoxic resistant clones that can develop after conventional TACE [6].

In terms of improving the delivery and targeting of TACE, there is a clear need to correlate bead location and tumour response. The novel design of this study allowed the assessment of radiopaque bead location on CT scans to be correlated with surgical resection specimens and allow an accurate calculation of ‘on-target’ and ‘off-target’ bead delivery. Despite a relatively low percentage of ‘on-target’ bead delivery in mCRC patients, necrosis levels of 90-100% were still evident. This suggests that it is not just bead delivery directly to the tumour that impacts tumour response but also bead delivery to the area surrounding the

tumour. Although TACE involves deposition of beads into the vessels feeding the tumour, direct access into the tumour can vary depending on the size of the tumour and underlying tumour vascularity. In the cases in which 'on-target' bead delivery was low, beads may have still been deposited in key feeding vessels in the area surrounding the tumour, thus still leading to significant ischaemia. Furthermore, despite low 'on-target' delivery, vandetanib concentrations within the tumour were therapeutic. The mechanism of action of BTG-002814 has yet to be fully elucidated and may be multi-factorial: the effect may be due to the embolisation effect, the local vandetanib effect or a combination of the two mechanisms [7].

In this trial, we analysed 39 key cytokines in order to explore overall trends in biomarker response to BTG-002814. Most pronounced changes from baseline to post-TACE were evident in leptin, osteopontin and sTie, which are likely to reflect the local inflammatory process post-TACE. Although VEGF was seen to rise post-TACE in three out of the five patients with recordable levels, for three patients, VEGF was unrecordable at all visits from baseline to visit 4. However, as anticipated, a decrease in soluble VEGF receptor 2 (sVEGFR-2) was not seen post-TACE. Increases in VEGF and decreases in sVEGFR-2 have been reported in early phase studies of VEGFR tyrosine kinase inhibitors (TKIs) [4, 8], whilst serum VEGF levels have been reported to peak 14 days post-TACE in HCC patients, with ineffective TACE cases showing higher serum VEGF levels on day 14 compared to effective cases [9]. As such, further studies are required in larger HCC and mCRC cohorts after treatment with BTG-002814.

As exploratory endpoints, we utilised two modalities to assess changes in perfusion following treatment with BTG-002814; perfusion computed tomography (pCT) and dynamic contrast-enhanced magnetic resonance imaging (DCE-MRI). Both CT and MRI are widely used in routine oncologic imaging, and functional studies can be incorporated relatively easily with routine examinations. Although CT and MRI techniques can provide qualitative and quantitative assessments of tumour vascularity, quantification by DCE-MRI is technically more challenging due to the lack of a direct relationship between MRI signal intensity and contrast agent concentration. However, a downside to

pCT imaging is that it does increase radiation exposure. Both pCT and DCE-MRI imaging have been utilised in clinical trials of TACE and vandetanib, but to date no trial has compared the function of both modalities. Although we did not see a significant change in any of the parameters examined, we have shown that the incorporation of perfusion imaging into an early-stage clinical trial of an anti-angiogenic medical device is feasible. Incorporating these endpoints into subsequent phases of trial development should therefore be achievable. However, further work is required to improve the baseline variability in DCE-MRI parameters in liver tumours before this approach can be reliably utilised.

Although the anti-tumour efficacy of TACE was not an endpoint of this study, the degree of tumour necrosis seen in our cohort is impressive, with a median necrosis of 90%. Information on the pathological response to TACE is limited, yet as discussed in chapter 4, our response rates are comparable with recent studies [7, 10] despite each patient receiving the same dose regardless of tumour size. Based on our phase 0 data, phase I-II studies of BTG-002814 appear to be warranted to explore this further.

In Chapter 6, we demonstrate that SBRT offers 1-year local control (LC) rates of 94% for small HCC tumours (<5 cm), and 1-year LC rates of 92% for patients with larger HCC tumours. The results from these two studies further demonstrate that SBRT can be used safely in patients that have previously received TACE. Although these studies are small and based at a single institution, the results are in keeping with other key trials showing that SBRT can provide LC rates of 87–100% at 1-year, especially for tumours <3 cm [11-13].

In Chapter 7, we demonstrate that the RO beads used in TACE are visible on the modalities for IGRT and show that matching between CBCT and AVE-IP scans was feasible in all clinical cases. Changes in centre of mass of RO beads between CBCT and radiotherapy planning scans was 1.7-3.5 mm. As such, their role as fiducial markers is feasible and warrants further exploration in SBRT studies.

8.2 FUTURE DIRECTIONS

8.2.1 TACE with vandetanib-eluting beads (BTG-002814)

Although TACE has traditionally been performed with cytotoxic agents, since the approval of sorafenib for advanced HCC, small molecule multi-TKIs have gained particular attention. The loading of LC Beads with sorafenib has been investigated but early studies did not show efficacy in HCC cell lines [14]. Loading of sunitinib into DC Beads™ has also been investigated, as has the correlation of in vitro release with in vivo pharmacokinetics along with the antitumor effects in a rabbit VX2 embolisation model [15-17]. Although these studies have shown promise and demonstrate feasibility for locoregional delivery, the toxicity seen with oral sunitinib has led to the search for alternative agents in HCC [18, 19].

The recommended size of beads for standard DEB-TACE is 100-300 μm based on the fact that small particles can be transported inside the tumour or close to the tumour margin leading to a more distal embolisation and obstruction of collateral vessels [20]. These smaller beads (100-300 μm) have been shown to be associated with significantly higher survival rates and lower complications than TACE with beads measuring >300 μm [21]. In the VEROnA study, we demonstrate that RO beads measuring 60-160 μm are safe, able to penetrate into tumours, and cause necrosis as a result of being deposited near to the tumour. Given the feasibility and minimal side effect profile of intra-arterial delivery of vandetanib loaded-beads, it seems rational to move forwards with this drug and bead size combination into a phase I study.

In the VEROnA study, a maximum dose of 100 mg of vandetanib was delivered to all patients regardless of tumour size. However, in DEB-TACE with doxorubicin, the extent of liver cancer burden is taken in account when planning the dose delivered [22]. A dose escalation study is therefore required in order to determine the maximum tolerated dose of intra-arterial vandetanib. In a model-based escalation study, tolerance of escalating doses of vandetanib could be assessed in pairs of patients at separate dose levels and sub-stratified according to tumour burden. Given our experience from the VEROnA trial, it would be feasible to incorporate pCT imaging into this early phase trial in addition to our

novel bead algorithm in order to correlate RO bead location with change in perfusion parameters and radiological response. With regards to further cytokine exploration, given the mechanism of action of vandetanib, it would be of particular interest to see if changes in sVEGFR-2, VEGF and EGF and EGFR varied depending on the dose of vandetanib delivered. Following this dose-escalation trial, a phase II study to determine efficacy would be required. The novel radiopacity of the beads would also enable undertreated parts of tumours to be targeted in a second TACE procedure.

8.2.2 TACE in combination with SBRT

With the safety and efficacy of SBRT now well established in patients with well-compensated liver disease, one of the unanswered questions regarding SBRT for HCC remains how to optimally incorporate this modality into the larger schema of treatment options. Although TACE is the standard treatment in intermediate-stage patients it is not a truly “ablative” treatment. As such, SBRT is an appealing adjuvant therapy in this population [23].

A meta-analysis has shown that TACE plus radiotherapy is associated with superior LC and disease-free survival compared to TACE alone, although radiation in most of the included studies in this analysis predates use of SBRT [24]. More recently, evidence has emerged to support the role for SBRT in the adjuvant and salvage setting [25-27]. A phase II study examined the combination of TACE and SBRT for single HCC ≤4 cm in treatment naive patients and reported a 3-year LC rate of 96.3%. However, TACE was only performed in 64% of patients, and TACE involved treatment with lipiodol plus doxorubicin or cisplatin as opposed to DEB-TACE.

A recent retrospective study of 103 patients using DEB-TACE (doxorubicin) has shown that the combination of DEB-TACE followed by SBRT for HCC achieved overall response rates of 88.43% using mRECIST with LC rates of 91% and 89% at one and two-years. While the population in this study was heterogeneous, 70.2% were BCLC B or C and over half of the patients had tumours greater than ≥3 cm. These results therefore compare favourably with the overall response rates for DEB-TACE alone in this population which range from 51–73% [28-30].

As stated by the authors, what is more encouraging is the complete response of 62.1% in this series compared to the 5–26.8% reported with DEB-TACE alone [23].

Studies of TACE and SBRT have so far been retrospective or early phase in nature but there is now a phase III randomised control study currently recruiting that is comparing the efficacy of TACE vs TACE combined with SBRT as a primary treatment for unresectable HCC (NCT03338647) [31]. The results of this study are therefore eagerly anticipated.

Although further efficacy data on vandetanib-loaded beads is required, RO beads are already commercially available in the United States (as LC Bead LUMI™) for the treatment of hypervascular tumours. In Canada, Europe, Australia, South Korea, Taiwan, Hong Kong, Brazil, Mexico and Argentina, DC Bead LUMI™ is approved for the treatment of HCC in combination with doxorubicin. Preliminary experience on DC Bead LUMI™ for HCC has already been published and has shown that this approach is well tolerated with minimal side-effects [32].

As DEB-TACE with doxorubicin is frequently used for HCC, this creates the opportunity for a number of future clinical trials, namely the combination of DC Bead LUMI™ TACE with SBRT, and the combination of BTG-002814 with SBRT. On the basis of the results from a retrospective study of DEB-TACE and SBRT, in which a statistically improved overall response of planned DEB-TACE and SBRT was seen when compared to salvage SBRT, it would seem reasonable to investigate the role of SBRT immediately following DEB-TACE. It is likely that there is a synergistic effect by performing these two treatments together [23]. The main cohort of patients that are likely to benefit from this combination approach are the patients with unresectable HCC tumour measuring >3 cm, in which TACE and RFA are found to be less effective [33]. Furthermore, by utilising radiopaque beads, SBRT could be utilised to deliver an integrated boost to areas that might need a higher radiation dose to overcome inadequate bead delivery.

By combining SBRT with RO bead TACE (BTG-002814 or DC Bead LUMI™), the role of RO beads as fiducial markers in the clinical setting could also be further investigated. This would enable the creation of fiducial internal target volumes

(ITV) based on RO bead position, whilst imaging with CBCT pre- and post-SBRT would enable intra- and inter-fraction errors to be calculated. However, in view of the auto-contouring method used in our study, further phantom pre-planning studies would be required to ensure that the RO beads could be contoured if this study was to be performed at sites that did not have auto-contouring on their planning system.

8.2.3 SBRT and novel immunotherapy drugs

Although not a focus of this thesis, it would be amiss to not mention that future treatment algorithms for liver tumours are likely to combine liver directed-therapies, such as SBRT, with newly emerging immunotherapy drugs. As discussed in Chapter 7, the combination of SBRT with sorafenib is already being explored in the RTOG 1112 trial [34]. However, novel emerging immunotherapy drugs, with particular reference to PD-L1 inhibitors, have already demonstrated exciting new treatment options for patients with HCC. As outlined in Chapter 1, the recently reported IMbrave150 trial has shown a promising role for the combination of Bevacizumab with Atezolizumab, a PD-L1 inhibitor [35]. Furthermore, in the CheckMate 040 study, the anti-PD-1 inhibitor Nivolumab has shown substantial tumour response (15–20%) with promising duration of response favourable survival, and a manageable toxicity profile in advanced HCC patients who have previously received or were intolerant to Sorafenib [36]. In the KEYNOTE-224 study, another anti-PD-1 inhibitor Pembrolizumab has reported similar findings [37]. The combination of SBRT with Nivoloumab has already been explored in phase I clinical trials, and the combination of SBRT with immunotherapy drugs is likely to dominate the future of clinical trials in HCC patients [38].

8.3 CONCLUSIONS

In conclusion, the results from the VEROnA study have shown that vandetanib-eluting RO beads can be safely delivered to patients with liver tumours prior to surgical resection, with preliminary data from a small cohort of patients showing promising anti-tumour activity. The ability to safely deliver vandetanib locally to tumours *via* TACE is a novel approach and warrants further exploration in future clinical trials in patients with intermediate-stage HCC and non-resectable mCRC

liver metastases. Cytokines and perfusion imaging should be further investigated in larger cohorts as biomarkers of response. SBRT has been shown to be an effective local treatment for small and large HCCs and the role of RO beads as fiducial markers is feasible and warrants further exploration in clinical trials of TACE combined with SBRT.

8.4 REFERENCES

[1] Llovet JM, Bruix J. Systematic review of randomized trials for unresectable hepatocellular carcinoma: Chemoembolization improves survival. Hepatology (Baltimore, Md). 2003;37:429-42.

[2] Kinugasa H, Nouso K, Takeuchi Y, Yasunaka T, Onishi H, Nakamura S, et al. Risk factors for recurrence after transarterial chemoembolization for early-stage hepatocellular carcinoma. J Gastroenterol. 2012;47:421-6.

[3] Akinwande O, Dendy M, Ludwig JM, Kim HS. Hepatic intra-arterial injection of irinotecan drug eluting beads (DEBIRI) for patients with unresectable colorectal liver metastases: A systematic review. Surg Oncol. 2017;26:268-75.

[4] Hsu C, Yang TS, Huo TI, Hsieh RK, Yu CW, Hwang WS, et al. Vandetanib in patients with inoperable hepatocellular carcinoma: a phase II, randomized, double-blind, placebo-controlled study. Journal of hepatology. 2012;56:1097-103.

[5] Ryan AJ, Wedge SR. ZD6474--a novel inhibitor of VEGFR and EGFR tyrosine kinase activity. Br J Cancer. 2005;92 Suppl 1:S6-13.

[6] Bowyer C, Lewis AL, Lloyd AW, Phillips GJ, Macfarlane WM. Hypoxia as a target for drug combination therapy of liver cancer. Anticancer Drugs. 2017;28:771-80.

[7] Jones RP, Malik HZ, Fenwick SW, Terlizzo M, O'Grady E, Stremitzer S, et al. PARAGON II - A single arm multicentre phase II study of neoadjuvant therapy using irinotecan bead in patients with resectable liver metastases from colorectal cancer. Eur J Surg Oncol. 2016;42:1866-72.

[8] Hanrahan EO, Lin HY, Kim ES, Yan S, Du DZ, McKee KS, et al. Distinct patterns of cytokine and angiogenic factor modulation and markers of benefit for vandetanib and/or chemotherapy in patients with non-small-cell lung cancer. J Clin Oncol. 2010;28:193-201.

[9] Chao Y, Wu CY, Kuo CY, Wang JP, Luo JC, Kao CH, et al. Cytokines are associated with postembolization fever and survival in hepatocellular carcinoma patients receiving transcatheter arterial chemoembolization. Hepatol Int. 2013;7:883-92.

[10] Najmi Varzaneh F, Pandey A, Aliyari Ghasabeh M, Shao N, Khoshpouri P, Pandey P, et al. Prediction of post-TACE necrosis of hepatocellular carcinoma

usingvolumetric enhancement on MRI and volumetric oil deposition on CT, with pathological correlation. Eur Radiol. 2018;28:3032-40.
[11] Bujold A, Massey CA, Kim JJ, Brierley J, Cho C, Wong RK, et al. Sequential phase I and II trials of stereotactic body radiotherapy for locally advanced hepatocellular carcinoma. J Clin Oncol. 2013;31:1631-9.
[12] Andolino DL, Johnson CS, Maluccio M, Kwo P, Tector AJ, Zook J, et al. Stereotactic Body Radiotherapy for Primary Hepatocellular Carcinoma. International Journal of Radiation Oncology*Biology*Physics. 2011;81:e447-e53.
[13] Huertas A, Baumann AS, Saunier-Kubs F, Salleron J, Oldrini G, Croise-Laurent V, et al. Stereotactic body radiation therapy as an ablative treatment for inoperable hepatocellular carcinoma. Radiother Oncol. 2015;115:211-6.
[14] Lahti SJ, Zeng D, Jia JB, Xing M, Kim HS. 5:27 PM, Abstract No. 171 - Sorafenib loaded drug-eluting beads: loading and eluting kinetics and in vitro viability study. Journal of Vascular and Interventional Radiology. 2015;26:S80-S1.
[15] Fuchs K, Bize PE, Dormond O, Denys A, Doelker E, Borchard G, et al. Drug-eluting beads loaded with antiangiogenic agents for chemoembolization: In vitro sunitinib loading and release and in vivo pharmacokinetics in an animal model. Journal of Vascular and Interventional Radiology. 2014;25:379-87.e2.
[16] Fuchs K, Bize PE, Denys A, Borchard G, Jordan O. Sunitinib-eluting beads for chemoembolization: Methods for in vitro evaluation of drug release. International Journal of Pharmaceutics. 2015;482:68-74.
[17] Bize P, Duran R, Fuchs K, Dormond O, Namur J, Decosterd LA, et al. Antitumoral Effect of Sunitinib-eluting Beads in the Rabbit VX2 Tumor Model. Radiology. 2016;280:425-35.
[18] Cheng AL, Kang YK, Lin DY, Park JW, Kudo M, Qin S, et al. Sunitinib versus sorafenib in advanced hepatocellular cancer: results of a randomized phase III trial. J Clin Oncol. 2013;31:4067-75.
[19] Hagan A, Phillips GJ, Macfarlane WM, Lloyd AW, Czuczman P, Lewis AL. Preparation and characterisation of vandetanib-eluting radiopaque beads for locoregional treatment of hepatic malignancies. Eur J Pharm Sci. 2017;101:22-30.

[20] Lewis AL, Dreher MR, O'Byrne V, Grey D, Caine M, Dunn A, et al. DC BeadM1: towards an optimal transcatheter hepatic tumour therapy. J Mater Sci Mater Med. 2016;27:13.
[21] Prajapati HJ, Xing M, Spivey JR, Hanish SI, El-Rayes BF, Kauh JS, et al. Survival, efficacy, and safety of small versus large doxorubicin drug-eluting beads TACE chemoembolization in patients with unresectable HCC. AJR Am J Roentgenol. 2014;203:W706-14.
[22] Lencioni R, de Baere T, Burrel M, Caridi JG, Lammer J, Malagari K, et al. Transcatheter treatment of hepatocellular carcinoma with Doxorubicin-loaded DC Bead (DEBDOX): technical recommendations. Cardiovasc Intervent Radiol. 2012;35:980-5.
[23] Buckstein M, Kim E, Fischman A, Blacksburg S, Facciuto M, Schwartz M, et al. Stereotactic body radiation therapy following transarterial chemoembolization for unresectable hepatocellular carcinoma. J Gastrointest Oncol. 2018;9:734-40.
[24] Huo YR, Eslick GD. Transcatheter Arterial Chemoembolization Plus Radiotherapy Compared With Chemoembolization Alone for Hepatocellular Carcinoma: A Systematic Review and Meta-analysis. JAMA Oncol. 2015;1:756-65.
[25] Takeda A, Sanuki N, Tsurugai Y, Iwabuchi S, Matsunaga K, Ebinuma H, et al. Phase 2 study of stereotactic body radiotherapy and optional transarterial chemoembolization for solitary hepatocellular carcinoma not amenable to resection and radiofrequency ablation. Cancer. 2016;122:2041-9.
[26] Paik EK, Kim MS, Jang WI, Seo YS, Cho CK, Yoo HJ, et al. Benefits of stereotactic ablative radiotherapy combined with incomplete transcatheter arterial chemoembolization in hepatocellular carcinoma. Radiation oncology (London, England). 2016;11:22.
[27] Jacob R, Turley F, Redden DT, Saddekni S, Aal AK, Keene K, et al. Adjuvant stereotactic body radiotherapy following transarterial chemoembolization in patients with non-resectable hepatocellular carcinoma tumours of >/= 3 cm. HPB (Oxford). 2015;17:140-9.
[28] Lammer J, Malagari K, Vogl T, Pilleul F, Denys A, Watkinson A, et al. Prospective randomized study of doxorubicin-eluting-bead embolization in the treatment of hepatocellular carcinoma: results of the PRECISION V study. Cardiovasc Intervent Radiol. 2010;33:41-52.

[29] Malagari K, Pomoni M, Kelekis A, Pomoni A, Dourakis S, Spyridopoulos T, et al. Prospective randomized comparison of chemoembolization with doxorubicin-eluting beads and bland embolization with BeadBlock for hepatocellular carcinoma. Cardiovasc Intervent Radiol. 2010;33:541-51.
[30] Moreno-Luna LE, Yang JD, Sanchez W, Paz-Fumagalli R, Harnois DM, Mettler TA, et al. Efficacy and safety of transarterial radioembolization versus chemoembolization in patients with hepatocellular carcinoma. Cardiovasc Intervent Radiol. 2013;36:714-23.
[31] ClinicalTrials.gov. SBRT or TACE for Advanced HCC.
[32] Aliberti C, Carandina R, Sarti D, Pizzirani E, Ramondo G, Cillo U, et al. Transarterial chemoembolization with DC Bead LUMI radiopaque beads for primary liver cancer treatment: preliminary experience. Future Oncol. 2017;13:2243-52.
[33] Wahl DR, Stenmark MH, Tao Y, Pollom EL, Caoili EM, Lawrence TS, et al. Outcomes After Stereotactic Body Radiotherapy or Radiofrequency Ablation for Hepatocellular Carcinoma. J Clin Oncol. 2016;34:452-9.
[34] ClinicalTrials.gov. Sorafenib Tosylate With or Without Stereotactic Body Radiation Therapy in Treating Patients With Liver Cancer.
[35] Finn RS, Qin S, Ikeda M, Galle PR, Ducreux M, Kim TY, et al. Atezolizumab plus Bevacizumab in Unresectable Hepatocellular Carcinoma. The New England journal of medicine. 2020;382:1894-905.
[36] El-Khoueiry AB, Sangro B, Yau T, Crocenzi TS, Kudo M, Hsu C, et al. Nivolumab in patients with advanced hepatocellular carcinoma (CheckMate 040): an open-label, non-comparative, phase 1/2 dose escalation and expansion trial. The Lancet. 2017;389:2492-502.
[37] Zhu AX, Finn RS, Edeline J, Cattan S, Ogasawara S, Palmer D, et al. Pembrolizumab in patients with advanced hepatocellular carcinoma previously treated with sorafenib (KEYNOTE-224): a non-randomised, open-label phase 2 trial. The Lancet Oncology. 2018;19:940-52.
[38] Smith WH, McGee HM, Schwartz M, Sung M, Rosenzweig K, Buckstein M. The Safety of Nivolumab in Combination with Prior or Concurrent Radiation Therapy Among Patients with Hepatocellular Carcinoma. International Journal of Radiation Oncology*Biology*Physics. 2019;105:E227-E8.

APPENDIX A: VEROnA Trial Standard Operating Procedues

VERONA

A pilot, open label, single-arm, phase 0, window of opportunity study of vandetanib-eluting radiopaque embolic beads (BTG-002814) in patients with resectable liver malignancies

DEB-TACE PROCEDURE

Version 1.0 – 11/05/2017

INTRODUCTION

The purpose of this document is to describe the VEROnA DEB-TACE procedure.

All patients will receive one treatment of BTG-002814, 7 to 21 days before surgical resection of the liver.

PRE-PROCEDURE

On the day of the procedure, the following are required for the study:

(The following assessments will be completed in UCLH Clinical Research Facility)

- Vital Signs
- Record of Concurrent Medications
- Assessment and record of Adverse Events
- ECG
- Blood sample for biomarkers
- Serum Tumour markers
- Blood sample for vandetanib levels

(*Patient transferred to Interventional Radiology Department P02 imaging reception for the following assessments)*

- MRI (with DCE protocol)
- CT (with perfusion protocol)

The relevant CRF pages should be completed with the required information.

PREPARATION of BTG-002814

BTG-002814 will be prepared in Production Pharmacy. Preparation includes Rehydration, addition of Non-Ionic Contrast Medium and Transfer to the Syringe. Preparation instructions are provided in the VEROnA Study Summary of Drug Arrangements.

Once prepared the syringe will be left ready for collection from the Chemo Dispatch 2nd floor of the University College London Macmillan Cancer Centre. The syringe will be packed in a heat-sealed plastic bag and the collector will be given a yellow cytotoxic bag to carry the dose to Interventional Oncology Services.

EMBOLISATION PROCEDURE

Using a unilateral femoral approach, selective catheterisation of the hepatic artery will be performed. Diagnostic visceral arteriography will be performed to delineate the arterial supply to the tumour, determine the presence of variant arterial anatomy and to confirm patency of the portal vein. Once the patient's arterial anatomy is understood, a catheter is advanced into the right

or left hepatic artery distal to the cystic artery (if visualised). The treatment plan is based on the fluoroscopic appearances during arteriography. For the purposes of this study, since all eligible patients have resectable disease, it is not a requirement of the protocol that all lesions visible on CT are treated with BTG-002814. This decision will be at the discretion of the treating investigator. For example, if a right hemi-hepatectomy is the operation planned, it is not necessary to treat all the lesions in the anterior and posterior sector; the lesions to be treated may be those deemed to be at highest risk of a positive surgical resection margin and therefore at highest risk of tumour recurrence following surgery. Visualisation of the beads on 4D CT will be attempted the day after the embolisation procedure.

Once the catheter is in place within the artery feeding the tumour, the re-constituted BTG-002814 suspension will be slowly infused into the artery (approximately 1 mL per minute). Catheter selection will be by operator preference. There will not be any issues with a 4- or 5-Fr catheter, but the choice of a microcatheter (2.4Fr. to 2.8Fr.), in case of tortuous, narrow or spastic vessels must be consistent with the size of embolic agent used (see IFU). The end point of the procedure is either full delivery of the reconstituted bead volume (i.e. 1 mL vandetanib loaded beads in contrast) or near-stasis in the tumoural vessel over 6 cardiac cycles. Undelivered volume of reconstituted embolic solution must be recorded.

For HCC patients, a super selective (segmental/subsegmental) approach should be taken with the catheter placed as selectively as possible whilst maintaining sufficient flow to the tumour. For mCRC patients, it is generally a lobar approach, by placing the catheter tip beyond the origin of the cystic artery (or any other arteries supplying extrahepatic organs) and maintaining forward flow.

The catheter will then be removed and haemostasis achieved by manual compression or with a percutaneous closure device. Each patient will be admitted for overnight care.

Normal procedures should be adopted for vasodilation.

Delivery Procedure

Ease of Vandetanib Bead delivery through a catheter will be improved by ensuring a homogenous suspension of beads within the water/ contrast medium.

1. Prime a microcatheter (2.4 Fr to 2.8Fr.) by flushing through 5 ml of Omnipaque 350 contrast.
2. Attach the 20 ml syringe to a 3 ml syringe using a three-way connector.
3. Expel any trapped air.
4. Gently move the Vandetanib Bead between the two syringes to create a homogenous suspension.
5. Draw an aliquot of the suspension into the 3 ml syringe.
6. Check the 3 ml syringe for bead aggregation and remove air if necessary.
7. Attach the catheter to the 3 ml delivery syringe via the three-way connector.
8. Inject Vandetanib Bead into the delivery catheter using short, controlled pulses to match blood flow while observing the contrast flow rate (recommended speed 1ml/min).
9. Carefully monitor the bead density in the catheter hub. If beads accumulate in the hub, then attempt the following steps:
    i. Gently increase the pressure exerted on the 3 ml syringe plunger to push the beads into the catheter, or
    ii. Tilt the catheter hub and the syringe to disperse the beads away from the catheter neck, or
    iii. Flush the catheter hub with Omnipaque 350

10. Flush the catheter with minimum 5 ml of Omnipaque 350 to ensure all beads have been delivered from the catheter.

Data to be Recorded

The amount and type of contrast agent delivered to the patient during the procedure and skin dose of x-rays from fluoroscopy during the procedure will be recorded. The vessels embolised will be noted and the amount of embolic agent used will be recorded. All medications used during the procedure will be recorded, including pain management regime.

The volume of BTG-002814 delivered will be recorded. If the full volume is not given the reason for this will be captured. Any TACE procedure complications will be recorded. The type of microcatheter used, the microcatheter size and the microcatheter dead space volume will also be recorded.

POST PROCEDURE

Patients will be admitted for overnight care. The following are required for the study:

(These assessments will be completed on the ward or recovery suite by a member of the Comprehensive Clinical Trials Unit. The VERONA Research Fellow or a person from UCLH Clinical Research Facility will perform any assessments due after 5pm in the evening).

Post Procedure – Day of BTG-002814 administration – Visit 2

- Vital Signs
- Record of Concurrent Medications
- Assessment and record of Adverse Events
- ECG
- Blood sample for vandetanib levels at 2 hours post treatment
- Blood sample for vandetanib levels at 4 hours post treatment

Day 1 after treatment – Visit 3

- Vital Signs
- Record of Concurrent Medications
- Assessment and record of Adverse Events
- Biochemistry
- Haematology
- 4D CT (performed in the radiotherapy unit)
- Blood sample for biomarkers
- Blood sample for vandetanib levels at 24 hours post treatment
- If the patient requires a longer hospital stay, one more (optional) blood sample for vandetanib levels should be taken after 36 hours and up to time of discharge.

The relevant CRF pages should be completed with the required information.

APPENDIX 1

VANDETANIB BEAD INSTRUCTION FOR USE

Vandetanib Bead – 100mg vandetanib, supplied as a lyophilised powder

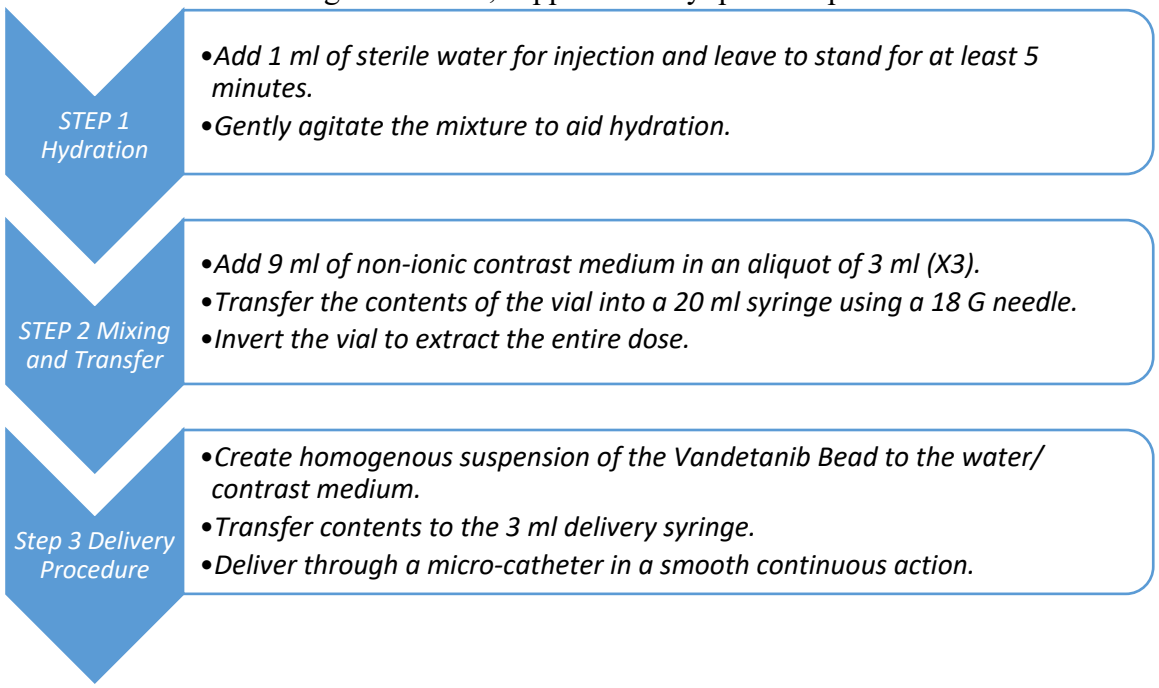

VEROnA

A pilot, open label, single-arm, phase 0, window of opportunity study of vandetanib-eluting radiopaque embolic beads (BTG-002814) in patients with resectable liver malignancies

PROCECURES FOR HANDLING AND TRANSPORT OF RESECTED LIVER TISSUE INCLUDING:

Contacts and communication

Surgical Requirements

Transporting Tissue

Ex-vivo scanning

Histopathology procedures

Version 3.0 - 18/02/2019

1. INTRODUCTION

The purpose of this document is to describe the transfer, imaging and sectioning of liver tissue samples for the VEROnA study.

All patients will undergo liver surgery at the Royal Free Hospital and the resected liver tissue will be collected and prepared for transfer by the Research Fellow or Tissue Collection Officer as back up.

1.2 SAMPLE PROCESSING FLOWCHART

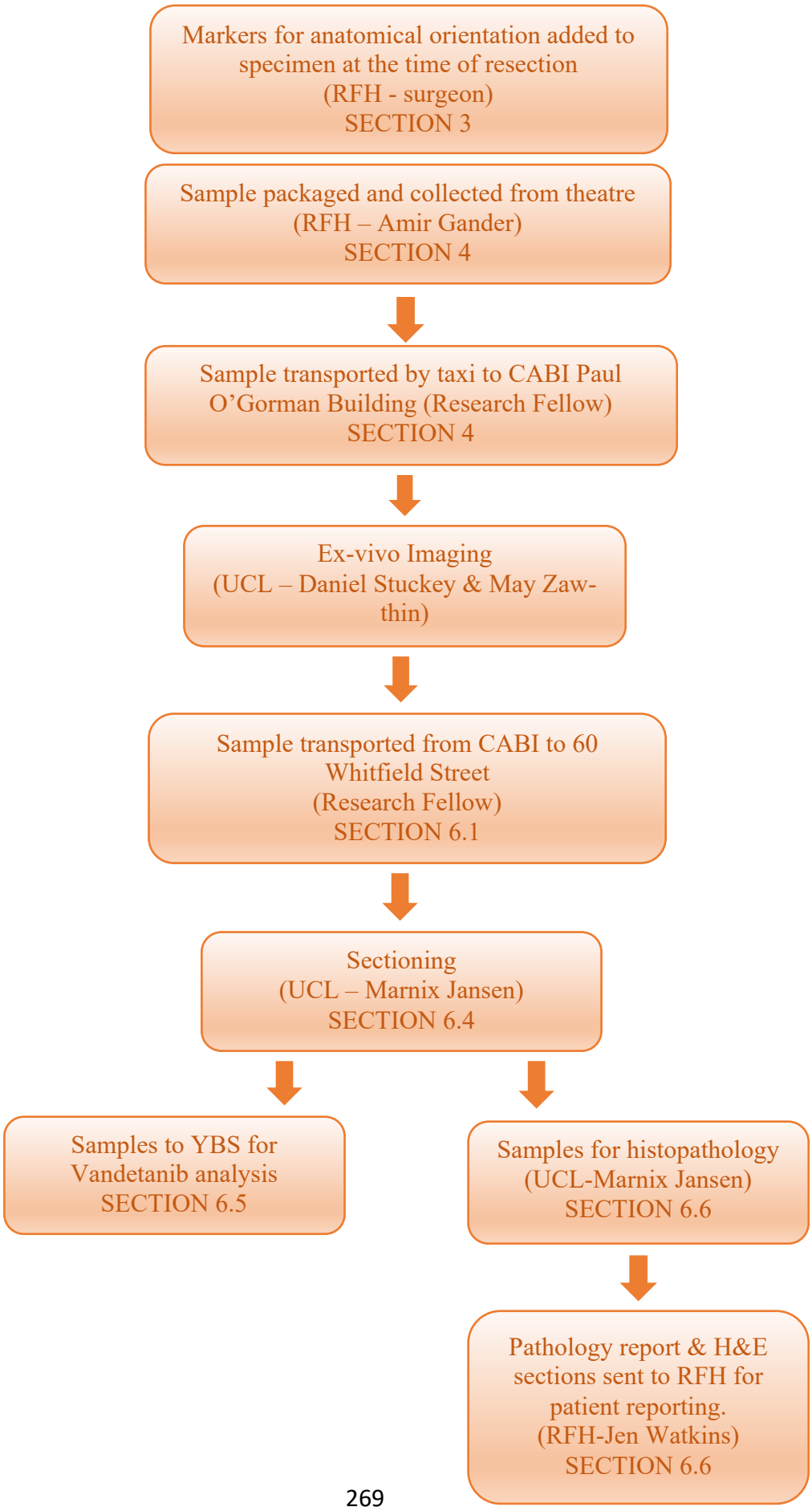

2. NOTIFICATION & PREPARATION PRIOR TO PATIENT SURGERY

2.1 NOTIFICATION OF SURGERY DATE

- When the patient is registered on the study, UCL CTC will alert all of the contacts listed in Table 1.1. An email will be sent confirming Patient Registration, ID number and provisional or confirmed date of surgery.
- If date of surgery is not confirmed at registration or surgery date is changed the TCO or Research Fellow will update UCL CTC with the date of surgery. If the TCO is unavailable UCL CTC will liaise with the surgical admissions team at RFH for HPB who will be able to provide information on surgery dates. UCL CTC will then inform all contacts in Table 1.1.
- The TCO/HBSM will add the patient onto the biobank system (for easy traceability and easy HTA reporting). This will produce a 'G' number for the sample and a subject ID for the patient for any future samples.

2.2 DAY OF SURGERY

- On the morning of surgery the TCO/HBSM will inform the surgeon of the VEROnA study patient and remind the surgeon of the trial procedures for marking the resection specimen. The TCO/HBSM will provide the surgeon with the radiopaque surgical slings required to mark the surgical specimen.
- The TCO/HBSM will phone Jorge Cardoso to advise of expected delivery time.
- The TCO/HBSM will phone Daniel Stuckey to advise of expected delivery time.
- The TCO/HBSM will also phone Marnix Jansen to advise of expected delivery time.
- The Research Fellow (RF) will provide back up for the TCO/HBSM on the day of surgery.

3. ORIENTATION OF LIVER SPECIMEN

3.1 ORIENTATION

Specimens will be marked using 1.5mm sterile surgical slings impregnated with radiopaque material. These will be provided by the TCO/HBSM (with Research Fellow as back up) on the day of surgery. These will be knotted and fixed to the specimen using a standard suture.
The specimen(s) should be oriented by the surgeons, adding one marker in each plane, as follows:

1 knot = Superior
2 knots = Anterior
3 knots = Medial

Specimen orientation will be marked by the surgeon in theatre following directions from the operating surgeon.

4. SAMPLE PREPERATION & DELIVERY

- The resected sample should by measured by the TCO/HBSM (with the Research Fellow as back up) and the measurements recorded on the surgical sample processing & shipment form.
- The resected sample will be placed within a plastic bag. As much air as possible should be excluded from the bag. The bag should be placed on ice in an insulated container. The specimen should not be in direct contact with ice or liquid. The TCO/HBSM will provide additional plastic bags with the sample packaging for later use if the sample needs re-packaging.
- The specimen will be logged onto Cerner adding a comment that it is to be processed in UCLH.
- Information about the specimen will be logged on the biobank system (time of collection, conditions, any comments etc.) then will be packed according to Category B, UN3373 for transport to UCLH.
- The TCO/HBSM will ensure that the sample has been correctly packaged for transfer.
- If the size of the resected sample is less than 8 x 8 x 20 cm the Research Fellow (with TCO/HBSM as back up) will deliver the sample by taxi (Black cab) to Daniel Stuckey & May Zaw-thin in the UCL Centre for Advanced Biomedical Imaging (CABI) Paul O'Gorman Building.
- If the size of the resected sample is greater than 8 x 8 x 20 cm the research fellow (with TCO/HBSM as back up) will deliver the sample by taxi (Black cab) to Marnix Jansen in the Histopathology Laboratory, 60 Whitfield Street.
- Marnix Jansen will halve or quarter the specimen to facilitate scanning, whilst maintaining integrity of the excision margins and specimen orientation.
- Once cut, the Research Fellow (with TCO/HBSM as back up) will deliver the sample by foot to Daniel Stuckey & May Zaw-thin in the UCL Centre for Advanced Biomedical Imaging (CABI) Paul O'Gorman Building.

5. IMAGING PROCEDURE

- Micro CT imaging will be performed on a Mediso nanoScan PET/CT.
- A CT image will be acquired with a 96 x 117 mm FOV at 125 microns of resolution.
- Sample will be placed inside a HDPE container (80 x 110 mm in-plain) to ensure sample coverage.
- The HDPE container will be secured to the Mediso imaging bed.
- Preparation and scanning should take approximately 20 minutes.
- After imaging is complete, the sample is then transferred to the Histopathology Laboratory, 60 Whitfield Street.
- Aim for minimum handling and minimum delay between removal from patient to sectioning in pathology lab.

6. PATHOLOGY PROCEDURE

6.1 SAMPLE DELIVERY

- After imaging, the Research Fellow/TCO/HBSM will deliver the sample to Marnix Jansen at the Histopathology Laboratory, 60 Whitfield Street.
- Cases will be booked in to CoPath as UCLH cases and processed and reported in the Histopathology Laboratory, 60 Whitfield Street.
- Reports will be automatically transferred onto CDR. Marnix Jansen will email these to RFH (Histopath) so the final histology report will be also available on the patients' notes at RFH.

6.2 BACKGROUND

- Specimens should be processed according to the RCPath dataset guidelines
- (http://www.rcpath.org/resources/pdf/G050DatasetLiverSept07-AR.pdf), with the following additions as specified in the following sections below:
    - 6.3
    - 6.4
    - 6.5
- Please contact Marnix Jansen (MJ) to cut-up any specimens from this trial.

6.3 MULTIPLE LESIONS

- Where multiple lesions have been resected from the same patient, correlation between radiology and pathology will be performed for 3D imaging and biobanking (details), which should be clearly indicated on the pathology request form.
- Treat each lesion according to protocol below.

6.4 RESECTION

- Where orientation and margins permit, cut the specimen in **intervals of 2-5 mm, using a guide**.
- **Photograph** the cut specimen with markers for orientation and size.
- **Biobanking** refer to section 6.5.
- **All-embed the metastasis serially** (from superior to inferior if cut in the transverse / axial plane). If the metastasis is too large to all embed, pin out the slices that are not embedded and leave a copy of the pathology request form with a note.

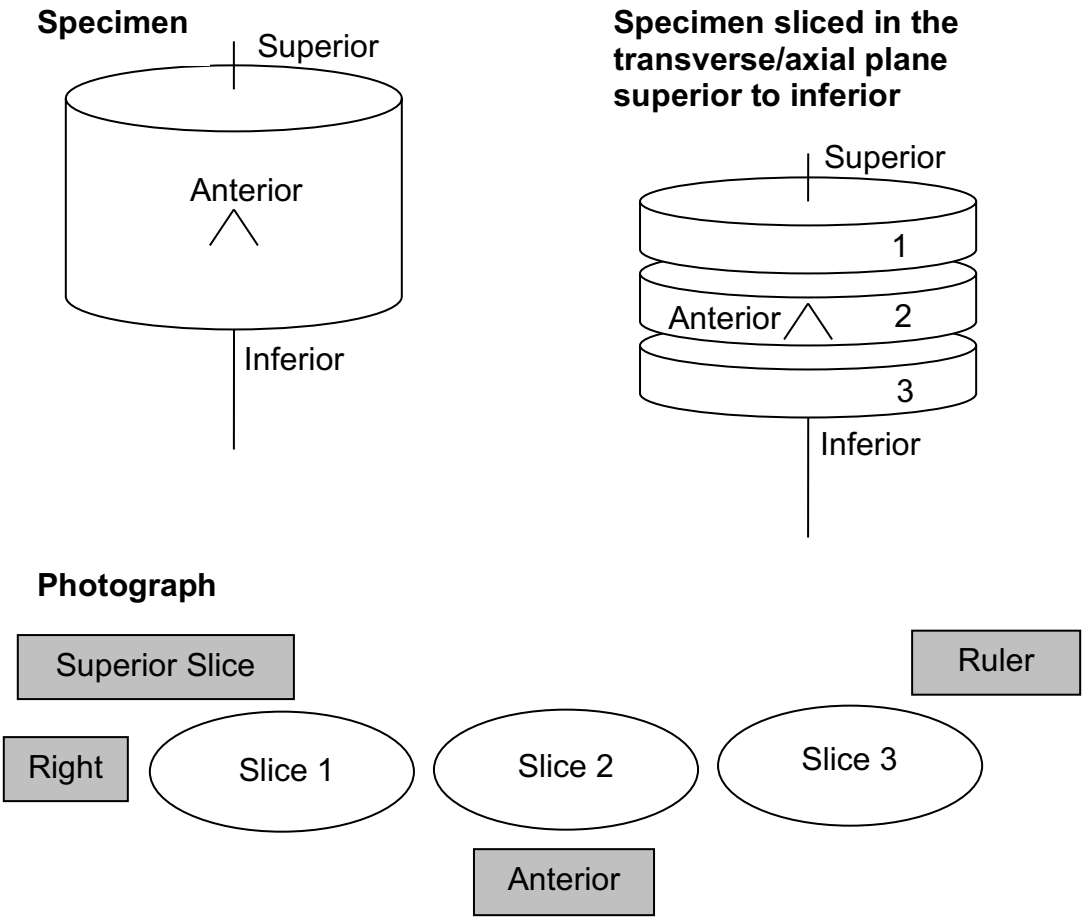

6.5 SAMPLES FOR VANDETANIB AND METABOLITE ANALYSIS

6.5.1 Requirements

- **Four samples** are frozen from each lesion, as follows (see diagram below):
  - One from centre of tumour (Location 1 - Centre)
  - One midway between centre of the tumour and edge (Location 2 - Mid)
  - One from tumour's edge (Location 3 - Edge)
  - One sample taken 1 cm away from tumour/normal tissue control) (Location 4 – Normal)
- Minimum of 0.6g tissue per sample is snap frozen

0.6 g each

6.5.2 Storage

- Sample to be wrapped in foil (provided by CTC) and snap frozen in liquid nitrogen. This could be via using a metal basket that is dropped into the liquid nitrogen. After a few minutes, the samples to be removed
- Place each foiled sample in a small plastic bag pre-labelled with the patient ID and location from which sample was taken (labels provided by UCL CTC). Labels to be used shown below:

BTG-002814 VEROnA Patient:_____ Location 1 – Centre Liver Vandetanib	BTG-002814 VEROnA Patient:_____ Location 2 – Mid Liver Vandetanib
BTG-002814 VEROnA Patient:_____ Location 3 – Edge Liver Vandetanib	BTG-002814 VEROnA Patient:_____ Location 4 – Normal Liver Vandetanib

- Place the small bags into a larger bag pre-labelled with the patient ID. Labels to be used shown below:

BTG-002814 VEROnA
Patient:_____
Liver Vandetanib
Visit 5

- Store samples at -80°C (range -70°C to -90°C) until ready for shipment.
- **All samples are frozen without OCT compound**

6.5.3 Shipment to York Bioanalytical Solutions

- Ship samples on dry ice. Samples to be within dry ice to ensure sufficient coverage. Ensure samples shipped at approximately -80C or below and in appropriate packing material containing sufficient dry ice to keep samples frozen during shipment.
- Do not ship on the day before a weekend or holiday. Notice and expected arrival times of the samples should be given in advance to York Bioanalytical Solutions.
- A sample inventory and surgical sample processing and shipment form should be included with each shipment. A copy of the form should be kept.
- The surgical sample processing and shipment forms will be stored at UCLH Clinical Research Facility in the laboratory folder in the laboratory. These will be transferred to the Histopathology Laboratory, 60 Whitfield Street, when the specimens are collected by the research fellow.

6.6 HISTOPATHOLOGY

- Marnix Jansen will also create H&E slides for histopathology.
- Fresh resection specimens will be inked according to standard operating procedure and serially sliced at 5 mm intervals. Lesion size, macroscopic extent of tumour necrosis and minimum distance to nearest margin and/or anatomic landmarks will be recorded at specimen dissection. All sections will then be paraffin-embedded in large 3x2 inch cassettes.
- Slides are needed for MDT review at RFH. H&E (haematoxylin-eosin) sections will be sent to Jen Watkins at Royal Free Pathology for standard patient reporting.
- Remaining tissue will also be embedded
- Research tissue including slides and paraffin blocks will be stored by Marnix Jansen during the study and sent to the UCL BioBank after completion
- Histopathological assessment of samples of resected liver tissue (both tumour and non-tumour) will include microscopic examination to correlate radiologic extent of tumour cell necrosis to microscopic extent of tumour cell necrosis.
- Patients may have multiple lesions, some of which may be untreated, comparison to be made by Marnix where possible regarding tumour necrosis, viable tumour and any vascular changes.

6.7 3D PATHOLOGY MODELLING

Standard H&E sections (4 µm thick) will be cut from every block onto large microscopy slides. All slides will be scanned using Aperio Technologies AT slide scanner using a ×40 objective, producing images with a final resolution of 0.25 µm per pixel. Scanned data sets will be uploaded and registered using a sequential slice-to-slice image-based registration approach. One virtual slide (the section closest to the centre of the tissue, because this section generally contains the most tissue and allows for the definition of the volume size before registration commences) is then used as a reference. Serial sections directly next to this reference section will be non-rigidly aligned to the reference using a slice-to-slice image-based registration technique. Alignment proceeds out from the centre, with subsequent images aligned to their neighbours. The set of aligned images will then be concatenated to form a 3D volumetric data set. This result will then be used as input to a non-rigid registration method that divides the image into a set of regularly spaced square patches that are individually aligned. The volume generated will then be used to

generate a 3D volume rendering and segmentation of each data set. Volumes will be digitally resliced and individual images imported for 3-dimensional reconstruction. These 3D models will be compared to the 3D models generated from clinical imaging.

VEROnA

A pilot, open label, single-arm, phase 0, window of opportunity study of vandetanib-eluting radiopaque embolic beads (BTG-002814) in patients with resectable liver malignancies

PATIENT IMAGING PROCEDURES

Version 1.0 – 26/04/2017

1. BACKGROUND

As changes in tissue perfusion may improve understanding of liver tumour biology and behaviour, patients in this study will undergo dynamic contrast enhanced (DCE) magnetic resonance imaging (MRI) and perfusion Computed Tomography (pCT) at time points stated in the table below. Anatomical, dual energy and 4D CT scanning will also be used to evaluate distribution of BTG-002814 within the liver.

Imaging protocols and scanner parameters for all patients and visits will be standardised.

2. TIMING

At each visit, CT scanning should occur before, or at least 1 hour after, MRI to avoid CT image contamination with Gadolinium contrast. CT and MRI studies will be performed at baseline, within one day of treatment and 1 day prior to surgical resection.

Study Visit	**Visit 0**	**Visit 1**	**Visit 2**		**Visit 3**	**Visit 4**	**Visit 5**	**Visit 6**
	Screening	**Baseline**	**Treatment Day**					**End of Study**
	Up to 7 days before registration	Up to 7 days before treatment and following registration	Pre-treatment	Post-treatment	Day 1 after treatment	-1 day prior to surgical resection	Surgical resection (7 to 21 days after treatment)	30-32 days post-surgery
Liver MRI, Incorporating DCE-MRI		X	X			X		
CT scan chest, abdomen, liver, pelvis, incorporating perfusion CT of liver		X	X			X		
4D CT scan liver					X			

3. MRI (incorporating DCE-MRI)

MRI including a dynamic contrast enhanced series will be performed using a 3T MRI scanner. Patients will lie supine on the scanner table and an intravenous cannula placed in the antecubital fossa. No oral contrast is required. Standard clinical liver sequences will be acquired, and include a T2 weighted TSE axial plane; axial and coronal mDixon based sequences and diffusion weighted imaging with 8 b-values.

T1 mapping will be performed using three-dimensional volumetric gradient echo imaging with varying flip angles. A series of T1–weighted three-dimensional volumetric images will be acquired at baseline and sequentially during administration of a bolus of intravenous paramagnetic MR contrast agent Gd-DOTA (gadoterate dimeglumine, Dotarem®, Guerbet, Roissy, France) (10ml Gd-DOTA mixed with 10ml normal saline injected at a rate of 4 mL/s followed by a 20ml saline flush). Each acquisition takes approximately 5 seconds during which time patients are asked to hold their breath in full expiration or if necessary, to breathe in a shallow fashion. The entire post contrast DCE series takes approximately 3-5 minutes. The MRI protocol will finish with a final T1 map at 5 minutes post contrast.

MRI should be performed after, or at least 90 minutes before any CT examination to prevent CT image contamination with gadolinium contrast.

Summary of the MRI protocol:

- T2 weighted turbo spin echo sequence in an Axial
- mDixon series in Axial + Coronal plane
- mDixon Quantitative axial sequence
- Diffusion weighted images with 8 b-values
- T1 map by MOLLI/LL (modified look locker/Look Locker)
- T1 map by MFA (Multi flip angle)
- B1 map
- DCE series, using 3d TFE
- T1 map by MFA at 5 minutes post contrast

4. DERIVED MRI PARAMETERS

Liver parenchyma and tumour signal intensity curves will be used to calculate semiquantitative and quantitative tissue parameters describing tumour perfusion, blood flow and vascularity before and following treatment with BTG-002814.

Quantitative parameters including Ktrans, Kep and Ve will be derived using a dual compartment model with an arterial and portal venous input function.

Estimated semiquantitative perfusion parameters will include portal venous (PV) perfusion; total liver blood flow (TLBF); hepatic arterial fraction (HF); distribution volume (DV) and mean transit time (MTT).

5. CT INCORPORATING PERFUSION CT

CT will incorporate dual energy (DECT) and perfusion imaging (pCT) of the liver, in addition to standard clinical contrast enhanced imaging of the chest, abdomen and pelvis. CT should be performed before or at least 90 minutes after the MRI scan. Images will be acquired in a supine position using a cannula placed in the antecubital fossa. No oral contrast is required.

A combined CT protocol will be carried out as follows, with each volume acquired in inspiration:

1. dual energy (80+135 kV) acquisition of the liver prior to contrast administration
2. bolus of 0.5 mL/kg of iodinated contrast (300 mgI/mL) injected at a rate of no less than 5 mL/s (total <8 seconds).
3. volume perfusion acquisition of the liver, with intermittent scanning over 90 seconds
4. interval of at least 3 minutes to allow contrast washout
5. bolus of 1 mL/kg of iodinated contrast (300 mgI/mL) injected at a rate of 3-5 mL/s
6. late arterial phase (35 seconds post contrast bolus) volume of the chest and liver
7. portal venous phase (60 seconds post contrast bolus) volume of the abdomen and pelvis

6. CT PARAMETERS DERIVED

Perfusion CT time-attenuation data will be used to derived tissue parameters describing tumour perfusion, blood flow and vascularity. Arterial blood flow (AF), portal venous blood flow (PF) and perfusion index will be derived using a dual input maximum slope method. Blood volume (BV) and permeability surface-area product (PS) will be derived using Patlak analysis.

7. 4D CT

Following treatment with BTG-002814 a 4D CT scan will be performed to check and track the positioning of the beads in 'real time'. This scan should be performed without contrast.

Proposed Schedule of Events for Radiotherapy procedures for Verona

Referral/Consent:	Prof Sharma to produce notification proforma
Ward:	Notification of Discharge.
CT (30 mins):	Wing board, sup locator, arms up, combifix, pen marks
	No IV or oral contrast, no drinking and fasting
	4D CT (120 kV Standard 100mA)
	T10-L4 (liver) Dose 38.6 mSv
Plan Preparation (120mins):	Analysis of binned data
	Creation of AVE-IP, M-IP, Min-IP
	Import into ARIA
	Creation of Set-Up plan
Linac (30 mins):	Patient set up as per CT scan
	Pelvis CBCT (125 kV, 60 mA, 20ms, 1080 mAs)
	T10-L4 Dose 5.8 mSv
Review point:	Post 1st patient scan to assess visibility/feasibility
	Post 3rd patient -decision to continue protocol

8. DATA STORAGE

Scan data will be on the local PACS system. All images must display the patient trial number and initials only; all other identifiable details such as name and/or date of birth must be removed.

Image data will be downloaded for image analysis using the standard UCL Centre for Medical Imaging pseudo-anonymisation protocol by an authorised member of the trial team.

9. QUALITY CONTROL/QUALITY INSURANCE

Each imaging dataset will be specifically checked for the following:

a) that the dataset acquired is complete
b) that the images cover the anatomy of interest and are free of significant artefacts
c) acquisition corresponds closely to the imaging protocol

All scans will be assessed within three days of acquisition, to allow referral to the supervising radiologists for consideration of rescanning.

Quality assurance procedures should be employed to characterise the performance of measurements obtained using clinical MRI and CT systems. QA schedule should be performed as per departmental protocol.

VEROnA

A pilot, open label, single-arm, phase 0, window of opportunity study of vandetanib-eluting radiopaque embolic beads (BTG-002814) in patients with resectable liver malignancies

LABORATORY MANUAL

For the Collection, Processing, Storage and Shipping of Blood Samples for Translational Research

Version 3.0 – 08/06/2018

1 INTRODUCTION

The purpose of this laboratory manual is to describe the collection, processing, storage and transportation of blood and archival tissue samples for the VEROnA study.

Archival tumour tissue (where available) and blood samples will be collected from **all patients at all participating sites** and shipped to various UK laboratories as part of the translational research aspect of this study.

In order to preserve the integrity of the patient samples, designated staff at each participating site are responsible for ensuring that research samples are collected, handled, processed and stored at their site in accordance with the instructions in this manual and the current approved version of the study protocol. Designated staff should be fully trained and listed on the Site Staff Delegation Log as authorised by the Principal Investigator to carry out these tasks before any study related activities and procedures can be performed by them.

It is important that site staff ensure that all research samples are transported to the central laboratories within the time frames specified in the study protocol and as set out in this document, and that **samples are not shipped to arrive at the laboratories either on a weekend or bank holiday**.

For each sample, complete the relevant Sample Collection Form and log the samples on the patients Biological Sample Inventory Log found in the laboratory section of the Investigator Site File (ISF) (spreadsheet supplied electronically). Completed logs can be filed in individual patient files or a study specific laboratory documents folder if preferred. Sample Inventory Logs must be sent to the VEROnA Trial Coordinator once all samples for a patient have been collected, and also as and when requested by UCL CTC.

1.2 SAMPLES DESTINATION AND SHIPPING TIMELINES

SAMPLE	DESTINATION	COURIER REQUIRED?	SHIPPING TIMELINE:
Archival Tumour Tissue (if available)	Department of Histopathology, Rockerfeller Building, UCL, London	No - send direct to destination	As soon as possible after patient registration
Plasma samples for biomarker analysis	UCL ECMC GCLP Facility, UCL Cancer Institute, London	Yes, contact UCL CTC	At the end of the study*
Plasma samples for vandetanib and N-desmethyl metabolite analysis	York Bioanalytical Solutions Limited, York	Yes, contact UCL CTC	Within 4 months after sample is taken

* *If storage space is limited then samples may be shipped more frequently. Please discuss this with the VEROnA Trial Coordinator.*

A. CONSUMABLES AND SHIPPING PROVIDED BY UCL CTC

The following consumables will be provided to Sites by UCL CTC:

- Cryovials (1 & 1.8 mL)
- Cryolabels
- Vacutainer© EDTA tubes (4 mL)
- Vacutainer© tubes (lithium heparin) (6 mL)
- Pipettes
- Freezer boxes
- Sample shipping forms

For samples to be shipped on dry ice, UCL CTC will arrange and pay for the courier. The courier will provide dry ice and packaging required for shipment.

2 PLASMA SAMPLES FOR BIOMARKER ANALYSIS

For the timing of samples to be collected please refer to **Appendix 1**.

2.1 EQUIPMENT REQUIRED

REQUIRED ITEM	SUPPLIED BY UCL CTC
4 mL Vacutainer© EDTA tubes	Yes
Temperature Controlled Centrifuge	No
Calibrated pipette to measure 100 µL	No
Cryovials (1 mL)	Yes
Labels for Samples	Yes
Non water-soluble ink pen	No
Freezer boxes for sample storage	Yes
Biomarker Sample Collection Form	Yes
–70°C (or colder) Freezer – storage space	No
Biological samples inventory log	Yes

2.2 PROCESSING PROCEDURE

- Label 1 x 4 mL Vacutainer© EDTA tube with the patient's trial number and initials
- Collect whole blood into the labelled Vacutainer© EDTA tube
- Within **30 minutes of collection** centrifuge the sample at **1000 x g** for **10 minutes** at room temperature
- UCL CTC will supply 8 x 1 mL pre-labelled cryovials to the site in per patient per visit plastic bags with the relevant biomarker sample collection forms. The patient's trial number, date of sample collection (DD/MM/YY), time of sample collection (HH:MM in 24 hour format, e.g. 13:40) and tube number (aliquot number) should be added to the labels in the space provided. Examples of the labels used are shown below for Baseline (Visit 1):

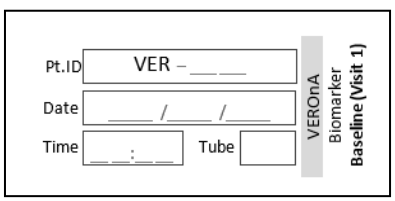

- Additional labels will be supplied by UCL CTC and can be found in the Laboratory section of the Investigator Site File (ISF).
- Pipette the plasma as 100 µL (0.1 mL) aliquots into the labelled cryovials
    - **NB** a minimum of 6 (ideally 8) aliquots are required per sample
- Discard the blood collection tube and the rest of its contents
- Complete a separate **Biomarker Sample Collection Form (Appendix 6)** for each time point a sample is taken
- Enter sample details on the **Biological Samples Inventory Log (Appendix 9)** (spreadsheet supplied electronically; a hardcopy is also available in the ISF).

2.3 STORAGE

- The labelled cryovials must be stored at –70°C or colder.
- The cryovials must be stored in the freezer boxes. With a non-water soluble pen label the freezer box lid and freezer box side with 'VEROnA biomarker samples, patient trial number'.
- Make sure the freezer boxes are stored with the label facing forward.
- There should be one freezer box per patient.
- Record the final storage location (freezer) of the cryovials for each sample time point on the **biological samples inventory log (Appendix 9).**
- Please refer to **Appendix 4** for more detailed information on the storage of samples in the freezer box.

2.4 SHIPPING

- The samples will be stored at site until the end of the study; however, if storage space is limited, then samples may be shipped in batches more frequently. This should be discussed and agreed with UCL CTC
- UCL CTC will arrange for the samples to be collected by a specialist courier company. The courier will provide the dry ice and packaging required for shipment.
- The samples must be shipped in the freezer boxes provided.
- Before shipping photocopy the completed **biomarker sample collection form** (Appendix 6) and fax a copy to UCL CTC. Keep a copy at site in the VEROnA laboratory file.
- Place the original completed **biomarker sample collection form (Appendix 9)** in the box with the samples
- Record details of shipping on the **biological samples inventory log (Appendix 9)**
- The shipping container must be clearly labelled 'VEROnA' and addressed to Helen Lowe.
- On receipt of each shipment the UCL ECMC GCLP Facility will complete the lower portion of the collection form and fax to the VEROnA team. Any discrepancies or inconsistencies will be raised by UCL CTC with the Site.

3 PLASMA SAMPLES FOR VANDETANIB & N-DESMETHYL VANDETANIB ANALYSIS

For the timing of samples to be collected please refer to **Appendix 1**. **NB** the collection of the post-treatment samples should be timed from the **START** of the BTG-002814 infusion.

3.2 EQUIPMENT REQUIRED

REQUIRED ITEM	SUPPLIED BY UCL CTC
6 mL Vacutainer© tubes (lithium heparin)	Yes
Temperature Controlled Centrifuge	No
Pipettes	Yes
Cryovials (1.8 mL)	Yes
Labels for Samples	Yes
Non water soluble ink pen	No
Freezer boxes for sample storage	Yes
Vandetanib Sample Collection Form	Yes
–70°C (or colder) Freezer – storage space	No
Biological samples inventory log	Yes

3.3 PROCESSING PROCEDURE

- Label 1 x 6 mL Vacutainer© tube containing lithium heparin with the patient's trial number, initials and time point
- Collect whole blood into the labelled Vacutainer© tube
- Immediately following collection, gently invert the blood tube multiple times to ensure the anticoagulant has adequately mixed with the blood sample
- Within **30 minutes of collection** centrifuge the sample at **1000 x g** for **10 minutes** at 4°C
- UCL CTC will supply 2 x 1.25 mL pre-labelled cryovials per sample time point to the site in per patient per visit plastic bags with the relevant vandetanib sample collection forms

- One cryovial per sample timepoint will be labelled with a yellow “primary sample” label and the other will be labelled with a blue “Back-up sample” label. The patient’s trial number is to be added to the labels in the space provided. Examples of the labels to be used are shown below for Visit 2 2 hour:

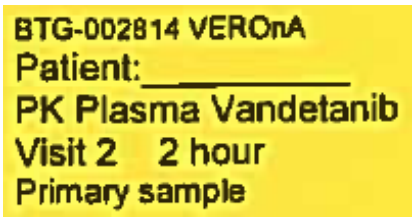

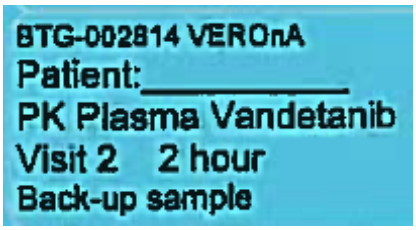

- Additional labels will be supplied to the site by UCL CTC and can be found in the Laboratory section of the Investigator Site File (ISF).
- Pipette **0.5 mL of the plasma** into **each of the** labelled cryovials, taking care not to disturb the buffy coat layer
- Cap the cryovials securely and store at **-70°C (or below), within 60 minutes of collection**
- Discard the blood collection tube and the rest of its contents
- Complete a separate **Vandetanib Sample Collection Form (Appendix 7)** for each time point a sample is taken
- Enter sample details on the **Biological Samples Inventory Log (Appendix 9)** (spreadsheet supplied electronically; a hardcopy is also available in the ISF).

3.4 STORAGE

- The samples must be stored at –70°C or colder.
- The yellow primary sample cryovials must be stored in one freezer box and the blue back-up sample cryovials must be stored in another freezer box. With a non-water soluble pen label the freezer box lid and freezer box side with ‘VEROnA Vandetanib samples PRIMARY’ or ‘Vandetanib samples BACK-UP’ and each box should be assigned a reference number.
- Make sure the freezer boxes are stored with the label facing forward.
- Record the final storage location (freezer and freezer box number) of the cryovials for each study time point on the **biological samples inventory log (Appendix 9).**
- Please refer to **Appendix 5** for more detailed information on the storage of samples in the freezer box.

3.5 SHIPPING

- The samples will be stored at site and shipped on request to York Bioanalytical Solutions (YBS)

- UCL CTC will arrange for the samples to be collected by a specialist courier company. The courier will provide the dry ice, packaging and temperature datalogger required for shipment.
- The samples must be shipped in the freezer boxes.

  Please note: Primary and back up samples should never be included in the same shipment. UCL CTC will advise the site which samples are to be shipped.
- Before shipping complete the **Vandetanib Plasma PK samples shipping form (Appendix 8)** photocopy the completed **vandetanib sample collection forms** and fax a copy to UCL CTC. Keep a copy at site in the VEROnA laboratory file.
- Place the original completed **vandetanib sample collection forms (Appendix 7)** in the box with the samples
- Record details of shipping on the **biological samples inventory log (Appendix 9)**
- On receipt of each shipment YBS will complete the lower portion of the collection form). Any discrepancies or inconsistencies will be raised by UCL CTC with the Site.

4 ARCHIVAL TUMOUR TISSUE

For the timing of samples to be collected, please refer to **Appendix 1** and section **7.3.16** of the protocol.

4.2 EQUIPMENT REQUIRED

REQUIRED ITEM	SUPPLIED BY UCL CTC?
Protective packaging for shipping, e.g. bubble-wrap	No
Archival Tumour Tissue Shipment Form	Yes

4.3 PROCESSING PROCEDURE

- Where patients have consented, pathology material from previous surgery or biopsy for HCC or colorectal cancer should be obtained by site staff from the relevant Pathology department as each patient is entered into the study.
- Complete an **Archival Tumour Tissue Shipment Form** for each patient.

4.4 SHIPPING

- Pathology material should be shipped in a padded envelope as soon as possible after the patient is entered into the study.
- Photocopy the completed **Archival Tumour Tissue shipment form** and fax a copy to the UCL CTC. Keep a copy at site.
- Place the original completed **Archival Tumour Tissue Shipment Form** for each block in the package. Keep copies at site.

Send the blocks and the original Archival Tumour Tissue shipment forms to Dr Marnix Jansen

Appendix 1: Summary of Sample Collection Timepoints

Timepoint for Sample Collection	Analysis	Type of Sample	No. of Samples
ASAP AFTER REGISTRATION			
Archival tumour tissue	Comparison with pathology material post BTG-002814	All available pathology material	All available pathology material
VISIT 1 (BASELINE) - PRIOR TO COMMENCING TREATMENT			
Within 7 days prior to treatment	Biomarker	Blood – plasma	1
VISIT 2 (TREATMENT DAY)			
Prior to treatment with BTG-002814	Biomarker	Blood – plasma	1
Prior to treatment with BTG-002814	Vandetanib levels	Blood – plasma	1
Post BTG-002814 treatment	Vandetanib levels	Blood – plasma	2*
VISIT 3			
Day 1 after treatment	Biomarker	Blood – plasma	1
Day 1 after treatment	Vandetanib levels	Blood – plasma	2**
VISIT 4			
-1 day prior to surgical resection	Biomarker	Blood – plasma	1±
-1 day prior to surgical resection	Vandetanib levels	Blood – plasma	1±
VISIT 6			
End of study visit	Biomarker	Blood – plasma	1
End of study visit	Vandetanib levels	Blood – plasma	1

Samples for Analysis: *Vandetanib levels (plasma)* *Blood Biomarkers*

** 2 & 4 hours post treatment (timed from the **START** of the infusion)*
***24 hours post treatment (timed from the **START** of the infusion); if patients require longer hospital stay an optional additional sample can be taken after 36 hours and up to time of hospital discharge*
±if surgery is delayed by >7 days an additional sample should be collected

Please refer to **section 7.0** of the protocol for more information.

Appendix 2: Centrifuge Table

Use a centrifuge with a swing-out rotor. If it is not possible to enter the speed in "g" on the centrifuge to be used, please use the table below showing the relation between radius of the rotor and speed. Centrifuge the tubes at the appropriate time and "g" (note g ≠ rpm).

$$rpm = 1000 \times \sqrt{\frac{g}{11.18 \times r}}$$

RADIUS OF CENTRIFUGE ROTOR (CM)	RPM EQUIAVLENT OF 1000XG
5	17889
6	14908
7	12778
8	11181
9	9938
10	8945
11	8131
12	7454
13	6880
14	6389
15	5963
16	5590
17	5261
18	4969
19	4708
20	4472
21	4259
22	4066
23	3889
24	3727
25	3578
26	3440
27	3313
28	3194
29	3084
30	2982

APPENDIX 3: SEPARATION OF BLOOD CELLS

PLASMA

The diagram below illustrates the separation of plasma from blood cells after centrifugation.

After centrifugation, the blood separates into several layers; white blood cells (WBC) and platelets will be in a whitish layer (buffy coat) just under the plasma layer (see diagram below).

The top layer is the plasma; when aspirating the plasma, take care not to place the tip of the pipette too close to where the cellular layers below begin, as this may disturb these layers and result in contamination of the plasma with cells.

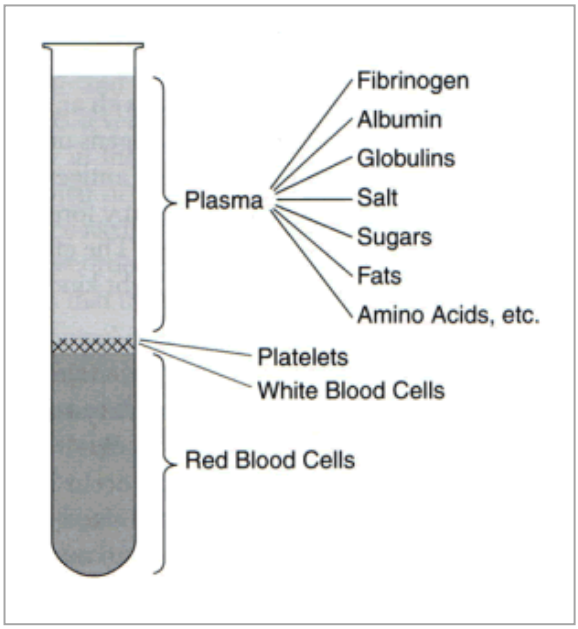

APPENDIX 4: STORAGE BOX INSTRUCTIONS FOR BLOOD BIOMARKER SAMPLES

The blood biomarker plasma samples for each patient should be stored together in one freezer box. They should be organised in the freezer boxes by Visit number. With a non-water-soluble pen label the freezer box lid and side of the base of the freezer box 'VEROnA biomarker samples, patient trial number'.

Samples for each collection time point (visit number) should be placed all in the same row. Each row should be labelled with the visit number as shown below.

The location of each freezer box must be noted on the **Biological samples inventory log**, to allow the laboratory easily to identify and locate samples as required.

The following grid reference should be used for each freezer box for each patient:

V1	V2	V3	V4	V6				

APPENDIX 4:

APPENDIX 5: STORAGE BOX INSTRUCTIONS FOR VANDETANIB SAMPLES

PRIMARY and BACK-UP Vandetanib blood plasma samples should be stored in separate freezer boxes. One freezer box should be clearly labelled 'VEROnA Vandetanib samples PRIMARY' and the other 'VEROnA Vandetanib samples BACK-UP'.

Samples should be stored in the boxes according to the layout below.

Each freezer box must be numbered sequentially and the location of each freezer box and freezer box number must be noted on the **Biological samples inventory log**, to allow the laboratory easily to identify and locate samples as required.

	VER-XX	VER-XX	VER-XX	VER-XX	VER-XX	VER-XX	VER-XX	VER-XX	VER-XX
0 hr									
2 hr									
4hr									
24hr									
>36hr									
V4									
V6									

APPENDIX 6: Example of biomarker SAMPLE collection form

VEROnA Biomarker sample collection form

This form should be completed on the day the samples are collected

Please complete one form for EACH sample timepoint. Fax [redacted] copy to the VEROnA trial coordinator when ready for shipping. File one copy in the site file or patient notes. Include the original copy with the relevant samples when shipped.

Patient trial no. VER - ☐☐	Site	
Date of collection	☐☐/☐☐/☐☐☐☐ dd/mm/yyyy	

Sample collection timepoint *[tick one box only]*

Baseline (Visit 1) ☐	Pre-Treatment (Visit 2) ☐	Day after treatment (Visit 3) ☐
Prior to surgery (Visit 4) ☐	End of Study (Visit 6) ☐	

Sample processing:

Time collected hh mm ☐☐ ☐☐ *Time centrifuged hh mm* ☐☐ ☐☐ *Time frozen at -70°C or below hh mm* ☐☐ ☐☐

No. of alliquots ☐

Were the samples processed following procedure in the Lab Manual? Yes ☐ No ☐

If no, please describe in detail the deviation(s) from the protocol below.
(e.g not processed within 30 mins of collection or centrifuged at 1500 x g instead of 1000 x g)

To be completed by the person processing the samples:

Name

Signature Date

Shipping details:

Date Staff Responsible

Signature

To be completed by the UCL ECMC GCLP Facility on receipt of samples:

Date samples received ☐☐/☐☐/☐☐☐☐ (dd/mm/yyyy) **No. of aliquots** ☐

Were any samples damaged, defrosted, lost, etc? ☐ Yes ☐ No
If yes, please describe in below (include affected aliquot number if appropriate).

Name of person checking samples

Signature Date

Upon receipt please fax the completed form to the VEROnA trial coordinator [redacted]

VEROnA biomarker sample collection form v2.0 20Mar19

Appendix 7: Example of vandetanib sample collection form

VEROnA Vandetanib sample collection form

This form should be completed on the day the samples are collected

Please complete one form for EACH sample timepoint. File one copy in the site file or patient notes.

Patient trial no. VER - ☐☐	Site	
Date of collection	☐☐/☐☐/☐☐☐☐	dd/mm/yyyy

Sample collection timepoint *[tick one box only]*

Visit 2 Pre-dose ☐	Visit 2 2 hour ☐	Visit 2 4 hour ☐	Visit 3 24 hours ☐
OPTIONAL: Visit 3 >36 hrs ☐	Visit 4 Prior to surgery ☐	Visit 6 End of Study ☐	

Sample processing:

Time collected hh mm ☐☐☐☐ *Time centrifuged* hh mm ☐☐☐☐ *Time frozen at -70°C or below* hh mm ☐☐☐☐

Primary sample aliquot created: **Yes** ☐ **No** ☐

Back-up sample aliquot created: **Yes** ☐ **No** ☐

Were the samples processed following procedure in the Lab Manual? **Yes** ☐ **No** ☐

If no, please describe in detail the deviation(s) from the protocol below.
(e.g not processed within 30 mins of collection or not stored within 60 minutes of collection)

Storage:

Primary aliquot stored in PRIMARY freezer box: **Yes** ☐ **No** ☐

Back-up aliquot stored in BACK-UP freezer box: **Yes** ☐ **No** ☐

To be completed by the person processing the samples:

Name

Signature Date

Please [redacted] or email [redacted] the completed form to the VEROnA trial coordinator at UCL CTC

VEROnA Vandetanib sample collection form v2 19Mar2018

Appendix 8: example of vandetanib PLASMA PK SAMPLES shipping for

VEROnA

Vandetanib Plasma PK samples
Dry Ice Sample shipping form

[redacted]

Section 1: To be completed by person shipping the samples				Section 2: To be completed by person receiving the samples	
Date shipped: D D - M M - Y Y Y Y				Date received: D D - M M - Y Y Y Y	
Patient Trial No.	**Date of sample collection** *(DD-MM-YYYY)*	**Timepoint[1]**	**Aliquot shipped** *(P=Primary; B=Backup)*	**Aliquot received** *(P=Primary; B=Backup)*	**Comments**
VER-					
VER-					
VER-					
VER-					
VER-					
VER-					
VER-					
VER-					
VER-					
VER-					
VER-					
VER-					
VER-					
VER-					
VER-					

[1] Visit 2 Pre-dose; Visit 2 2hr; Visit 2 4hr; Visit 3 24hr; Visit 3 >36hr; Visit 4 Prior to surgery; Visit 6 End of study

Name :	Name :
Signature:	Signature:
Date: D D - M M - Y Y Y Y	Date: D D - M M - Y Y Y Y

VEROnA Vandetanib PK Shipping V1 20/03/2018

Appendix 9: Biological sample inventory log

VEROnA - Plasma for blood biomarkers Sample Inventory Log

Patient trial ID: _____ **Patient Initials:** _____ **Trial Site:** _____

Protocol Time point	Date of collection *(dd/mm/yyyy)*	If sample not taken please give reason:	No. of aliquots created	Nominal storage temp (°C)	Storage Location (e.g. freezer)	Date shipped to lab *(dd/mm/yyyy)*	Name of person shipping sample
Visit 1 Baseline							
Visit 2 Pre-Treatment							
Visit 3 Day after treatment							
Visit 4 Day before surgery							
Visit 6 End of study							

VEROnA - Plasma for Vandetanib N-desmethyl metabolite Sample Inventory Log

Patient trial ID: _____ **Patient Initials:** _____ **Trial Site:** _____

Protocol Time point	Aliquot[1]	Date of collection[2] *(dd/mm/yyyy)*	If sample not taken please give reason	Aliquot created (Y/N)	Nominal storage temp (°C)	Storage Location (freezer/ box ID)	Date shipped to YBS *(dd/mm/yyyy)*	Initials of person shipping sample
Visit 2 Pre-dose	P							
	B							
Visit 2 2hr	P							
	B							
Visit 2 4hr	P							
	B							
Visit 3 24hr	P							
	B							
Visit 3 >36hr	P							
	B							
Visit 4 Prior to Surgery	P							
	B							
Visit 6 End of Study	P							
	B							

1 P=primary; B=back-up
2 if sample not taken, enter ND

UCL Cancer Institute

Document No. : **ONC/076/Version 1**

Title : **Preparation of VEROnA Clinical Samples for Analysis**

Effective Date : **12/06/2019**
Review Due Date : **12/06/2022**

Training Implications; *(Please tick appropriate box)*	**A**	**B**	**C** √	**D**

A = New procedure requiring documented assessment of competence
B = Modified procedure requiring documented reassessment of competence
C = Familiarity with new procedure required (no assessment of competence necessary)
D = Familiarity with changes required (no assessment of competence necessary)

Revision History:
ONC/076/V1: First version. Effective date: 12/06/2019

	Signature	**Name**	**Date**
Prepared by		Leah Ensell	
Reviewed by		Helen Lowe	
Authorised by		John Hartley	

Manual Number 2

1. INTRODUCTION

1.1. This SOP describes the preparation for analysis of plasma samples collected as part of VEROnA: A window of opportunity study of vandetanib-eluting radiopaque beads (BTG-002814) in patients with resectable liver malignancies, EudraCT Number: 2016-004164-19

1.2. Samples are to be analysed using Luminex xMAP technology, on the Bio-Plex 200 system in the GCLP Facility.

1.3. Samples will each be analysed using six separate Milliplex® Kits, comprising a total of 39 biomarkers. In order to minimise the quantity of sample used, and reduce freeze-thawing of samples, this SOP details which kits should be used together where possible.

2. SCOPE

2.1. This SOP applies to all plasma samples received at the UCL ECMC GCLP Facility from the VEROnA clinical trial.

2.2. For sample numbers and time points, refer to the active version of the Analytical Plan.

3. RESPONSIBILITIES

3.1. It is the responsibility of members of staff of the UCL ECMC GCLP Facility who are trained in this SOP to carry out the procedure as detailed.

3.2. Any deviations should be reported to the Analytical Project Manager and a deviation filed according to Facility procedures.

4. RELATED DOCUMENTS

4.1. QUP/001/Vx (where x denotes version number) – Quality Policy

4.2. QUA/006/Vx (where x denotes version number) – Deviation Procedure

4.3. QUA/004/Vx (where x denotes version number) – Corrective and Preventative Action

4.4. Analytical Plan AP/VEROnA/Vx (where x denotes the active version)- VEROnA: A window of opportunity study of vandetanib-eluting radiopaque beads (BTG-002814) in patients with resectable liver malignancies; EudraCT Number: 2016-004164-19

4.5. ONC/058/Vx (where x denotes version number) - Using the HAGP1MAG-12K MILLIPLEX MAP kit

4.6. ONC/059/Vx (where x denotes version number) - Using the HANG2MAG-12K MILLIPLEX MAP kit

4.7. ONC/060/Vx (where x denotes version number) - Using the HCYTOMAG-60K MILLIPLEX MAP kit

4.8. ONC/061/Vx (where x denotes version number) - Using the HIGFBMAG-53K MILLIPLEX MAP kit

4.9. ONC/062/Vx (where x denotes version number) - Using the HMMP2MAG-55K MILLIPLEX MAP kit

4.10. ONC/063/Vx (where x denotes version number) - Using the HSP1MAG-63K MILLIPLEX MAP kit

4.11. ONC/058/F1/Vx (where x denotes version number) - MILLIPLEXMAP Kit Process Sheet

4.12. LAB/008/Vx (where x denotes the version number) - Amending sample details in Freezerworks

4.13. EQU/006/Vx (where x denotes the version number) – Routine use and cleaning of micro-centrifuges

PROCEDURE

4.14. Plasma samples for the VEROnA clinical trial are stored below -70^{o}C until analysis.

4.15. Samples are stored in aliquots of 100uL, with up to 8 aliquots per patient timepoint. Samples should be thawed and prepared as per this SOP to minimize freeze-thawing, and maximise the amount of sample available for re-analysis as required.

4.16. For each reagent kit, the manufacturer supplies a recommended sample dilution in order to bring analyte concentrations within the assay range. These are detailed in Table 1. Initial analysis will be carried out on samples diluted according to these recommendations; if the analytical results fall outside of the assay range, samples will be re-analysed at a higher or lower dilution as applicable.

4.17. Where possible a single aliquot should be used for multiple plates on the same day, as detailed in table 1.

Aliquot Number	Milliplex Kit ID	Assay procedure	Recommended sample dilution	Minimum plasma volume required	SOP Number
1	HAGP1MAG-12K	2 day	1:2 in Assay Buffer	50uL	ONC/058
	HANG2MAG-12K	2 day	1:5 in Assay Buffer	20uL	ONC/059
2	HIGFBMAG-53K	2 day	1:25 in Assay Buffer	5uL	ONC/061
	HSP1MAG-63K	2 day	1:40 in Serum Matrix	5uL	ONC/063
3	HMMP2MAG-53K	1 day	1:20 in Assay Buffer	5uL	ONC/062
4	HCYTOMAG-60K	2 day	Undiluted	100uL	ONC/060

Table 1: Recommended dilutions for Milliplex kits

4.18. Where possible all of a patient's samples should be assayed in the same plate. Each plate can be used to analyse up to 25 samples in triplicate.

4.19. On the day of analysis, one aliquot per patient timepoint to be assayed should be retrieved and thawed on ice.

4.20. For aliquots 1 and 4 as detailed in Table 1:

4.20.1. Once thawed, vortex thoroughly and centrifuge at 10,000g for 10 minutes at 4^{o}C.

4.21. For aliquots 2 and 3 as detailed in Table 1:

4.21.1. Once thawed, vortex thoroughly and transfer 50ul to a clean labelled 1.5ml micro-centrifuge tube.

4.21.2. Return the original sample vial containing the remaining plasma to storage at below -70^{o}C.

4.21.3. Centrifuge the 50ul of plasma at 10,000g for 10 minutes at 4^{o}C.

4.22. Transfer the supernatant to a clean, labelled microcentrifuge tube, leaving any pellet or debris in the sample tube.

4.23. Place the clarified supernatant on ice, before continuing analysis as per the relevant Milliplex kit SOP.

4.24. Update the sample record (analysis date, aliquot volumes and number of thaws) in Freezerworks according to SOP LAB/008/Vx.

4.25. If re-analysis is required a fresh aliquot must be thawed and processed as above, using a new dilution if necessary.

4.26. Previously thawed and refrozen aliquots should only be used for analysis or re-analysis if no other sample is available. In this instance, a comment should be made on the ONC/058/F1/Vx sample processing form and recorded alongside the final result.

UCL Cancer Institute

Document No. : **ONC/058/Version 2**

Title : **Using the HAGP1MAG-12K MILLIPLEX MAP Human Angiogenesis / Growth Factor Magnetic Bead Panel 1 for biomarker analysis of plasma samples**

Effective Date : **12/06/2019** **Review Due Date** : **12/06/2022**

Training Implications; *(Please tick appropriate box)*	**A**	**B**	**C**	**D** √
A = New procedure requiring documented assessment of competence **B = Modified procedure requiring documented reassessment of competence** **C = Familiarity with new procedure required (no assessment of competence necessary)** **D = Familiarity with changes required (no assessment of competence necessary)**				

Revision History:
ONC/058/V1: First version. Effective date 04/05/2018.
ONC/058/V2: Preparation of plasma samples updated. Addition of carryover samples in analysis. Storage conditions of reagents removed. QC ranges removed as lot-dependant. Acceptance and Repeat analysis criteria updated. Effective date 12/06/2019

	Signature	**Name**	**Date**
Prepared by		Alexia Gali	
Reviewed by		Helen Lowe	
Authorised by		John Hartley	

5. INTRODUCTION/ OBJECTIVES

5.1. To describe the procedure for using the HAGP1MAG-12K MILLIPLEX MAP Human Angiogenesis / Growth Factor Magnetic Bead Panel 1 to quantify the concentrations of Angiopoietin-2, Endoglin, Follistatin, HB-EGF, HGF, Leptin, PLGF, VEGF-C and VEGF-D biomarkers in VEROnA clinical study samples.

6. SCOPE

6.1. Applicable to samples where biomarker quantification is part of a clinical trial or study within the UCL ECMC GCLP Facility, UCL Cancer Institute, Paul O'Gorman Building, UCL, 72 Huntley Street, WC1E 6DD.

7. RESPONSIBILITIES

7.1. It is the responsibility of members of staff of the ECMC GCLP Facility who are trained in this SOP to carry out the procedure as detailed.

7.2. Any deviations should be reported to the Analytical Project Manager and a deviation filed according to Facility procedures.

8. RELATED DOCUMENTS

8.1. QUP/001/Vx (where x denotes version number) – Quality Policy

8.2. QUA/006/Vx (where x denotes version number) – Deviation Procedure

8.3. QUA/004/Vx (where x denotes version number) – Corrective and Preventative Action

8.4. Human Cytokine/Chemokine Magnetic Bead Panel Instructions Manuals, as follows:

8.5. Instructions Manual of kit **HAGP1MAG-12K**. The cytokines that will be quantified using this kit are: Angiopoietin-2, Endoglin, Follistatin, HB-EGF, HGF, Leptin, PLGF, VEGF-C and VEGF-D

8.6. EQU/037/Vx (where x denotes version number) - Use and Maintenance of the Bio-Plex 200 System

8.7. EQU/038/Vx (where x denotes version number) - Creating an assay using the Bio-Plex Manager Software

8.8. EQU/041/Vx (where x denotes the version number) – Use and maintenance of the Bio-Plex Pro wash station

8.9. EQU/005/Vx (where x denotes version number) – Routine Use and Cleaning of Centrifuges (Eppendorf 5810R)

8.10. ONC/058/F1/Vx (where x denotes version number) – MILLIPLEX MAP kit Processing Sheet

8.11. ONC/076/Vx (where x denotes version number) - Preparation of VEROnA Clinical Samples for Analysis

9. **REAGENTS/INSTRUMENTATION**

Kit components	*Additional Instrumentation & Reagents*
Human Cytokine / Chemokine Standard	Luminex Sheath Fluid
Human Cytokine Quality Controls 1 and 2	Reagent Reservoirs
Serum Matrix	Aluminum Foil
Set of one 96-Well Plate with 2 Sealers	Absorbent Pads
Assay Buffer	Adjustable Pipettes
10X Wash Buffer	Multichannel Pipettes
Human Cytokine Detection Antibodies	Titer Plate Shaker
Streptavidin-Phycoerythrin	Vortex Mixer
Bead Diluent	Bio-Plex 200 System
Mixing Bottle	Bio-Plex Pro Wash Station
	Sonicating water bath

10. **PROCEDURE**

10.1. Allow all reagents to warm to room temperature (20-25^{o}C) before use in the assay. Assay steps must be recorded on an ONC/058/F1/Vx form.

10.2. **Dilution of Plasma Samples**

10.2.1. Follow the preparation of plasma samples as per SOP ONC/076/Vx.

10.2.2. Remove samples from ice. In a new Eppendorf tube, add 50µL of plasma and 50µL of Assay Buffer to dilute the sample at 1:2.

10.2.3. Keep plasma sample and dilution on ice until use in the assay.

10.3. **Preparation of Antibody-Immobilized Beads**

10.3.1. Sonicate each individual antibody-bead vial for 30 seconds and then vortex for 1 minute.

10.3.2. Add 150 µL from each antibody-bead vial to the Mixing Bottle and bring final volume to 3.0 mL by adding 1650 µL of Bead Diluent.

10.3.3. Vortex the mixed beads well.

10.4. **Preparation of Quality Controls**

10.4.1. Carefully open the vials containing lyophilized Quality Control 1 and Quality Control 2 and reconstitute in 250 µL deionized water to each vial. To open the vials, gently tap them to get the powder on the bottom of the bottle. Slowly remove the lid until the lid slot appears and then pipette the deionized water

through the lid slot. Swirl the vials and tap again to get all the solution on the bottom.

10.4.2. Allow vials to sit for 5-10 minutes and then transfer the entire contents of the vials to appropriately labelled polypropylene microfuge tubes. Reconstituted quality controls **should not** be stored/transferred in glass vials.

10.5. **Preparation of Wash Buffer**

10.5.1. Bring the 10x Wash Buffer to room temperature and mix to bring all salts into solution. Dilute 60 mL of 10X Wash Buffer with 540 mL deionized water. Store unused portion at 2-8^{o}C for next day use in the assay.

10.6. **Preparation of Serum Matrix**

10.6.1. Carefully open the bottle containing lyophilized Serum Matrix and add 1.0 mL deionized water to it. To open the vial, gently tap it to get the powder on the bottom of the bottle. Slowly remove the lid until the lid slot appears and then pipette the deionized water through the lid slot. Swirl the vial and tap again to get all the solution on the bottom.

10.6.2. Allow at least 10 minutes for complete reconstitution.

10.7. **Preparation of Human Cytokine Standard**

10.7.1. Carefully open the bottle containing lyophilized the Human Cytokine Standard and reconstitute with 250µL deionized water. To open the vial, gently tap it to get the powder on the bottom of the bottle. Slowly remove the lid until the lid slot appears and then pipette the deionized water through the lid slot. Swirl the vial and tap again to get all the solution at the bottom.

10.7.2. Invert the vial several times to mix. Vortex the vial for 10 seconds.

10.7.3. Allow the vial to sit for 5-10 minutes and then transfer the standard to an appropriately labelled polypropylene microfuge tube. This will be used as the top standard. Reconstituted cytokine standard **should not** be stored/transferred in glass vials.

10.8. **Preparation of Working Standards**

10.8.1. Label seven polypropylene microfuge tubes as: Standard 6, Standard 5, Standard 4, Standard 3, Standard 2, Standard 1 and Background.

10.8.2. Add 200 µL of Assay Buffer to each of the seven tubes.

10.8.3. Using a new tip with each dilution, and pre-wetting it before taking the desired volume, prepare serial dilutions by:

adding 100 µL of the reconstituted Standard 7 to the Standard 6 tube, mix well and
transfer 100 µL of the Standard 6 to the Standard 5 tube, mix well and
transfer 100 µL of the Standard 5 to the Standard 4 tube, mix well and
transfer 100 µL of the Standard 4 to Standard 3 tube, mix well and

transfer 100 µL of the Standard 3 to the Standard 2 tube, mix well and transfer 100 µL of the Standard 2 to the Standard 1 tube and mix well.

Background sample (0 pg/mL) will only contain Assay Buffer.

10.8.4. The standards prepared by serial dilution must be used **within 1 hour of preparation**. Discard any unused working standards.

Preparation of the human cytokine standard working standards

Standard Concentration (Tube #)	Volume of Deionized Water to Add	Volume of Standard to Add
Standard 7	250 µL	0
Standard Concentration (Tube #)	**Volume of Assay Buffer to Add**	**Volume of Standard to Add**
Standard 6	200 µL	100 µL of Standard 7
Standard 5	200 µL	100 µL of Standard 6
Standard 4	200 µL	100 µL of Standard 5
Standard 3	200 µL	100 µL of Standard 4
Standard 2	200 µL	100 µL of Standard 3
Standard 1	200 µL	100 µL of Standard 2

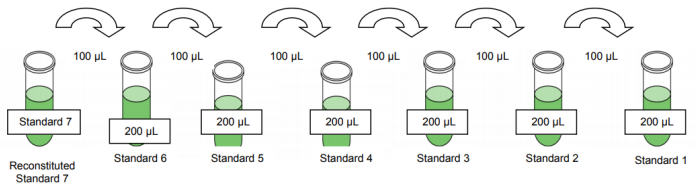

10.9. **Carryover Sample Preparation**

10.9.1. In the 96-well format of the plate, ensure that two wells containing Assay Buffer only are included after the top standard curve sample, for carryover assessment.

10.10. **Immunoassay Procedure**

10.10.1. Blank samples and standard samples can be analysed in duplicate, whereas plasma samples should be run in triplicate.

10.10.2. It is possible to run a portion of a plate initially, then reuse the plate with other samples later. Cover the wells that are not being used.

10.10.3. Add 200 µL of Wash Buffer into each well of the plate. Seal and mix on a plate shaker (500-800 rpm) for 10 minutes at room temperature.

10.10.4. Decant Wash Buffer and remove the residual amount from all wells by inverting the plate and tapping it smartly onto absorbent towels several times.

10.10.5. Add 25 µL of each Standard or Control into the appropriate wells. **Pipette to the sides of the wells** and be sure all fluid is expressed out of the pipette tips.

10.10.6. Add 25 µL of Assay Buffer to the background, carryover and sample wells. Assay Buffer should be **added before** the Serum Matrix.

10.10.7. Add 25 µL of Serum Matrix solution to the background, standards, and control wells.

10.10.8. Add 25 µL of sample (**diluted 1 part of plasma to 2 parts of Assay Buffer**) to appropriate wells.

10.10.9. Sonicate the Mixing Bottle for 30 seconds, mix by vortexing for 1 minute and add 25 µL of the Mixed or Premixed Beads to each well. (Note: During addition of Beads, shake bead bottle intermittently to avoid settling.)

10.10.10. Seal the plate with a plate sealer. Wrap the plate with foil and bring plate to a medium shake (~300 rpm), then slowly (over 10-20 seconds), bring to full speed (~1200 rpm). This will fully disrupt beads, equivalent to vortexing the plate. Keep at full speed about 10 seconds, then bring back down to 400-600 rpm.

10.10.11. Incubate with agitation (~600rpm) on a plate shaker overnight (16 – 18 hours) at 4°C.

10.10.12. Store all kit reagents at 2-8°C overnight.

10.10.13. Following an overnight incubation, allow plate to warm to room temperature (20-25°C) before subsequent use. In addition, allow all reagents to warm to room temperature before use in the assay.

10.10.14. Carefully remove sealing film to avoid splattering transfers.

10.10.15. Wash the plate by using the '3WASHES' program of the Bio-Plex Pro Wash station.

10.10.16. Add 25 µL of Detection Antibodies into each well. (Note: Allow the Detection Antibodies to warm to room temperature prior to addition).

10.10.17. Seal, cover with foil, bring slowly to full shake, then ramp down to 500 rpm. Incubate with agitation on a plate shaker for 1 hour at room temperature. **DO NOT ASPIRATE AFTER INCUBATION** and do not exceed incubation time.

10.10.18. Add 25 µL Streptavidin-Phycoerythrin (SAPE) to each well containing the 25 µL of Detection Antibodies.

10.10.19. Seal, cover with foil and bring slowly to full shake, then ramp down to 300 rpm. Incubate with agitation on a plate shaker for 30 minutes at room temperature. Do not exceed the dictated times of SAPE incubation as this will result in higher background signals.

10.10.20. Wash the plate by using the '3WASHES' program of the Bio-Plex Pro Wash station.

10.10.21. Add 100 µL of Sheath Fluid to all wells. (Note: This is performed because there has to be 50 µL excess well content to what the Bio-Plex 200 System will aspirate.)

10.10.22. Resuspend the beads with a longer shake, using the same gradual process as before. Agitate the plate on the plate shaker at room temperature for 5-10 minutes and at 500rpm. Keep the time to a minimum between shaking and reading so that beads do not settle.

10.10.23. Create an assay, as per SOP EQU/038/Vx - Creating an assay using the Bio-Plex Manager Software and read plate on a Bio-Plex 200 System, using the Bio-Plex Manager Software 6.1 (Security Edition). The information for the creation of the assay should be entered according to the kit's instruction manual for the standards concentration, magnetic bead region and quality control concentration.

10.10.24. Enter the appropriate Quality Control concentration for each bead/analyte during creation of an assay. The Quality Control concentration that should be entered for each analyte is the average value of the high and low range number provided by the kit manufacturer.

10.10.25. Ensure that the 'beads per region' field is set to 50, the samples size is set to 50 µL and the gate settings are between 8,000 and 15,000. Do not run at High RP1 target and click on the 'Auto Save after Run' button to save the results in an appropriate computer folder after completion of reading. Select the 'Optimise curves after run' button in order to allow the software to set outliers for the standard curve.

10.10.26. A second trained analyst should QC check the information entered in the created assay and sign the ONC/058/F1/Vx form.

10.10.27. Read plate by clicking on the 'Start' button in the 'Run Protocol' section. The plate should be read immediately after the assay is finished. If, however, the plate cannot be read immediately, seal the plate, cover with aluminium foil or an opaque lid, and store the plate at 2-8^{o}C for up to 24 hours. Delay in reading a plate may result in decreased sensitivity for some analytes.

Table 2: Bead Region and Concentration of Top Standard of Human Angiogenesis/Growth Factor Panel 1 Antibody-Immobilized Magnetic Beads.

Bead/Analyte Name	Luminex Magnetic Bead Region	Concentration of Top Standard (pg/mL)
Angiopoietin-2	14	10,000
Endoglin	22	20,000
Follistatin	43	20,000
HB-EGF	47	1,000
HGF	45	20,000
Leptin	28	100,000
PLGF	52	1,000
VEGF-C	54	5,000
VEGF-D	56	5,000

10.10.28. After reading the plate, export the data in the Report Table to an Excel workbook, by clicking the Export Report Table button in the toolbar and selecting the Single analyte format. A results file (.rbx) must be generated, which will be a file containing the results of a reading, including the raw data, the settings information from the Protocol, and tools for analysing and exporting the data (tables, a standard curve, export functions, etc.).

10.10.29. Using a USB drive, the report table and results file (.rbx) should be exported and stored in the appropriate trial folder, on the UCL ECMC GCLP S: drive.

11. ACCEPTANCE AND REPEAT ANALYSIS CRITERIA

11.1. Acceptance Criteria

11.1.1. Optimisation of the curve will be performed by the Bio-Plex Manager software.

11.1.2. Both QC 1 and QC 2 samples should demonstrate concentrations between the concentration ranges provided by the manufacturer for each sample.

11.2. Repeat Analysis Criteria

11.2.1. If one or both of the QC 1 and QC 2 samples shows a concentration outside the ranges provided by the manufacturer for each sample, the assay must be repeated.

11.2.2. Results above the ULOQ will be reported as > OOR (Out of Range), and the assay will be repeated, where sufficient sample is available, by further diluting the sample to within the assay range.

12. TROUBLESHOOTING

12.1. In the event that troubleshooting is required for an assay, describe the steps taken in form ONC/058/F1/Vx (Comments box).

12.2. If the detection antibody has been accidentally aspirated off or poured off before adding SAPE to the well, it is possible to recover the assay. Please refer to kit instructions manual and follow the outlined steps.

12.3. If samples fall outside the dynamic range of the assay, further dilute the samples with the appropriate diluent and repeat the assay.

12.4. If fluidics fail, or if there is any problem with how the data was obtained, the samples can still be rerun. Take the sample plate, remove the sheath fluid using a handheld magnet or using the Bio-Plex Pro Wash Station and resuspend the beads in fresh sheath fluid. Load the plate, check the Rerun/Recovery Mode box, and select those wells to be re-run. Start the run. The new values will be displayed for the re-run samples in the data file created on the first attempt. Sufficient beads are present for several re-runs.

Appendix B: FACT-HEP and EORTC QUESTIONNAIRES

(Chapter 6)

FACT-Hep (Version 4)

Below is a list of statements that other people with your illness have said are important. ***Please circle or mark one number per line*** to indicate your response as it applies to the past 7 days.

	PHYSICAL WELL-BEING	Not at all	A little bit	Some-what	Quite a bit	Very much
GP1	I have a lack of energy	0	1	2	3	4
GP2	I have nausea	0	1	2	3	4
GP3	Because of my physical condition, I have trouble meeting the needs of my family	0	1	2	3	4
GP4	I have pain	0	1	2	3	4
GP5	I am bothered by side effects of treatment	0	1	2	3	4
GP6	I feel ill	0	1	2	3	4
GP7	I am forced to spend time in bed	0	1	2	3	4

	SOCIAL/FAMILY WELL-BEING	Not at all	A little bit	Some-what	Quite a bit	Very much
GS1	I feel close to my friends	0	1	2	3	4
GS2	I get emotional support from my family	0	1	2	3	4
GS3	I get support from my friends	0	1	2	3	4
GS4	My family has accepted my illness	0	1	2	3	4
GS5	I am satisfied with family communication about my illness	0	1	2	3	4
GS6	I feel close to my partner (or the person who is my main support)	0	1	2	3	4
Q1	*Regardless of your current level of sexual activity, please answer the following question. If you prefer not to answer it, please mark this box* ☐ *and go to the next section.*					
GS7	I am satisfied with my sex life	0	1	2	3	4

EMOTIONAL WELL-BEING

		Not at all	A little bit	Some-what	Quite a bit	Very much
GE1	I feel sad	0	1	2	3	4
GE2	I am satisfied with how I am coping with my illness	0	1	2	3	4
GE3	I am losing hope in the fight against my illness	0	1	2	3	4
GE4	I feel nervous	0	1	2	3	4
GE5	I worry about dying	0	1	2	3	4
GE6	I worry that my condition will get worse	0	1	2	3	4

FUNCTIONAL WELL-BEING

		Not at all	A little bit	Some-what	Quite a bit	Very much
GF1	I am able to work (include work at home)	0	1	2	3	4
GF2	My work (include work at home) is fulfilling	0	1	2	3	4
GF3	I am able to enjoy life	0	1	2	3	4
GF4	I have accepted my illness	0	1	2	3	4
GF5	I am sleeping well	0	1	2	3	4
GF6	I am enjoying the things I usually do for fun	0	1	2	3	4
GF7	I am content with the quality of my life right now	0	1	2	3	4

	ADDITIONAL CONCERNS	Not at all	A little bit	Some-what	Quite a bit	Very much
C1	I have swelling or cramps in my stomach area	0	1	2	3	4
C2	I am losing weight	0	1	2	3	4
C3	I have control of my bowels	0	1	2	3	4
C4	I can digest my food well	0	1	2	3	4
C5	I have diarrhea (diarrhoea)	0	1	2	3	4
C6	I have a good appetite	0	1	2	3	4
Hep 1	I am unhappy about a change in my appearance	0	1	2	3	4
CNS 7	I have pain in my back	0	1	2	3	4
Cx6	I am bothered by constipation	0	1	2	3	4
H17	I feel fatigued	0	1	2	3	4
An7	I am able to do my usual activities	0	1	2	3	4
Hep 2	I am bothered by jaundice or yellow color to my skin	0	1	2	3	4
Hep 3	I have had fevers (episodes of high body temperature)	0	1	2	3	4
Hep 4	I have had itching	0	1	2	3	4
Hep 5	I have had a change in the way food tastes	0	1	2	3	4
Hep 6	I have had chills	0	1	2	3	4
HN 2	My mouth is dry	0	1	2	3	4
Hep 8	I have discomfort or pain in my stomach area	0	1	2	3	4

EORTC QLQ-C30 (Version 3)

We are interested in some things about you and your health. Please answer all of the questions yourself by circling the number that best applies to you. There are no "right" or "wrong" answers. The information that you provide will remain strictly confidential.

	Not at all	A little	Quite a bit	Very much
Do you have any trouble doing strenuous activities, like carrying a heavy shopping bag or a suitcase? …	1	2	3	4
Do you have any trouble taking a long walk? …….	1	2	3	4
Do you have any trouble taking a short walk outside of the house? …….	1	2	3	4
Do you need to stay in bed or a chair during the day?	1	2	3	4
5. Do you need help with eating, dressing, washing yourself or using the toilet? ……	1	2	3	4

During the past week:	**Not at all**	**A little**	**Quite a bit**	**Very much**
Were you limited in doing either your work or other daily activities? …….	1	2	3	4
Were you limited in pursuing your hobbies or other leisure time activities? …….	1	2	3	4
Were you short of breath? …….	1	2	3	4
Have you had pain? ……	1	2	3	4
Did you need to rest? …….	1	2	3	4
Have you had trouble sleeping? ……	1	2	3	4
Have you felt weak? ……	1	2	3	4
Have you lacked appetite? ……	1	2	3	4
Have you felt nauseated? …….	1	2	3	4
Have you vomited? ……	1	2	3	4
Have you been constipated? ……	1	2	3	4

During the past week:	**Not at all**	**A little**	**Quite a bit**	**Very much**
Have you had diarrhea? ……	1	2	3	4
Were you tired? ……..	1	2	3	4
Did pain interfere with your daily activities? ……	1	2	3	4
Have you had difficulty in concentrating on things, like reading a newspaper or watching television? ….	1	2	3	4
Did you feel tense? …….	1	2	3	4
Did you worry? …….	1	2	3	4
Did you feel irritable? ……..	1	2	3	4
Did you feel depressed? …….	1	2	3	4
Have you had difficulty remembering things? …….	1	2	3	4
Has your physical condition or medical treatment interfered with your family life? ……..	1	2	3	4
Has your physical condition or medical treatment interfered with your social activities? ……	1	2	3	4
Has your physical condition or medical treatment caused you financial difficulties? ……..	1	2	3	4

For the following questions, circle the number between 1 and 7 that best applies to you

How would you rate your overall health during the past week?

1	2	3	4	5	6	7
Very poor						Excellent

How would you rate your overall quality of life during the past week?

1	2	3	4	5	6	7
Very poor						Excellent

Appendix C: List of peer-reviewed publications arising from this project

1. Stereotactic body radiotherapy for large unresectable hepatocellular carcinomas- a single Institution phase II study.
   Beaton L, Dunne EM, Yeung R, Rackley T, Weber B, et al.
   Clinical Oncology. 2020 Feb 21. doi: 10.1016/j.clon.2020.01.028

2. Stereotactic Body Radiotherapy for Small Unresectable Hepatocellular Carcinomas
   Yeung R*, **Beaton L***, Rackley T, Weber B, Hamm J, Lee R, et al. (***Joint first author**)
   Clinical Oncology. 2019;31(6):365-373. doi.org/10.1016/j.clon.2019.01.012

3. VEROnA protocol: a pilot, open label, single-arm, phase 0, window-of-opportunity study of vandetanib-eluting radiopaque embolic beads (BTG-002814) in patients with resectable liver malignancies.
   Beaton L, Tregidgo HFJ, Znati SA, Forsyth S, Clarkson MJ, Bandula S, et al.
   JMIR Res Protoc. 2019 Oct 2;8(10):e13696. doi: 10.2196/13696

4. How Rapid Advances in Imaging are Defining the Future of Precision Radiation Oncology.
   Beaton L, Bandula S, Gaze MN, Sharma RA.
   Br J Cancer. 2019 Apr;120(8):779-790. doi: 10.1038/s41416-019-0412-y.

Appendix D: List of peer reviewed publications during the timescale of this project not direclty related to this project

1. PET/CT of breast cancer regional nodal recurrences: an evaluation of contouring atlases.
   Beaton L, Nica L, Tyldesley S, Sek K, Ayre G, Aparicio M, Gondara L, Speers C, Nichol A.
   Radiation Oncology 2020 doi: 10.1186/s13014-020-01576-6

2. Whole brain radiotherapy versus stereotactic radiosurgery in poor-prognosis patients with one to 10 brain metastases; a randomized feasibility study.
   Clinical Oncology Feb 2020 doi: 10.1016/j.clon.2020.02.001
   Raman S, Mou B, Hsu F, Valev B, Cheung A, Vallieres I, Ma R, McKenzie M, **Beaton L,** Rackley T, Gondara L, Nichol A.

3. In the era after the EORTC 'boost' study, is the additional radiotherapy to the breast tumour bed still beneficial for young women?
   Beaton L, Chan EK, Laura Beaton, Tyldesley S, Gondara L, Speers C, Nichol A. *Clinical Oncology Feb 2020.* doi: 10.1016/j.clon.2020.01.025.

4. Cardiac death after breast radiotherapy and the QUANTEC cardiac guidelines.
   Beaton L, Bergman A, Nichol A, Aparicio M, Wong G, Gondara L, et al.
   Clin Transl Radiat Oncol (2019); **19**: 39-45 doi.org/10.1016/j.ctro.2019.08.001

5. Recommendations for clinical translation of nanoparticle-enhanced radiotherapy.
   Ricketts K, Ahmad R, **Beaton L**, Cousins B, Critchley K, Davies M, et al.
   Br J Radiol. (2018) Dec;91(1092):20180325. doi: 10.1259/bjr.20180325.

6. Proton Beam Therapy (Book Chapter)
   Walter and Miller's Textbook of Radiotherapy: Radiation Physics, Therapy and Oncology. May 2019.
   Gains J, **Beaton L**, Amos A, Sharma R

Appendix E: Posters, presentations and abstracts

1. VEROnA protocol: a pilot, open label, single-arm, phase 0, window-of-opportunity study of vandetanib-eluting radiopaque embolic beads (BTG-002814) in patients with resectable liver malignancies
   Beaton L, Tregidgo HFJ, Znati, SA, Forsyth S, Clarkson MJ, Bandula S, et al. *Cancer Institute and Cancer Research UK-UCL Centre Conference, UCL, London. Poster presentation November 2018.*

2. Outcomes of Stereotactic Ablative Radiotherapy for Lymph Node Oligometastases
   Zhao Y, Yeung Y, **Beaton LE**, Liu M, Olson R.
   American Society for Radiation Oncology (ASTRO)
   Poster Presentation October 2018

3. A planning feasibility study of intensity-modulated proton therapy for re-irradiation of large pelvic in-field recurrences.
   Eminowicz, G, Rompokos V, Amos A, **Beaton L,** Payne, H et al.
   Particle Therapy Co-operative Group. Cincinnati, USA.
   Poster presentation May 2018